STRUCTURAL AND FUNCTIONAL STUDIES OF ALIX IN RETROVIRAL BUDDING

by

Qianting Zhai

A dissertation submitted to the faculty of
The University of Utah
in partial fulfillment of the requirements for the degree of

Doctor of Philosophy

Department of Biochemistry

The University of Utah

August 2011

The University of Utah Graduate School

STATEMENT OF DISSERTATION APPROVAL

The dissertation of **Qianting Zhai**

has been approved by the following supervisory committee members:

Christopher P. Hill	, Chair	**May 11th, 2011** Date Approved
Wesley I. Sundquist	, Member	**May 11th, 2011** Date Approved
Michael S. Kay	, Member	**May 11th, 2011** Date Approved
Martin P. Horvath	, Member	**May 11th, 2011** Date Approved
Darrell R. Davis	, Member	**May 11th, 2011** Date Approved

and by **Christopher P. Hill**, Chair of the Department of **Biochemistry**

and by Charles A. Wight, Dean of The Graduate School.

ABSTRACT

The cellular protein ALIX and other ESCRT proteins facilitate topologically equivalent membrane abscission events, including viral envelope separation from host membranes, biogenesis of multi-vesicular bodies, and midbody scission at the late stage of cytokinesis. Late domain motifs displayed by retroviral Gag polyproteins are responsible for recruiting ESCRT proteins. The three best-characterized classes of late domains are: the "P(S/T)AP" late domains that bind TSG101 of the ESCRT-I complex, the "PPXY" late domains that bind NEDD4 family ubiquitin E3 ligases, and the "YPXnL" late domains that bind ALIX. ALIX also binds the ESCRT-III protein CHMP4, which recruits other ESCRT-III subunits and VPS4 complexes to carry out membrane fission.

My work in this dissertation is centered on how ALIX is recruited by various retroviruses and how ALIX function is regulated in viral budding. We first determined crystal structures of $ALIX_{Bro1}$, $ALIX_{V}$ and $ALIX_{Bro1\text{-}V}$. Second, in order to understand how the viral Gag proteins hijack ALIX, we determined the structure of $ALIX_{Bro1\text{-}V}$ in complex with HIV and EIAV YPXnL late motifs. Third, we used surface plasmon resonance (SPR) to map a new type of ALIX-binding elements from certain SIV strains, which do not contain

the canonical YPXnL late domains and still package ALIX in the virions. Furthermore, the new ALIX-binding motifs were crystallized with $ALIX_{Bro1\text{-}V}$. All these late-domain ligands adopt different conformations of backbones to interact with the equivalent interface on the ALIX V domain. Based on sequence analysis, nearly every known primate lentiviruses contains an ALIX-binding site, suggesting that the ability to recruit ALIX provide a strong selective advantage for viruses. Fourth, we discovered that the full-length ALIX is autoinhibited by its C-terminal proline-rich region (PRR), which blocks the interaction of viral late domains based on the results of isothermal titration calorimetry (ITC), SPR and small-angle X-ray scattering (SAXS). The mutation that opens the closed conformation of the V domain partitioned ALIX into membrane-containing fractions and enhanced virus budding. These observations suggest that the function of ALIX is highly regulated, and ALIX activation requires dissociation of the autoinhibitory PRR, opening of the V domain, and probably protein dimerization.

TABLE OF CONTENTS

ACKNOWLEDGMENTS

I would like to express my deepest gratitude to my advisor Chris Hill for the guidance and support. In addition to his broad scientific knowledge, his active role in the campaign for sustainable energy has been an inspiration to me. I would like to thank Wes Sundquist for constant scientific guidance and being a role model for an integral and passionate scientist. I also thank my thesis committee: Michael Kay, Martin Horvath and Darrell Davis for critical review of my work.

I would also like to acknowledge my co-workers, Robert Fisher, Michael landsman, Hyo-young Chung, David G. Myszka and Prof. Jill Trewhella, whose contributions are instrumental in this work. I thank Rob Fisher, Heidi Schubert and Frank Whitby for helpful guidance regarding crystallography, and Steven Alam for help in ITC and NMR experiments. I thank all the members of the Hill and Sundquist labs, who have provided a scientifically and socially enjoyable environment. Finally, I am also thankful for my friends and family who provided constant encouragement and support during my graduate work.

CHAPTER 1

INTRODUCTION

Retroviruses and Hosts

Retroviruses Life Cycle

Viruses are abundant and are estimated to total 10^{31} particles on earth. Viruses infect mammals, plants, bacteria, and archaea (Breitbart and Rohwer, 2005). Viruses can be formidable pathogens, and viruses can also be useful tools for the study of the cellular biology and evolution of virus-host relationships. Diverse viruses are grouped at different hierarchical levels, based on their similar properties rather than on the identity of their hosts (Lwoff et al., 1962). Viruses can be classified into families, based on their type of genome and the method of replication (Baltimore, 1974). For example, Hepatitis A is a single-stranded RNA virus of the family *Picornaviridae*, while Hepatitis B virus is a DNA virus of the *hepadnaviridae* family (Baron, 1996). Human immunodeficiency viruses types 1 and 2 (HIV-1, HIV-2) and human T-cell leukemia viruses all belong to the family *Retroviridea*. A standard retrovirus contains a dimer of positive-sense single-stranded RNA, enclosed in a capsid, which in turn is surrounded by a lipid bilayer envelope (Ganser-Pornillos et al., 2008).

Retrovirus replication has many steps in common with the replication of other viruses, as well as several steps that are unique to their lifestyle (Figure 1.1). Retroviruses bind to specific receptors on the cell surface, and then, like all enveloped viruses, fuse the virion membrane with the host membrane, either at the cell surface or after internalization into endosomes,

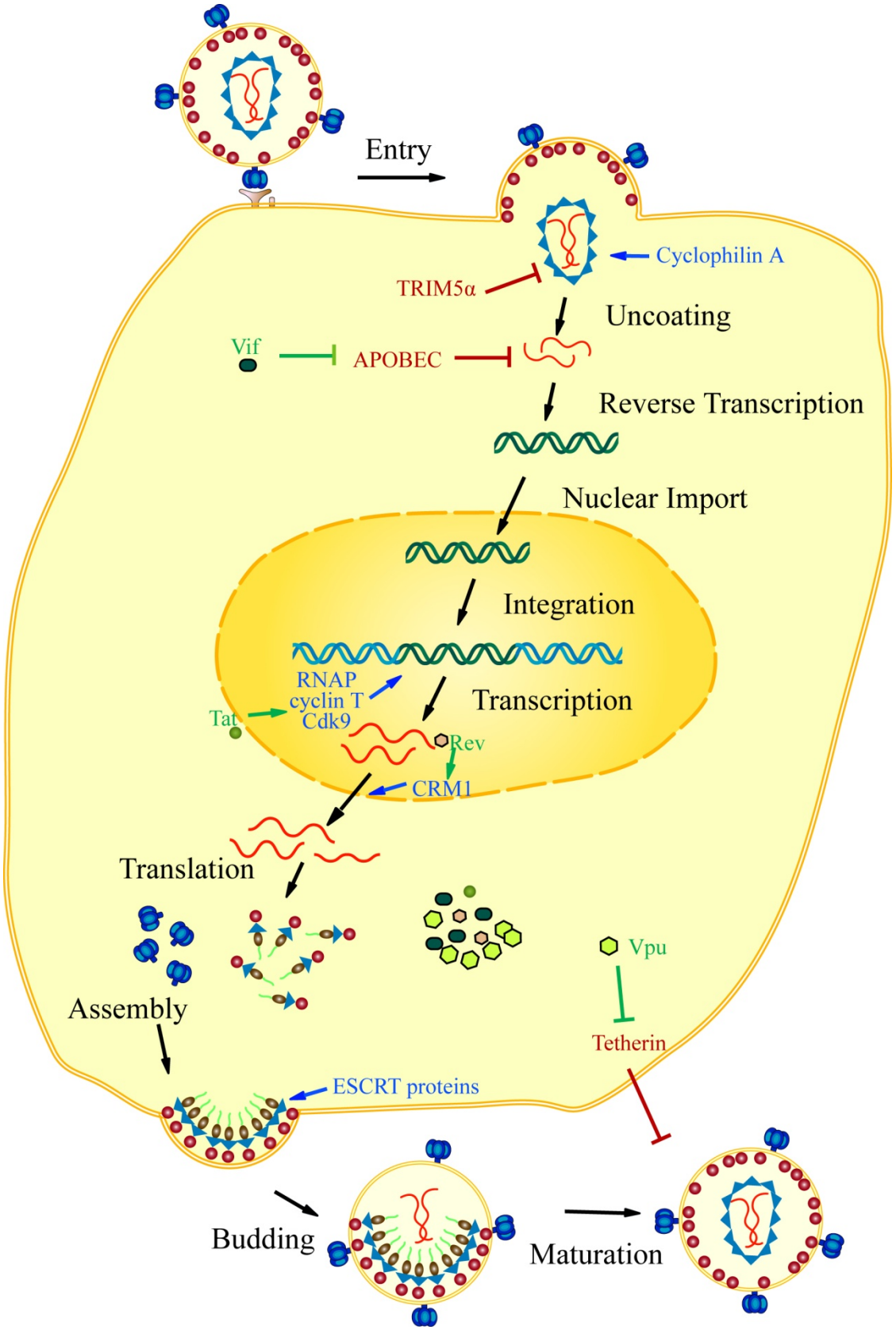

Figure 1.1. Retrovirus life cycle and interactions with host proteins.

to deliver the virion core to the cytoplasm (Hughson, 1997). The single-stranded positive-sense RNA genome is reverse transcribed into double-stranded linear DNA. This DNA is delivered into the nucleus in the form of a pre-integration complex (PIC) that contains both viral and host proteins, and is inserted into the host genome to form the integrated provirus. In the late phase of the life cycle, the viral DNA is transcribed by the host RNA polymerase II (RNAP) complex, and the viral RNAs are processed and exported to the cytoplasm by highly regulated mechanisms. Three viral structural protein precursors – group-specific-antigen protein (Gag), polymerase (Pol) and the envelope protein (Env) – are translated in the cytoplasm, and transported to the plasma membrane by vesicular, cytoskeletal or other routes. Nascent virions are assembled from these proteins on host membranes, and immature particles are released from the cells. Finally, maturation of the virions is triggered by the viral protease, which cleaves the Gag into its constituent protein molecules to drive a dramatic reorganization of the core and the acquisition of virus infectivity (Ganser-Pornillos et al., 2008; Goff, 2007; Wolf and Goff, 2008).

The numerous host proteins involved in retrovirus replication are characterized into two categories. The first category is innate immunity factors, which host organisms have evolved to perform multiple defensive mechanisms to limit or restrict virus replication by interfering with many stages of the retroviral life cycle. The other category is of the many host

proteins exploited by retrovirus in each step of replication to overcome the limited genome size and content of retroviruses (Goff, 2007; Wolf and Goff, 2008).

Restriction Factors

Host cell proteins that mediate antiviral activities by inhibiting the viral life cycle are known collectively as restriction factors, and include the proteins TRIM5α, APOBECs, tetherin and ZAP. At the same time, many retroviruses have developed various offensive strategies to inactivate or overcome the blocks to infection. As a result, a balance exists between host defense and viral offence, and this conflict is a powerful driver of evolutionary change.

TRIM5α blocks retroviral replication early in the life cycle, after viral entry but before reverse transcription. Although the exact mechanism of TRIM5α action is still not fully understood, TRIM5α binds to and multimerizes around incoming capsids, inducing premature uncoating of the viral capsids, which is detrimental to reverse transcription. TRIM5α proteins from a variety of species have different capabilities to restrict HIV-1 and other retroviruses. For instance, human TRIM5α potently restricts N-tropic MLV but not B-tropic MLV, HIV-1, or SIVmac, whereas rhesus macaque TRIM5α potently restricts HIV-1, N-tropic MLV but not SIVmac (Huthoff and Towers, 2008; Wolf and Goff, 2008).

APOBEC3G was identified as a cellular factor that renders human cells nonpermissive for infection by HIV viruses lacking a Vif gene (Sheehy et al., 2002). APOBEC family members convert cytidines into uracils in the negative sense single-stranded DNA that is generated during HIV-1 reverse transcription. As a result, these mutations might inactivate viral gene products or regulatory genetic elements. In addition, APOBEC3G can also be incorporated into nascent virus particles, and continues to edit during reverse transcription upon infection of the next target cell. However, the HIV-1 encoded Vif protein (viral infectivity factor) counteracts APOBEC3G by targeting it for ubiquitylation and subsequent degradation by the proteasome (Huthoff and Towers, 2008; Wolf and Goff, 2008).

Tetherin, also known as BST-2, was identified as a restriction factor that prevents retroviral particle release from the cell surface (Van Damme et al., 2008). This restriction factor is only effective against Vpu-minus HIV-1, because Vpu reduces cell surface levels of tetherin, with reported mechanisms including lysosomal degradation, proteasomal degradation, and sequestrating tetherin to the trans-Golgi network (Douglas et al., 2010). In the presence of tetherin, large numbers of Vpu-minus HIV-1 virions retained at the cell surface are fully formed and mature (Neil et al., 2008; Van Damme et al., 2008).

Host Proteins Exploited by Retroviruses

In contrast to cellular restriction factors, a number of host proteins are hijacked by viruses and used to facilitate viral replication and intracellular movements. For example, cyclophilin A is a host factor that binds directly to the HIV-1 capsid (Franke et al., 1994; Howard et al., 2003). While TRIM5α restricts viral infection, cyclophilin A modulates the sensitivity of HIV-1 to host restriction factors (Towers et al., 2003). Retroviral transcription of the integrated provirus DNA involves a large number of transcription proteins and the entire RNAP machinery (Wu, 2004). Viral Tat protein enhances expression from HIV-1 long-terminal repeat (LTR) by association with host cyclin T and cyclin kinase (Cdk9) (Yankulov and Bentley, 1998). The nuclear export factor CRM1 is exploited by the viral protein Rev to export the viral RNA from the nucleus to the cytoplasm (Daelemans et al., 2002; Strebel, 2003). The most extensive host machinery that is required for retrovirus budding uses endosomal sorting complex required for transport (ESCRT) proteins. Gag recruits the ESCRT machinery, and its membrane pinching activity, which normally drives the abscission step of cytokinesis and budding of vesicles into late endosomes, is used to bud virions from the cell. The rest of my dissertation will focus on Gag and ESCRT proteins in retrovirus budding (Bieniasz, 2009).

Retrovirus Budding

Gag Composition

The Gag protein is central to the assembly of HIV-1 and other retroviruses. Gag proteins alone are sufficient to assemble and produce non-infectious, spherical virus-like particles in the absence of other viral proteins or viral RNA (Freed, 1998). The structural proteins of HIV-1 are all derived from the Gag polyprotein. The functional organization of HIV-1 Gag is typical of retroviruses: matrix (MA), capsid (CA) protein, P2, nucleocapsid (NC) protein, P1 and p6 protein (Bieniasz, 2009).

The MA domain can interact directly with PI(4,5)P2, thereby explaining how high levels of PI(4,5)P2 in the plasma membrane act as a membrane anchor for HIV-1 Gag association (De Matteis and Godi, 2004; Ono et al., 2004; Saad et al., 2006). Gag proteins self-oligomerize and trigger the exposure of a hydrophobic N-terminal myristate of the MA domain, which further contributes to membrane association (Waheed and Freed, 2010). In freshly budded particles, the Gag polyproteins are located around the periphery of the particle under the lipid envelope, which is derived from the plasma membrane (Briggs et al., 2004; Carlson et al., 2008).

Upon assembly and budding, the viral protease is activated to cleave Gag into its constituent domains, and the newly processed proteins reassemble to form the distinct layers of the mature virion. The N-myristoylated MA targets the inner viral membrane, CA assembles into the

conical capsid, and NC coats the viral RNA genome (Ganser-Pornillos et al., 2008).

Late Domains

The p6 region of Gag is crucial for the release or pinching-off of assembled virions from the cell plasma membrane. Deletion of p6 from the HIV-1 Gag precursor protein leads to accumulation of assembled immature virus particles tethered to the plasma membrane (Gottlinger et al., 1991). Mutational analysis of the viral p6 region reveals short sequence motifs, termed "late domains", that are required for particle release. Thus far, three different classes of late domains from retroviruses have been well characterized.

The particle-release activity of HIV-1 p6 maps primarily to a P(T/S)AP late domain near the N-terminus of p6. The second position in this tetrapeptide motif can be either a threonine or a serine (Huang et al., 1995). P(T/S)AP motifs are highly conserved among lentiviruses, and have been shown to function in HTLV-1, MPMV, the VP40 protein of the Ebola virus, and the Z proteins of some arenaviruses (Morita and Sundquist, 2004). The P(T/S)AP motif recruits the cellular protein, TSG101, that normally functions in the sorting of proteins to multivesicular bodies (Garrus et al., 2001; Martin-Serrano et al., 2001; VerPlank et al., 2001).

Another commonly used late domain is the PPXY motif, which functions in diverse retroviruses, such as RSV, MMuLV, HHTLV-1, MPMV,

rhabdoviruses, filoviruses, and arenaviruses (Morita and Sundquist, 2004). Several groups have demonstrated that the Nedd4 family of ubiquitin E3 ligases can bind viral PPXY late domains (Kikonyogo et al., 2001; Macias et al., 2002).

A third late domain, the YPDL motif, was identified in the C-terminal p9 domain of equine infectious anemia virus (EIAV) Gag, which does not contain the P(T/S)AP or PPXY motifs (Puffer et al., 1997). A variant YPX_3L motif was also found in the p6 domain of Gag encoded by HIV, and shown to bind ALIX (Strack et al., 2003). The viral motifs recruiting ALIX are collectively called the YPXL late domain.

In a number of cases, retroviral Gag proteins have been shown to contain multiple late domains. For example, HIV-1 contains both PTAP and YPXL late domains, and MLV contains PSAP, YPXL and PPXY late domains. The advantage of multiple late domains within a virus is not entirely clear, but one possibility is that they provide the advantage of redundancy to recruit different cellular factors, in order to bud efficiently from different types of cell.

Late domain function is largely insensitive to the motif's position within a viral protein, and late domains are often exchangeable between retroviruses. For example, the YPDL late domain of EIAV can be functionally replaced with the PPPY late domain from RSV or the PTAP segment from HIV-1 p6 (Li et al., 2002). EM analysis reveals that late domain mutations

cause the same phenotype as deletion of the entire HIV-1 p6 region, with immature particles remaining tethered to the cell surface (Demirov et al., 2002; Gottlinger et al., 1991). The receptors for characterized late domains, TSG101and ALIX, are members of ESCRT proteins, and Nedd4 family ubiquitin ligases can ubiquitylate ESCRT-I components (Chung et al., 2008; Morita and Sundquist, 2004). These proteins normally function at the surface of the endosome to induce the budding of small vesicles into the multivesicular bodies (MVB). In infected cells, HIV-1 Gag redirects the ESCRT machinery to the plasma membrane and uses it to bud out of the cell.

ESCRT Machinery

MVB Sorting

Vesicle formation in MVB and viral particle budding on the cell surface share the same topology: they all bud away from the cytosol. MVB sorting plays important roles in the down-regulation of numerous activated growth factor receptors and membrane proteins. Downregulation of cell surface proteins is often facilitated by the posttranslational attachment of ubiquitin to the cytoplasmic domains (Joazeiro et al., 1999; Katzmann et al., 2002). Those membrane proteins are then sorted into the luminal vesicles (ILVs) of morphologically distinctive late endosomes known as MVBs. Fusion of the limiting membrane of the MVB with the lysosomal membrane results in MVB vesicles and their cargoes being exposed to the hydrolytic interior of the lysosome (Katzmann et al., 2002; Raiborg and Stenmark, 2009).

Genetic studies of yeast vacuoles, which correspond to the lysosomes of higher eukaryotes, led to the discovery of many components of the cellular MVB pathway (Raymond et al., 1992). The proteins essential for MVB sorting are now known as class E vacuolar vesicle protein sorting (VPS) proteins. Class E VPS mutants not only block MVB formation, but also produce large aberrant late endosomes consisting of stacked flat cisternae-like membranes, in contrast to roughly spherical wild-type endosomes filled with spherical ~24nm intraluminal vesicles (ILVs) (Nickerson et al., 2006; Raymond et al., 1992). Importantly, class E proteins are highly conserved from yeast to human. Many of these proteins are core subunits of four complexes required for transport (ESCRTs): ESCRT-0, ESCRT-I, ESCRT-II and ESCRT-III. Other class E VPS proteins include the AAA+ ATPase VPS4, and the ESCRT-associated protein Bro1 domain-containing protein ALIX.

Ubiquitylation is the principal signal for cargo to be directed into the MVB pathway. The conserved ESCRT/MVB machinery performs three distinct but connected functions: first, it recognizes ubiquitylated cargoes and enriches them on the endosome membrane; second, it deforms the membrane and maintains the membrane curvature to allow cargo to be enclosed by endosomal invagination; third, it catalyzes membrane abscission, forming ILV that contains the cargo.

ESCRT-0

Human ESCRT-0 is a heterodimer composed of HRS (hepatocyle growth factor-regulated tyrosine kinase substrate) and STAM (signal transducing adaptor molecule), which correspond to VPS27 and Hse in yeast, respectively (Table 1.1). Both human and yeast ESCRT-0 core complexes are connected by antiparallel coiled coils (Figure 1.2) (Prag et al., 2007; Ren et al., 2009).

Table 1. ESCRT complex subunits

Protein Complex	Yeast protein	Human protein	Ubiquitin binding domain	Membrane interaction domain
ESCRT-0	VPS27	HRS	VHS	FYVE
	Hse1	STAM1, 2	UIM, VHS	–
ESCRT-I	VPS23	TSG101	UEV	–
	VPS28	VPS28	–	–
	VPS37	VPS37A,B,C,D	–	VPS37 1-21
	MVB12	MVB12	–	–
ESCRT-II	VPS36	EAP45	GLUE	GLUE
	VPS22	EAP30	–	–
	VPS25	EAP20	–	–
ESCRT-III				N-terminal
	VPS20	CHMP6	–	myristate
	VPS32/Snf7	CHMP4A,B,C	–	–
	VPS24	CHMP3	–	–
	VPS2/Did4	CHMP2A,B	–	–
	VPS46/Did2	CHMP1A,B	–	–
	Ist1	IST1	–	–
	VPS60	CHMP5	–	–
other	VPS4	VPS4A,B	–	–
ESCRT	Vta1	LIP5	–	–
	Bro1	ALIX	V	Bro1?

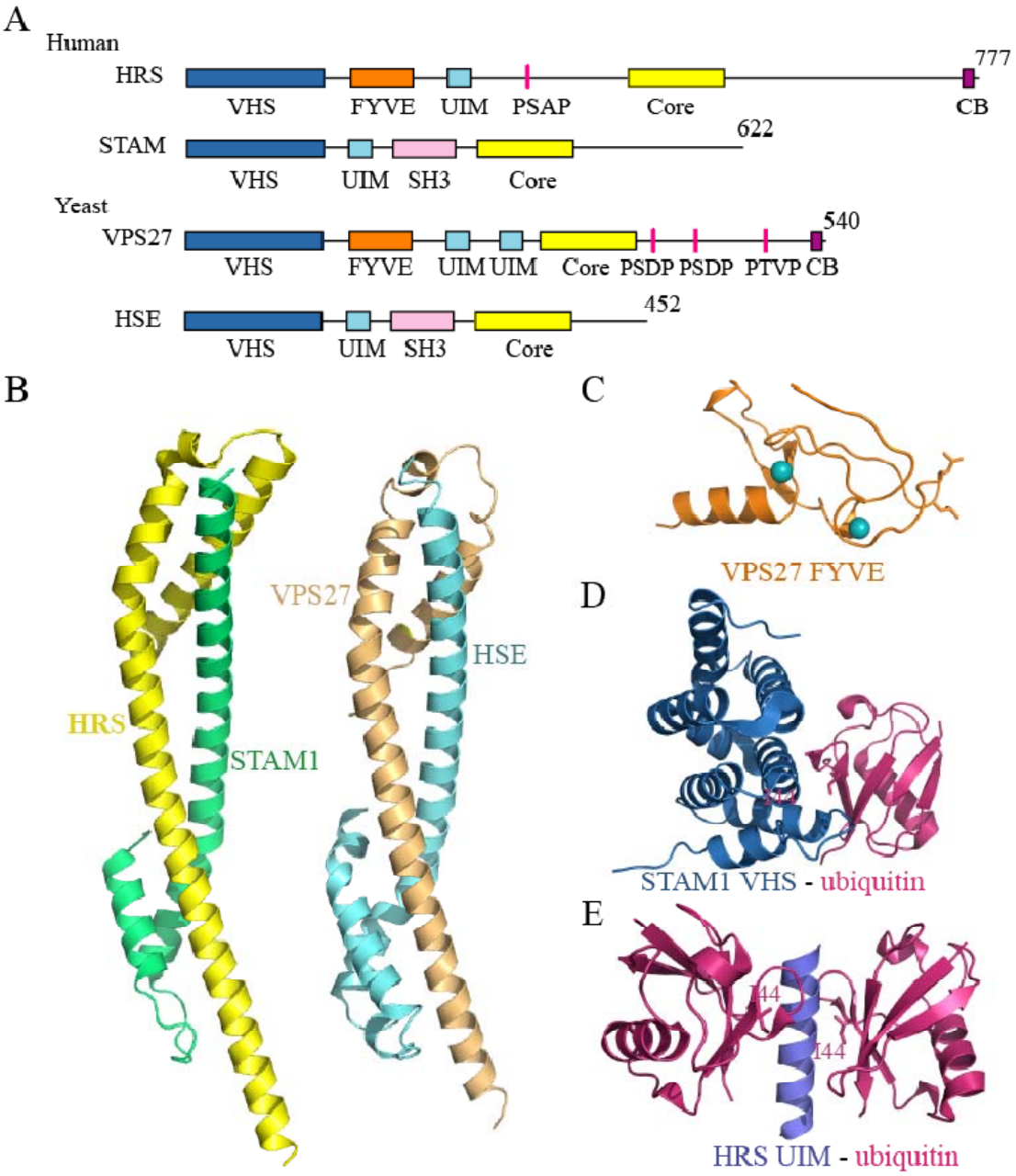

Figure 1.2. Domain organizations and known structures of the ESCRT-0 proteins. (A) Domain organization of human HRS, human STAM1, yeast VPS27 and yeast HSE. Domain name abbreviations are as follows: VHS, VPS-HRS-STAM domain; UIM, ubiquitin interaction motif; FYVE, (Fab1, YOTB, Vac1 and EEA1) zinc finger domain; CB, clathrin-binding. (B) Structure of the ESCRT-0 core complex: left, human; right: yeast. (C) Structure of the FYVE domain from yeast VPS27 with two zinic ions are colored in cyan. (D) Structure of the STAM VHS domain in complex with ubiquitin. (E) Structure of the complex between HRS UIM and two ubiquitin molecules.

The ESCRT-0 complex contains multiple domains that enable it to capture ubiquitylated cargo on endosomal membranes and initiate downstream sorting. First, ESCRT-0 targets to endosomes via the FYVE domain of HRS, which specifically binds to the endosomal lipid PI(3)P (phosphatidylinositol 3-phosphate) (Misra and Hurley, 1999; Raiborg et al., 2001b). Second, both subunits of ESCRT-0 complexes are equipped with multiple ubiquitin-interaction domains: the UIM and VHS domains, which provide the initial recognition of MVB cargoes (Bache et al., 2003b; Bilodeau et al., 2002; Raiborg et al., 2002; Ren and Hurley, 2010). The UIM and VHS motifs bind rather weakly to ubiquitin, with dissociation constants (K_D) of 200-300 μM and 100 μM-2mM, respectively. Nevertheless, ESCRT-0 binds Lys63-linked tetraubiquitin 50 times more tightly than monoubiquitin, indicating multiple ubiquitin-binding domains cooperatively binding to polyubiquitin (Hirano et al., 2006; Raiborg et al., 2002; Ren and Hurley, 2010). Third, HRS binds clathrin through a C-terminal clathrin-box motif, and localizes to flat clathrin lattices on early endosomes (Raiborg et al., 2002; Raiborg et al., 2001a; Raiborg et al., 2006). As a result, the concentration of local ESCRT-0 proteins and ubiquitylated cargoes are increased, which further facilitates the ESCRT-0-ubiquitin interaction. Finally, HRS recruits TSG101/ESCRT-I to endosomal membranes via the “PSAP” motif (Bache et al., 2003a). In conclusion, ESCRT-0 functions to recruit, concentrate and

cluster ubiquitylated cargoes to endosome membranes for downstream ESCRT proteins to continue the cargo sorting.

HIV-1 Gag can be viewed as an analogue of the ESCRT-0 complex based on the following observations. 1) HIV-1 Gag has an intrinsic property to polymerize, and Gag can be induced to assemble *in vitro* spontaneously into protein spheres that resemble ESCRT-0 clustering mediated by clathrin (Campbell et al., 2001; Campbell and Rein, 1999). 2) MA functionally substitutes for the FYVE domain of ESCRT-0. The HIV-1 MA domain specifically recognizes $PI(4,5)P_2$, which is enriched in plasma membranes (Ono et al., 2004; Saad et al., 2006), and $PI(4,5)P_2$ binding induces the N-terminal myristate of MA to adopt an exposed conformation, which further increases membrane-binding affinity and Gag multimerization (Saad et al., 2006; Tang et al., 2004). 3) The HIV-1 Gag PTAP late domain mimics the PSAP motif of Hrs/ESCRT-0, and thereby recruits ESCRT-I and other components of the MVB vesicle fission machinery to facilitate budding (Pornillos et al., 2003).

ESCRT-I

The ESCRT-I complex is a hetrotetramer formed by four subunits: TSG101, VPS28, VPS37 and Mvb12 (Chu et al., 2006; Katzmann et al., 2001; Morita et al., 2007a). The crystal structure of the yeast ESCRT-I complex core revealed a dramatic feature of the heterotetramer structure with a rigid 130 Å stalk (Kostelansky et al., 2007). Together with structures of the yeast

VPS23 UEV domain (Sundquist et al., 2004; Teo et al., 2004b), and VPS28 C-terminal domain (CTD) (Pineda-Molina et al., 2006), the overall structure of the ESCRT-I complex can be modeled (Figure 1.3).

ESCRT-I is recruited through the UEV domain of TSG101, which interacts with P(T/S)AP motifs in Hrs/VPS27 or viral Gag (Bache et al., 2003a; Katzmann et al., 2003; Pornillos et al., 2003). Additionally, the UEV domain may also bind ubiquitylated cargoes (Sundquist et al., 2004; Teo et al., 2004b). However, unlike ESCRT-0, ESCRT-I alone binds acidic phospholipids to a modest extent, but associates with membranes tightly in the presence of ESCRT-II (Kostelansky et al., 2007). ESCRT-1 in turn recruits ESCRT-II through the C-terminal domain of VPS28, which is at the opposite end of the stalk to the UEV domain (Gill et al., 2007).

Markedly, all ESCRT ubiquitin-binding domains interact with the same Ile44 patch on ubiquitin (Hurley and Emr, 2006; Saksena et al., 2007). The simplest model indicated by these observations is a "hand-off" model in which ESCRT complexes sequentially bind to cargoes. However, one ESCRT-II complex cannot simultaneously interact with the ubiquitin caught by the UEV domain and the VPS28 subunit of one ESCRT-I complex, which are separated by 130Å. The architecture of the ESCRT-I complex therefore provides direct evidence against the "hand-off" model between ESCRT-I and II. Instead, ESCRT-I and ESCRT-II likely co-assemble and cluster multiple ubiquitylated transmembrane proteins for packaging into ILVs.

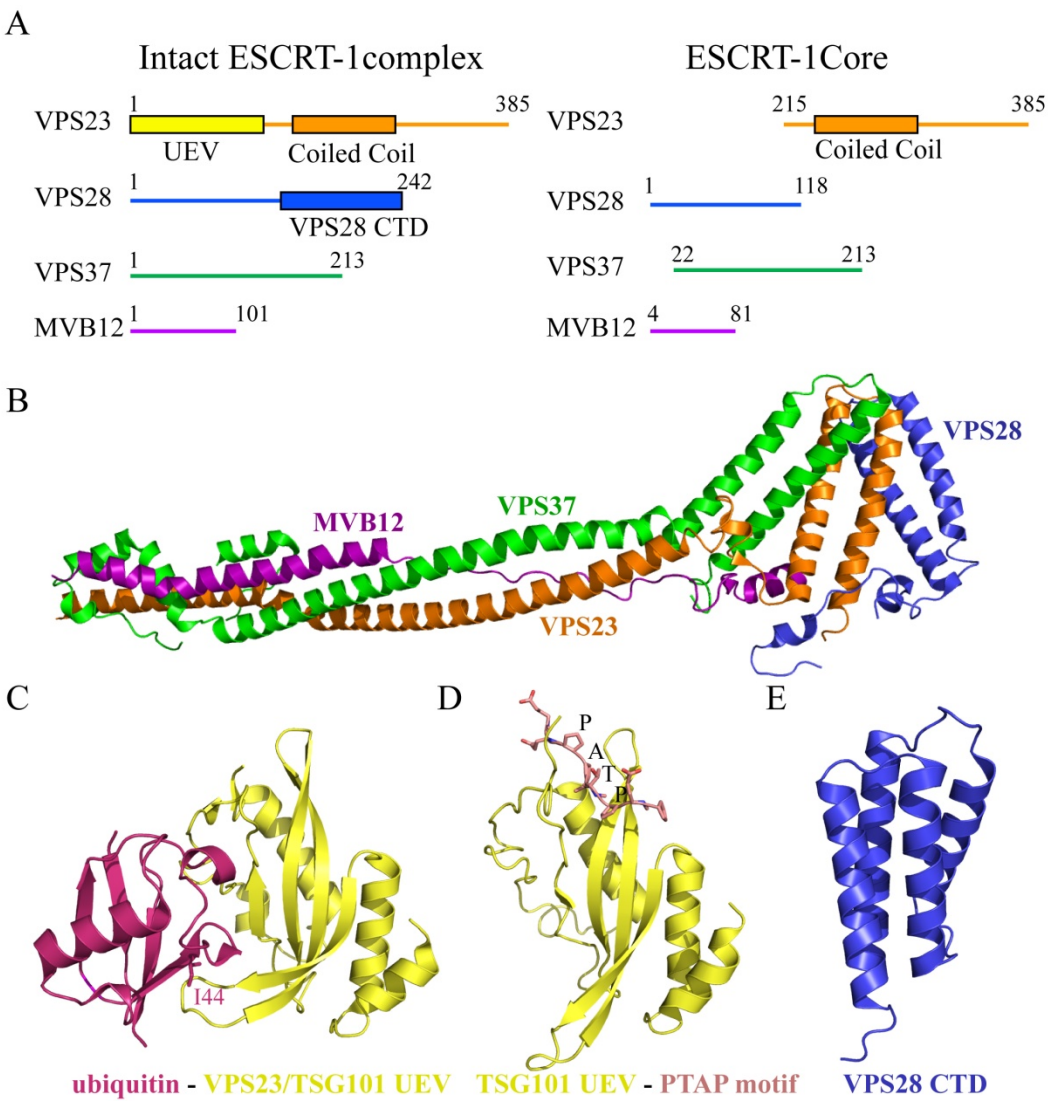

Figure 1.3. Domain organization and structures of ESCRT-I complex and subunits. (A) Domain organization of the intact ESCRT-I complex and the ESCRT-I core. (B) Structure of the ESCRT-I core. (C) Superposition of the human (yellow, red) and yeast (gray) complexes of the TSG101/Vps23 UEV domain with ubiquitin. (D) Overlay of the TSG101 UEV domain (yellow) in complex with the HIV-1 PTAP late domain (green) and the HRS PSAP motif (magenta). (E) Structure of the VPS28 C-terminal domain.

ESCRT-II

The ESCRT-II complex consists of one VPS36 subunit, one VPS22 subunit, and two copies of VPS25 (Babst et al., 2002b). Even though the three subunits do not share sequence homology, they all possess two repeats of a superimposable WH (winged-helix) domain. The cores of the both human and yeast ESCRT-II complexes are shaped like the letter "Y", with two branches each formed by one VPS25 protein, and the stalk composed of VPS22 and VPS36 (Hierro et al., 2004; Im and Hurley, 2008; Teo et al., 2004a) (Figure 1.4A).

The structure of the GLUE domain, which was missing from the core structure, was determined in complex with ubiquitin and in complex with the C-terminal domain of the VPS28 ESCRT-I subunit, respectively (Figure 1.4B) (Alam et al., 2006). Indeed, both human and yeast GLUE domains can bind ubiquitin, membranes, and ESCRT-I (Im and Hurley, 2008; Slagsvold et al., 2005; Teo et al., 2006). Nevertheless, two NZF domains are inserted in the yeast GLUE domain: the first NZF domain of VPS36 interacts with ESCRT-I and the second NZF possesses ubiqutin-binding activity (Gill et al., 2007; Slagsvold et al., 2005; Teo et al., 2006). ESCRT-II subsequently recruits ESCRT-III through direct interactions between VPS25/ESCRT-II and VPS20/ESCRT-III (Babst et al., 2002b; Im et al., 2009; von Schwedler et al., 2003; Yorikawa et al., 2005).

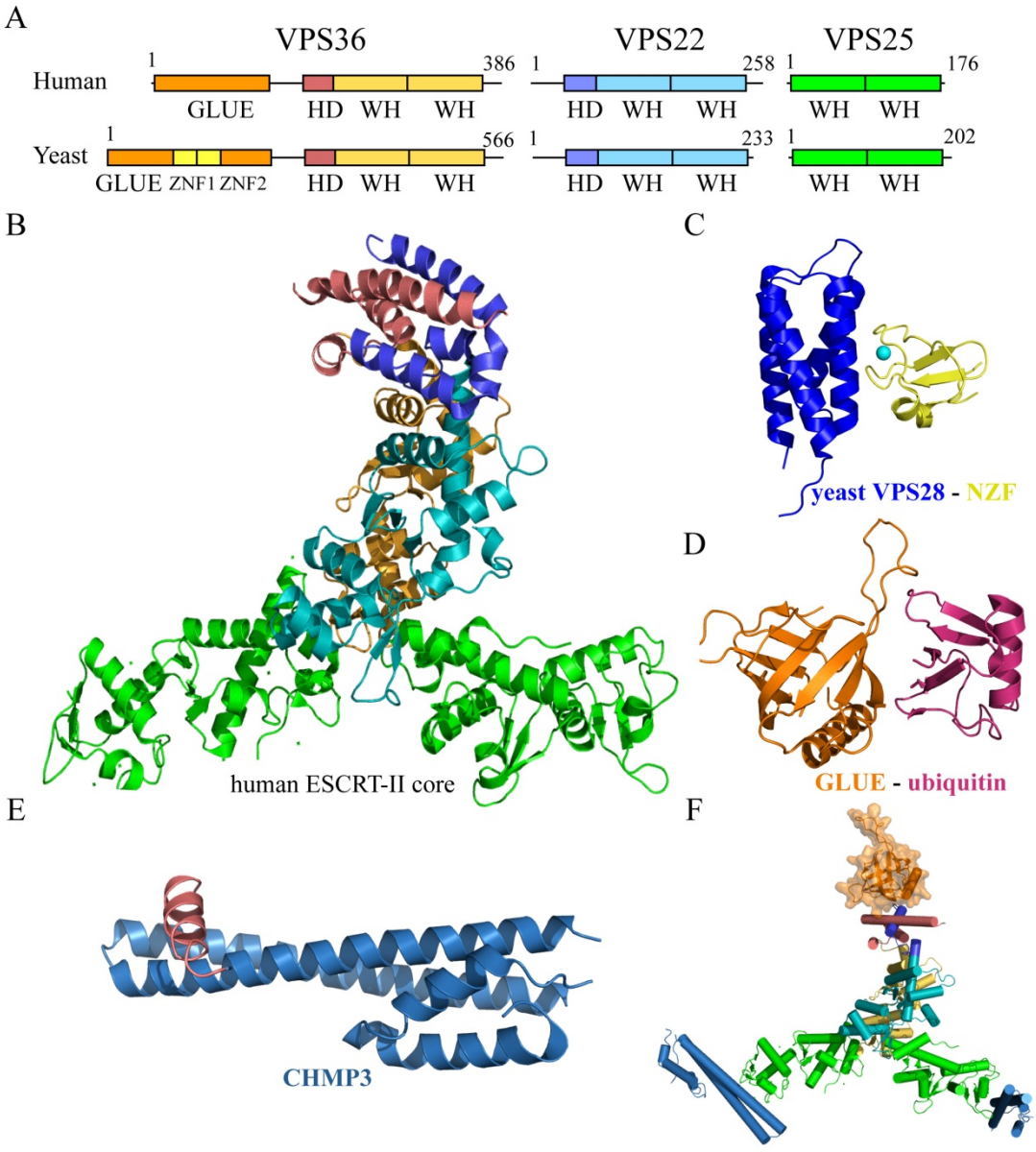

Figure 1.4. Domain organization and structures of ESCRT-II proteins and ESCRT-III proteins. (A) Domain organization of human and yeast ESCRT-II complex. (B) Overall structure of the human ESCRT-II core, in which the GLUE domain is absent. The color is same in (A). One VPS25 with one WH2 domain poorly visible in the electron density is modeled in the figure using the other subunit. (C) Structure of the yeast ESCRT-I VPS28 CTD (blue) in complex with the NZF-N domain (yellow) from ESCRT-II. (D) The complex structure between the human GLUE domain and ubiquitin. (E) Crystal structure of human CHMP3. The CHMP3 core is blue and the autoinhibitory domain is salmon. (F) The composite structure of the ESCRT-II complex nucleating ESCRT-III subunits.

ESCRT-III

The ESCRT-III complex consists of four core subunits: CHMP6, CHMP4, CHMP3, CHMP2, and accessory proteins CHMP1, IST1 and CHMP5 (Babst et al., 2002a; Nickerson et al., 2006). ESCRT-III subunits are recruited from the cytosol to the endosomal membrane, where they assemble into high order oligomers. ESCRT-III proteins are similar in both size (221-241 residues) and domain organization, with an N-terminal basic core followed by a C-terminal acidic region, despite considerable variation in their primary sequences. Structural studies on CHMP3 indicate that the core domain contains 70 Å-long helices that are required for membrane association and homo- or hetro-dimerization (Figure 1.4E) (Muziol et al., 2006). The C terminal segment packs against the core and prevents premature assembly, while deletion of the autoinhibitory region produces a dominant inhibitor of HIV-1 budding (Bajorek et al., 2009; Lata et al., 2008; Muziol et al., 2006; Zamborlini et al., 2006).

ESCRT-III subunits were proposed to play an important role in membrane deformation, based on the following observations. First, ESCRT-III subunits can interact directly with membranes and removal of autoinhibiton induces membrane targeting (Babst et al., 2002a; Lin et al., 2005; Muziol et al., 2006). Second, ESCRT-III subunits can assemble into high order complexes on the membranes. For example, co-incubation of monomeric CHMP2A and CHMP3, both with C-terminal regions deleted,

assemble *in vitro* into tubular structures with their membrane-interaction sites exposed on the outside of the tubule (Lata et al., 2008). Other ESCRT-III subunits can also form high order helical structures, such as VPS24, CHMP1B and IST1 (Bajorek et al., 2009; Ghazi-Tabatabai et al., 2008). Finally, ESCRT-III not only associates with membranes, but also its assembly is capable of driving membrane deformation. Overexpression of CHMP4 in mammalian cells produces buds and tubules from the top surface of cells, and CHMP4 assembles into interconnected circular arrays of filaments around sites of membrane protrusion (Hanson et al., 2008). Thus, assembly of ESCRT-III proteins is sufficient to drive membrane deformation with the appropriate curvature for viral and MVB budding.

Based on biochemical and genetic studies, ESCRT-III subunits appear to be recruited sequentially (Saksena et al., 2009; Teis et al., 2008). VPS20 is the first ESCRT-III protein to associate with ESCRT-II on the endosome, where it adopts a conformation that is required to nucleate oligomerization of SNF7 at the endosome. Subsequent endosomal recruitment of the VPS24-VPS2 subcomplex appears to be dependent on the VPS20-Snf7 subcomplex (Babst et al., 2002a). Emr and colleagues reported that the Snf7 oligomer contributes the major building block of the ESCRT-III complex. The VPS24-VPS2 subcomplex caps and terminates the Snf7 oligomer by recruiting VPS4, which then disassembles the ESCRT-III complex by hydrolyzing ATP (Saksena et al., 2009; Teis et al., 2008).

VPS4

VPS4 is a member of the AAA+ (ATPase associated with diverse cellular activities) ATPase family, members of which typically function as oligomeric rings and use energy from ATP hydrolysis to remodel the conformation of their substrates (Erzberger and Berger, 2006; Ogura and Wilkinson, 2001; Sauer et al., 2004). VPS4 is composed of an N-terminal microtubule-interacting and transport (MIT) domain, a large ATPase domain, a small ATPase helical domain, a ß domain and a C-terminal helix (Figure 1.5) (Scott et al., 2005a). VPS4 also functions as an oligomer that is, by most accounts, a dodecamer comprised of two stacked rings that are conformationally distinct (Landsberg et al., 2009; Yu et al., 2008), although there also has been a report of a tetradecameric form (Hartmann et al., 2008). Nevertheless, the central pore and the ATP hydrolysis activity of VPS4 are critical for MVB sorting, enveloped virus budding, and late stage of cytokinesis (Gonciarz et al., 2008; Scott et al., 2005a). Hence, current evidence favors a model in which VPS4 pumps ESCRT-III subunits from the membrane-bound state, through the central pore, and into the cytosol.

The Vta1/LIP5 cofactor promotes and stabilizes the double ring structure of the VPS4 complex, and stimulates ATPase activity (Azmi et al., 2006; Yang and Hurley, 2010; Yu et al., 2008). LIP5 is composed of two MIT domains at its N terminus, a dimeric VPS4-binding VSL domain at its C terminus, and a long flexible linker (Xiao et al., 2008). Hence, the VPS4-LIP5

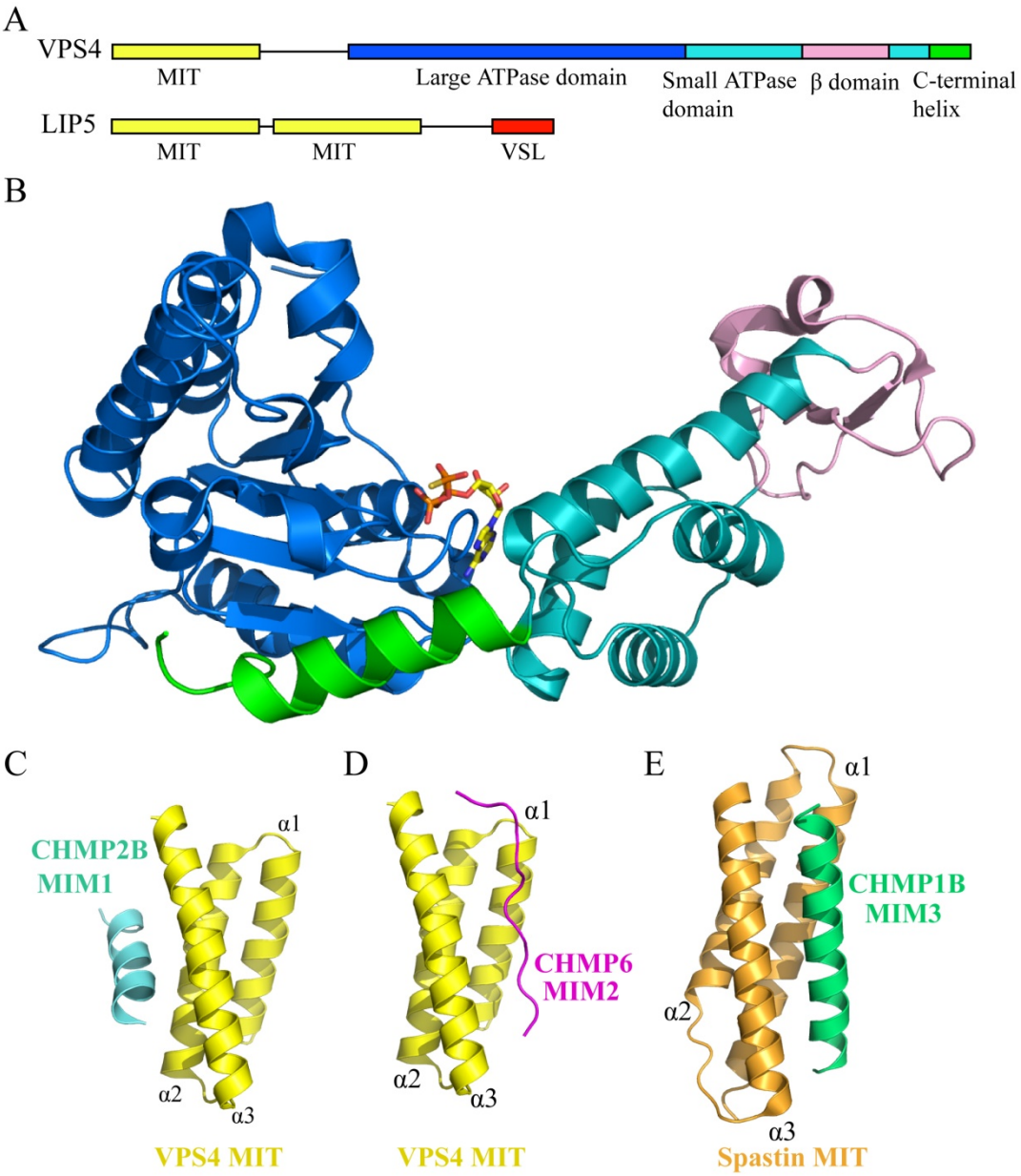

Figure 1.5. Domain organization and structures of VPS4 proteins. (A) Domain organization of human and yeast VPS4 proteins and VTA1. (B) Structure of yeast VPS4 missing the MIT domain in complex with ATPγS. (C) Structure of human VPS4 MIT in complex with MIM1 element from CHMP2B. (D) Structure of human VPS4 MIT in complex with MIM2 element from CHMP6. (E) Structure of Spastin MIT domain in complex with MIM3 element from CHMP1B.

ATPase supercomplex displays a total of 24 MIT domains, 1 from each of the 12 VPS4 subunits and 2 from each of the 6 associated Vta1 cofators (Azmi et al., 2008; Yu et al., 2008). Recruitment of ESCRT-III subunits is critically dependent on the MIT domain, which is composed of an antiparallel three-helix bundle (Scott et al., 2005b). The MIT domain can bind ESCRT-III proteins in diverse ways. Type 1 MIT interacting motifs (MIM1), such as the C-terminus helix of CHMP1A, CHMP2B or VPS2 C-terminus, contact the VPS4 MIT domain via a surface groove formed by helices α2 and α3 of the MIT domain (Obita et al., 2007; Stuchell-Brereton et al., 2007). Type 2 MIT interacting motifs (MIM2) incorporated in the CHMP6 C-terminus can bind to the VPS4 MIT domain in the groove between helices α1 and α3 with an extended strand (Kieffer et al., 2008). In addition, a helix at the C-terminus of CHMP1B can fill the groove formed by helices α1 and α3 of the MIT domain in spastin, which is a microtubule- severing enzyme (Yang et al., 2008).

Membrane Abscission Mechanism

The key question for understanding the mechanisms of vial budding and MVB biogenesis is how do the ESCRTs mediate scission of the narrow membrane neck connecting the nascent vesicle with the limiting membrane? ESCRT-III and VPS4 were initially believed to perform membrane fission based on the following two observations. (1) Activated ESCRT-III subunits assemble into a detergent-insoluble complex on the endosomal membrane,

and overexpression of CHMP4 leads to plasma membrane invaginations that are coated on the inside (Babst et al., 2002a; Hanson et al., 2008; Zamborlini et al., 2006). (2) ESCRT-III proteins and VPS4 are the most ancient and conserved of the ESCRTs. Counterparts to ESCRT-III and VPS4, but not other MVB pathway components, have been found in archaebacteria, in which there is no endomembrane system, and *sulfolobus* ESCRT-III and VPS4 are crucial for cell division (Ghazi-Tabatabai et al., 2009).

Important insights to the mechanism of membrane scission were provided by Wollert and Hurley, who reconstituted the membrane fission process by ESCRT machinery *in vitro* by using fluorescence microscopy visualization of bilayer giant unilamellar vesicles (GUVs) (Wollert et al., 2009). This work demonstrated that the ESCRT-III proteins alone have the intrinsic ability to drive the detachment of ILVs (Wollert et al., 2009). The model system recapitulates the ordered recruitment of ESCRT-III and VPS4 established in yeast. After the membrane scission step, VPS4 acts to recycle ESCRT-III proteins (Saksena et al., 2009; Teis et al., 2008). Wollert and Hurley subsequently added to this model by demonstrating that ESCRT-III subunits alone are not sufficient to produce buds at physiological concentrations in the GUV assay (Wollert and Hurley, 2010). After further dissecting the roles of upstream ESCRTs, they demonstrated that ESCRT-0 clusters ubiquitin, consistent with its several ubiquitin-interacting domains (Bache et al., 2003b; Bilodeau et al., 2002; Raiborg et al., 2002; Ren and

Hurley, 2010). Nevertheless, the biggest surprise from this study was that ESCRT-I and -II together at subphysiological concentrations induce membrane bud formation. Furthermore, both ESCRT-I and -II localize to the necks membrane buds and confine the cargo within the buds by an unknown mechanism. Finally, ESCRT-III subunits colocalize with ESCRT-I and -II at membrane necks and complete scission efficiently (Wollert and Hurley, 2010).

This model has been challenged, however, on the basis of live-cell visualization of the *in vivo* assembly and disassembly of ESCRT proteins, which favors the alternative view that VPS4 plays a more active role in the membrane scission event than simply recycling the ESCRT components (Baumgartel et al., 2011; Jouvenet et al., 2011). This conclusion is driven by three principal observations: (1) The ESCRT-III and VPS4A proteins were recruited coincidently with the completion of Gag accumulation. (2) VPS4A localizes to viral budding sites before disappearance of the nascent virions, suggesting that it acts before particle release. (3) Expression of VPS4 dominant negative protein both blocks virion release and leads to colocalization of ESCRT-III protein with VLPs, which is contradictory to the Hurley model that predicts that VLPs should not be associate with ESCRT proteins over time.

ALIX

ALIX Functions in the MVB Pathway, Retrovirus release, and Cytokinesis

Role of ALIX in the MVB pathway. Bro1, the ALIX homologue in yeast, has been identified as an accessory class E VPS factor for the MVB pathway. Bro1 is important for sorting of carboxypeptidase S (CPS) and Ste2-GFP (Odorizzi et al., 1998; Odorizzi et al., 2003), whereas deletion of Bro1 only causes minor aberrant secretion of the soluble vacuolar enzyme carboxypeptidase Y (CPY) (Odorizzi et al., 2003). Bro1 appears to function at a late step of the MVB pathway, after the endosome-associated ESCRT-III proteins and before or in conjunction with Doa4, the ubiquitin hydrolase that mediates deubiquitylation prior to cargo incorporation into MVB vesicles (Katzmann et al., 2001; Nikko et al., 2003). Hence Bro1 dysfunction might lead to incorporation of ubiquitylated cargoes into intraluminal vesicles and depletion of the cytosolic ubiquitin pool, although this effect is subtle and delayed compared to mutations of other ESCRT components. In addition, Bro1 was shown to enhance the stability of ESCRT-III *in vivo* and inhibits Vps4-mediated disassembly of ESCRT-III complex *in vitro* (Wemmer et al., 2011). A Snf7 mutant that cannot bind Bro1 dramatically reduces the number of ILVs. These results implicate that Bro1 regulates ESCRT-III dissembly and membrane scission activity.

Role of ALIX in retrovirus release. ALIX plays a major role in promoting EIAV particle release. First, ALIX was shown to interact with the EIAV p9 protein, which contains a YPDL motif, the only late domain of EIAV. Second, mutations in the YPDL motif of EIAV Gag that prevent the interaction between ALIX and EIAV p9 disrupt virus budding (Martin-Serrano et al., 2003a; Strack et al., 2003). Third, expression of a truncated dominate negative form of ALIX, or ALIX depletion induced by small interfering RNA, specifically inhibits EIAV virus production (Martin-Serrano et al., 2003a; Strack et al., 2003; Vincent et al., 2003).

Although ALIX is crucial for EIAV budding, the role of ALIX in HIV-1 release is less established. The p6 region of HIV contains both PTAP and YPXL late domains, which bind directly to the TSG101/ESCRT-I and ALIX proteins, respectively (Martin-Serrano et al., 2003b; Pornillos et al., 2003; Strack et al., 2003). The TSG101-PTAP interaction is essential for efficient release of HIV-1 from 293T cells and human T cell lines (Garrus et al., 2001). In contrast, mutations that abrogate the ALIX-YPXL interaction or siRNA-mediated ALIX depletion have only a trivial impact on HIV-1 release from COS-7, Hela and 293T cells (Demirov et al., 2002; Gottlinger et al., 1991).

Nevertheless, several observations indicate a greater role for ALIX in HIV-1 release. Overexpression of an ALIX fragment (residues 365-716) dramatically inhibits HIV-1 release (Munshi et al., 2007). Furthermore, ALIX stimulates the release and infectivity of HIV-1 proviral constructs that

contain ΔPTAP mutations (Fisher et al., 2007; Usami et al., 2007). ALIX therefore provides an alternative route for virus-particle egress, when the ability of TSG101 to promote virus release is eliminated. The presence of two late domains in HIV-1, presumably, provides advantages of optimal virus production and release in a variety of cell types.

Role of ALIX in midbody abscission. The membrane scission event at the final step in cell division is topologically equivalent to MVB formation and viral particle budding. Accumulating evidence indicates that the ESCRT machinery participates in this step, for example, ALIX, TSG101/TSG101, ESCRT-III proteins and VPS4 are all important for cytokinesis (Carlton and Martin-Serrano, 2007; Morita et al., 2010; Morita et al., 2007b). Among ESCRT proteins, the role of ALIX in cytokinesis is the most characterized. First of all, a concentration of ALIX is revealed at the midbodies of dividing cells. ALIX is recruited by CEP55, which functions in the organization of midbodies and recruitment of proteins required for abscission (Lee et al., 2008). Moreover, depletion of ALIX by siRNAs, or disruption of the ALIX-CEP55 interaction, causes cytokinesis defects with most of the cells exhibiting multiple nuclei and unusual remnants of arrested midbodies (Carlton et al., 2008; Carlton and Martin-Serrano, 2007; Morita et al., 2007b).

Mechanism of ALIX in promoting particle release

ALIX bridges viral Gag and the ESCRT machinery. ALIX is composed of three regions: an N-terminal Bro1 domain (residues 1-359), a central V

domain (residues 360-702), and finally a C-terminal proline-rich region (PRR; residues 703-868) that is predicted to lack persistent secondary or tertiary structure (Fujii et al., 2007).

The ALIX V domain binds the YPXL late domain of Gag. The V domain consists of two extended arms, each of which comprises three long helices. The two arms are arranged at an angle of ~30° to each other in the shape of the letter V (Fisher et al., 2007; Lee et al., 2007). The YPXL late domain binding site on the V domain is centered on the highly conserved hydrophobic groove on arm2 (Fisher et al., 2007; Zhai et al., 2008). The ALIX V domain can accommodate different conformations of the late domain peptide backbones. The YPXL late domains of HIV-1 $p6^{Gag}$ and EIAV $p9^{Gag}$ are mapped to the core sequences of $_{35}$L**YP**LTS**L**$_{41}$ and $_{22}$L**YP**D**L**$_{26}$ respectively (important residues are boldface) (Strack et al., 2003). Göttlinger and colleagues also reported that $p6^{Gag}$ proteins from SIV_{agm} and SIV_{mac239} can bind and package ALIX into virions, although the ALIX binding sites were not obvious from sequence comparisons (Strack et al., 2003).

The Bro1 domain is the common feature shared by all the ALIX homologues: two human ALIX homologues-HD-PTP and Brox, and the yeast Bro1 protein (Ichioka et al., 2008). The structures of the Bro1 domains are similar both for human ALIX and yeast Bro1 (Fisher et al., 2007; Kim et al., 2005). The ALIX Bro1 domain contains ten α-helices and a small ß-sheet. The surface of Bro1 domain is characterized with two conserved hydrophobic

patches. The first patch is centered on the exposed residue Tyr319, which forms the docking site for Src kinase (Schmidt et al., 2005), although the absence of Src in yeast suggests that this feature is conserved to support some other interaction. The second patch, centered on residue Ile212, forms the binding site for the CHMP4/ESCRT-III protein, which functions to mediate membrane fission (Fisher et al., 2007; Kim et al., 2005; McCullough et al., 2008; Wollert et al., 2009). ALIX therefore facilitates viral budding by binding directly to Gag proteins and recruiting CHMP4/ESCRT-III complexes, which then mediate membrane fission (Fujii et al., 2007). ALIX recruitment by Gag can also be augmented by interactions between the Bro1 domain and the NC domain of HIV-1 Gag (Dussupt et al., 2009; Popov et al., 2008, 2009).

ALIX modulates membrane curvature. ALIX can recruit binding partners that are capable of inducing or stabilizing membrane curvature. ALIX was shown to be associated with the cellular protein CIN85/SETA-endophilin complex (Schmidt et al., 2004; Soubeyran et al., 2002). Bar-domain containing endophilins are lysophophatidic acid acyltransferases that modify membrane phospholipids and are believed to induce negative curvature and invagination of the plasma membrane during the early steps of endocytosis (Farsad et al., 2001; Schmidt et al., 1999). Furthermore, endophilin-2 binds and facilitates MLV Gag protein release (Wang et al., 2003). However, the ALIX-endophilin interaction is dispensable in retroviral

budding, because the ALIX construct lacking of endophilin-binding-activity still facilitates HIV-1 release (Fisher et al., 2007).

ALIX might bind or modify membrane curvature directly. First, The Bro1 domain has a convex shape and basic residues that could target negatively curved membranes produced during viral budding or MVB biogenesis (Kim et al., 2005). Second, the ALIX Bro1 domain and the Brox protein have been shown to stimulate the "minimal" Gag protein to produce virus-like particles (Dussupt et al., 2009; Popov et al., 2008, 2009). The minimal Gag construct lacks all the Gag-Gag interactions, and was therefore thought to be attenuated in its ability bend the plasma away from the cytosol. Bro1 domains are thought to assist Gag in the deformation of cellular membranes due to its membrane binding character. Third, 2,2' lysobisphosphatidic acid (2,2'-LBPA), which is abundant in MVB and involved in protein and lipid trafficking, can induce formation of vesicles and recruit ALIX (Kobayashi et al., 1998; Lebrand et al., 2002; Matsuo et al., 2004). However, Gruenberg and his colleagues also shown that ALIX represses and attenuates internal vesicle formation of LBPA lipsome, which is hard to reconcile with the positive role of ALIX in viral budding (Fujii et al., 2007; Matsuo et al., 2004). Therefore, it still remains elusive that whether ALIX can directly bind to membrane.

ALIX-Ubiquitin interaction. Ubiquitin serves as an important sorting signal during endocytosis and protein trafficking from the limiting membrane

of the endosome into MVB vesicles (Katzmann et al., 2001; Raiborg and Stenmark, 2009). The upstream complexes ESCRT-0,-I and -II all contain ubiquitin-binding domains that directly bind to an overlapping hydrophobic patch of ubiquitin that includes Ile44 (Hurley and Emr, 2006; Katzmann et al., 2002). Although the precise functional role of ubiquitin in retrovirus release remains elusive, there are several lines of evidence that support a role for Gag ubiquitylation. (1) High levels of ubiquitin are incorporated in retroviruses (Ott et al., 1998; Putterman et al., 1990). (2) Gag proteins are ubiquitylated at multiple sites (Ott et al., 2000). (3) Mutations of multiple lysine residues in HIV-1 and Rous sarcoma virus (RSV) Gag inhibits virus budding (Gottwein et al., 2006; Ott et al., 2000; Spidel et al., 2004). (4) The PPXY late domain can recruit NEDD4 family ubiquitin ligase; either NEDD4-2 or NEDD4-2s stimulates the release of HIV-1 constructs that lack TSG101-and ALIX- binding domains (Chung et al., 2008; Usami et al., 2008).

Freed and colleagues recently reported that ALIX can associate with ubiquitin, and substitution of the YPXL late domain with ubiquitin largely rescues VLP release in an ALIX dependent manner (Joshi et al., 2008). Furthermore, a ubiquitin E3-ligase, POSH, which has been shown to augment HIV-1 particle release, can bind and ubiquitylate ALIX (Alroy et al., 2005; Tsuda et al., 2006; Votteler et al., 2009). Thus, ALIX association with ubiquitin and ubiquitylated Gag might further augment retroviral release.

Other functions of ALIX

ALIX has also been implicated in a number of other important cellular processes, as indicated by the variety of ALIX-binding partners. Roles for ALIX in apoptosis and regulation of JNK signaling pathway are implicated by interactions with the calcium-binding EF-hand protein ALG-2 and the ubiquitin E3 enzyme POSH (Sadoul, 2006; Tsuda et al., 2006; Vito et al., 1996). A role for ALIX in cell-surface-receptor downregulation is indicated by direct interactions with cell-surface receptors and through antagonism of the Cbl-SETA/CIN85-endophilin complex (Geminard et al., 2004; Schmidt et al., 2004). Finally, a role for ALIX in regulating cytoskeleton assembly and cell adhesion is indicated by an interaction with actin (Zhou et al., 2009; Zhou et al., 2008).

Goal of this dissertation

ALIX performs important functions in the endosomal pathway, in midbody separation, and during retrovirus budding from cell membrane. ALIX can bind directly to viral Gag and cellular ESCRT proteins, and these interactions facilitate virus budding. However, the structural and mechanistic basis of ALIX function is unclear. This dissertation was motivated by a desire to address following questions. 1) How is ALIX recruited to sites of viral budding and, more specifically, how do HIV-1 and EIAV recruit ALIX through difference sequences, and how do the viruses that lack YPXL motifs incorporate ALIX in the nascent virions? Chapters 2-4 are

focused on these questions of ALIX recruitment mechanisms. 2) How is ALIX regulated and, more specifically, does ALIX cycle between inactive (soluble) and active (membrane-associated) states, like other ESCRT proteins? Chapter 5 is centered on regulation of ALIX function. 3) Do human ALIX homologues share similar structural and functional features? Chapter 6 reports studies of an ALIX homologue.

My central approach has been to determine relevant molecular structures by X-ray crystallography. This has been complemented by biochemical binding assays, collaborative studies on the solution conformation by small angle X-ray scattering, and by collaborative functional studies on viral particle release.

Outline of Chapters

Chapter 2: Structural and Biochemical Studies of ALIX/AIP1 and Its Role in Retrovirus Budding

The work described in Chapter 2 was originally published in the March 9, 2007 issue of the Cell and is reprinted here in its published format. The focus of this work was about understanding how ALIX functions in viral budding through structure analysis of apo ALIX proteins. A former graduate student, Rob Fisher, determined the structures of isolated $ALIX_{Bro1}$ and $ALIX_{V}$ domains and obtained poor quality crystals of an $ALIX_{Bro1\text{-}V}$ construct. I improved $ALIX_{Bro1\text{-}V}$ crystals by introducing K268Y and K269Y mutations on a loop region, which turn out to stabilize a crystal contact. Hyo-Young

Chuang, a former graduate student in the Sundquist lab, carried out an assay to characterize ALIX function in EIAV and HIV-1 ΔPTAP budding. This work concludes that both the conserved hydrophobic pocket on the V domain and the conserved hydrophobic patch on the Bro1 domain are required for virus budding. Overall, the work in this chapter shows in structural detail that ALIX serves as a scaffold that connects retroviral Gag proteins to ESCRT-III proteins.

Chapter 3: Structural and Functional Studies of ALIX Interactions with YPX_nL Late Domains of HIV and EIAV

The work described in Chapter 3 was originally published in the January, 2008 issue of the Nature Structural & Molecular Biology and is reprinted here in its published format. This work centers on understanding how ALIX is recruited by the HIV-1 p6 YPL(T/A)SL and EIAV p9 YPDL late domains. I co-crystallized ALIX with YPXnL motifs from HIV-1 and EIAV and determined the structures, which reveal that ALIX primarily recognizes the conserved LYP element by binding the Tyr residue deep in a conserved hydrophobic pocket and anchoring its OH group with a hydrogen bonding interaction at the bottom of the pocket. However, the HIV-1 and EIAV ligands adopt different backbone conformations to reach the fourth binding site of ALIX; the leucine of the EIAV late domain is spaced by one residue after LYP, whereas for HIV-1 there are three intervening residues following the LYP before the fourth anchor site leucine. Rob Fisher performed binding

experiments that showed that those peptides bind the ALIX construct with similar affinity, while the $p6^{Gag}$ and $p9^{Gag}$ proteins have distinct dissociation constants, indicating that the rest of proteins affect ALIX recruitment. Hyo-Young Chuang performed viral budding assays to verify the importance of key interface residues.

Chapter 4: Identification and Structural Characterization of the ALIX-Binding Late Domain of Simian Immunodeficiency Virus SIV_{mac239} and $SIV_{agmTan-1}$

Chapter 4 was originally published in the January, 2011 issue of the Journal of Virology. This work was undertaken to understand how certain SIVagm and SIVmac strains lacking a canonical YPX_nL motif recruit ALIX to virions (Strack et al., 2003). I mapped the ALIX-binding elements and determined their crystal structures in complex with $ALIX_{Bro1-V}$. Both peptides begin to form an α-helix with the tyrosine, which superimposes closely to those from HIV-1 and EIAV. Michael Landsman, a graduate student in Sundquist lab, performed the viral budding assays reported in this paper to confirm that the newly identified late domains were ALIX responsive. Sequence analysis of $p6^{Gag}$ indicates that the α-helix mode is the most common type of ALIX-binding late domain throughout primate lentiviruses.

Chapter 5: Activation of the Retroviral Budding Factor ALIX

Chapter 5 is a manuscript in preparation and was submitted to the Journal of Virology for publication. Previous studies have suggested that the soluble ALIX protein adopts an autoinhibited state and the conformational changes coincide with ALIX activation (Fisher et al., 2007; Pires et al., 2009; Zhou et al., 2008). I expressed and purified full length ALIX using a baculovirus-insect cell expression system, performed binding studies and showed that full length ALIX did not bind detectably to the EIAV p9 peptide. Together with SAXS analysis by Adam Dierkers and Cy Jeffries, postdocs in the Trewhella lab, we determined that the C-terminal PRR of ALIX folds back against the V domain and inhibits access by viral late domains. Hyo-Young Chung discovered that the R649E mutation, which was designed to open the closed conformation of the V domain, was more potent than the wild type protein in stimulating virus release and infectivity. Michael Landesman showed that this R649E protein partitions into membrane-containing fractions to a greater extent that the wild-type protein. Based on these data, we propose that ALIX is activated to facilitate virus budding through a series of conformational changes, including PRR release from Bro1-V domains, opening of the V domain, membrane recruitment of ALIX, and dimerization.

Chapter 6: Structural and Functional Studies of Brox in Virus Budding

Work in this chapter describes the structure of Brox, which is a human homologue of ALIX. Most of the Brox structure overlaps closely with the known structures of other Bro1 domains. However, extra C-terminal residues of Brox reach the convex interface, which is unique compared with the known Bro1 domains. Two hydrophobic patches that have been described for the ALIX Bro1 domain are also conserved on the Brox surface. I performed binding experiments to verify that the CHMP4 interacts with Brox directly via the putative interface. Michael Landesman performed a minimal Gag budding assay and showed that Brox-CHMP4 interaction is required for VLP formation of the minimal Gag construct.

Chapter 7: Summary and Respective

Chapter 7 summarizes structural and biochemical studies of ALIX described in Chapter 2-6. In addition, it discusses some ALIX-binding proteins, which may regulate ALIX function in viral budding. This chapter includes an initial binding study of the ALIX-ubiquitin interaction. I performed binding experiments and showed that ubiquitin can interact with the ALIX V domain with a K_D of 1 mM, I44A mutation on ubiquitin can abolish this interaction. ALIX-ubiquitin interaction and ALIX-ubiquitylation may provide alternative pathways for virus budding and regulate ALIX

function. It concludes with a discussion of future directions for understanding ALIX activation.

Appendix: Structural and Functional Studies on the Extracellular Domain of BST2/Tetherin in Reduced and Oxidized conformations

The appendix was originally published in the October 19, 2010 issue of the PNAS and is reproduced here in its published form. The focus of this work is to determine the structure of BST2, which prevents the release of budded viruses from the cell surface. Heidi Schubert was able to obtain native crystals of the extracellular domain under reducing conditions and compute an initial electron density map. However, the map was too poor to interpret. While Heidi was on maternity leave, I grew selenium- methionine crystals, solved the phase problem of crystallography and determined its structure. The BST2 extracellular domain forms a single long helix that associates as a parallel coiled coil over the C-terminal two thirds of the construct, while the N-terminal third of the protein forms an antiparallel four-helix bundle with another dimer. Roberto Steiner group determined the BST2 structure expressed on the surface of HEK293T cells, which forms a dimer in the crystal. I collaborated with Debra Eckert to characterize the oligomeric states of BST2. Consistent with the two crystal structures, we found that BST2 forms a stable tetramer under reducing conditions and converts into a stable dimer upon oxidation.

References

Alam, S.L., Langelier, C., Whitby, F.G., Koirala, S., Robinson, H., Hill, C.P., and Sundquist, W.I. (2006). Structural basis for ubiquitin recognition by the human ESCRT-II EAP45 GLUE domain. Nat Struct Mol Biol *13*, 1029-1030.

Alroy, I., Tuvia, S., Greener, T., Gordon, D., Barr, H.M., Taglicht, D., Mandil-Levin, R., Ben-Avraham, D., Konforty, D., Nir, A.*, et al.* (2005). The trans-Golgi network-associated human ubiquitin-protein ligase POSH is essential for HIV type 1 production. Proc Natl Acad Sci U S A *102*, 1478-1483.

Azmi, I., Davies, B., Dimaano, C., Payne, J., Eckert, D., Babst, M., and Katzmann, D.J. (2006). Recycling of ESCRTs by the AAA-ATPase Vps4 is regulated by a conserved VSL region in Vta1. J Cell Biol *172*, 705-717.

Azmi, I.F., Davies, B.A., Xiao, J., Babst, M., Xu, Z., and Katzmann, D.J. (2008). ESCRT-III family members stimulate Vps4 ATPase activity directly or via Vta1. Dev Cell *14*, 50-61.

Babst, M., Katzmann, D.J., Estepa-Sabal, E.J., Meerloo, T., and Emr, S.D. (2002a). Escrt-III: an endosome-associated heterooligomeric protein complex required for mvb sorting. Dev Cell *3*, 271-282.

Babst, M., Katzmann, D.J., Snyder, W.B., Wendland, B., and Emr, S.D. (2002b). Endosome-associated complex, ESCRT-II, recruits transport machinery for protein sorting at the multivesicular body. Dev Cell *3*, 283-289.

Bache, K.G., Brech, A., Mehlum, A., and Stenmark, H. (2003a). Hrs regulates multivesicular body formation via ESCRT recruitment to endosomes. J Cell Biol *162*, 435-442.

Bache, K.G., Raiborg, C., Mehlum, A., and Stenmark, H. (2003b). STAM and Hrs are subunits of a multivalent ubiquitin-binding complex on early endosomes. J Biol Chem *278*, 12513-12521.

Bajorek, M., Schubert, H.L., McCullough, J., Langelier, C., Eckert, D.M., Stubblefield, W.M., Uter, N.T., Myszka, D.G., Hill, C.P., and Sundquist, W.I. (2009). Structural basis for ESCRT-III protein autoinhibition. Nat Struct Mol Biol *16*, 754-762.

Baltimore, D. (1974). The strategy of RNA viruses. Harvey Lect *70 Series*, 57-74.

Baron, S. (1996). Medical Microbiology (The University of Texas Medical Branch at Galveston).

Baumgartel, V., Ivanchenko, S., Dupont, A., Sergeev, M., Wiseman, P.W., Krausslich, H.G., Brauchle, C., Muller, B., and Lamb, D.C. (2011). Live-cell visualization of dynamics of HIV budding site interactions with an ESCRT component. Nat Cell Biol *13*, 469-474.

Bieniasz, P.D. (2009). The cell biology of HIV-1 virion genesis. Cell Host Microbe *5*, 550-558.

Bilodeau, P.S., Urbanowski, J.L., Winistorfer, S.C., and Piper, R.C. (2002). The Vps27p Hse1p complex binds ubiquitin and mediates endosomal protein sorting. Nat Cell Biol *4*, 534-539.

Breitbart, M., and Rohwer, F. (2005). Here a virus, there a virus, everywhere the same virus? Trends Microbiol *13*, 278-284.

Briggs, J.A., Simon, M.N., Gross, I., Krausslich, H.G., Fuller, S.D., Vogt, V.M., and Johnson, M.C. (2004). The stoichiometry of Gag protein in HIV-1. Nat Struct Mol Biol *11*, 672-675.

Campbell, S., Fisher, R.J., Towler, E.M., Fox, S., Issaq, H.J., Wolfe, T., Phillips, L.R., and Rein, A. (2001). Modulation of HIV-like particle assembly in vitro by inositol phosphates. Proc Natl Acad Sci U S A *98*, 10875-10879.

Campbell, S., and Rein, A. (1999). In vitro assembly properties of human immunodeficiency virus type 1 Gag protein lacking the p6 domain. J Virol *73*, 2270-2279.

Carlson, L.A., Briggs, J.A., Glass, B., Riches, J.D., Simon, M.N., Johnson, M.C., Muller, B., Grunewald, K., and Krausslich, H.G. (2008). Three-dimensional analysis of budding sites and released virus suggests a revised model for HIV-1 morphogenesis. Cell Host Microbe *4*, 592-599.

Carlton, J.G., Agromayor, M., and Martin-Serrano, J. (2008). Differential requirements for Alix and ESCRT-III in cytokinesis and HIV-1 release. Proc Natl Acad Sci U S A *105*, 10541-10546.

Carlton, J.G., and Martin-Serrano, J. (2007). Parallels between cytokinesis and retroviral budding: a role for the ESCRT machinery. Science *316*, 1908-1912.

Chu, T., Sun, J., Saksena, S., and Emr, S.D. (2006). New component of ESCRT-I regulates endosomal sorting complex assembly. J Cell Biol *175*, 815-823.

Chung, H.Y., Morita, E., von Schwedler, U., Muller, B., Krausslich, H.G., and Sundquist, W.I. (2008). NEDD4L overexpression rescues the release and

infectivity of human immunodeficiency virus type 1 constructs lacking PTAP and YPXL late domains. J Virol *82*, 4884-4897.

Daelemans, D., Afonina, E., Nilsson, J., Werner, G., Kjems, J., De Clercq, E., Pavlakis, G.N., and Vandamme, A.M. (2002). A synthetic HIV-1 Rev inhibitor interfering with the CRM1-mediated nuclear export. Proc Natl Acad Sci U S A *99*, 14440-14445.

De Matteis, M.A., and Godi, A. (2004). PI-loting membrane traffic. Nat Cell Biol *6*, 487-492.

Demirov, D.G., Orenstein, J.M., and Freed, E.O. (2002). The late domain of human immunodeficiency virus type 1 p6 promotes virus release in a cell type-dependent manner. J Virol *76*, 105-117.

Douglas, J.L., Gustin, J.K., Viswanathan, K., Mansouri, M., Moses, A.V., and Fruh, K. (2010). The great escape: viral strategies to counter BST-2/tetherin. PLoS Pathog *6*, e1000913.

Dussupt, V., Javid, M.P., Abou-Jaoude, G., Jadwin, J.A., de La Cruz, J., Nagashima, K., and Bouamr, F. (2009). The nucleocapsid region of HIV-1 Gag cooperates with the PTAP and LYPXnL late domains to recruit the cellular machinery necessary for viral budding. PLoS Pathog *5*, e1000339.

Erzberger, J.P., and Berger, J.M. (2006). Evolutionary relationships and structural mechanisms of AAA+ proteins. Annu Rev Biophys Biomol Struct *35*, 93-114.

Farsad, K., Ringstad, N., Takei, K., Floyd, S.R., Rose, K., and De Camilli, P. (2001). Generation of high curvature membranes mediated by direct endophilin bilayer interactions. J Cell Biol *155*, 193-200.

Fisher, R.D., Chung, H.Y., Zhai, Q., Robinson, H., Sundquist, W.I., and Hill, C.P. (2007). Structural and biochemical studies of ALIX/AIP1 and its role in retrovirus budding. Cell *128*, 841-852.

Franke, E.K., Yuan, H.E., and Luban, J. (1994). Specific incorporation of cyclophilin A into HIV-1 virions. Nature *372*, 359-362.

Freed, E.O. (1998). HIV-1 gag proteins: diverse functions in the virus life cycle. Virology *251*, 1-15.

Fujii, K., Hurley, J.H., and Freed, E.O. (2007). Beyond Tsg101: the role of Alix in 'ESCRTing' HIV-1. Nat Rev Microbiol *5*, 912-916.

Ganser-Pornillos, B.K., Yeager, M., and Sundquist, W.I. (2008). The structural biology of HIV assembly. Curr Opin Struct Biol *18*, 203-217.

Garrus, J.E., von Schwedler, U.K., Pornillos, O.W., Morham, S.G., Zavitz, K.H., Wang, H.E., Wettstein, D.A., Stray, K.M., Cote, M., Rich, R.L.*, et al.* (2001). Tsg101 and the vacuolar protein sorting pathway are essential for HIV-1 budding. Cell *107*, 55-65.

Geminard, C., De Gassart, A., Blanc, L., and Vidal, M. (2004). Degradation of AP2 during reticulocyte maturation enhances binding of hsc70 and Alix to a common site on TFR for sorting into exosomes. Traffic *5*, 181-193.

Ghazi-Tabatabai, S., Obita, T., Pobbati, A.V., Perisic, O., Samson, R.Y., Bell, S.D., and Williams, R.L. (2009). Evolution and assembly of ESCRTs. Biochem Soc Trans *37*, 151-155.

Ghazi-Tabatabai, S., Saksena, S., Short, J.M., Pobbati, A.V., Veprintsev, D.B., Crowther, R.A., Emr, S.D., Egelman, E.H., and Williams, R.L. (2008). Structure and disassembly of filaments formed by the ESCRT-III subunit Vps24. Structure *16*, 1345-1356.

Gill, D.J., Teo, H., Sun, J., Perisic, O., Veprintsev, D.B., Emr, S.D., and Williams, R.L. (2007). Structural insight into the ESCRT-I/-II link and its role in MVB trafficking. Embo J *26*, 600-612.

Goff, S.P. (2007). Host factors exploited by retroviruses. Nat Rev Microbiol *5*, 253-263.

Gonciarz, M.D., Whitby, F.G., Eckert, D.M., Kieffer, C., Heroux, A., Sundquist, W.I., and Hill, C.P. (2008). Biochemical and structural studies of yeast Vps4 oligomerization. J Mol Biol *384*, 878-895.

Gottlinger, H.G., Dorfman, T., Sodroski, J.G., and Haseltine, W.A. (1991). Effect of mutations affecting the p6 gag protein on human immunodeficiency virus particle release. Proc Natl Acad Sci U S A *88*, 3195-3199.

Gottwein, E., Jager, S., Habermann, A., and Krausslich, H.G. (2006). Cumulative mutations of ubiquitin acceptor sites in human immunodeficiency virus type 1 gag cause a late budding defect. J Virol *80*, 6267-6275.

Hanson, P.I., Roth, R., Lin, Y., and Heuser, J.E. (2008). Plasma membrane deformation by circular arrays of ESCRT-III protein filaments. J Cell Biol *180*, 389-402.

Hartmann, C., Chami, M., Zachariae, U., de Groot, B.L., Engel, A., and Grutter, M.G. (2008). Vacuolar protein sorting: two different functional states of the AAA-ATPase Vps4p. J Mol Biol *377*, 352-363.

Hierro, A., Sun, J., Rusnak, A.S., Kim, J., Prag, G., Emr, S.D., and Hurley, J.H. (2004). Structure of the ESCRT-II endosomal trafficking complex. Nature *431*, 221-225.

Hirano, S., Kawasaki, M., Ura, H., Kato, R., Raiborg, C., Stenmark, H., and Wakatsuki, S. (2006). Double-sided ubiquitin binding of Hrs-UIM in endosomal protein sorting. Nat Struct Mol Biol *13*, 272-277.

Howard, B.R., Vajdos, F.F., Li, S., Sundquist, W.I., and Hill, C.P. (2003). Structural insights into the catalytic mechanism of cyclophilin A. Nat Struct Biol *10*, 475-481.

Huang, M., Orenstein, J.M., Martin, M.A., and Freed, E.O. (1995). p6Gag is required for particle production from full-length human immunodeficiency virus type 1 molecular clones expressing protease. J Virol *69*, 6810-6818.

Hughson, F.M. (1997). Enveloped viruses: a common mode of membrane fusion? Curr Biol *7*, R565-569.

Hurley, J.H., and Emr, S.D. (2006). The ESCRT complexes: structure and mechanism of a membrane-trafficking network. Annu Rev Biophys Biomol Struct *35*, 277-298.

Huthoff, H., and Towers, G.J. (2008). Restriction of retroviral replication by APOBEC3G/F and TRIM5alpha. Trends Microbiol *16*, 612-619.

Ichioka, F., Kobayashi, R., Katoh, K., Shibata, H., and Maki, M. (2008). Brox, a novel farnesylated Bro1 domain-containing protein that associates with charged multivesicular body protein 4 (CHMP4). Febs J *275*, 682-692.

Im, Y.J., and Hurley, J.H. (2008). Integrated structural model and membrane targeting mechanism of the human ESCRT-II complex. Dev Cell *14*, 902-913.

Im, Y.J., Wollert, T., Boura, E., and Hurley, J.H. (2009). Structure and function of the ESCRT-II-III interface in multivesicular body biogenesis. Dev Cell *17*, 234-243.

Joazeiro, C.A., Wing, S.S., Huang, H., Leverson, J.D., Hunter, T., and Liu, Y.C. (1999). The tyrosine kinase negative regulator c-Cbl as a RING-type, E2-dependent ubiquitin-protein ligase. Science *286*, 309-312.

Joshi, A., Munshi, U., Ablan, S.D., Nagashima, K., and Freed, E.O. (2008). Functional replacement of a retroviral late domain by ubiquitin fusion. Traffic *9*, 1972-1983.

Jouvenet, N., Zhadina, M., Bieniasz, P.D., and Simon, S.M. (2011). Dynamics of ESCRT protein recruitment during retroviral assembly. Nat Cell Biol *13*, 394-401.

Katzmann, D.J., Babst, M., and Emr, S.D. (2001). Ubiquitin-dependent sorting into the multivesicular body pathway requires the function of a conserved endosomal protein sorting complex, ESCRT-I. Cell *106*, 145-155.

Katzmann, D.J., Odorizzi, G., and Emr, S.D. (2002). Receptor downregulation and multivesicular-body sorting. Nat Rev Mol Cell Biol *3*, 893-905.

Katzmann, D.J., Stefan, C.J., Babst, M., and Emr, S.D. (2003). Vps27 recruits ESCRT machinery to endosomes during MVB sorting. J Cell Biol *162*, 413-423.

Kieffer, C., Skalicky, J.J., Morita, E., De Domenico, I., Ward, D.M., Kaplan, J., and Sundquist, W.I. (2008). Two distinct modes of ESCRT-III recognition are required for VPS4 functions in lysosomal protein targeting and HIV-1 budding. Dev Cell *15*, 62-73.

Kikonyogo, A., Bouamr, F., Vana, M.L., Xiang, Y., Aiyar, A., Carter, C., and Leis, J. (2001). Proteins related to the Nedd4 family of ubiquitin protein ligases interact with the L domain of Rous sarcoma virus and are required for gag budding from cells. Proc Natl Acad Sci U S A *98*, 11199-11204.

Kim, J., Sitaraman, S., Hierro, A., Beach, B.M., Odorizzi, G., and Hurley, J.H. (2005). Structural basis for endosomal targeting by the Bro1 domain. Dev Cell *8*, 937-947.

Kobayashi, T., Stang, E., Fang, K.S., de Moerloose, P., Parton, R.G., and Gruenberg, J. (1998). A lipid associated with the antiphospholipid syndrome regulates endosome structure and function. Nature *392*, 193-197.

Kostelansky, M.S., Schluter, C., Tam, Y.Y., Lee, S., Ghirlando, R., Beach, B., Conibear, E., and Hurley, J.H. (2007). Molecular architecture and functional model of the complete yeast ESCRT-I heterotetramer. Cell *129*, 485-498.

Landsberg, M.J., Vajjhala, P.R., Rothnagel, R., Munn, A.L., and Hankamer, B. (2009). Three-dimensional structure of AAA ATPase Vps4: advancing structural insights into the mechanisms of endosomal sorting and enveloped virus budding. Structure *17*, 427-437.

Lata, S., Schoehn, G., Jain, A., Pires, R., Piehler, J., Gottlinger, H.G., and Weissenhorn, W. (2008). Helical structures of ESCRT-III are disassembled by VPS4. Science *321*, 1354-1357.

Lebrand, C., Corti, M., Goodson, H., Cosson, P., Cavalli, V., Mayran, N., Faure, J., and Gruenberg, J. (2002). Late endosome motility depends on lipids via the small GTPase Rab7. Embo J *21*, 1289-1300.

Lee, H.H., Elia, N., Ghirlando, R., Lippincott-Schwartz, J., and Hurley, J.H. (2008). Midbody targeting of the ESCRT machinery by a noncanonical coiled coil in CEP55. Science *322*, 576-580.

Lee, S., Joshi, A., Nagashima, K., Freed, E.O., and Hurley, J.H. (2007). Structural basis for viral late-domain binding to Alix. Nat Struct Mol Biol *14*, 194-199.

Li, F., Chen, C., Puffer, B.A., and Montelaro, R.C. (2002). Functional replacement and positional dependence of homologous and heterologous L domains in equine infectious anemia virus replication. J Virol *76*, 1569-1577.

Lin, Y., Kimpler, L.A., Naismith, T.V., Lauer, J.M., and Hanson, P.I. (2005). Interaction of the mammalian endosomal sorting complex required for transport (ESCRT) III protein hSnf7-1 with itself, membranes, and the AAA+ ATPase SKD1. J Biol Chem *280*, 12799-12809.

Lwoff, A., Horne, R., and Tournier, P. (1962). A system of viruses. Cold Spring Harb Symp Quant Biol *27*, 51-55.

Macias, M.J., Wiesner, S., and Sudol, M. (2002). WW and SH3 domains, two different scaffolds to recognize proline-rich ligands. FEBS Lett *513*, 30-37.

Martin-Serrano, J., Yarovoy, A., Perez-Caballero, D., and Bieniasz, P.D. (2003a). Divergent retroviral late-budding domains recruit vacuolar protein sorting factors by using alternative adaptor proteins. Proc Natl Acad Sci U S A *100*, 12414-12419.

Martin-Serrano, J., Zang, T., and Bieniasz, P.D. (2001). HIV-1 and Ebola virus encode small peptide motifs that recruit Tsg101 to sites of particle assembly to facilitate egress. Nat Med *7*, 1313-1319.

Martin-Serrano, J., Zang, T., and Bieniasz, P.D. (2003b). Role of ESCRT-I in retroviral budding. J Virol *77*, 4794-4804.

Matsuo, H., Chevallier, J., Mayran, N., Le Blanc, I., Ferguson, C., Faure, J., Blanc, N.S., Matile, S., Dubochet, J., Sadoul, R.*, et al.* (2004). Role of LBPA

and Alix in multivesicular liposome formation and endosome organization. Science *303*, 531-534.

McCullough, J., Fisher, R.D., Whitby, F.G., Sundquist, W.I., and Hill, C.P. (2008). ALIX-CHMP4 interactions in the human ESCRT pathway. Proc Natl Acad Sci U S A *105*, 7687-7691.

Misra, S., and Hurley, J.H. (1999). Crystal structure of a phosphatidylinositol 3-phosphate-specific membrane-targeting motif, the FYVE domain of Vps27p. Cell *97*, 657-666.

Morita, E., Colf, L.A., Karren, M.A., Sandrin, V., Rodesch, C.K., and Sundquist, W.I. (2010). Human ESCRT-III and VPS4 proteins are required for centrosome and spindle maintenance. Proc Natl Acad Sci U S A *107*, 12889-12894.

Morita, E., Sandrin, V., Alam, S.L., Eckert, D.M., Gygi, S.P., and Sundquist, W.I. (2007a). Identification of human MVB12 proteins as ESCRT-I subunits that function in HIV budding. Cell Host Microbe *2*, 41-53.

Morita, E., Sandrin, V., Chung, H.Y., Morham, S.G., Gygi, S.P., Rodesch, C.K., and Sundquist, W.I. (2007b). Human ESCRT and ALIX proteins interact with proteins of the midbody and function in cytokinesis. Embo J *26*, 4215-4227.

Morita, E., and Sundquist, W.I. (2004). Retrovirus budding. Annu Rev Cell Dev Biol *20*, 395-425.

Munshi, U.M., Kim, J., Nagashima, K., Hurley, J.H., and Freed, E.O. (2007). An Alix fragment potently inhibits HIV-1 budding: characterization of binding to retroviral YPXL late domains. J Biol Chem *282*, 3847-3855.

Muziol, T., Pineda-Molina, E., Ravelli, R.B., Zamborlini, A., Usami, Y., Gottlinger, H., and Weissenhorn, W. (2006). Structural basis for budding by the ESCRT-III factor CHMP3. Dev Cell *10*, 821-830.

Neil, S.J., Zang, T., and Bieniasz, P.D. (2008). Tetherin inhibits retrovirus release and is antagonized by HIV-1 Vpu. Nature *451*, 425-430.

Nickerson, D.P., West, M., and Odorizzi, G. (2006). Did2 coordinates Vps4-mediated dissociation of ESCRT-III from endosomes. J Cell Biol *175*, 715-720.

Nikko, E., Marini, A.M., and Andre, B. (2003). Permease recycling and ubiquitination status reveal a particular role for Bro1 in the multivesicular body pathway. J Biol Chem *278*, 50732-50743.

Obita, T., Saksena, S., Ghazi-Tabatabai, S., Gill, D.J., Perisic, O., Emr, S.D., and Williams, R.L. (2007). Structural basis for selective recognition of ESCRT-III by the AAA ATPase Vps4. Nature *449*, 735-739.

Odorizzi, G., Babst, M., and Emr, S.D. (1998). Fab1p PtdIns(3)P 5-kinase function essential for protein sorting in the multivesicular body. Cell *95*, 847-858.

Odorizzi, G., Katzmann, D.J., Babst, M., Audhya, A., and Emr, S.D. (2003). Bro1 is an endosome-associated protein that functions in the MVB pathway in Saccharomyces cerevisiae. J Cell Sci *116*, 1893-1903.

Ogura, T., and Wilkinson, A.J. (2001). AAA+ superfamily ATPases: common structure--diverse function. Genes Cells *6*, 575-597.

Ono, A., Ablan, S.D., Lockett, S.J., Nagashima, K., and Freed, E.O. (2004). Phosphatidylinositol (4,5) bisphosphate regulates HIV-1 Gag targeting to the plasma membrane. Proc Natl Acad Sci U S A *101*, 14889-14894.

Ott, D.E., Coren, L.V., Chertova, E.N., Gagliardi, T.D., and Schubert, U. (2000). Ubiquitination of HIV-1 and MuLV Gag. Virology *278*, 111-121.

Ott, D.E., Coren, L.V., Copeland, T.D., Kane, B.P., Johnson, D.G., Sowder, R.C., 2nd, Yoshinaka, Y., Oroszlan, S., Arthur, L.O., and Henderson, L.E. (1998). Ubiquitin is covalently attached to the p6Gag proteins of human immunodeficiency virus type 1 and simian immunodeficiency virus and to the p12Gag protein of Moloney murine leukemia virus. J Virol *72*, 2962-2968.

Pineda-Molina, E., Belrhali, H., Piefer, A.J., Akula, I., Bates, P., and Weissenhorn, W. (2006). The crystal structure of the C-terminal domain of Vps28 reveals a conserved surface required for Vps20 recruitment. Traffic *7*, 1007-1016.

Pires, R., Hartlieb, B., Signor, L., Schoehn, G., Lata, S., Roessle, M., Moriscot, C., Popov, S., Hinz, A., Jamin, M.*, et al.* (2009). A Crescent-Shaped ALIX Dimer Targets ESCRT-III CHMP4 Filaments. Structure *17*, 843-856.

Popov, S., Popova, E., Inoue, M., and Gottlinger, H.G. (2008). Human immunodeficiency virus type 1 Gag engages the Bro1 domain of ALIX/AIP1 through the nucleocapsid. J Virol *82*, 1389-1398.

Popov, S., Popova, E., Inoue, M., and Gottlinger, H.G. (2009). Divergent Bro1 domains share the capacity to bind human immunodeficiency virus type 1 nucleocapsid and to enhance virus-like particle production. J Virol *83*, 7185-7193.

Pornillos, O., Higginson, D.S., Stray, K.M., Fisher, R.D., Garrus, J.E., Payne, M., He, G.P., Wang, H.E., Morham, S.G., and Sundquist, W.I. (2003). HIV Gag mimics the Tsg101-recruiting activity of the human Hrs protein. J Cell Biol *162*, 425-434.

Prag, G., Watson, H., Kim, Y.C., Beach, B.M., Ghirlando, R., Hummer, G., Bonifacino, J.S., and Hurley, J.H. (2007). The Vps27/Hse1 complex is a GAT domain-based scaffold for ubiquitin-dependent sorting. Dev Cell *12*, 973-986.

Puffer, B.A., Parent, L.J., Wills, J.W., and Montelaro, R.C. (1997). Equine infectious anemia virus utilizes a YXXL motif within the late assembly domain of the Gag p9 protein. J Virol *71*, 6541-6546.

Putterman, D., Pepinsky, R.B., and Vogt, V.M. (1990). Ubiquitin in avian leukosis virus particles. Virology *176*, 633-637.

Raiborg, C., Bache, K.G., Gillooly, D.J., Madshus, I.H., Stang, E., and Stenmark, H. (2002). Hrs sorts ubiquitinated proteins into clathrin-coated microdomains of early endosomes. Nat Cell Biol *4*, 394-398.

Raiborg, C., Bache, K.G., Mehlum, A., Stang, E., and Stenmark, H. (2001a). Hrs recruits clathrin to early endosomes. Embo J *20*, 5008-5021.

Raiborg, C., Bremnes, B., Mehlum, A., Gillooly, D.J., D'Arrigo, A., Stang, E., and Stenmark, H. (2001b). FYVE and coiled-coil domains determine the specific localisation of Hrs to early endosomes. J Cell Sci *114*, 2255-2263.

Raiborg, C., and Stenmark, H. (2009). The ESCRT machinery in endosomal sorting of ubiquitylated membrane proteins. Nature *458*, 445-452.

Raiborg, C., Wesche, J., Malerod, L., and Stenmark, H. (2006). Flat clathrin coats on endosomes mediate degradative protein sorting by scaffolding Hrs in dynamic microdomains. J Cell Sci *119*, 2414-2424.

Raymond, C.K., Howald-Stevenson, I., Vater, C.A., and Stevens, T.H. (1992). Morphological classification of the yeast vacuolar protein sorting mutants: evidence for a prevacuolar compartment in class E vps mutants. Mol Biol Cell *3*, 1389-1402.

Ren, X., and Hurley, J.H. (2010). VHS domains of ESCRT-0 cooperate in high-avidity binding to polyubiquitinated cargo. Embo J *29*, 1045-1054.

Ren, X., Kloer, D.P., Kim, Y.C., Ghirlando, R., Saidi, L.F., Hummer, G., and Hurley, J.H. (2009). Hybrid structural model of the complete human ESCRT-0 complex. Structure *17*, 406-416.

Saad, J.S., Miller, J., Tai, J., Kim, A., Ghanam, R.H., and Summers, M.F. (2006). Structural basis for targeting HIV-1 Gag proteins to the plasma membrane for virus assembly. Proc Natl Acad Sci U S A *103*, 11364-11369.

Sadoul, R. (2006). Do Alix and ALG-2 really control endosomes for better or for worse? Biol Cell *98*, 69-77.

Saksena, S., Sun, J., Chu, T., and Emr, S.D. (2007). ESCRTing proteins in the endocytic pathway. Trends Biochem Sci *32*, 561-573.

Saksena, S., Wahlman, J., Teis, D., Johnson, A.E., and Emr, S.D. (2009). Functional reconstitution of ESCRT-III assembly and disassembly. Cell *136*, 97-109.

Sauer, R.T., Bolon, D.N., Burton, B.M., Burton, R.E., Flynn, J.M., Grant, R.A., Hersch, G.L., Joshi, S.A., Kenniston, J.A., Levchenko, I.*, et al.* (2004). Sculpting the proteome with AAA(+) proteases and disassembly machines. Cell *119*, 9-18.

Schmidt, A., Wolde, M., Thiele, C., Fest, W., Kratzin, H., Podtelejnikov, A.V., Witke, W., Huttner, W.B., and Soling, H.D. (1999). Endophilin I mediates synaptic vesicle formation by transfer of arachidonate to lysophosphatidic acid. Nature *401*, 133-141.

Schmidt, M.H., Dikic, I., and Bogler, O. (2005). Src phosphorylation of Alix/AIP1 modulates its interaction with binding partners and antagonizes its activities. J Biol Chem *280*, 3414-3425.

Schmidt, M.H., Hoeller, D., Yu, J., Furnari, F.B., Cavenee, W.K., Dikic, I., and Bogler, O. (2004). Alix/AIP1 antagonizes epidermal growth factor receptor downregulation by the Cbl-SETA/CIN85 complex. Mol Cell Biol *24*, 8981-8993.

Scott, A., Chung, H.Y., Gonciarz-Swiatek, M., Hill, G.C., Whitby, F.G., Gaspar, J., Holton, J.M., Viswanathan, R., Ghaffarian, S., Hill, C.P.*, et al.* (2005a). Structural and mechanistic studies of VPS4 proteins. Embo J *24*, 3658-3669.

Scott, A., Gaspar, J., Stuchell-Brereton, M.D., Alam, S.L., Skalicky, J.J., and Sundquist, W.I. (2005b). Structure and ESCRT-III protein interactions of the MIT domain of human VPS4A. Proc Natl Acad Sci U S A *102*, 13813-13818.

Sheehy, A.M., Gaddis, N.C., Choi, J.D., and Malim, M.H. (2002). Isolation of a human gene that inhibits HIV-1 infection and is suppressed by the viral Vif protein. Nature *418*, 646-650.

Slagsvold, T., Aasland, R., Hirano, S., Bache, K.G., Raiborg, C., Trambaiolo, D., Wakatsuki, S., and Stenmark, H. (2005). Eap45 in mammalian ESCRT-II binds ubiquitin via a phosphoinositide-interacting GLUE domain. J Biol Chem *280*, 19600-19606.

Soubeyran, P., Kowanetz, K., Szymkiewicz, I., Langdon, W.Y., and Dikic, I. (2002). Cbl-CIN85-endophilin complex mediates ligand-induced downregulation of EGF receptors. Nature *416*, 183-187.

Spidel, J.L., Craven, R.C., Wilson, C.B., Patnaik, A., Wang, H., Mansky, L.M., and Wills, J.W. (2004). Lysines close to the Rous sarcoma virus late domain critical for budding. J Virol *78*, 10606-10616.

Strack, B., Calistri, A., Craig, S., Popova, E., and Gottlinger, H.G. (2003). AIP1/ALIX is a binding partner for HIV-1 p6 and EIAV p9 functioning in virus budding. Cell *114*, 689-699.

Strebel, K. (2003). Virus-host interactions: role of HIV proteins Vif, Tat, and Rev. AIDS *17 Suppl 4*, S25-34.

Stuchell-Brereton, M.D., Skalicky, J.J., Kieffer, C., Karren, M.A., Ghaffarian, S., and Sundquist, W.I. (2007). ESCRT-III recognition by VPS4 ATPases. Nature *449*, 740-744.

Sundquist, W.I., Schubert, H.L., Kelly, B.N., Hill, G.C., Holton, J.M., and Hill, C.P. (2004). Ubiquitin recognition by the human TSG101 protein. Mol Cell *13*, 783-789.

Tang, C., Loeliger, E., Luncsford, P., Kinde, I., Beckett, D., and Summers, M.F. (2004). Entropic switch regulates myristate exposure in the HIV-1 matrix protein. Proc Natl Acad Sci U S A *101*, 517-522.

Teis, D., Saksena, S., and Emr, S.D. (2008). Ordered assembly of the ESCRT-III complex on endosomes is required to sequester cargo during MVB formation. Dev Cell *15*, 578-589.

Teo, H., Gill, D.J., Sun, J., Perisic, O., Veprintsev, D.B., Vallis, Y., Emr, S.D., and Williams, R.L. (2006). ESCRT-I core and ESCRT-II GLUE domain structures reveal role for GLUE in linking to ESCRT-I and membranes. Cell *125*, 99-111.

Teo, H., Perisic, O., Gonzalez, B., and Williams, R.L. (2004a). ESCRT-II, an endosome-associated complex required for protein sorting: crystal structure and interactions with ESCRT-III and membranes. Dev Cell *7*, 559-569.

Teo, H., Veprintsev, D.B., and Williams, R.L. (2004b). Structural insights into endosomal sorting complex required for transport (ESCRT-I) recognition of ubiquitinated proteins. J Biol Chem *279*, 28689-28696.

Towers, G.J., Hatziioannou, T., Cowan, S., Goff, S.P., Luban, J., and Bieniasz, P.D. (2003). Cyclophilin A modulates the sensitivity of HIV-1 to host restriction factors. Nat Med *9*, 1138-1143.

Tsuda, M., Seong, K.H., and Aigaki, T. (2006). POSH, a scaffold protein for JNK signaling, binds to ALG-2 and ALIX in Drosophila. FEBS Lett *580*, 3296-3300.

Usami, Y., Popov, S., and Gottlinger, H.G. (2007). Potent rescue of human immunodeficiency virus type 1 late domain mutants by ALIX/AIP1 depends on its CHMP4 binding site. J Virol *81*, 6614-6622.

Usami, Y., Popov, S., Popova, E., and Gottlinger, H.G. (2008). Efficient and specific rescue of human immunodeficiency virus type 1 budding defects by a Nedd4-like ubiquitin ligase. J Virol *82*, 4898-4907.

Van Damme, N., Goff, D., Katsura, C., Jorgenson, R.L., Mitchell, R., Johnson, M.C., Stephens, E.B., and Guatelli, J. (2008). The interferon-induced protein BST-2 restricts HIV-1 release and is downregulated from the cell surface by the viral Vpu protein. Cell Host Microbe *3*, 245-252.

VerPlank, L., Bouamr, F., LaGrassa, T.J., Agresta, B., Kikonyogo, A., Leis, J., and Carter, C.A. (2001). Tsg101, a homologue of ubiquitin-conjugating (E2) enzymes, binds the L domain in HIV type 1 Pr55(Gag). Proc Natl Acad Sci U S A *98*, 7724-7729.

Vincent, O., Rainbow, L., Tilburn, J., Arst, H.N., Jr., and Penalva, M.A. (2003). YPXL/I is a protein interaction motif recognized by aspergillus PalA and its human homologue, AIP1/Alix. Mol Cell Biol *23*, 1647-1655.

Vito, P., Lacana, E., and D'Adamio, L. (1996). Interfering with apoptosis: Ca(2+)-binding protein ALG-2 and Alzheimer's disease gene ALG-3. Science *271*, 521-525.

von Schwedler, U.K., Stuchell, M., Muller, B., Ward, D.M., Chung, H.Y., Morita, E., Wang, H.E., Davis, T., He, G.P., Cimbora, D.M.*, et al.* (2003). The protein network of HIV budding. Cell *114*, 701-713.

Votteler, J., Iavnilovitch, E., Fingrut, O., Shemesh, V., Taglicht, D., Erez, O., Sorgel, S., Walther, T., Bannert, N., Schubert, U.*, et al.* (2009). Exploring the functional interaction between POSH and ALIX and the relevance to HIV-1 release. BMC Biochem *10*, 12.

Waheed, A.A., and Freed, E.O. (2010). The Role of Lipids in Retrovirus Replication. Viruses *2*, 1146-1180.

Wang, M.Q., Kim, W., Gao, G., Torrey, T.A., Morse, H.C., 3rd, De Camilli, P., and Goff, S.P. (2003). Endophilins interact with Moloney murine leukemia virus Gag and modulate virion production. J Biol *3*, 4.

Wemmer, M., Azmi, I., West, M., Davies, B., Katzmann, D., and Odorizzi, G. (2011). Bro1 binding to Snf7 regulates ESCRT-III membrane scission activity in yeast. J Cell Biol *192*, 295-306.

Wolf, D., and Goff, S.P. (2008). Host restriction factors blocking retroviral replication. Annu Rev Genet *42*, 143-163.

Wollert, T., and Hurley, J.H. (2010). Molecular mechanism of multivesicular body biogenesis by ESCRT complexes. Nature *464*, 864-869.

Wollert, T., Wunder, C., Lippincott-Schwartz, J., and Hurley, J.H. (2009). Membrane scission by the ESCRT-III complex. Nature *458*, 172-177.

Wu, Y. (2004). HIV-1 gene expression: lessons from provirus and non-integrated DNA. Retrovirology *1*, 13.

Xiao, J., Xia, H., Zhou, J., Azmi, I.F., Davies, B.A., Katzmann, D.J., and Xu, Z. (2008). Structural basis of Vta1 function in the multivesicular body sorting pathway. Dev Cell *14*, 37-49.

Yang, D., and Hurley, J.H. (2010). Structural role of the Vps4-Vta1 interface in ESCRT-III recycling. Structure *18*, 976-984.

Yang, D., Rismanchi, N., Renvoise, B., Lippincott-Schwartz, J., Blackstone, C., and Hurley, J.H. (2008). Structural basis for midbody targeting of spastin by the ESCRT-III protein CHMP1B. Nat Struct Mol Biol *15*, 1278-1286.

Yankulov, K., and Bentley, D. (1998). Transcriptional control: Tat cofactors and transcriptional elongation. Curr Biol *8*, R447-449.

Yorikawa, C., Shibata, H., Waguri, S., Hatta, K., Horii, M., Katoh, K., Kobayashi, T., Uchiyama, Y., and Maki, M. (2005). Human CHMP6, a myristoylated ESCRT-III protein, interacts directly with an ESCRT-II component EAP20 and regulates endosomal cargo sorting. Biochem J *387*, 17-26.

Yu, Z., Gonciarz, M.D., Sundquist, W.I., Hill, C.P., and Jensen, G.J. (2008). Cryo-EM structure of dodecameric Vps4p and its 2:1 complex with Vta1p. J Mol Biol *377*, 364-377.

Zamborlini, A., Usami, Y., Radoshitzky, S.R., Popova, E., Palu, G., and Gottlinger, H. (2006). Release of autoinhibition converts ESCRT-III components into potent inhibitors of HIV-1 budding. Proc Natl Acad Sci U S A *103*, 19140-19145.

Zhai, Q., Fisher, R.D., Chung, H.Y., Myszka, D.G., Sundquist, W.I., and Hill, C.P. (2008). Structural and functional studies of ALIX interactions with YPX(n)L late domains of HIV-1 and EIAV. Nat Struct Mol Biol *15*, 43-49.

Zhou, X., Pan, S., Sun, L., Corvera, J., Lee, Y.C., Lin, S.H., and Kuang, J. (2009). The CHMP4b- and Src-docking sites in the Bro1 domain are autoinhibited in the native state of Alix. Biochem J *418*, 277-284.

Zhou, X., Pan, S., Sun, L., Corvera, J., Lin, S.H., and Kuang, J. (2008). The HIV-1 p6/EIAV p9 docking site in Alix is autoinhibited as revealed by a conformation-sensitive anti-Alix monoclonal antibody. Biochem J *414*, 215-220.

CHAPTER 2

STRUCTRUAL AND BIOCHEMICAL STUDIES OF ALIX/AIP1 AND ITS ROLE IN RETROVIRUS BUDDING

Robert D. Fisher, Hyo-Young Chung, Qianting Zhai, Howard Robinson, Wesley I. Sundquist and Christopher P. Hill

This research was originally published in the Cell 128(5):841-52, 2007.

Structural and Biochemical Studies of ALIX/AIP1 and Its Role in Retrovirus Budding

Robert D. Fisher,[1,3] Hyo-Young Chung,[1,3] Qianting Zhai,[1] Howard Robinson,[2] Wesley I. Sundquist,[1,*] and Christopher P. Hill[1,*]
[1] Department of Biochemistry, University of Utah School of Medicine, Salt Lake City, UT 84112, USA
[2] Department of Biology, Brookhaven National Laboratory, Upton, NY 11973, USA
[3] These authors contributed equally to this work.
*Correspondence: wes@biochem.utah.edu (W.I.S.), chris@biochem.utah.edu (C.P.H.)
DOI 10.1016/j.cell.2007.01.035

SUMMARY

ALIX/AIP1 functions in enveloped virus budding, endosomal protein sorting, and many other cellular processes. Retroviruses, including HIV-1, SIV, and EIAV, bind and recruit ALIX through YPX_nL late-domain motifs (X = any residue; n = 1–3). Crystal structures reveal that human ALIX is composed of an N-terminal Bro1 domain and a central domain that is composed of two extended three-helix bundles that form elongated arms that fold back into a "V." The structures also reveal conformational flexibility in the arms that suggests that the V domain may act as a flexible hinge in response to ligand binding. YPX_nL late domains bind in a conserved hydrophobic pocket on the second arm near the apex of the V, whereas CHMP4/ESCRT-III proteins bind a conserved hydrophobic patch on the Bro1 domain, and both interactions are required for virus budding. ALIX therefore serves as a flexible, extended scaffold that connects retroviral Gag proteins to ESCRT-III and other cellular-budding machinery.

INTRODUCTION

Many enveloped RNA viruses use short peptide motifs, termed "late domains," to recruit cellular factors that facilitate budding (reviewed in Bieniasz, 2006; Demirov and Freed, 2004; Morita and Sundquist, 2004). Two of the best characterized late domains are the PTAP motif, which binds and recruits TSG101 (*t*umor *s*usceptibility *g*ene 101; Demirov et al., 2002; Garrus et al., 2001; Gottlinger et al., 1991; Huang et al., 1995; Martin-Serrano et al., 2001; VerPlank et al., 2001), and the YPX_nL motif (where X can vary in sequence and length), which binds ALIX/AIP1 (*AL*G-2-*i*nteracting protein *X*; Chen et al., 2005; Puffer et al., 1997; Strack et al., 2003; Vincent et al., 2003). YPX_nL late domains can vary in sequence and can function alone or together with PTAP late domains. For example, the structural $p6^{Gag}$ protein of HIV-1_{NL4-3} contains $_{7}PTAP_{10}$ and $_{36}YPLASL_{41}$ late domains that function in tandem, whereas the analogous EIAV $p9^{Gag}$ protein contains a single $_{23}YPDL_{26}$ late domain. In principle, multiple late domains could synergistically enhance virus release and/or expand viral tropism.

Both TSG101 (Vps23p in yeast) and ALIX (Bro1p) help sort membrane proteins into vesicles that bud into the lumen of multivesicular bodies (MVB), which supports the idea that virus budding and MVB vesicle formation are highly related processes. The requirements for MVB protein sorting and vesicle formation are best understood in yeast, where the process requires the action of at least 18 different "Class E" proteins. Most, but not all, Class E proteins are stable subunits of the three ESCRT complexes (*e*ndosomal *s*orting *c*omplexes *r*equired for *t*ransport; Hurley and Emr, 2006). Humans have at least one homolog of every yeast Class E protein, and MVB vesicle sorting therefore appears to be a highly conserved process, albeit one that occurs with considerably greater complexity in mammals.

TSG101 functions as the central subunit of ESCRT-I, which recognizes ubiquitylated membrane-protein cargoes and helps recruit the downstream machinery necessary for protein sorting and MVB vesicle formation (Hurley and Emr, 2006). This downstream machinery includes the ESCRT-III and VPS4-LIP5 complexes, which appear to be intimately involved in the actual mechanics of protein sorting and vesicle formation. ALIX is also a Class E protein and can interact directly with both ESCRT-I and ESCRT-III but is not a stable subunit of either complex (reviewed in Odorizzi, 2006). The yeast homolog Bro1p also recruits the deubiquitylating enzyme Doa4p, which removes ubiquitin from cargoes as they are sorted into MVB vesicles (Dejournett et al., 2006; Luhtala and Odorizzi, 2004).

In addition to its roles in virus budding and MVB cargo sorting, ALIX has also been implicated in a number of other important cellular processes, including (1) MVB vesicle fission and back fusion via regulation of the conical lipid,

lysobisphosphatidic acid (LBPA; reviewed in van der Goot and Gruenberg, 2006); (2) endocytosis via interactions with the membrane-curvature-sensing endophilins (Chatellard-Causse et al., 2002; Gallop and McMahon, 2005); (3) cell-surface-receptor downregulation via direct interactions with cell-surface receptors (Geminard et al., 2004) and through antagonism of the Cbl-SETA/CIN85-endophilin complex (Schmidt et al., 2004); (4) spatial distribution of endosomes via regulation of cortical actin (Cabezas et al., 2005); (5) cell motility/adhesion via interactions with FAK (*f*ocal *a*dhesion *k*inase), PYK2 (*p*roline-rich *t*yrosine *k*inase *2*; Schmidt et al., 2003), and possibly also RabGAPLP (*Rab G*TPase-*a*ctivating *p*rotein-*l*ike *p*rotein; Ichioka et al., 2005); (6) apoptosis via interactions with the calcium-binding EF-hand protein ALG-2 (*a*poptosis-*l*inked *g*ene-2; reviewed in Sadoul, 2006); (7) regulation of the JNK signaling pathway via interactions with ALG-2 and the ubiquitin E3 ligase POSH (*p*lenty *o*f *SH*3 domains; Tsuda et al., 2006). The latter observation is of particular interest because POSH is also required for HIV-1 release (Alroy et al., 2005), which raises the possibility that the ALIX-POSH-ALG-2 complex could function in HIV-1 budding.

In summary, it is now apparent that ALIX performs a series of important functions in the endosomal pathway, in cytoskeletal dynamics, and in enveloped virus budding. However, the mechanistic bases for these seemingly diverse ALIX functions are not known. Our studies were therefore undertaken with the goals of elucidating the structure of ALIX, determining how it interacts with retroviral Gag proteins, and testing its requirements for functioning in virus budding.

RESULTS

Structural Studies of Human ALIX

As illustrated in Figure 1A, human ALIX can be subdivided into three regions; the Bro1 domain (residues 1–358), the "V" domain (362–702), and the proline-rich region (PRR; 703–868). Constructs containing the PRR did not express well in *E. coli*, but constructs spanning the Bro1 and V domains could be expressed and purified. A series of $ALIX_{Bro1\text{-}V}$ proteins with loop mutations were surveyed to identify a protein that would crystallize. The $KK_{268,269}YY$ mutation enabled crystallization (apparently because Tyr268 makes an important crystal contact), and the structure of this protein (hereafter termed $ALIX_{Bro1\text{-}V}$) was determined at a resolution of 3.3 Å (R_{free} = 31.7%; Figures 1B and S1; Table S1). Isolated wild-type Bro1 and V domains were also crystallized and their structures were determined at higher resolutions (2.55 Å, R_{free} = 27.4% and 2.6 Å, R_{free} = 30.2%, respectively; see Figures 1C–1E). The V-domain crystals contained two molecules in the asymmetric unit, and the different structures therefore provided three independent views of the ALIX V domain.

Global Architecture of $ALIX_{Bro1\text{-}V}$

As illustrated in Figure 1B, the $ALIX_{Bro1\text{-}V}$ protein adopts an extended conformation in which the Bro1 and V domains form discrete elements. Like its yeast analog, Bro1p (Kim et al., 2005), $ALIX_{Bro1}$ is shaped like a banana, with a long dimension of ~100 Å. The domain is organized about a core tetratricopeptide repeat (TPR) composed of three helical hairpins that associate into a right-handed superhelix (Figure 1C). The ALIX V domain is composed of two extended arms that fold back on themselves at an angle of ~30° to form a V. The arms are 77 Å (arm1) and 90 Å (arm2) in length, and each is organized about an extended three-helix bundle (Figures 1D and 1E). The V-shaped conformation brings the N-terminal Bro1 domain and the C-terminal PRR (not present in the structure) into spatial proximity, thereby explaining how Src kinase can simultaneously dock to the Bro1 domain and phosphorylate Tyr residues in the ALIX C-terminal tail (Schmidt et al., 2005).

$ALIX_{Bro1\text{-}V}$ has a highly asymmetric shape because the long axes of the Bro1 and arm1 elements connect in parallel. As a result, $ALIX_{Bro1\text{-}V}$ is ~150 Å in its longest dimension but less than 50 Å in its other two. Small-angle X-ray scattering profiles fit the crystal model well (R.D.F. and H. Tsuruta, unpublished data), which indicates that the crystal structure provides a good model for the solution structure of the uncomplexed protein. Nevertheless, we speculate that the different domains could change their relative orientations in response to environmental cues like ligand binding because the Bro1 and V domains are connected by a single tripeptide linker ($_{359}VPV_{361}$) that makes only limited noncovalent contacts (Figures 1B and 2A). Moreover, the V-domain arm trajectories vary in the three different structures, which results in relative displacements of up to 10 Å at their tips (Figure 2B). Finally, the loop region between the two arms of the V domain also has the potential to act as a hinge (Figure 2C and Discussion). Thus, the overall impression is that $ALIX_{Bro1\text{-}V}$ is a scaffold composed of extended domains that may reorient in response to ligand binding.

Structure of the Bro1 Domain

The three helical hairpins that comprise the $ALIX_{Bro1}$ TPR core (α4/5, α6/7, and α8/9) are each ~50 residues in length. They form a right-handed solenoid with a rotation of ~20° between each helical pair. The core is flanked on one side by α10 (left in Figure 1C) and on the other by a small β sheet (β1, β2) and a three-helix bundle (α1–3). Both the N and C termini adopt extended conformations that traverse opposite sides of the domain, with the first 17 residues extending along the convex surface and the final 43 residues extending across the concave surface.

As expected, human $ALIX_{Bro1}$ generally resembles its yeast counterpart (Kim et al., 2005), with an overall rmsd of 2.8 Å over 338 equivalent Cα positions (Figure S2). The character of the domain surface is also largely conserved, with two exposed hydrophobic patches centered about Tyr319 and Phe199. The first patch forms the docking site for Src kinase when Tyr319 is phosphorylated (Schmidt et al., 2005), and the second patch forms the binding site for the CHMP4B subunits of the ESCRT-III complex (Kim et al., 2005 and see below). A strongly

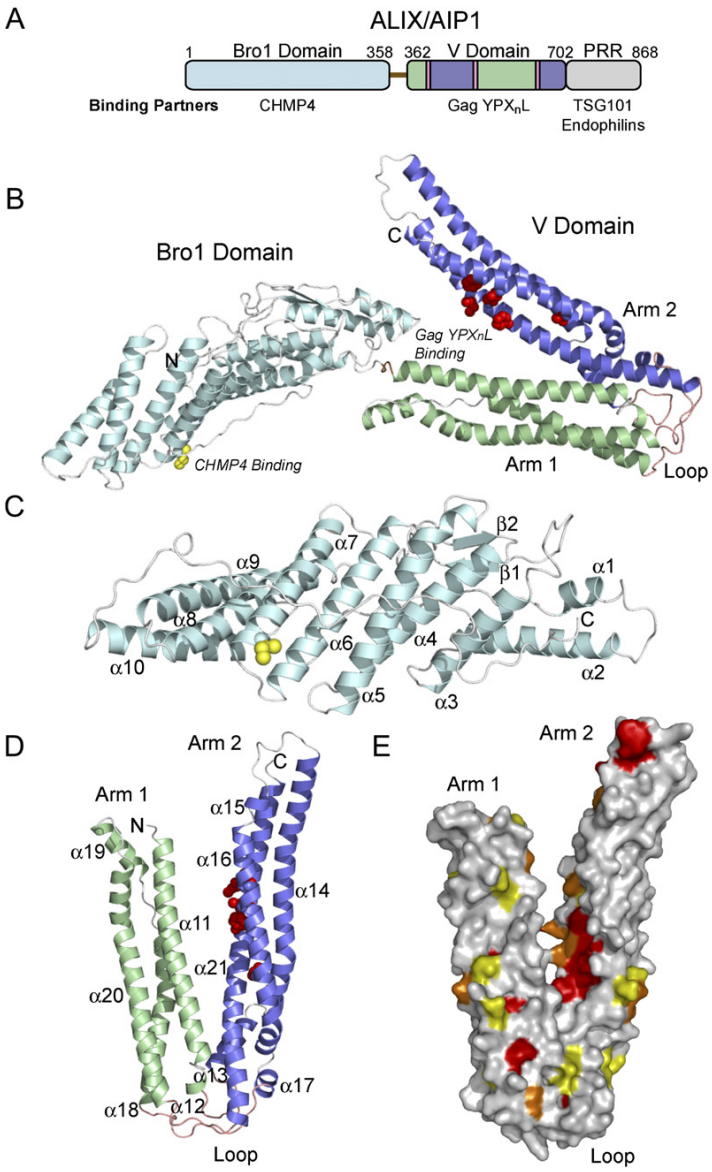

Figure 1. Structure of $ALIX_{Bro1-V}$

(A) shows domain structure of human ALIX. Sequences that compose the different elements are color coded here (and throughout) as follows: Bro1, turquoise; Bro1-V linker, brown; V-domain arm1, green; V-domain loop, salmon; V-domain arm2, blue; and Proline-rich region (PRR), gray.

(B) Ribbon representation of $ALIX_{Bro1-V}$ is shown. Residues implicated in CHMP4 binding (Ile212; yellow) or YPX_nL binding (Phe495, Val498, Ala509, Phe676, Leu680, and Ile683; red) are highlighted. The Bro1 and V domains are connected by a short hydrophobic linker ($_{359}VPV_{361}$). The limited set of interdomain hydrophobic packing interactions is made by Phe24 (α1, Bro1), Val359, Pro360, Val361, Val363 (α11, arm1, and V), and Leu585 (α19, arm1, and V).

(C) This ribbon diagram of $ALIX_{Bro1}$ shows the secondary-structure-labeling scheme. The view is from the underside of the orientation shown in (A).

(D) shows a ribbon diagram of $ALIX_V$ showing the secondary-structure-labeling scheme. As compared to (A), this orientation is rotated clockwise by ~60° relative to a line perpendicular to the plane of the paper.

(E) This surface rendering shows $ALIX_V$ sequence conservation. $ALIX_V$ sequences from seven divergent species were aligned using ESPript (Gouet et al., 1999); residues with scaled similarity scores are color coded as follows: 85–100 are red, 68–84 are orange, and 50–67 are yellow.

electropositive patch at one end of the yeast Bro1 domain is also basic in the human protein, albeit to a lesser extent.

The human and yeast Bro1 domains differ most at one end of the domain (right in Figure 1C), where N- and C-terminal elements differ in secondary structure and packing (Figure S2). Specifically, the C terminus of yeast Bro1p forms three consecutive helical segments that cross the concave side and then turn up into the domain, whereas the equivalent residues in the human protein (342–358) form an extended strand that traverses a similar path but terminates earlier. Thus, the C-terminal helix of the yeast protein packs between α3 and the α1–2 hairpin ($ALIX_{Bro1}$ numbering), whereas the human Bro1 C terminus is shifted by ~10 Å, and the first three helices of human $ALIX_{Bro1}$ collapse into a three-helix bundle (a maximal relative shift of ~12 Å). It appears possible that these distinct C-terminal conformations could alter the relative orientations of the Bro1 and V domains in the different proteins.

The Structure of the ALIX V Domain

Both arms of the ALIX V domain are composed of extended three-helix bundles, although a series of short breaks subdivide the major helices into 11 different segments (Figures 1D, S1, and S3). The topology of the V domain is notable in that the polypeptide chain crosses the arm1/arm2 "loop" region three times in the course of

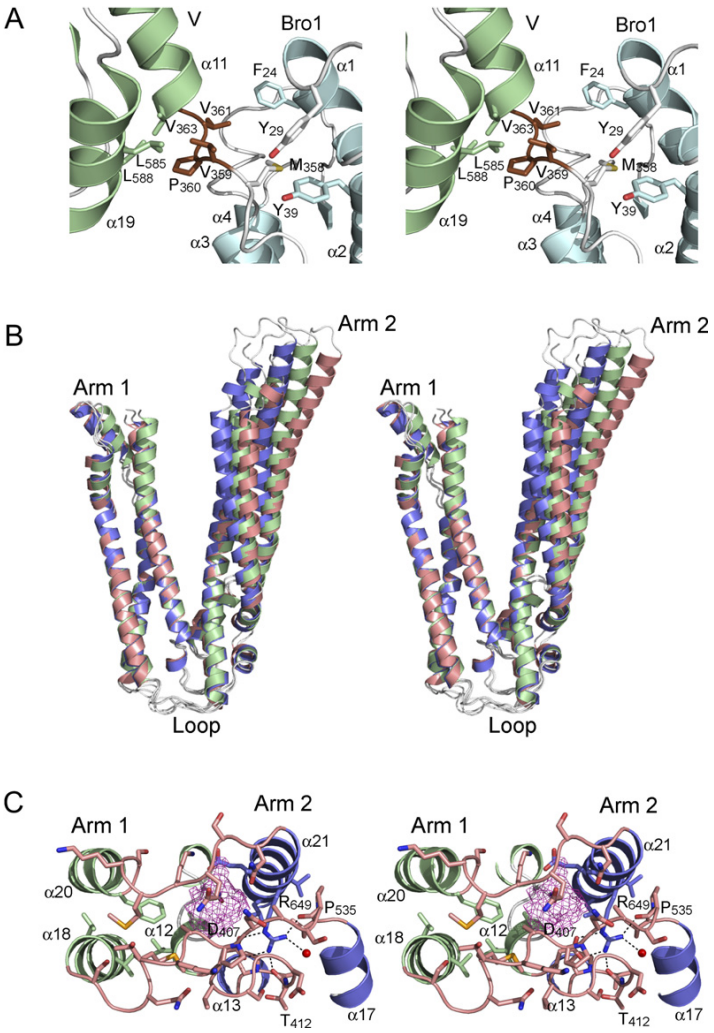

Figure 2. Interdomain Linkers and Conformational Flexibility of $ALIX_{Bro1-V}$

(A) Stereoview showing the linker between the Bro1 and V domains is shown. Secondary structures are color coded as in Figure 1B, and residues that contact the $_{359}VPV_{361}$ linker are shown explicitly.

(B) This stereoview illustrates conformational variability in different V-domain structures. The different trajectories of arm2 were visualized by superimposing only the arm1 regions from crystals of $ALIX_{Bro1-V}$ (salmon) and from the two different molecules in the $ALIX_V$ asymmetric unit (green and blue). The only other significant difference between the structures was in the position of Trp476 residue (α4/5 loop), which flips out of the core of arm2 in one of the two $ALIX_V$ structures to make a crystal contact.

(C) shows a stereoview illustrating the three-stranded loop region that connects the two arms of the V domain. Secondary structures are color coded as in Figure 1B. Side chains within the loop and adjacent residues are shown, and the stabilizing interactions of the Arg649 residue are shown explicitly. The purple cage denotes a pocket that appears to be occupied by a mix of ordered and disordered water molecules. The view is from the bottom of (B).

building the two helical bundles (Figure S3). Hence, the two arms are highly interconnected in primary sequence, and the entire V domain likely represents a single functional entity.

The two V-domain arms are primarily stabilized by hydrophobic side-chain-packing interactions that are based upon heptad repeats and that adopt canonical ''knobs into holes'' side-chain packing. This explains why the domain scored highly in coiled-coil prediction algorithms (Katoh et al., 2003; Odorizzi et al., 2003). In contrast, the three strands in the loops connecting arm1 and arm2 are stabilized almost exclusively by hydrophilic interactions, most of which are mediated by backbone atoms. An illustrative example is provided by the highly conserved Arg649 residue (α21, arm2), which forms a series of interactions that buttress the underside of the loop region; these include a buried salt bridge with Asp407 (α12/13 loop) and hydrogen-bonding interactions with a buried water molecule and with the backbone carbonyl oxygen atoms of Pro535 (α17/18 loop) and Thr412 (α12/13 loop). The loop region also encloses a hydrophilic interior cavity of ~67 $Å^3$ (purple in Figure 2C).

The V domain exhibits intrinsic conformational flexibility, as revealed by comparisons of the relative positions of the two arms in the different crystal structures. Isolated arm1 structures from the crystallographically independent models overlap well (rmsd = 1.4 Å), and the same is true for the arm2 structures, but overlapping on either arm causes the other to ''fan out'' into different positions. This is illustrated in Figure 2B for the case of overlap on arm1, where the relative arm2 displacements reach up to 10 Å at their distal ends. These global differences in the structures arise from small, cumulative changes in the interhelical packing interactions along both arms rather than from a dramatic reorganization of the loop region or elsewhere. Thus, the structures demonstrate that the V-domain arm

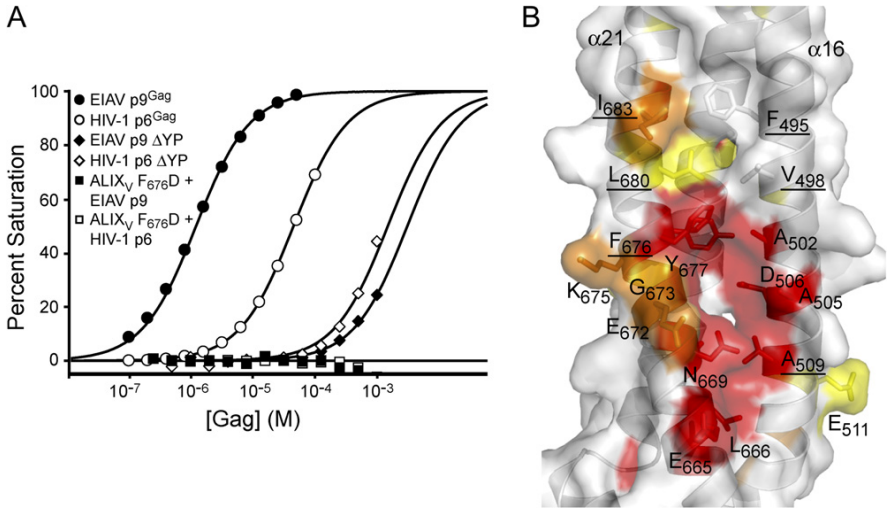

Figure 3. Identification of the YPX$_n$L-Binding Site on ALIX$_V$

(A) Biosensor binding isotherms for purified HIV-1 p6^{Gag} and EIAV p9^{Gag} constructs binding to immobilized ALIX$_V$ domain constructs are shown.
(B) YPX$_n$L-binding site on ALIX$_V$ arm2 is shown here as viewed from arm1. Residue conservation is color coded as in Figure 1E. Underlined residues were mutated and tested for YPX$_n$L-binding activity and/or for activity in the HIV-1 ΔPTAP rescue assay (see text).

positions can vary, although the biological significance of this observation remains to be elucidated.

The ALIX V Domain Binds HIV-1 p6^{Gag} and EIAV p9^{Gag} YPX$_n$L Late Domains

ALIX binds and facilitates budding of retroviral Gag proteins that contain YPX$_n$L late domains, but the interaction site is not yet known. We therefore performed biosensor binding experiments to map the YPX$_n$L-binding site and measure the binding affinities of the HIV-1 p6^{Gag} and EIAV p9^{Gag} proteins. As shown in Figure 3A, the immobilized ALIX V domain bound both HIV-1 p6^{Gag} and EIAV p9^{Gag}, with dissociation constants of 59 ± 15 μM and 1.2 ± 0.3 μM, respectively. In both cases, binding was specific for the YPX$_n$L late domain because YP to SR mutations (termed ΔYP; Strack et al., 2003) reduced binding affinities substantially (>15-fold). Very similar binding data were also obtained for the ALIX$_{Bro1-V}$ construct, which indicates that the Bro1 domain did not contribute to the binding interaction (Table S2).

Close inspection of the V-domain surface revealed a highly conserved hydrophobic groove on arm2 between helices 16 and 21, centered about Phe676, that was a strong candidate for the YPX$_n$L late-domain-binding site (Figures 1D, 1E, 3B, and S4). This site is exposed to solvent but is located near the base of the V, where the two arms are separated by only 5–10 Å. Phe676 sits at one end of a deep pocket (~10 Å) that is lined by a series of highly conserved residues (highlighted in red in Figure 3B). A shallower hydrophobic groove also extends ~7 Å above Phe676, although the residues that line this half of the site are less well conserved (Figures 3B, S1, and S4).

Mutational analyses confirmed that a series of conserved residues within the putative YPX$_n$L-binding site on arm2 were required for full-affinity HIV-1 p6^{Gag} and EIAV p9^{Gag} binding. As shown in Figure 3A, the Phe676Asp mutation abolished any detectable binding to either HIV-1 p6^{Gag} or EIAV p9^{Gag}, which represents a >1000-fold reduction in EIAV p9^{Gag} binding affinity. Mutations in two other binding-groove residues (Val498Asp and Ile683Asp) also reduced HIV-1 p6^{Gag} and EIAV p9^{Gag} binding affinities substantially (≥20 fold; see Table S2). These data indicate that retroviral Gag YPX$_n$L late domains bind the V domain of ALIX at a conserved site that spans the side and interior face of arm2.

Requirements for ALIX in EIAV and HIV-1 Release

Previous studies have indicated that ALIX can function in the release of both EIAV and HIV-1 (Chen et al., 2005; Martin-Serrano et al., 2003; Strack et al., 2003; von Schwedler et al., 2003). Importantly, however, EIAV p9^{Gag} contains a single known late domain (the $_{23}$YPDL$_{26}$-ALIX site), whereas HIV-1 p6^{Gag} contains two late domains: a $_{7}$PTAP$_{10}$-TSG101 site and a $_{36}$YPLASL$_{41}$-ALIX site. We therefore assessed the relative importance of ALIX for the release of both EIAV and HIV-1. As shown in Figure 4A, the release of virion-associated Gag-derived CA protein from HeLa cells expressing a wild-type EIAV vector was readily detected in western blot assays (lane 1, upper panel), but the ΔYP mutation in the p9^{Gag} ALIX-binding site reduced EIAV particle release 12-fold (compare lanes 1 and 2, panel 1). ALIX depletion similarly reduced the

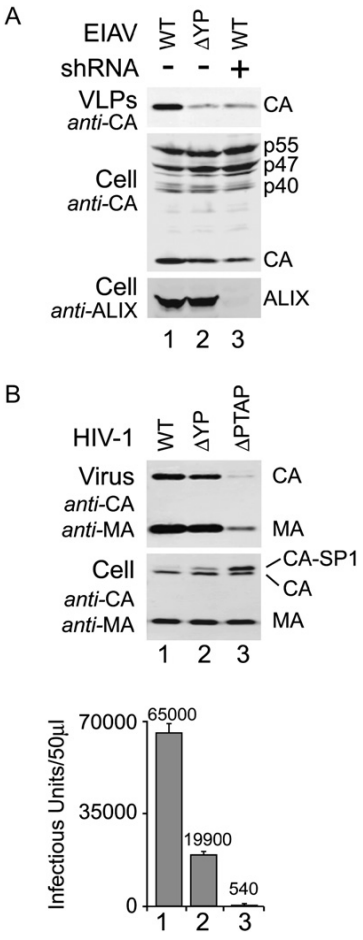

Figure 4. Requirement for ALIX in EIAV and HIV-1 Budding

(A) ALIX requirements for EIAV vector budding are shown as follows: lanes 1, wild-type (WT) EIAV vector expressed in wild-type HeLa cells (positive control); lanes 2, EIAV vector encoding a $_{23}SR_{24}$ mutation in the $_{23}YPDL_{26}$ late domain of $p9^{Gag}$ (ΔYP) expressed in wild-type HeLa cells; and lanes 3, wild-type EIAV vector expressed in cells depleted of ALIX using shRNA. Western blots are shown as follows: panel 1, virus-like particle (VLP) production (anti-CA antibody) reports the amount of successful budding and panel 2, cellular Gag protein levels (anti-CA antibody) control for expression. Note that CA corresponds to the processed central domain of Gag, p55 corresponds to full-length Gag protein, and p40 and p47 are intermediate Gag cleavage products. Cellular Gag levels were similar in all cases, although the processing was somewhat delayed in the ΔYP mutant and in the absence of ALIX. Panel 3 shows cellular ALIX levels (anti-ALIX antibody).

(B) The relative importance of ALIX and TSG101 binding for HIV-1 virus budding is shown. Lanes 1 show wild-type (WT) HIV-1 expressed in 293T cells (positive control), lanes 2 show HIV-1 encoding a $_{36}SR_{37}$ mutation in the $_{36}YPLASL_{41}$ late domain of $p6^{Gag}$ (ΔYP), and lanes 3 show wild-type HIV-1 encoding a $_{7}LIRL_{10}$ mutation in the $_{7}PTAP_{10}$ late domain of $p6^{Gag}$ (ΔPTAP). Western blots show virus production (panel 1) and cellular Gag protein levels (panel 2, anti-CA and anti-MA antibodies; MA is the processed N-terminal domain of Gag). Panel 3 shows viral titers measured in a single-cycle MAGIC assay (errors are standard deviations from three separate infectivity experiments). Note that cellular CA and MA levels were similar in all cases but that the CA-SP1-processing intermediate accumulated in the ΔYP and ΔPTAP constructs, which is a typical diagnostic of virus-budding inhibition.

release of wild-type EIAV 10-fold (compare lanes 1 and 3, upper panel). shRNA depletion of ALIX from HeLa cells was very efficient (lane 3, bottom panel), and EIAV Gag expression was not significantly affected by either the $p9^{Gag}$ ΔYP mutation or by ALIX depletion (middle panels). Gag processing was inhibited slightly, however, which is reminiscent of the Gag-processing delay observed upon inhibition of HIV-1 budding (Gottlinger et al., 1991). We therefore conclude that the $_{23}YPDL_{26}$-ALIX interaction plays a critical role in enhancing EIAV Gag release, which is in good agreement with previous studies (Martin-Serrano et al., 2003; Puffer et al., 1997; Strack et al., 2003).

The importance of ALIX for HIV-1 release was also tested by measuring the effect of the ΔYP mutation in the ALIX-binding site of HIV-1 $p6^{Gag}$. As shown in Figure 4B, this mutation reduced HIV-1 Gag release from 293T cells, as measured in both a western blot assay (compare lanes 1 and 2, panel 1) and by viral titers in a single-cycle MAGIC infectivity assay (lanes 1 and 2, panel 3). However, the reductions in release and infectivity were modest (~3-fold). In comparison, a mutation that blocked the $_{7}PTAP_{10}$-TSG101 interaction ($PTAP_{7\text{-}10}LIRL$, termed ΔPTAP) had a much more profound effect on HIV-1 release and reduced infectious titers more than 100-fold (Figure 4B, compare lanes 1 and 3). Neither late-domain mutation affected Gag protein expression, although both again delayed Gag processing, as evidenced by intracellular accumulation of the CA-SP1-processing intermediate, with the more profound effect again seen for the ΔPTAP mutation (Figure 4B, central panel). These experiments indicate that ALIX and TSG101 both enhance the release of wild-type HIV-1 from 293T cells but that the virus depends much more heavily upon the $_{7}PTAP_{10}$-TSG101 interaction. These studies again generally agree well with previous mutational analyses that utilized different HIV-1 constructs and cell types and were performed before the discovery of the $p6^{Gag}$ $_{36}YPLASL_{41}$-ALIX interaction (Demirov et al., 2002; Gottlinger et al., 1991; Huang et al., 1995).

ALIX Overexpression Rescues Release and Infectivity of HIV-1 ΔPTAP

The experiments described above demonstrate that the $p9^{Gag}$ $_{23}YPDL_{26}$-ALIX late-domain interaction plays a major role in facilitating EIAV release, yet the $p6^{Gag}$ $_{36}YPLASL_{41}$-ALIX interaction does not efficiently substitute for the $_{7}PTAP_{10}$-TSG101 interaction in supporting HIV-1 release. We hypothesized that this apparent discrepancy might reflect a reduced ability of HIV-1 to recruit ALIX owing to the lower affinity of the $p6^{Gag}$ YPX_nL-binding site. We therefore tested whether the inefficient release of the HIV-1 ΔPTAP virus from 293T cells could be "rescued" by increasing intracellular ALIX concentrations.

As shown in Figure 5, HIV-1 ΔPTAP release and infectivity were indeed stimulated very dramatically (~25-fold) by ALIX overexpression (Figure 5, panels 1 and 4, compare lanes 1 and 2). Hence, raising cellular ALIX levels could restore HIV-1 ΔPTAP infectivity to within ~20% of the wild-type virus. Importantly, ALIX overexpression did not alter intracellular Gag expression or processing (panel 2), which demonstrates that the enhancement occurred at late stages in particle assembly or budding. Control experiments also confirmed that the $p6^{Gag}{}_{36}YPLASL_{41}$-ALIX interaction was responsible for this enhancement because ALIX overexpression did not stimulate the release of an HIV-1 ΔPTAP virus that also lacked a functional ALIX-binding site (compare lanes 2 and 4). Indeed, the secondary ΔYP mutation actually reduced HIV-1 ΔPTAP release and infectivity by an additional 5-fold (compare lanes 3 and 4 to lane 1) presumably because the mutation also inhibited the ability of *endogenous* ALIX to mediate low-level release. These experiments demonstrate that ALIX can replace TSG101 in its role of supporting the efficient release of infectious HIV-1, provided ALIX is present at sufficient levels to overcome the modest affinity of the $_{36}YPLASL_{41}$-ALIX interaction.

ALIX YPX_nL-Binding Activity Is Required for Virus Release

The rescue of HIV-1 ΔPTAP release and infectivity upon ALIX overexpression provided a convenient assay for testing which ALIX activities were required for functional virus release. This assay was initially used to test whether ALIX mutations that inhibited YPX_nL binding in vitro also inhibited virus release through the ALIX pathway. As described previously, overexpression of wild-type ALIX enhanced the release and infectivity of HIV-1 ΔPTAP ~25-fold (Figure 6A, compare lanes 1 and 2). In contrast, ALIX proteins with point mutations that inhibited YPX_nL binding (Val498Asp, Phe676Asp, and Ile683Asp) failed to rescue HIV-1 ΔPTAP release or infectivity (compare lanes 2 and 3–5). These mutations did not affect ALIX expression or stability (panel 3), nor did they affect cellular Gag levels (panel 2). Similar data were obtained for a series of other mutations within the YPX_nL-binding site (Phe495Asp, Val509Asp, and Leu680Asp), whereas mutations in a second conserved hydrophobic patch located on arm1 (Leu401Asp, Ile405Asp, and Leu556Asp) did not diminish ALIX rescue significantly (<2-fold, data not shown). These data reinforce the idea that ALIX binds YPX_nL late domains within the site shown in Figure 2B and demonstrate that ALIX mutations that impair YPX_nL binding also inhibit virus release and infectivity.

ALIX Recruitment of CHMP4/ESCRT-III Is Required for HIV-1 ΔPTAP Release

In addition to binding YPX_nL late domains, ALIX also binds CHMP4/ESCRT-III proteins through the Bro1 domain, suggesting that ALIX may serve to connect retroviral Gag proteins to the ESCRT-III machinery (Katoh et al., 2003; Kim et al., 2005; Martin-Serrano et al., 2003; Odorizzi et al., 2003; Strack et al., 2003; von Schwedler et al., 2003). We therefore tested whether the interaction between ALIX and CHMP4A was required for virus budding. Previous work showed that mutations in an exposed hydrophobic patch on yeast Bro1p inhibited Snf7p (CHMP4) binding and prevented proper MVB sorting (Kim et al., 2005). We found that a mutation within the equivalent patch on human ALIX, Ile212Asp, similarly inhibited the $ALIX_{Bro1}$-CHMP4A interaction, as assayed in a GST pulldown experiment (Figure 6B). As expected, wild-type $ALIX_{Bro1}$ bound to a GST-CHMP4A fusion protein but not to GST alone (compare lanes 2 and 3). In contrast, the $ALIX_{Bro1,I212D}$ mutant did not bind GST-CHMP4A detectably (compare lanes 3 and 6).

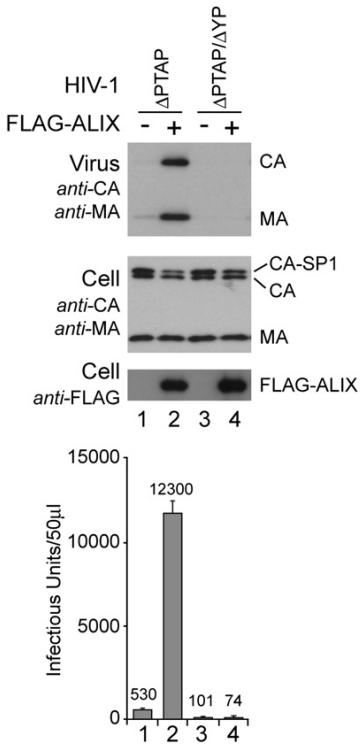

Figure 5. ALIX Overexpression Rescues HIV-1 ΔPTAP Release and Infectivity

Virus release, cellular Gag protein levels, exogenous ALIX expression, and viral infectivity are shown as analyzed by western blotting (panels 1–3) or MAGIC infectivity assays (panel 4). Lanes 1 show HIV-1 ΔPTAP cotransfected with an empty pCI-neo vector control, lanes 2 show HIV-1 ΔPTAP cotransfected with a vector expressing FLAG-ALIX, lanes 3 show HIV-1 ΔPTAP ΔYP cotransfected with an empty vector control, and lanes 4 show HIV-1 ΔPTAP ΔYP cotransfected with a vector expressing FLAG-ALIX. For reference, wild-type HIV-1 titers were typically ~65,000 IU/50 µl, and overexpression raised ALIX levels ~50-fold over endogenous protein levels as estimated by western blotting with anti-ALIX antibodies (not shown). Error bars in infectivity assays represent standard deviations of three separate infectivity experiments.

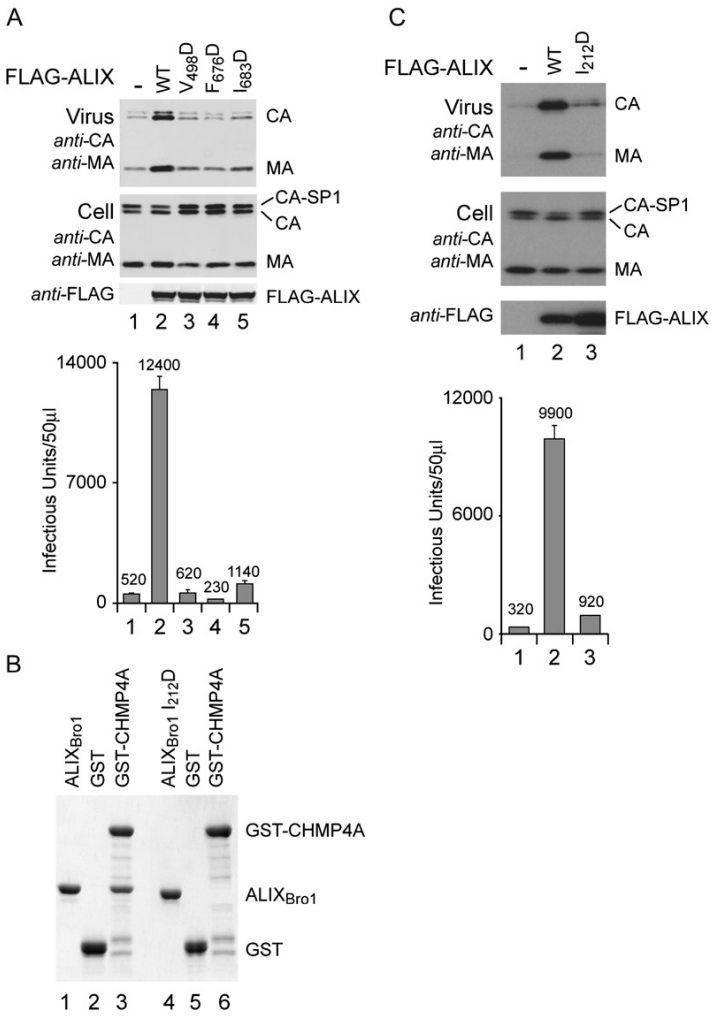

Figure 6. ALIX Mutants Lacking YPX_nL- and CHMP4-Binding Activities Do Not Support HIV-1 ΔPTAP Release and Infectivity

(A) HIV-1 ΔPTAP release and infectivity when coexpressed with an empty vector (−; lanes 1), with vectors expressing wild-type ALIX (lanes 2), or with ALIX mutants defective in YPX_nL binding (lanes 3–5) are shown. ALIX and Gag protein levels were analyzed by western blotting (panels 1–3), and infectious titers were analyzed using MAGIC assays (panel 4).

(B) This GST pulldown assay shows that the $ALIX_{Bro1}$ mutation Ile212Asp inhibits GST-CHMP4A binding. Binding experiments were performed with wild-type $ALIX_{Bro1}$ (lanes 1–3) and the $I_{212}D$ mutant (lanes 4–6). Lanes 1 and 4 show pure $ALIX_{Bro1}$ proteins (reference markers), lanes 2 and 4 show $ALIX_{Bro1}$ proteins binding to GST alone (negative controls), and lanes 3 and 6 show $ALIX_{Bro1}$ proteins binding to GST-CHMP4A.

(C) HIV-1 ΔPTAP release and infectivity are shown when coexpressed with an empty expression vector (−, lanes 1), with vectors expressing wild-type ALIX (lanes 2), or with the ALIX Ile212Asp mutant (lanes 3), which is defective in CHMP4A binding. In (A) and (C), HIV-1 ΔPTAP release, cellular Gag protein levels, exogenous ALIX expression, and viral infectivity were analyzed as described in Figure 4, with error bars representing standard deviations from three separate infectivity experiments.

We next tested whether the Ile212Asp mutation affected the ability of ALIX to rescue HIV-1 ΔPTAP infectivity. As shown in Figure 6C, the $ALIX_{I212D}$ mutant expressed well (panel 3, compare lanes 2 and 3) but failed to rescue HIV-1 ΔPTAP release or infectivity significantly (top and bottom panels, compare lanes 2 and 3). Hence, the Ile212Asp mutation strongly inhibited the ability of ALIX to support HIV-1 release, implying that one essential ALIX function in virus budding is to recruit CHMP4/ESCRT-III.

Other ALIX Functions in Virus Budding

The HIV-1 ΔPTAP rescue assay was also used to survey the functional importance of four other known ALIX properties: Tyr319 phosphorylation, TSG101 binding, endophilin binding, and interactions of the C-terminal PRR. ALIX mutants defective in each of these properties were generated and tested for their ability to rescue HIV-1 ΔPTAP release. In the first case, the ALIX Tyr319Phe mutation, which blocks phosphorylation and Src kinase binding (Schmidt et al., 2005), did not impair the rescue of HIV-1 ΔPTAP release and infectivity (Figure 7, lane 3). This result indicates that Src binding and phosphorylation do not play essential (or nonredundant) roles in ALIX virus-budding activity.

ALIX can also bind directly to the N-terminal UEV domain of TSG101 via a $_{717}PSAP_{720}$ motif located in the ALIX PRR (Martin-Serrano et al., 2003; Strack et al., 2003; von Schwedler et al., 2003). This interaction is of interest because it provides a potential mechanism for association of the two known late-domain-binding partners of HIV-1. As expected, mutation of the final proline in the $_{717}PSAP_{720}$ motif (Pro720Leu) eliminated TSG101 UEV binding entirely (Figure S5A). However, the $ALIX_{P720L}$ mutant fully rescued HIV-1 ΔPTAP release and infectivity (Figure 7, lane 4), which indicates that a functional TSG101-binding site was not required for ALIX to support virus budding. Indeed, we found that ALIX overexpression rescued HIV-1 ΔPTAP release even when TSG101 was

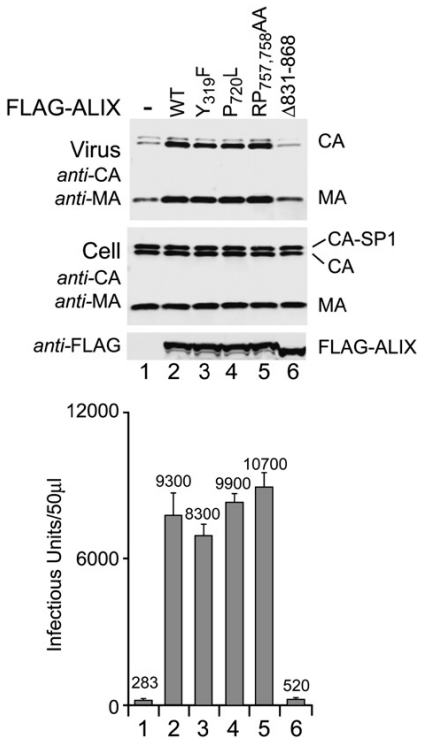

Figure 7. ALIX Requirements for HIV-1 ΔPTAP Release and Infectivity

HIV-1 ΔPTAP release and infectivity are shown when coexpressed with: an empty vector (−; lanes 1) with expression vectors for wild-type ALIX (lanes 2), with the ALIX $Y_{319}F$ mutant (lanes 3), which cannot be phosphorylated on residue 319, with the $ALIX_{P720L}$ mutant (lanes 4), which is defective in TSG101 binding, with the $ALIX_{RP757,758AA}$ mutant (lanes 5), which is defective in endophilin binding, or with the $ALIX_{\Delta831–868}$ mutant (lanes 6), which lacks the final 38 residues in the PRR. HIV-1 ΔPTAP release, cellular Gag protein levels, exogenous ALIX expression, and viral infectivity were analyzed as described in Figure 4, with error bars representing standard deviations from three separate infectivity experiments.

depleted from cells (not shown), which indicates that the ALIX and TSG101 virus-budding pathways can function independently.

Endophilins represent another interesting class of ALIX-binding partners because endophilins can bind membranes and can drive (or sense) membrane curvature. Moreover, endophilin-2 binds and facilitates MLV Gag protein release (Wang et al., 2003). Endophilins bind the $_{755}PXRPPPP_{761}$ sequence within the ALIX PRR (Chatellard-Causse et al., 2002; Shibata et al., 2004). We employed yeast two-hybrid assays to confirm that the ALIX $RP_{757,758}AA$ mutation inhibited binding to both endophilin-1 and -2 (Figure S5B). Despite lacking endophilin-binding activity, however, the $ALIX_{RP757,758AA}$ mutant efficiently rescued HIV-1 ΔPTAP release and infectivity, which indicates that endophilin binding was also dispensable for the virus-budding function of ALIX (Figure 7, lane 5).

Finally, we tested the general importance of the ALIX PRR using several deletion mutants, the shortest of which removed just the final 38 ALIX residues ($ALIX_{\Delta831–868}$). All of the C-terminal deletion mutants tested, including $ALIX_{\Delta831–868}$, failed to rescue HIV ΔPTAP release and infectivity (lane 6) despite equivalent expression levels of the mutant and wild-type proteins (panel 3, compare lanes 2 and 6). We therefore conclude that ALIX PRR interaction(s) are required for late budding activity.

DISCUSSION

$ALIX_{Bro1-V}$ Structure

The elongated Bro1 domain extends from the first arm of the central V domain, which gives $ALIX_{Bro1-V}$ the shape of a "check mark." This distinctive conformation explains how Src kinase can bridge the N-terminal Bro1 domain and the distal PRR tail and how it may similarly bring other Bro1- and PRR-binding proteins into close proximity. The $ALIX_{Bro1-V}$ structure also suggests several ways in which conformational changes could function in the numerous biological roles ascribed to ALIX. Two types of domain motion are attractive possibilities: (1) variation in the relative orientation of the Bro1 and V domains, which appears possible given the limited number of contacts made by the interdomain linker (Figure 2A), and (2) variation in the trajectories of the two arms of the V domain, as implied by differences in the three different V-domain structures (Figure 2B).

In addition to the modest variation in arm orientation observed between crystal structures, we speculate that the V domain might function as a "molecular hinge," with the structures reported here corresponding to the closed conformation. This idea is consistent with the lack of hydrophobic packing interactions throughout the loop region of the V domain (Figure 2C). The hydrophilic loop-packing interactions that do exist are well defined and geometrically constrained, however, which indicates that if the loop functions as a hinge, then activation energy will be required to break these interactions and open the V. In principle, hinge opening could be driven by posttranslational modifications and/or ligand binding and might expose new binding sites and thereby provide an elegant mechanism for transmitting signals for complex assembly and disassembly. YPX_nL late domains are obvious candidates for triggering a possible hinge-opening motion because they bind near the base of the V at a site located nearly between the two arms.

YPX_nL Binding

We have mapped the YPX_nL-binding site to a conserved, hydrophobic groove on arm2 of the ALIX V domain and demonstrated that YPX_nL binding is required for ALIX-mediated budding of both HIV-1 and EIAV. ALIX binds nearly 60× more tightly to EIAV $p9^{Gag}$ than to HIV-1 $p6^{Gag}$, which is consistent with the idea that the EIAV $_{23}YPDL_{26}$ late

domain is an optimized ALIX-binding site (Vincent et al., 2003). This presumably reflects the fact that EIAV contains just a single known late domain and therefore relies heavily on ALIX to bud from cells. In contrast, the weaker HIV-1 $_{36}$YPLASL$_{41}$-ALIX late-domain interaction implies that suboptimal binding must confer a selective advantage when a functional TSG101-binding site is also present. This same trend can be seen in many different SIV strains, where the absence of a TSG101-binding site appears to correlate with the presence of an optimized ALIX-binding site (and vice versa; Bibollet-Ruche et al., 2004). Hence, viral late domains are not necessarily optimized for high-affinity binding, particularly when a virus employs multiple late domains.

We also found that ALIX can efficiently support the release and infectivity of an HIV-1 construct that lacks a TSG101-binding site, provided that the cellular ALIX levels are high enough to overcome the relatively weak binding affinity. Importantly, virus release via ALIX does not require TSG101, and vice versa. Similarly, TSG101 is not required for release of a Δp6 HIV-1 chimera that buds via a fused EIAV p9^{Gag} element (Martin-Serrano et al., 2003) nor for ALIX stimulation of murine leukemia virus budding (Segura-Morales et al., 2005). These observations all indicate that although TSG101 and ALIX can bind one another and function together in the MVB pathway, they represent independent routes out of the cell. The decisions as to which late domain(s) are employed by a particular virus, how many late domains are used, and the affinity of each binding site presumably reflect a complex optimization of the different possible exit routes from relevant host cell types.

Although the precise mechanistic role of the different cellular Class E proteins in enveloped virus budding is not yet clear, there is increasing evidence that viruses may be mimicking cellular interactions that allow membrane proteins to recruit the MVB machinery and be sorted into MVB vesicles, which ultimately leads to lysosomal degradation or release within extracellular exosomes. Interestingly, both the AP-2 adaptor complex and ALIX can bind a Tyr-based motif found in the cytoplasmic tail of the transferrin receptor (TR; although the motif does not match the YPX$_n$L consensus; Geminard et al., 2004). Vidal and colleagues have argued that the AP-2 interaction directs TR endocytosis, and the ALIX interaction may then direct the TR into exosomes that are released by maturing reticulocyte cells (Geminard et al., 2004). Both AP-2 and ALIX also bind the EIAV p9^{Gag} late domain and function in virus release (Chen et al., 2005), which suggests that EIAV may bud via the same pathway that sorts cellular TRs into reticulocyte-derived exosomes.

To date, the only well-documented example in which an ALIX-like protein binds a nonviral YPX$_n$L motif is for an ALIX homolog in *Aspergillus nidulans*, PalA, which binds tandem YPXL/I tetrapeptide repeats within PacC, a protein involved in sensing and responding to pH changes (Vincent et al., 2003). The YPXL/I motifs are required for pH-dependent proteolytic activation of PacC, although the precise role of PalA in this process is not clear. Other cellular binding partners for the ALIX V domain presumably exist, but the lack of a strong consensus sequence for the YPX$_n$L-like binding motifs complicates their identification.

Other Functional Requirements

Our studies also show that one essential function of ALIX in virus budding is to recruit the CHMP4/ESCRT-III complex. It has been challenging to establish a direct role for the ESCRT-III proteins in virus budding because human cells express 11 distinct, but related, ESCRT-III subunits, and it is therefore difficult to differentiate between nonessential versus redundant functions (e.g., see Langelier et al., 2006). Our work provides the most direct demonstration to date that ESCRT-III recruitment is required for virus budding and is consistent with previous studies showing that dominant-negative ESCRT-III constructs can block virus release (Martin-Serrano et al., 2003; Strack et al., 2003; von Schwedler et al., 2003) and that artificial Gag fusions that recruit ESCRT-III subunits can substitute for the $_{23}$YPDL$_{26}$ late domain in supporting EIAV p9^{Gag} release (Pineda-Molina et al., 2006). Hence, there is now increasing evidence that while enveloped RNA viruses can enter into the MVB pathway via many different binding partners, they ultimately require access to the ESCRT-III and VPS4-LIP5 complexes, which appear to be the functional machinery of MVB protein sorting/vesicle formation.

The PRR of ALIX also provides essential function(s) in virus budding. While the terminal 38 residues of ALIX could play a structural role, the high Pro and Gln content of this region (34% and 24%, respectively) makes it more likely that the polypeptide is inherently unstructured and can adopt an extended conformation that serves as the docking site for other cellular proteins. We have shown that endophilin and TSG101 binding to the PRR appear to be dispensable (or redundant) for viral budding. Determining the subset of PRR interactions that are essential for virus budding will likely shed light on the mechanistic requirements for protein sorting/vesicle formation and will further reveal how ALIX can serve as an adaptable, multidomain scaffold that links retroviral Gag proteins to essential cellular budding machinery.

EXPERIMENTAL PROCEDURES

Summary of Protein Expression, Purification, and Structure Determination

For protein-interaction studies, HIV-1 p6^{Gag} and EIAV p9^{Gag} were expressed as GST fusions in *E. coli* and purified by affinity chromatography and gel filtration chromatography (following protolytic removal of GST). ALIX$_{Bro1-V}$, ALIX$_{Bro1}$, and SeMet ALIX$_V$ were similarly expressed as GST or 6×-His N-terminal fusion proteins in *E. coli* and affinity purified for binding studies and crystallization. The 6x-His tag was left on crystallized ALIX$_{Bro1}$ but removed from ALIX$_{Bro1-V}$ and ALIX$_V$. The crystallized ALIX$_{Bro1-V}$ protein had a KK$_{268,269}$YY mutation. Structures were determined by SAD (ALIX$_V$) or molecular replacement (ALIX$_{Bro1}$ and ALIX$_{Bro1-V}$) and refined as summarized in Table S1. Full details of

plasmid construction, protein expression, crystallization, and structure determination are provided in the Supplemental Data.

Protein-Protein Interaction Experiments

Biosensor binding experiments were performed as described (Garrus et al., 2001) with purified HIV-1 $p6^{Gag}$, EIAV $p9^{Gag}$, and HIV-1 $TSG101_{UEV}$ proteins binding to immobilized GST-$ALIX_{Bro1-V}$, GST-$ALIX_{V}$, GST-$ALIX_{Bro1}$, and GST-$ALIX_{714–723}$ proteins. Assay conditions and binding affinities are provided in Table S2. GST pulldown experiments were performed as described (von Schwedler et al., 2003) using purified $ALIX_{Bro1}$ proteins binding to GST or GST-CHMP4A proteins captured from clarified *E. coli* lysates.

Assays for HIV-1 ΔPTAP Release and Infectivity

293T cells (~8×10^5 cells/well in 6-well plates) were transfected with 1 μg of HIV-1 ΔPTAP plasmid (Garrus et al., 2001) + 1 μg of ALIX expression vector per well (10 μl Lipofectamine 2000, Invitrogen). Cytoplasmic proteins and sucrose-pelleted virions were harvested 24 hr posttransfection, analyzed by western blotting, and quantified using an Odyssey imaging system (Li-COR, Inc.). Primary antibodies were rabbit anti-CA and rabbit anti-MA at 1:15,000. HIV-infectious titers were assayed in single-cycle MAGIC assays in P4 cells. Additional experimental details are provided in von Schwedler et al. (2003).

EIAV VLP Production and ALIX Silencing

HeLa M cells (~4×10^5 cells/well, 6-well plate) were transiently transfected (10 μl; FuGene6, Roche Applied Science) with 5 μg of wild-type or $p9^{Gag}$ ΔYP pEV53B EIAV vector (Olsen, 1998). EIAV virus-like particles were harvested 48 hr posttransfection, concentrated through 20% sucrose cushions, and analyzed by western blotting using affinity-purified EIAV anti-CA antibody (1:10,000). For ALIX-depletion experiments, an shRNA targeting human ALIX nucleotides 1765–1783 (Chen et al., 2005) was delivered using the FG12 lentiviral expression vector (Qin et al., 2003; 8 μg/ml polybrene, moi = 15) 24 hr prior to transfection with pEV53B.

Supplemental Data

Supplemental Data include Experimental Procedures, References, five figures, and two tables and can be found with this article online at http://www.cell.com/cgi/content/full/128/5/841/DC1/.

ACKNOWLEDGMENTS

We thank Michael Landesman for performing the yeast two-hybrid experiment shown in Figure S5 and Heidi Schubert, Andrew VanDemark, and Frank Whitby for helpful guidance in the crystallography. Operations of the National Synchrotron Light Source (NSLS) are supported by the Office of Basic Energy Sciences at the U.S. Department of Energy and by the National Institutes of Health (NIH). Data collection at the NSLS was funded by the National Center for Research Resources. This work was supported by NIH Grants GM066521 (C.P.H. and W.I.S.) and AI051174 (W.I.S.).

Received: November 13, 2006
Revised: December 22, 2006
Accepted: January 5, 2007
Published: March 8, 2007

REFERENCES

Alroy, I., Tuvia, S., Greener, T., Gordon, D., Barr, H.M., Taglicht, D., Mandil-Levin, R., Ben-Avraham, D., Konforty, D., Nir, A., et al. (2005). The trans-Golgi network-associated human ubiquitin-protein ligase POSH is essential for HIV type 1 production. Proc. Natl. Acad. Sci. USA *102*, 1478–1483.

Bibollet-Ruche, F., Bailes, E., Gao, F., Pourrut, X., Barlow, K.L., Clewley, J.P., Mwenda, J.M., Langat, D.K., Chege, G.K., McClure, H.M., et al. (2004). New simian immunodeficiency virus infecting De Brazza's monkeys (Cercopithecus neglectus): evidence for a cercopithecus monkey virus clade. J. Virol. *78*, 7748–7762.

Bieniasz, P.D. (2006). Late budding domains and host proteins in enveloped virus release. Virology *344*, 55–63.

Cabezas, A., Bache, K.G., Brech, A., and Stenmark, H. (2005). Alix regulates cortical actin and the spatial distribution of endosomes. J. Cell Sci. *118*, 2625–2635.

Chatellard-Causse, C., Blot, B., Cristina, N., Torch, S., Missotten, M., and Sadoul, R. (2002). Alix (ALG-2-interacting protein X), a protein involved in apoptosis, binds to endophilins and induces cytoplasmic vacuolization. J. Biol. Chem. *277*, 29108–29115.

Chen, C., Vincent, O., Jin, J., Weisz, O.A., and Montelaro, R.C. (2005). Functions of early (AP-2) and late (AIP1/ALIX) endocytic proteins in equine infectious anemia virus budding. J. Biol. Chem. *280*, 40474–40480.

Dejournett, R.E., Kobayashi, R., Pan, S., Wu, C., Etkin, L.D., Clark, R.B., Bogler, O., and Kuang, J. (2006). Phosphorylation of the proline-rich domain of XP95 modulates XP95 interaction with partner proteins. Biochem. J. *401*, 521–531.

Demirov, D.G., and Freed, E.O. (2004). Retrovirus budding. Virus Res. *106*, 87–102.

Demirov, D.G., Orenstein, J.M., and Freed, E.O. (2002). The late domain of human immunodeficiency virus type 1 p6 promotes virus release in a cell type-dependent manner. J. Virol. *76*, 105–117.

Gallop, J.L., and McMahon, H.T. (2005). BAR domains and membrane curvature: bringing your curves to the BAR. Biochem. Soc. Symp. *72*, 223–231.

Garrus, J.E., von Schwedler, U.K., Pornillos, O.W., Morham, S.G., Zavitz, K.H., Wang, H.E., Wettstein, D.A., Stray, K.M., Cote, M., Rich, R.L., et al. (2001). Tsg101 and the vacuolar protein sorting pathway are essential for HIV-1 budding. Cell *107*, 55–65.

Geminard, C., De Gassart, A., Blanc, L., and Vidal, M. (2004). Degradation of AP2 during reticulocyte maturation enhances binding of hsc70 and Alix to a common site on TFR for sorting into exosomes. Traffic *5*, 181–193.

Gottlinger, H.G., Dorfman, T., Sodroski, J.G., and Haseltine, W.A. (1991). Effect of mutations affecting the p6 gag protein on human immunodeficiency virus particle release. Proc. Natl. Acad. Sci. USA *88*, 3195–3199.

Gouet, P., Courcelle, E., Stuart, D.I., and Metoz, F. (1999). ESPript: analysis of multiple sequence alignments in PostScript. Bioinformatics *15*, 305–308.

Huang, M., Orenstein, J.M., Martin, M.A., and Freed, E.O. (1995). p6Gag is required for particle production from full-length human immunodeficiency virus type 1 molecular clones expressing protease. J. Virol. *69*, 6810–6818.

Hurley, J.H., and Emr, S.D. (2006). The ESCRT complexes: structure and mechanism of a membrane-trafficking network. Annu. Rev. Biophys. Biomol. Struct. *35*, 277–298.

Ichioka, F., Horii, M., Katoh, K., Terasawa, Y., Shibata, H., and Maki, M. (2005). Identification of Rab GTPase-activating protein-like protein (RabGAPLP) as a novel Alix/AIP1-interacting protein. Biosci. Biotechnol. Biochem. *69*, 861–865.

Katoh, K., Shibata, H., Suzuki, H., Nara, A., Ishidoh, K., Kominami, E., Yoshimori, T., and Maki, M. (2003). The ALG-2-interacting protein Alix associates with CHMP4b, a human homologue of yeast Snf7 that is involved in multivesicular body sorting. J. Biol. Chem. *278*, 39104–39113.

Kim, J., Sitaraman, S., Hierro, A., Beach, B.M., Odorizzi, G., and Hurley, J.H. (2005). Structural basis for endosomal targeting by the Bro1 domain. Dev. Cell *8*, 937–947.

Langelier, C., von Schwedler, U., Fisher, R.D., De Dominco, I., White, P.L., Hill, C.P., Kaplan, J., Ward, D., and Sundquist, W.I. (2006). Human ESCRT-II complex and its role in human immunodeficiency virus type 1 release. J. Virol. *80*, 9465–9480.

Luhtala, N., and Odorizzi, G. (2004). Bro1 coordinates deubiquitination in the multivesicular body pathway by recruiting Doa4 to endosomes. J. Cell Biol. *166*, 717–729.

Martin-Serrano, J., Zang, T., and Bieniasz, P.D. (2001). HIV-1 and Ebola virus encode small peptide motifs that recruit Tsg101 to sites of particle assembly to facilitate egress. Nat. Med. *7*, 1313–1319.

Martin-Serrano, J., Yaravoy, A., Perez-Caballero, D., and Bieniasz, P.D. (2003). Divergent retroviral late-budding domains recruit vacuolar protein sorting factors by using alternative adaptor proteins. Proc. Natl. Acad. Sci. USA *100*, 12414–12419.

Morita, E., and Sundquist, W.I. (2004). Retrovirus budding. Annu. Rev. Cell Dev. Biol. *20*, 395–425.

Odorizzi, G. (2006). The multiple personalities of Alix. J. Cell Sci. *119*, 3025–3032.

Odorizzi, G., Katzmann, D.J., Babst, M., Audhya, A., and Emr, S.D. (2003). Bro1 is an endosome-associated protein that functions in the MVB pathway in Saccharomyces cerevisiae. J. Cell Sci. *116*, 1893–1903.

Olsen, J.C. (1998). Gene transfer vectors derived from equine infectious anemia virus. Gene Ther. *5*, 1481–1487.

Pineda-Molina, E., Belrhali, H., Piefer, A.J., Akula, I., Bates, P., and Weissenhorn, W. (2006). The crystal structure of the C-terminal domain of Vps28 reveals a conserved surface required for Vps20 recruitment. Traffic *7*, 1007–1016.

Puffer, B.A., Parent, L.J., Wills, J.W., and Montelaro, R.C. (1997). Equine infectious anemia virus utilizes a YXXL motif within the late assembly domain of the Gag p9 protein. J. Virol. *71*, 6541–6546.

Qin, X.F., An, D.S., Chen, I.S., and Baltimore, D. (2003). Inhibiting HIV-1 infection in human T cells by lentiviral-mediated delivery of small interfering RNA against CCR5. Proc. Natl. Acad. Sci. USA *100*, 183–188.

Sadoul, R. (2006). Do Alix and ALG-2 really control endosomes for better or for worse? Biol. Cell *98*, 69–77.

Schmidt, M.H., Chen, B., Randazzo, L.M., and Bogler, O. (2003). SETA/CIN85/Ruk and its binding partner AIP1 associate with diverse cytoskeletal elements, including FAKs, and modulate cell adhesion. J. Cell Sci. *116*, 2845–2855.

Schmidt, M.H., Hoeller, D., Yu, J., Furnari, F.B., Cavenee, W.K., Dikic, I., and Bogler, O. (2004). Alix/AIP1 antagonizes epidermal growth factor receptor downregulation by the Cbl-SETA/CIN85 complex. Mol. Cell. Biol. *24*, 8981–8993.

Schmidt, M.H., Dikic, I., and Bogler, O. (2005). Src phosphorylation of Alix/AIP1 modulates its interaction with binding partners and antagonizes its activities. J. Biol. Chem. *280*, 3414–3425.

Segura-Morales, C., Pescia, C., Chatellard-Causse, C., Sadoul, R., Bertrand, E., and Basyuk, E. (2005). Tsg101 and Alix interact with murine leukemia virus Gag and cooperate with Nedd4 ubiquitin ligases during budding. J. Biol. Chem. *280*, 27004–27012.

Shibata, H., Yamada, K., Mizuno, T., Yorikawa, C., Takahashi, H., Satoh, H., Kitaura, Y., and Maki, M. (2004). The penta-EF-hand protein ALG-2 interacts with a region containing PxY repeats in Alix/AIP1, which is required for the subcellular punctate distribution of the amino-terminal truncation form of Alix/AIP1. J. Biochem. (Tokyo) *135*, 117–128.

Strack, B., Calistri, A., Craig, S., Popova, E., and Gottlinger, H.G. (2003). AIP1/ALIX is a binding partner for HIV-1 p6 and EIAV p9 functioning in virus budding. Cell *114*, 689–699.

Tsuda, M., Seong, K.H., and Aigaki, T. (2006). POSH, a scaffold protein for JNK signaling, binds to ALG-2 and ALIX in Drosophila. FEBS Lett. *580*, 3296–3300.

van der Goot, F.G., and Gruenberg, J. (2006). Intra-endosomal membrane traffic. Trends Cell Biol. *16*, 514–521.

VerPlank, L., Bouamr, F., LaGrassa, T.J., Agresta, B., Kikonyogo, A., Leis, J., and Carter, C.A. (2001). Tsg101, a homologue of ubiquitin-conjugating (E2) enzymes, binds the L domain in HIV type 1 Pr55Gag. Proc. Natl. Acad. Sci. USA *98*, 7724–7729.

Vincent, O., Rainbow, L., Tilburn, J., Arst, H.N., Jr., and Penalva, M.A. (2003). YPXL/I is a protein interaction motif recognized by aspergillus PalA and its human homologue, AIP1/Alix. Mol. Cell. Biol. *23*, 1647–1655.

von Schwedler, U.K., Stuchell, M., Muller, B., Ward, D.M., Chung, H.Y., Morita, E., Wang, H.E., Davis, T., He, G.P., Cimbora, D.M., et al. (2003). The protein network of HIV budding. Cell *114*, 701–713.

Wang, M.Q., Kim, W., Gao, G., Torrey, T.A., Morse, H.C., 3rd, De Camilli, P., and Goff, S.P. (2003). Endophilins interact with Moloney murine leukemia virus Gag and modulate virion production. J. Biol. *3*, 4.

Accession Numbers

Coordinates and data have been deposited into the Protein Data Bank (www.pdb.org; PDB codes 20EV, 20EW, and 20EX).

Cell, Volume *128*

Supplemental Data

Structural and Biochemical Studies of ALIX/AIP1 and Its Role in Retrovirus Budding

Robert D. Fisher, Hyo-Young Chung, Qianting Zhai, Howard Robinson, Wesley I. Sundquist, and Christopher P. Hill

SUPPLEMENTAL EXPERIMENTAL METHODS

Plasmid Construction

ALIX Protein Expression Constructs. ALIX coding sequences were amplified and subcloned from an EST clone (von Schwedler et al., 2003), and ALIX proteins were expressed as either 6x-His or GST N-terminal fusion proteins. For $ALIX_{Bro1\text{-}V}$ (residues 1-698) and $ALIX_{V}$ (residues 360-702), ALIX coding sequences were amplified with 5'*Nde*I and 3'*BamH*I restriction sites and inserted into the pET151/D-TOPO vector (Invitrogen) following the manufacturer's instructions. $ALIX_{Bro1}$ (residues 1-359) was cloned between 5'*Nde*I and 3'*BamH*I restriction sites in a modified pET16b vector (Novagen) designed to contain a TEV protease cleavage site following the 6x-His tag. GST-ALIX expression constructs were generated by inserting ALIX coding sequences between 5'*Nde*I and 3'*BamH*I restriction sites in a pGEX2T vector (GE Healthcare) modified to contain a TEV protease cleavage site and 5'*Nde*I and 3'*BamH*I/*Bgl*II restriction sites following the GST gene (pGEX2T-TEV).

HIV-1 $p6_{Gag}$ and EIAV $p9^{Gag}$ Expression Constructs. Genes encoding $HIV\text{-}1_{NL4\text{-}3}$ $p6^{Gag}$ and EIAV $p9^{Gag}$ were amplified from the proviral R9 and pEV53B plasmids (see below), with 5'*Nde*I and 3'*BamH*I restriction sites, to allow expression as GST fusion proteins

from a pGEX2T vector (GE Healthcare) modified to contain 5'*Nde*I and 3'*BamH*I cloning sites (Garrus et al., 2001; von Schwedler et al., 2003). ALIX point mutants were generated by the Quickchange (Stratagene) method, following the manufacturer's protocol.

GST-CHMP4A Expression Construct. The GST-CHMP4A expression construct used in GST pulldown experiments was described previously (von Schwedler et al., 2003). Note, however, that the CHMP4A and CHMP4B designations have been reversed from our previous publication to follow the convention of Katoh et al. (Katoh et al., 2003).

ALIX Mammalian Expression Vector. FLAG-tagged human ALIX DNA was amplified and an *Nde*I-*BamH*I fragment was subcloned into a pCI-neo vector (Promega) engineered to express the protein with an N-terminal FLAG epitope tag. ALIX mutants were constructed using the quick change method following manufacturer's instruction (Stratagene).

Virus Expression Constructs. HIV-1 proviral expression constructs were based on HIV-1_{NL4-3} R9ΔApa (Swingler et al., 1997) (a gift from Didier Trono, University of Lausanne). The HIV-1 $p6^{Gag}$ ΔPTAP construct has been described previously (Garrus et al., 2001). The HIV-1 $p6^{Gag}$ ΔYP was constructed using megaprimer mutagenesis to introduce the $_{36}YP_{37}$ to $_{36}SR_{37}$ mutation in $p6^{Gag}$ without altering the overlapping pol reading frame. The vector pEV53B (Olsen, 1998) (a gift from John Olsen, UNC Chapel Hill) was used to produce EIAV virus like particles, and the $_{23}YP_{24}$ to $_{23}SR_{24}$ mutation was introduced using the megaprimer method.

shRNA Lentiviral Vector for ALIX Depletion. An shRNA targeting human ALIX nucleotides 1765-1783 (Chen et al., 2005), was built into the FG12 lentiviral delivery

vector (Qin et al., 2003) (a gift from David Baltimore, Caltech). Lentiviral vectors packing this shRNA expression construct were produced in 293T cells by calcium phosphate co-transfection (8.1 µg FG12-ALIX shRNA, 8.1 µg pCMVΔR8.91 (Zufferey et al., 1997), and 2.7 µg pMD.G (Ory et al., 1996), 10 cm plate, ~4×10^6). Virus like particles were collected from the cell culture supernatants on the third day posttransfection and concentrated 200-fold by centrifugation through a 20% sucrose cushion.

Purification of Recombinant ALIX Proteins

$ALIX_{Bro1-V}$, $ALIX_{Bro1}$, and $ALIX_V$ were expressed as 6x-His N-terminal fusion proteins in BL21(DE3) Codon+ (RIL) *E. coli* grown in auto-induction media, ZYP-5052 (Studier, 2005), at 37°C for 5-6 hours with vigorous shaking in baffled flasks before moving to 23°C to grow to saturation within 16-18 hours. SeMet $ALIX_V$ was prepared by expression in PASM-5052 media (Studier, 2005). Subsequent purification steps were performed at 4°C unless noted. Cells were lysed with sonication and lysozyme treatment (2.5 mg/ml in 50 mM Tris pH 8.0, 300 mM NaCl, 10 mM imidazole). Clarified supernatant was applied to Ni^{2+}-NTA resin (Qiagen), washed with lysis buffer, and eluted with 25 mM Tris pH 8.0, 100 mM NaCl, 250 mM imidazole. For $ALIX_{Bro1}$, EDTA and DTT were added to 1 mM and the solution was diluted to 50 mM NaCl with ddH_2O. For $ALIX_{Bro1-V}$ and $ALIX_V$, the eluted protein was dialyzed against 25 mM Tris pH 8.0, 100 mM NaCl, 2 mM β-mercaptoethanol while incubating with TEV protease (~18 h, 23°C), and the processed protein was collected as flow-through from a second pass over Ni^{2+}-NTA resin and diluted to 50 mM NaCl. For all three constructs, protein

solutions were applied to a Q Sepharose FF column (GE Healthcare) and washed with 25 mM Tris pH 8.0, 50 mM NaCl, 1 mM DTT before eluting with a gradient to 1 M NaCl. Monomeric ALIX was separated from dimer ($ALIX_{Bro1\text{-}V}$ and $ALIX_V$ samples) and aggregated species by size exclusion chromatography in 10 mM Tris pH 8.0, 100 mM NaCl, 1 mM DTT: $ALIX_{Bro1\text{-}V}$ (Superdex 200, GE Healthcare), $ALIX_{Bro1}$ and $ALIX_V$ (Superdex 75, GE Healthcare). In the case of $ALIX_{Bro1\text{-}V}$ and $ALIX_V$, monomeric ALIX was the predominant species, while dimeric ALIX was present in a much lower percentage. Furthermore, rigorous equilibrium analytical ultracentrifugation showed that monomeric $ALIX_V$ remained monomeric and that there was no appreciable equilibrium between monomer and dimer species.

Purification of Recombinant HIV-1 $p6^{Gag}$ and EIAV $p9^{Gag}$

GST-$p6^{Gag}$ and GST-$p9^{Gag}$ were expressed and lysed (50 mM Tris pH 8.0, 300 mM NaCl, 1 mM DTT) as for ALIX constructs. Clarified lysate was applied to a Glutathione GSTPrep column (GE Healthcare), washed, and eluted with lysis buffer supplemented with 20 mM glutathione. Protein fractions were combined, made to 2.5 mM $CaCl_2$, and incubated with thrombin (Novagen). Free GST and uncut GST fusion protein was separated from free HIV-1 p6 or EIAV p9 by size exclusion chromatography (Superdex 75, GE Healthcare) in 20 mM NaPhosphate pH 7.2, 150 mM NaCl. Residual GST was removed by an additional pass through the Glutathione GSTPrep column.

ALIX Crystallization and Data Collection

All crystals were grown in sitting drops using protein concentrated to 10 mg/ml in the size exclusion chromatography solution. SeMet $ALIX_V$ crystals grew at 4°C with a reservoir of 0.16-0.20 M Magnesium formate and 14% PEG-3350, and a drop of 1-2 μL reservoir and 2 μL protein solution. $ALIX_{Bro1}$ and $ALIX_{Bro1\text{-}V}$ both crystallized best at 13°C in drops with equal (0.5 – 2.0 μL) volumes of protein and reservoir solution: $ALIX_{Bro1}$ — 0.1 M NaMES pH 6.5, 10% PEG-20,000. $ALIX_{Bro1\text{-}V}$ – 8-9% PEG 4000, 0.10-0.25 M ammonium acetate, 0.10-0.15 M Magnesium acetate, 0.05 M Hepes pH 7.0.

$ALIX_{Bro1}$ and $ALIX_V$ crystals were cryoprotected in solutions of reservoir made up with 20% glycerol ($ALIX_V$; 5% and 10% intermediate steps). $ALIX_{Bro1\text{-}V}$ cryoprotection used reservoir made up with 30% MPD, achieved in 5% increments. Crystals were suspended in a nylon loop, plunged into liquid nitrogen, and maintained at 100 K during data collection. Crystallographic statistics are given in Supplemental Table S1.

ALIX Structure Solution and Refinement

The $ALIX_V$ structure was determined by the SAD method. The top 8 Se sites located with SHELX (Schneider and Pape, 2004; Sheldrick and Schneider, 1997) were used in SOLVE/RESOLVE (Terwilliger, 2002) to estimate phases at 3.1 Å. Phases were further improved in SIGMAA (Read, 1986) by averaging estimates obtained from two crystals, and used with amplitudes of crystal 1 for map calculation. Initial polyalanine models were built for the two molecules in the asymmetric unit and used to guide averaging of the map separately over the regions of arm1 and arm2 using MAMA

(Kleywegt and Jones, 1999) and AVE (Jones, 1992). This improved map allowed fitting of the amino acid sequence.

The $ALIX_{Bro1}$ and $ALIX_{Bro1\text{-}V}$ structures were solved by molecular replacement using PHASER (McCoy et al., 2005). The search model for $ALIX_{Bro1}$ was a mixed poly-Ser/homology model based on the yeast Bro1 structure (pdb code 1ZB1) (Kim et al., 2005). Search models for $ALIX_{Bro1\text{-}V}$ were the refined structures of $ALIX_{Bro1}$ and the two arms of $ALIX_{V}$. Modelbuilding was with O (Jones et al., 1991) and COOT (Emsley and Cowtan, 2004). Structures were refined with CNS (Brunger et al., 1998) and in the final cycles using REFMAC5 with TLS refinement using TLSMD (Merritt and Painter, 2006; Painter and Merritt, 2006), and TLSANL (Howlin et al., 1993) in the CCP4 suite (Group, November 4. 1994). Figures of the structure were generated in PyMol (DeLano, 2002). Coordinates and data have been deposited in the Protein Data Bank, www.pdb.org (PDB code 2OEV, 2OEW, 2OEX).

SUPPLEMENTAL REFERENCES

Brunger, A.T., Adams, P.D., Clore, G.M., DeLano, W.L., Gros, P., Grosse-Kunstleve, R.W., Jiang, J.S., Kuszewski, J., Nilges, M., Pannu, N.S., *et al.* (1998). Crystallography & NMR system: A new software suite for macromolecular structure determination. Acta Crystallogr. D Biol. Crystallogr. *54 (Pt 5)*, 905-921.

Chen, C., Vincent, O., Jin, J., Weisz, O.A., and Montelaro, R.C. (2005). Functions of early (AP-2) and late (AIP1/ALIX) endocytic proteins in equine infectious anemia virus budding. J. Biol. Chem. *280*, 40474-40480.

DeLano, W.L. (2002). The PyMOL Molecular Graphics System and Users Manual (San Carlos, CA, DeLano Scientific).

Emsley, P., and Cowtan, K. (2004). Coot: model-building tools for molecular graphics. Acta Crystallogr. D Biol. Crystallogr. *60*, 2126-2132.

Garrus, J.E., von Schwedler, U.K., Pornillos, O.W., Morham, S.G., Zavitz, K.H., Wang, H.E., Wettstein, D.A., Stray, K.M., Cote, M., Rich, R.L., *et al.* (2001). Tsg101 and the vacuolar protein sorting pathway are essential for HIV-1 budding. Cell *107*, 55-65.

Group, C.C.P. (November 4. 1994). The CCP4 Suite:Programs for Protein Crystallography. Acta Crystallogr. D50, 760-763.

Holm, L., and Sander, C. (1998). Touring protein fold space with Dali/FSSP. Nucleic Acids Res. *26*, 316-319.

Howlin, B., Butler, S.A., Moss, D.S., Harris, G.W., and Driessen, H.P.C. (1993). TLSANL: TLS parameter analysis program for segmented anisotropic refinement of macromolecular structures. J. Appl. Crystallogr. *26*, 622-624.

Johnsson, B., Lofas, S., and Lindquist, G. (1991). Immobilization of proteins to a carboxymethyldextran-modified gold surface for biospecific interaction analysis in surface plasmon resonance sensors. Anal Biochem. *198*, 268-277.

Jones, T.A. (1992). A, yaap, asap, @#*? A set of averaging programs. In Molecular Replacement, E.J. Dodson, S. Gover, and W. Wolf, eds. (Warrington, SERC Daresbury Laboratory), pp. 91-105.

Jones, T.A., Zou, J.Y., Cowan, S.W., and Kjeldgaard (1991). Improved methods for binding protein models in electron density maps and the location of errors in these models. Acta Crystallogr. A *47 (Pt 2)*, 110-119.

Katoh, K., Shibata, H., Suzuki, H., Nara, A., Ishidoh, K., Kominami, E., Yoshimori, T., and Maki, M. (2003). The ALG-2-interacting protein ALIX associates with CHMP4b, a human homologue of yeast Snf7 that is involved in multivesicular body sorting. J. Biol. Chem.

Kim, J., Sitaraman, S., Hierro, A., Beach, B.M., Odorizzi, G., and Hurley, J.H. (2005). Structural basis for endosomal targeting by the Bro1 domain. Dev. Cell *8*, 937-947.

Kleywegt, G.J., and Jones, T.A. (1999). Software for handling macromolecular envelopes. Acta Crystallogr. D Biol. Crystallogr. *55*, 941-944.

Laskowski, R.A., MacArthur, M.W., Moss, D.S., and Thornton, J.M. (1993). PROCHECK: a program to check the stereochemical quality of protein structures. J. Appl. Crystallogr. *26*, 283-291.

McCoy, A.J., Grosse-Kunstleve, R.W., Storoni, L.C., and Read, R.J. (2005). Likelihood-enhanced fast translation functions. Acta Crystallogr. D Biol. Crystallogr. *61*, 458-464.

Merritt, E.A., and Painter, J. (2006). TLSMD web server for the generation of multi-group TLS models. J. Appl. Crystallogr. *39*.

Myszka, D.G. (1999). Improving biosensor analysis. J. Mol. Recognit. *12*, 279-284.

Olsen, J.C. (1998). Gene transfer vectors derived from equine infectious anemia virus. Gene Ther. *5*, 1481-1487.

Ory, D.S., Neugeboren, B.A., and Mulligan, R.C. (1996). A stable human-derived packaging cell line for production of high titer retrovirus/vesicular stomatitis virus G pseudotypes. Proc. Natl. Acad. USA *93*, 11400-11406.

Otwinowski, Z., and Minor, W. (1997). Processing of X-ray diffraction data collected in oscillation mode. Methods in Enzymol. *276*, 307-326.

Painter, J., and Merritt, E.A. (2006). Optimal description of a protein structure in terms of multiple groups undergoing TLS motion. Acta Crystallogr. D Biol. Crystallogr. *62*, 439-450.

Qin, X.F., An, D.S., Chen, I.S., and Baltimore, D. (2003). Inhibiting HIV-1 infection in human T cells by lentiviral-mediated delivery of small interfering RNA against CCR5. Proc. Natl. Acad. USA *100*, 183-188.

Read, R. (1986). Improved Fourier coefficients for maps using phases from partial structures with errors. Acta Crystallogr. A *42*, 140-149.

Schneider, T., and Pape, T. (2004). HKL2MAP: a graphical user interface for phasing with SHELX programs. J. Appl. Crystallogr. *37*, 843-844.

Sheldrick, G.M., and Schneider, T. (1997). SHELXL: High resolution refinement. Methods Enzymol. *277*, 319-343.

Studier, F.W. (2005). Protein production by auto-induction in high density shaking cultures. Protein Expr. Purif. *41*, 207-234.

Swingler, S., Gallay, P., Camaur, D., Song, J., Abo, A., and Trono, D. (1997). The Nef protein of human immunodeficiency virus type 1 enhances serine phosphorylation of the viral matrix. J. Virol. *71*, 4372-4377.

Terwilliger, T.C. (2002). Automated structure solution, density modification and model building. Acta Crystallogr. D Biol. Crystallogr. *58*, 1937-1940.

Thompson, J.D., Higgins, D.G., and Gibson, T.J. (1994). CLUSTAL W: improving the sensitivity of progressive multiple sequence alignment through sequence weighting, position-specific gap penalties and weight matrix choice. Nucleic Acids Res. *22*, 4673-4680.

von Schwedler, U.K., Stuchell, M., Muller, B., Ward, D.M., Chung, H.Y., Morita, E., Wang, H.E., Davis, T., He, G.P., Cimbora, D.M.*, et al.* (2003). The protein network of HIV budding. Cell *114*, 701-713.

Zufferey, R., Nagy, D., Mandel, R.J., Naldini, L., and Trono, D. (1997). Multiply attenuated lentiviral vector achieves efficient gene delivery in vivo. Nat. Biotechnol. *15*, 871-875.

Table S1. Data Collection and Refinement Statistics

	$ALIX_{Bro1-V}$ [a]	$ALIX_{Bro1}$ [a]	$ALIX_V$ [a]	
Data Collection [b]				
			Crystal 1	Crystal 2
Space Group	C2	C2	$P2_1$	$P2_1$
Cell Parameters (Å)	a = 144.0	a = 120.7	a = 63.9	a = 63.2
	b = 98.5	b = 63.2	b = 50.0	b = 49.8
	c = 72.2	c = 76.4	c = 130.2	c = 129.6
	ß = 105.6	ß = 122.1	ß = 101.1	ß = 101.2
Wavelength (Å)	1.1	1.54180	0.9792	0.9792
Resolution (Å)	30-3.30	30-2.55	50-2.60	50-2.60
Outer Shell (Å)	3.42-3.30	2.64-2.55	2.69-2.60	2.69-2.60
Number of reflections				
Total	727,803	178,235	1,048,903	1,677,930
Unique	14,236	15,487	23,601	22,229
Completeness (%)	94.6 (64.9)	96.5 (79.3)	92.4 (64.0)	89.8 (57.7)
R_{sym} (%)[b]	8.7 (28.8)	5.3 (24.0)	7.8 (20.4)	10.6 (29.7)
Mean I/s(I)	21.1 (3.5)	19.6 (3.6)	12.3 (3.6)	16.1 (3.2)
Refinement				
R factor/R_{free} (%)[c,d]	23.5/31.7	20.8/27.4	22.8/30.2	
Nonhydrogen atoms				
Total	5486	2910	5489	
Solvent	0	79	91	
RMSD from ideal geometry [e]				
Bond lengths (Å)	0.009	0.016	0.010	
Bond angles (º)	1.153	1.544	1.293	
Average B-factor ($Å^2$)	140.7	60.3	48.5	
Ramachandran plot, nonglycine residue in				
Most favorable region (%)	83.7	88.8	93.9	
Additional allowed region (%)	15.7	10.3	6.0	
Generous allowed region (%)	0.6	0.9	0.2	
Disallowed region (%)	0.0	0	0.0	

Values in parenthesis are for the highest resolution shell.

[a] The $ALIX_{Bro1-V}$ construct crystallized comprises ALIX residues Met1-Arg698 preceded by the vector sequence GIDPFTH. Of these, ALIX residues 2-698 are ordered in the refined model. The $ALIX_{Bro1}$ construct comprises ALIX residues Met1-Val359 preceded by MHHHHHHHHHHSGQNLYFQGH, and ALIX residues 1-358 are ordered. The $ALIX_V$ construct comprises ALIX residues Pro360-Arg702 preceded by GIDPFTHM, and ALIX residues 361-702 (molecule A) and 362-702 (molecule B) are ordered.

[b] Data were collected from single crystals at beamline X29 at the National Synchrotron Light Source, Brookhaven National Laboratory ($ALIX_V$ and $ALIX_{Bro1-V}$) or on a rotating anode source ($ALIX_{Bro1}$). Data were integrated and scaled with the HKL package (Otwinowski and Minor, 1997).

[b] $R_{sym} = (|(\sum I - \langle I \rangle)|)/(\sum I)$, where $\langle I \rangle$ is the average intensity of multiple measurements.

[c] R factor = $\sum_{hkl}||F_{obs}(hkl)|| - F_{calc}(hkl)||/\sum_{hkl}|F_{obs}(hkl)|$

[d] R_{free} = the crossvalidation R factor for 5% of reflections against which the model was not refined (7% for $ALIX_{Bro1-V}$).

[e] Geometry was analyzed in PROCHECK (Laskowski et al., 1993)

Table S2. ALIX Binding to HIV-1 $p6^{Gag}$ and EIAV $p9^{Gag}$

	Estimated Dissociation Constant (μM, 20°C)[a]				
	$ALIX_{Bro1\text{-}V}$ (WT)	$ALIX_V$ (WT)	$ALIX_V$ ($V_{498}D$)	$ALIX_V$ ($F_{676}D$)	$ALIX_V$ ($I_{683}D$)
HIV-1 $p6^{Gag}$	57 ± 21[b]	59 ± 15[b]	NB[c]	NB[c]	>1000[d]
HIV-1 $p6^{Gag}$ ΔYP	>1000[d]	>1000[d]	-	-	-
EIAV $p9^{Gag}$	1.5 ± 0.3[b]	1.2 ± 0.3[b]	18 ± 1	NB[b]	580 ± 20
EIAV $p9^{Gag}$ ΔYP	>1000[d]	>1000[d]	-	-	-

[a]Binding was measured using Biacore 2000 and 3000 optical biosensors (Biacore AB, Uppsala, Sweden) equipped with CM4 sensor chips derivatized with anti-GST antibodies through amine-coupling (Johnsson et al., 1991). GST (control) and GST-ALIX fusion proteins were captured from crude *E. coli* lysates to densities of 1000-1800 RU, and chip surfaces were over-coated with recombinant GST to minimize non-specific interactions. Purified wild-type and mutant HIV-1 $p6^{Gag}$ and EIAV $p9^{Gag}$ were diluted in running buffer (20 mM NaPhosphate, 150 mM NaCl, 0.2 mg/mL BSA, 0.005% P20, pH 7.2), and injected in duplicate from concentrations of 0 μM to 1000 μM. Affinity parameters were obtained by plotting the equilibrium responses against the analyte concentration and fitting to a simple 1:1 binding model (e.g., see Figure 3A)(Myszka, 1999).

[b]Average ± difference between 8 ($ALIX_{Bro1\text{-}V}$) or 6 ($ALIX_V$) independent measurements (errors in other measurements were estimated from statistical fits of the binding data).

[c]NB = No detectable binding.

[d]Weak binding was detectable, but could not be accurately quantified because half-maximal binding was not achieved.

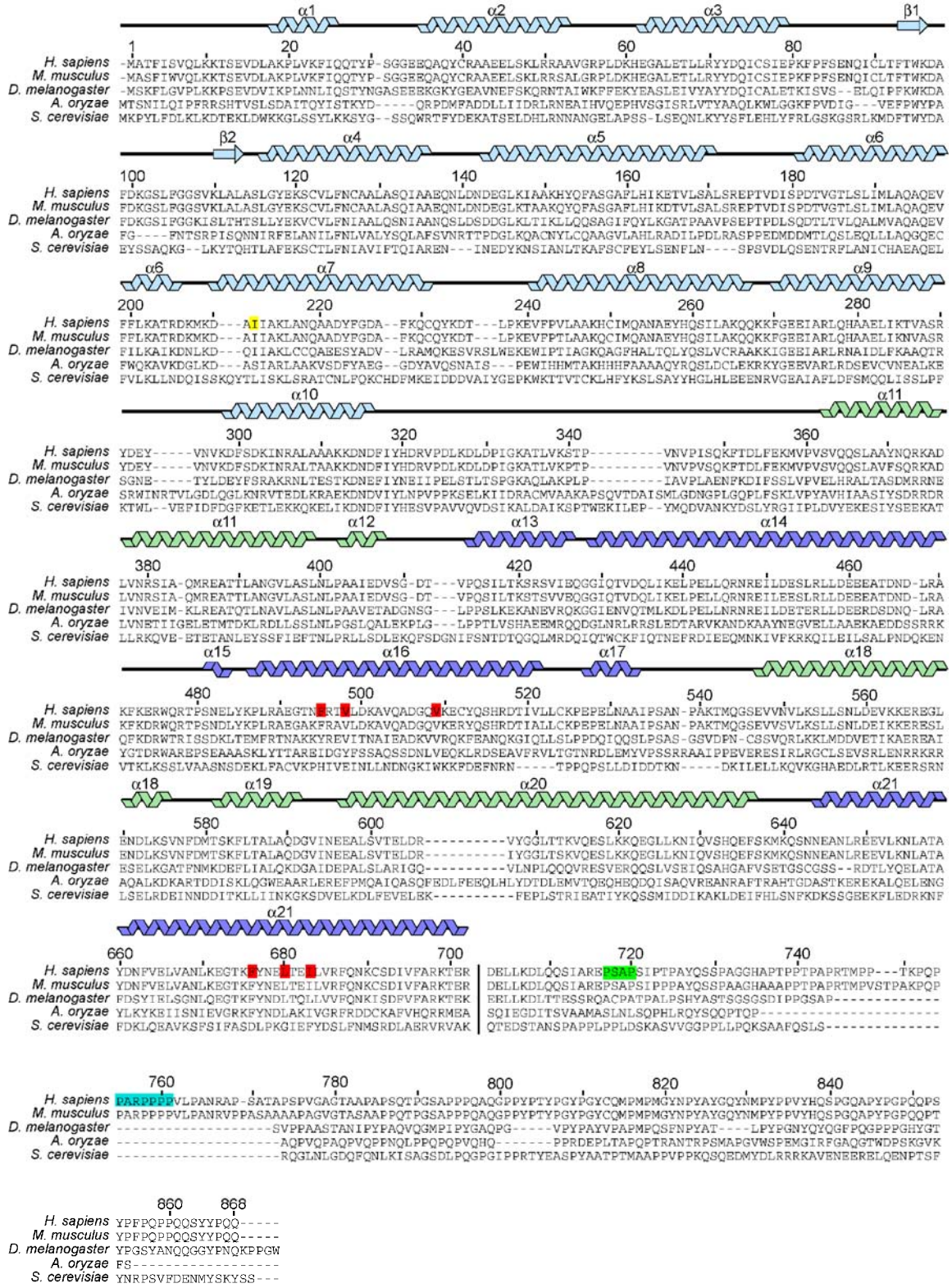
α1 α2 α3 β1
1 20 40 60 80
H. sapiens -MATFISVQLKKTSEVDLAKPLVKFIQQTYP-SGGEEQAQYCRAAEELSKLRRAAVGRPLDKHEGALETLLRYYDQICSIEPKFPFSENQICLTFTWKDA
M. musculus -MASFIWVQLKKTSEVDLAKPLVKFIQQTYP-SGGEEQAQYCRAAEELSKLRRSALGRPLDKHEGALETLLRYYDQICSIEPKFPFSENQICLTFTWKDA
D. melanogaster -MSKFLGVPLKKPSEVDVIKPLNNLIQSTYNGASEEEKGKYGEAVNEFSKQRNTAIWKPFEKYEASLEIVYAYYDQICALETKISVS--ELQIPFKWKDA
A. oryzae MTSNILQIPFRRRSHTVSLSDAITQYISTKYD-----QRPDMFADDLLIIDRLRNEAIHVQEPHVSGISRLVTYAAQLKWLGGKFPVDIG---VEFPWYPA
S. cerevisiae MKPYLFDLKLKDTEKLDWKKGLSSYLKKSYG--SSQWRTFYDEKATSELDHLRNNANGELAPSS-LSEQNLKYYSFLEHLYFRLGSKGSRLKMDFTWYDA
β2 α4 α5 α6
100 120 140 160 180
H. sapiens FDKGSLFGGSVKLALASLGYEKSCVLFNCAALASQIAAEQNLDNDEGLKIAAKHYQFASGAFLHIKETVLSALSREPTVDISPDTVGTLSLIMLAQAQEV
M. musculus FDKGSLFGGSVKLALASLGYEKSCVLFNCAALASQIAAEQNLDNDEGLKTAAKQYQFASGAFLHIKDTVLSALSREPTVDISPDTVGTLSLIMLAQAQEV
D. melanogaster FDKGSIFGGKISLTHTSLLYEKVCVLFNIAALQSNIAANQSLDSDDGLKLTIKLLQQSAGIFQYLKGATPAAVPSEPTPDLSQDTLTVLQALMVAQAQEV
A. oryzae FG----FNTSRPISQNNIRFELANILFNLVALYSQLAFSVNRTTPDGLKQACNYLCQAAGVLAHLRADILPDLRASPPEDMDDMTLQSLEQLLLAQGQEC
S. cerevisiae EYSSAQKG--LKYTQHTLAFEKSCTLFNIAVIFTQIAREN---INEDYKNSIANLTKAFSCFEYLSENFLN----SPSVDLQSENTRFLANICHAEAQEL
α6 α7 α8 α9
200 220 240 260 280
H. sapiens FFLKATRDKMKD---AIIAKLANQAADYFGDA--FKQCQYKDT---LPKEVFPVLAAKHCIMQANAEYHQSILAKQQKKFGEEIARLQHAAELIKTVASR
M. musculus FFLKATRDKMKD---AIIAKLANQAADYFGDA--FKQCQYKDT---LPKEVFPTLAAKQCIMQANAEYHQSILAKQQKKFGEEIARLQHAAELIKNVASR
D. melanogaster FILKAIKDNLKD---QIIAKLCCQAEESYADV--LRAMQKESVRSLWEKEWIPTIAGKQAGFHALTQLYQSLVCRAAKKIGEEIARLRNAIDLFKAAQTR
A. oryzae FWQKAVKDGLKD---ASIARLAAKVSDFYAEG--GDYAVQSNAIS---PEWIHHMTAKHHHFAAAAQYRQSLDCLEKRKYGEEVARLRDSEVCVNEALKE
S. cerevisiae FVLKLLNDQISSKQYTLISKLSRATCNLFQKCHDFMKEIDDDVAIYGEPKWKTTVTCKLHFYKSLSAYYHGLHLEEENRVGEAIAFLDFSMQQLISSLPF
α10 α11
300 320 340 360
H. sapiens YDEY-----VNVKDFSDKINRALAAAKKDNDFIYHDRVPDLKDLDPIGKATLVKSTP---------VNVPISQKFTDLFEKMVPVSVQQSLAAYNQRKAD
M. musculus YDEY-----VNVKDFSDKINRALTAAKKDNDFIYHDRVPDLKDLDPIGKATLVKPTP---------VNVPVSQKFTDLFEKMVPVSVQQSLAVFSQRKAD
D. melanogaster SGNE-----TYLDEYFSRAKRNLTESTKDNEFIYNEIIPELSTLTSPGKAQLAKPLP---------IAVPLAENFKDIPSSLVPVELHRALTASDMRRNE
A. oryzae SRWINRTVLGDLQGLKNRVTEDLKRAEKDNDVIYLNPVPPKSELKIIDRACMVAAKAPSQVTDAISMLGDNGPLGQPLFSKLVPYAVHIAASIYSDRRDR
S. cerevisiae KTWL--VEPIDFDGFKETLEKKQKELIKDNDFIYHESVPAVVQVDSIKALDAIKSPTWEKILEP--YMQDVANKYDSLYRGIIPLDVYEKESIYSEEKAT
α11 α12 α13 α14
380 400 420 440 460
H. sapiens LVNRSIA-QMREATTLANGVLASLNLPAAIEDVSG-DT---VPQSILTKSRSVIEQGGIQTVDQLIKELPELLQRNREILDESLRLLDEBEATDND-LRA
M. musculus LVNRSIA-QMREATTLANGVLASLNLPAAIEDVSG-DT---VPQSILTKSTSVVEQGGIQTVDQLIKELPELLQRNREILEESLRLLDEBEATDND-LRA
D. melanogaster IVNVEIM-KLREATQTLNAVLASLNLPAAVETADGNSG---LPPSLKEKANEVRQKGGIENVQTMLKDLPELLNRNREILDETERLLDEERDSDNQ-LRA
A. oryzae LVNETIIGELETMTDKLRDLLSSLNLPGSLQALEKPLG---LPPTLVSHAEEMRQQDGLNRLRRSLEDTARVKANDKAAYNEGVELLAAEKAEDDSSRRK
S. cerevisiae LLRKQVE-ETETANLEYSSFIEFTNLPRLLSDLEKQFSDGNIFSNTDTQGQLMRDQIQTWCKFIQTNEFRDIEEQMNKIVFKRKQILEILSALPNDQKEN
α15 α16 α17 α18
480 500 520 540 560
H. sapiens KFKERWQRTPSNELYKPLRAEGTNERTNLDKAVQADGQKECYQSHRDTIVLLCKPEPELNAAIPSAN-PAKTMQGSEVVNVLKSLLSNLDEVKKEREGL
M. musculus KFKDRWQRTPSNDLYKPLRAEGAKFRAVLDKAVQADGQVKERYQSHRDTIALLCKPEPELNAAIPSAN-PAKTMQGSEVVSVLKSLLSNLDEIKKERESL
D. melanogaster QFKDRWTRISSDKLTEMFRTNAKKYREVITNAIEADKVVRQKFEANQKGIQLLSLPPDQIQQSLPSAS-GSVDPN-CSSVQRLKKLMDDVETIKAEREAI
A. oryzae YGTDRWAREPSEAAASKLYTTAREIDGYFSSAQSSDNLVEQKLRDSEAVFRVLTGTNRDLEMYVPSSRRAAIPPEVERESIRLRGCLSEVSRLENRRKRR
S. cerevisiae VTKLKSSLVAASNSDEKLFACVKPHIVEINLLNDNGKIWKKFDEFNRN-----TPPQPSLLDIDDTKN-----DKILELLKQVKGHAEDLRTLKEERSRN
α18 α19 α20 α21
580 600 620 640
H. sapiens ENDLKSVNFDMTSKFLTALAQDGVINEEALSVTELDR----------VYGGLTTKVQESLKKQEGLLKNIQVSHQEFSKMKQSNNEANLREEVLKNLATA
M. musculus ENDLKSVNFDMTSKFLTALAQDGVINEEALSVTELDR----------IYGGLTSKVQESLKKQEGLLKNIQVSHQEFSKMKQSNNEANLREEVLKNLATA
D. melanogaster ESELKGATFNMKDEFLIALQKDGAIDEPALSLARIGQ----------VLNPLQQQVRESVERQQSLVSEIQSAHGAFVSETGSCGSS--RDTLYQELATA
A. oryzae AQALKDKARTDDISKLQGWEAARLEREFPMQAIQASQFEDLFEEQLHLYDTDLEMVTQEQHEQDQISAQVREANRAFTRAHTGDASTKEREKALQELENG
S. cerevisiae LSELRDEINNDDITKLLIINKGKSDVELKDLFEVELEK----------FEPLSTRIEATIYKQSSMIDDIKAKLDEIFHLSNFKDKSSGEEKFLEDRKNF
α21
660 680 700 720 740
H. sapiens YDNFVELVANLKEGTKEYNEITELLVRFQNKCSDIVFARKTER | DELLKDLQQSIAREPSAPSIPTPAYQSSPAGGHAPTPPTPAPRTMPP---TKPQP
M. musculus YDNFVELVANLKEGTKFYNELTEILVRFQNKCSDIVFARKTER | DELLKDLQQSIAREPSAPSIPPPAYQSSPAAGHAAAPPTPAPRTMPVSTPAKPQP
D. melanogaster FDSYIRLSGNLQEGTKFYNDLTQLLVVFQNKISDFVFARKTEK | EELLKDLTTRSSRQACPATPALPSHYASTSGSGSDIPPGSAP----------
A. oryzae YLKYKEIISNIEVGRKFYNDLAKIVGRFRDDCKAFVHQRRMEA | SQIEGDITSVAAMASLNLSQPHLRQYSQQPTQP----------
S. cerevisiae FDKLQEAVKSFSIFASDLPKGIEFYDSLFNMSRDLAERVRVAK | QTEDSTANSPAPPLPPLDSKASVVGGPPLLPQKSAAFQSLS----------
760 780 800 820 840
H. sapiens PARPPPPVLPANRAP-SATAPSPVGAGTAAPAPSQTPGSAPPPQAQGPPYPTYPGYPGYCQMPMPMGYNPYAYGQYNMPYPPVYHQSPGQAPYPGPQQPS
M. musculus PARPPPPVLPANRVPPASAAAAPAGVGTASAAPPQTPGSAPPPQAQGPPYPTYPGYPGYCQMPMPMGYNPYAYGQYNMPYPPVYHQSPGQAPYPGPQQPT
D. melanogaster ----------SVPPAASTANIPYPAQVQGMPIPYGAQPG-----VPYPAYVPAPMPQSFNPYAT----LPYPGNYQYQGFPQGPPPGHYGT
A. oryzae ----------AQPVQPAQPVQPPNQLPPQPQPVQHQ-------PPRDEPLTAPQPTRANTRPSMAPGVWSPEMGIRFGAQGTWDPSKGVK
S. cerevisiae ----------RQGLNLGDQFQNLKISAGSDLPQGPGIPPRTYEASPYAATPTMAAPPVPPKQSQEDMYDLRRRKAVENEERELQENPTSF
860 868
H. sapiens YPFPQPPQQSYYPQQ-----
M. musculus YPFPQPPQQSYYPQQ-----
D. melanogaster YPGSYANQQGGYPNQKPPGW
A. oryzae FS----------
S. cerevisiae YNRPSVFDENMYSKYSS---

Figure S1. Sequence Alignments, Secondary Structure, and Topology of Human ALIX$_{Bro1-V}$.

Sequence alignments of Bro1/ALIX proteins from five representative species, chosen because they are the most highly studied ALIX/Bro1 proteins. The secondary structure of human ALIX$_{Bro1-V}$ is shown above, together with the numbering scheme. The color coding is the same as in Fig. 1B, with the TSG101 binding site shown in lime green and the Endophilin binding site shown in turquoise. Sequence alignments were performed using the ClustalW server www.ebi.ac.uk/clustalw (Thompson et al., 1994), and match structure-based alignments for the Bro1 domain.

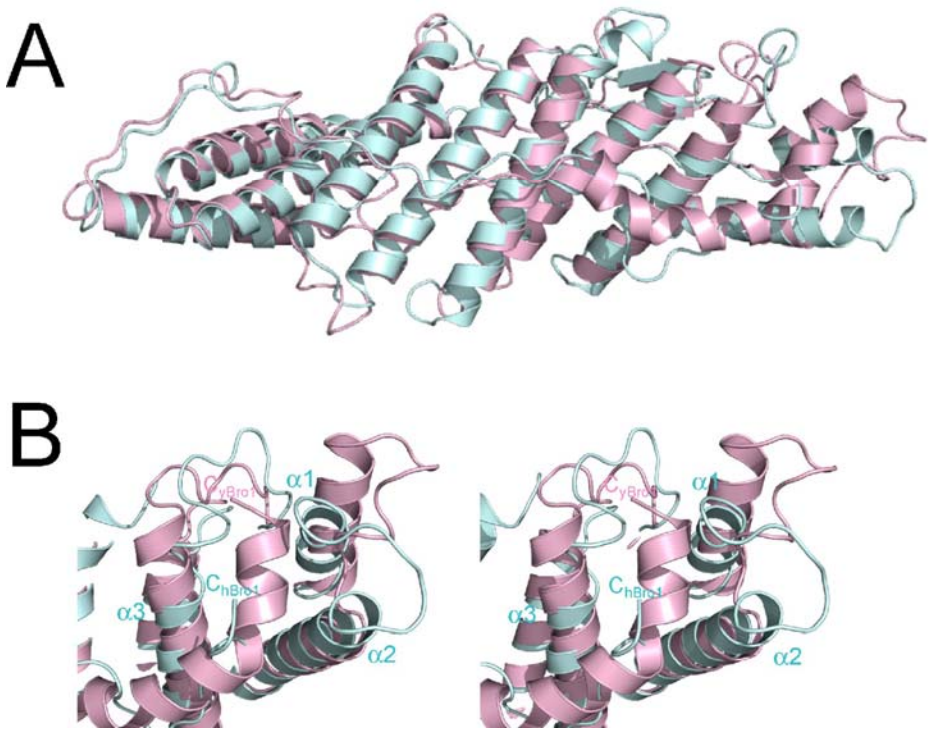

Figure S2. Comparison of the Human and Yeast Bro1 Domains.

(A) Superposition of human $ALIX_{Bro1}$ (turquoise) and yeast $Bro1_{Bro1}$ (magenta). Alignments were performed using the DALI server: http://www.ebi.ac.uk/dali (Holm and Sander, 1998).

(B) Stereoview showing a closeup view of the region with the greatest divergence between human $ALIX_{Bro1}$ (turquoise) and yeast $Bro1_{Bro1}$ (magenta). The region corresponds to the right edge of the image in (A). Helices a1-3 in human $ALIX_{Bro1}$ are labeled, as are the C-termini of human $ALIX_{Bro1}$ (C_{hBro1}) and yeast $Bro1_{Bro1}$ (C_{yBro1}).

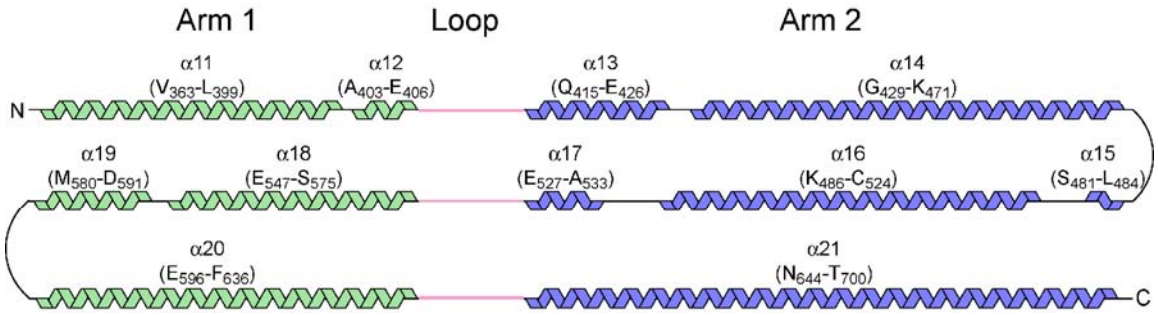

Figure S3. Topology of the ALIX$_V$ domain.

The figure illustrates how the polypeptide strand crosses the arm1/arm2 loop three times in the course of building the V domain. Color coding and numbering schemes are the same as in Fig. 1D.

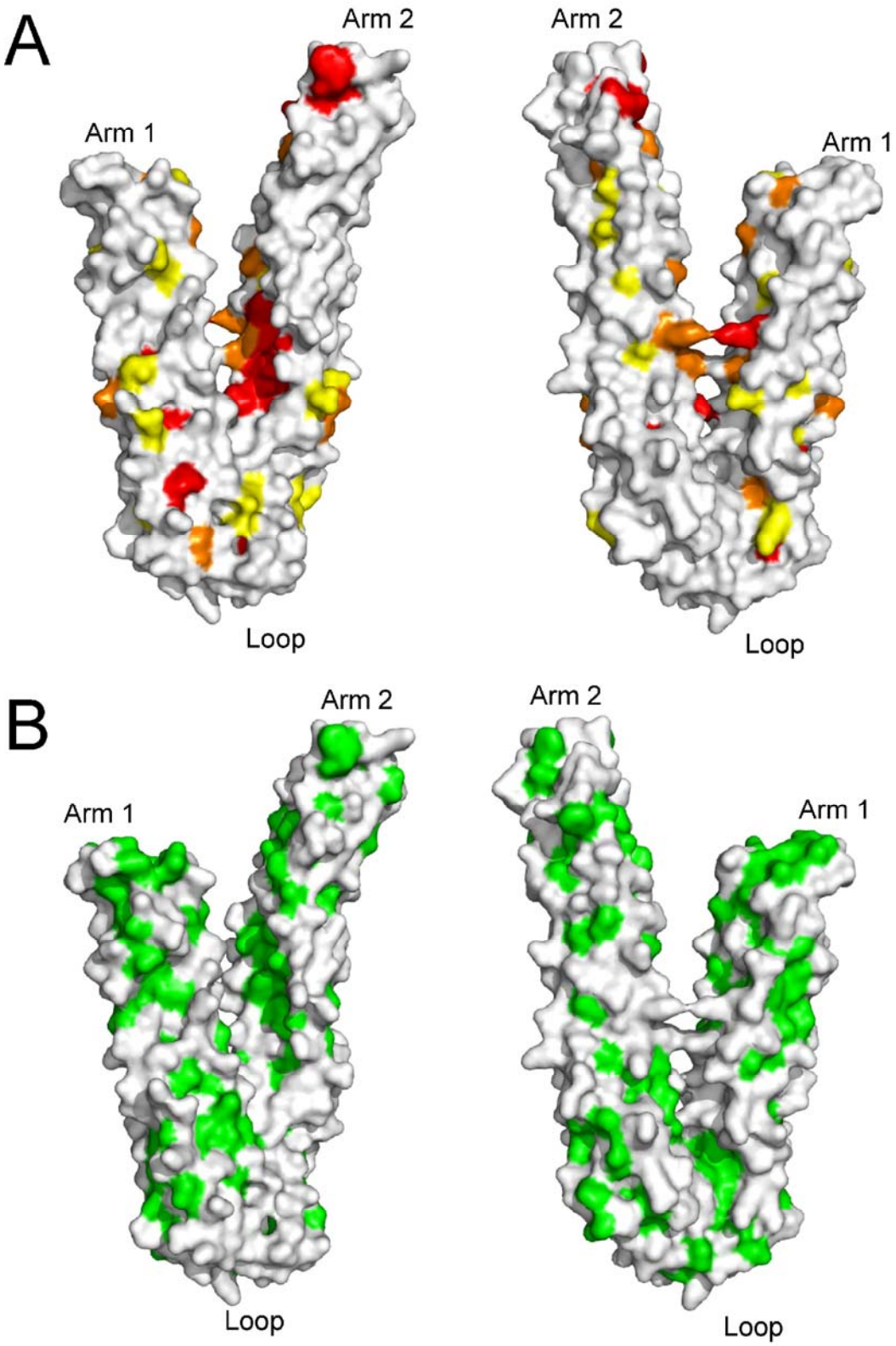
A
Arm 2
Arm 1
Loop
Arm 2
Arm 1
Loop
B
Arm 2
Arm 1
Loop
Arm 2
Arm 1
Loop

Figure S4. ALIX$_V$ Surface Conservation and Hydrophobicity

(A) Surface representation of Alilx$_V$ highlighting amino acid conservation. Coloring and orientation of the left molecule are the same as in Fig. 1E. The right molecule is the view from the "back" of the left. The nine species used in the alignment to define conservation are: *Homo sapiens* (Human), *Mus musculus* (Mouse), *Gallus gallus* (Chicken), *Xenopus laevis* (African clawed frog), *Drosophila melanogaster* (Fruit fly), *Caenorhabditis elegans*, *Dictyostelium discoideum* (Slime mold), *Arabidopsis thaliana* (Mouse-ear cress), and *Aspergillus oryzae*.

(B) Surface representation of ALIX$_V$ with surface residues colored by residue type. Hydrophobic residues are colored green, polar blue, and acidic/basic residues white. The molecule orientations are the same as in (A), except that the left molecule has been slightly rotated around the vertical axis to view the YPX$_n$L binding site on Arm2.

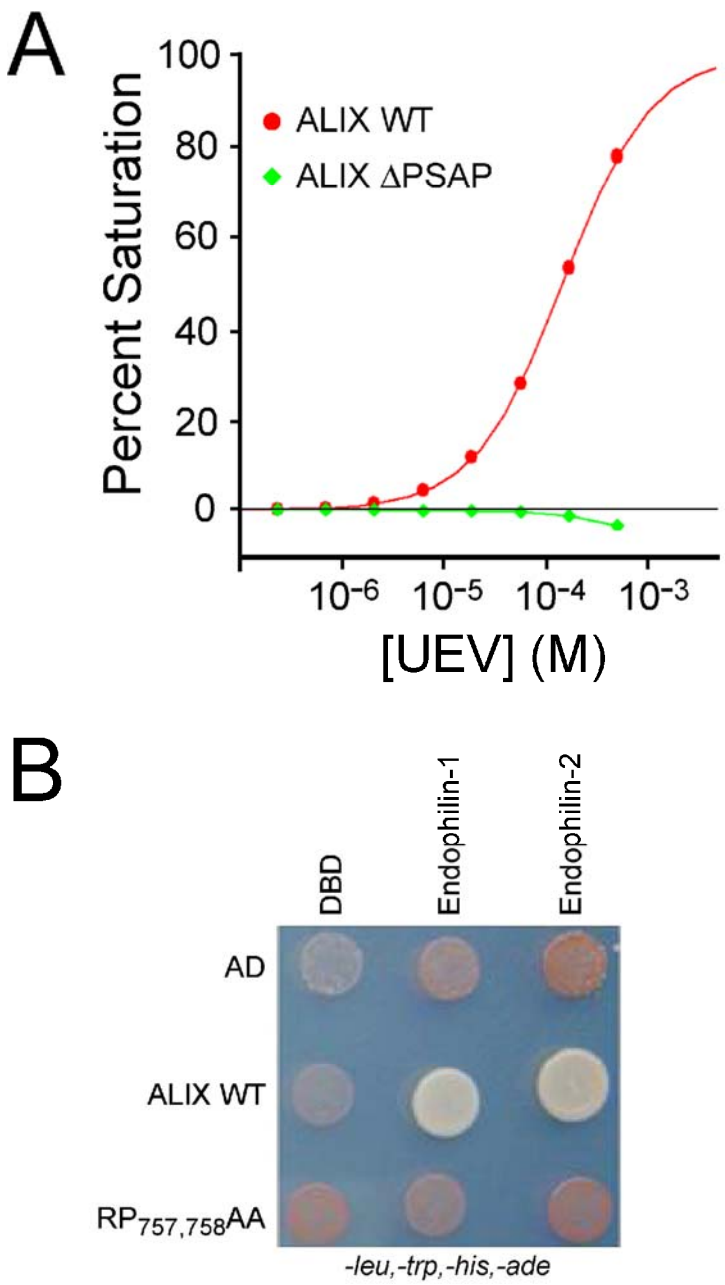

Figure S5. Characterization of ALIX Mutations that Block Endophilin and TSG101 Binding

(A) Biosensor binding isotherms showing that the TSG101 UEV domain binds a GST fusion construct spanning the wild type ALIX $_{717}$PSAP$_{720}$ motif (GST-ALIX$_{714-723}$,

K_d=146±1 μM), and that the Pro720Leu mutation (GST-$ALIX_{714\text{-}723,\ P720L}$) eliminated binding.

(B) Yeast two hybrid assay showing that human ALIX binds endophilins-1 and -2, and that the interactions are inhibited by the ALIX $RP_{757,758}AA$ mutation. Directed yeast two hybrid assays were performed using the Matchmaker GAL4 Yeast Two Hybrid 3 system (Clontech). AH-109 *Saccharomyces cerevisiae* were co-transformed with pGADT7 or pGBKT7 cloning vectors (Clontech) containing inserts encoding wild type (WT) and mutant human ALIX (Activation Domain fusions, AD) and endophilins-1 and -2 (DNA Binding Domain fusions, DBD). Transformed yeast colonies were grown for three days at 30 °C on YPD plates with -Leu, -Trp selection. 10-100 colonies were pooled, resuspended in a liquid culture of SB (-Leu, -Trp), selected on SB (-Leu, -Trp, -Ade, -His) plates, and allowed to grow for 3 days. Growth on -Leu,-Trp,-His,-Ade media reflects positive binding interactions between ALIX and the endophilins, whereas failure to grow reflects a lack binding activity ($ALIX_{RP757,758AA}$ mutants and negative controls).

CHAPTER 3

STRUCTURAL AND FUNCTIONAL STUDIES OF ALIX INTERACTIONS WITH YPX_NL LATE DOMAINS OF HIV AND EIAV

Qianting Zhai, Robert D. Fisher, Hyo-Young Chung, David G. Myszka, Wesley I. Sundquist1 & Christopher P. Hill

This research was originally published in the Nature Structurial & Molecular Biology 15(1):43-9,2008.

nature
structural &
molecular biology

Structural and functional studies of ALIX interactions with YPX$_n$L late domains of HIV-1 and EIAV

Qianting Zhai[1,3], Robert D Fisher[1,3], Hyo-Young Chung[1], David G Myszka[2], Wesley I Sundquist[1] & Christopher P Hill[1]

Retrovirus budding requires short peptide motifs (late domains) located within the viral Gag protein that function by recruiting cellular factors. The YPX$_n$L late domains of HIV and other lentiviruses recruit the protein ALIX (also known as AIP1), which also functions in vesicle formation at the multivesicular body and in the abscission stage of cytokinesis. Here, we report the crystal structures of ALIX in complex with the YPX$_n$L late domains from HIV-1 and EIAV. The two distinct late domains bind at the same site on the ALIX V domain but adopt different conformations that allow them to make equivalent contacts. Binding studies and functional assays verified the importance of key interface residues and revealed that binding affinities are tuned by context-dependent effects. These results reveal how YPX$_n$L late domains recruit ALIX to facilitate virus budding and how ALIX can bind YPX$_n$L sequences with both $n = 1$ and $n = 3$.

Retroviruses such as HIV-1 bud through limiting host cell membranes to acquire a lipid envelope and exit the cell. Efficient budding requires short peptide motifs, known as late domains, that are found in varying numbers and combinations in the viral Gag protein. Late domains function by recruiting *trans*-acting cellular factors that facilitate viral budding[1–3]. HIV-1 p6^{Gag} contains two late domains: a $_{7}$P(S/T)AP$_{10}$ motif that recruits the cellular protein TSG101 and a $_{35}$LYPLTSLRSLF$_{45}$ motif that recruits ALIX (also known as AIP1) (refs. 4–12). The HIV-1 $_{35}$LYPLTSL$_{41}$ motif belongs to the YPX$_n$L family of late domains, in which n frequently is a single residue (that is, $n = 1$) but can be three residues ($n = 3$), as is the case for HIV-1 (refs. 10,12). Unlike HIV-1, the related EIAV p9^{Gag} protein lacks a PTAP late domain and contains a single $_{22}$LYPDL$_{26}$ late domain that binds ALIX[10–15].

Both TSG101 and ALIX are components of the ESCRT pathway, which helps to sort membrane proteins into vesicles that bud into late endosomal compartments called multivesicular bodies[16–18]. The ESCRT pathway also functions in the final abscission step of cytokinesis, in which the thin membrane stalk that connects the mother and daughter cells is pinched off to produce two discrete cells[19]. Both of these membrane fission processes are topologically equivalent to viral budding, and it appears that late domains function by redirecting ESCRT machinery to sites of virus assembly where it can facilitate budding[3].

Principal components of the human ESCRT pathway include three multiprotein endosomal sorting complexes required for transport (ESCRT-I (which contains a TSG101 subunit), ESCRT-II and ESCRT-III), ALIX and the VPS4–LIP5 complex[16]. Although mechanistic details are lacking, the ESCRT-III proteins are thought to form a membrane-associated lattice that is essential for protein sorting, membrane fission or both[20]. The machinery is reset by the action of the VPS4–LIP5 ATPase, which binds ESCRT-III components and disassembles the lattice. Although the ESCRT pathway is often represented as a series of sequential steps, it may be better described as a complex protein interaction network, as illustrated by the ability of ALIX to bind both to ESCRT-I and to the CHMP4 subunits of ESCRT-III and by the apparent absence of a role for ESCRT-II in HIV-1 budding[10,11,15,21–23].

The mechanism by which HIV-1 accesses the ESCRT machinery has been best characterized for the p6^{Gag}–ESCRT-I interaction. Extensive biochemical and structural work has shown that the ubiquitin E2 variant (UEV) domain of TSG101 binds the PTAP late domain of HIV p6^{Gag} and that mutations in the PTAP motif or UEV domain that block their interaction also inhibit efficient virus budding[4–6,9,24,25]. In situations where the PTAP-TSG101 interaction is impaired, HIV-1 budding becomes much more dependent upon the YPX$_n$L-ALIX interaction[26,27]. Furthermore, other lentiviruses, including EIAV and some SIV strains, naturally lack PTAP late domains and therefore rely on YPX$_n$L-ALIX interactions to bud from cells[10,26,28].

Crystal structures[22,26,29] have revealed that ALIX is composed of three regions: an N-terminal Bro1 domain (named for the apparent yeast homolog, Bro1p) that binds the CHMP4 subset of ESCRT-III proteins[10,11,15,22,30]; a central V domain that is formed by two three-helix bundles disposed in a 'V' shape[26,29]; and a C-terminal proline-rich region (PRR, not present in the crystal structures) that serves as a docking site for a number of proteins, including TSG101 and SH3

[1]Department of Biochemistry and [2]Center for Biomolecular Interactions Analysis, University of Utah School of Medicine, Salt Lake City, Utah 84112-5650, USA. [3]These authors contributed equally to this work. Correspondence should be addressed to C.P.H. (chris@biochem.utah.edu) or W.I.S. (wes@biochem.utah.edu).

Received 3 July; accepted 21 September; published online 9 December 2007; doi:10.1038/nsmb1319

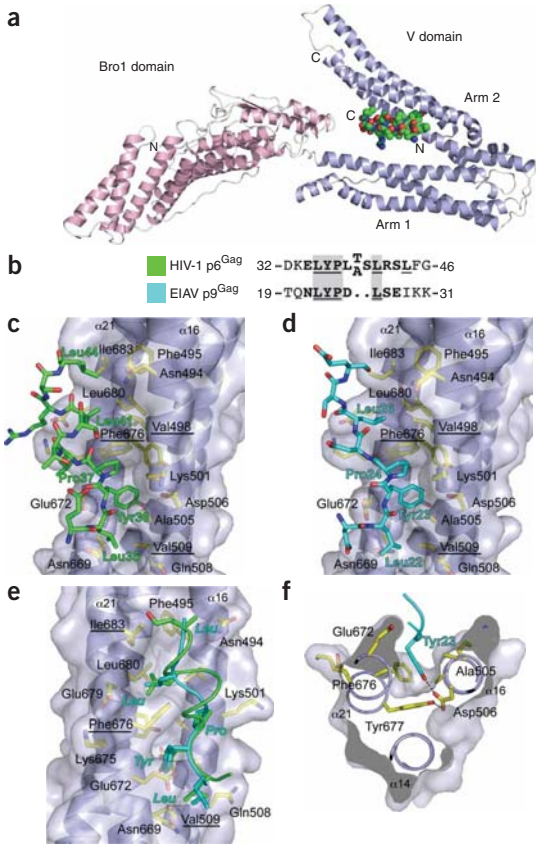

Figure 1 Structure of $ALIX_{Bro1\text{-}V}$–YPX_nL complexes. (**a**) Ribbon diagram of $ALIX_{Bro1\text{-}V}$ in complex with the HIV-1 $p6^{GagT}$ YPX_nL late-domain peptide (CPK). (**b**) HIV-1 $p6^{GagT}$ $p6^{GagA}$ and EIAV $p9^{Gag}$ YPX_nL late-domain peptide sequences used for crystallography and binding studies aligned on the basis of the crystal structures. Residues modeled in the crystal structures are in boldface, and residues that lack electron density are in normal font; the first included residue (HIV Glu34; EIAV Asn21) has some density, although the conformation is ambiguous. Structurally equivalent residues are on a gray background. Residues that contact the protein are underlined. (**c,d**) Close-up views of YPX_nL late domains (sticks) for HIV-1 $p6^{GagT}$ (green) and EIAV $p9^{Gag}$ (turquoise). ALIX is represented as a blue ribbon and surface with residues in the binding site highlighted as yellow sticks. ALIX residues previously shown by mutagenesis to be important for $p6^{Gag}$ and $p9^{Gag}$ binding and ALIX function in viral budding are underlined[26,29]. (**e**) Overlay of the HIV-1 $p6^{Gag}$ and EIAV $p9^{Gag}$ crystal structures. The intervening $_{38}LTS_{40}$ residues of the HIV-1 YPX_nL motif form a helical turn to position Leu41 in a position equivalent to that of EIAV $p9^{Gag}$ Leu26. (**f**) Cutaway view of EIAV $p9^{Gag}$ binding to ALIX. Viewed along the axis of arm 2 from the V-domain apex, rotated ~90° into the page relative to **d**. The YPX_nL tyrosine binds in a deep pocket and forms hydrogen-bonding interactions with ALIX Asp506, which is optimally oriented by hydrogen bonding with Tyr677. Figure generated using PyMol[52].

domain–containing proteins,[11,31–35]. The V domain binds the YPX_nL late domains of HIV $p6^{Gag}$ and EIAV $p9^{Gag}$ and this interaction is required for ALIX-dependent viral budding[10,15,26,27,29,36]. To understand how ALIX is recruited to sites of viral budding, we have determined crystal structures of human ALIX complexes with HIV-1 and EIAV YPX_nL late-domain peptides and have performed binding and functional assays that confirm and extend the structural studies.

RESULTS

Structure determination

We determined crystal structures of $ALIX_{Bro1\text{-}V}$ (residues 1–698) in complex with peptides spanning the HIV-1 and EIAV late-domain motifs to 2.8-Å resolution and R_{free} values of 28% (**Fig. 1**). This $ALIX_{Bro1\text{-}V}$ construct contains a $KK_{268,269}YY$ double mutation that stabilizes a crystal contact but does not alter the protein structure and is distant from known ligand-binding sites[26]. The peptides used correspond to residues 32–46 of $p6^{Gag}$ in HIV-1 strains NL4-3 ($p6^{GagA}$) and HXB2 ($p6^{GagT}$) and to residues 19–31 of $p9^{Gag}$ in EIAV (**Fig. 1b**). The two HIV-1 peptides differ only in the presence of alanine ($p6^{GagA}$) or threonine ($p6^{GagT}$) at position 39, whereas the only identical residues in the EIAV peptide are the conserved residues of the YPX_nL motif and a conserved leucine that precedes the tyrosine.

Overall structure

The overall structure of $ALIX_{Bro1\text{-}V}$ in the three peptide complexes closely resembles that of the unliganded protein[26], with differences primarily within flexible loops. All three late-domain ligands bind to a largely hydrophobic groove on arm 2 of the ALIX V domain that was previously implicated in binding by mutagenesis studies[26,29,36]. The peptides lie approximately parallel to arm 2, on the side facing arm 1, and with their N termini pointing toward the base of the V. The binding site, located between ALIX helices α16 and α21, is lined by the conserved residues Ala502, Ala505, Asp506, Val509, Glu665, Asn669, Glu672, Gly673, Lys675, Phe676, Tyr677, Leu680 and Ile683 and by the less-well-conserved residues Phe495 and Val498. Minor local changes in ALIX conformation are induced by peptide binding. In particular, a segment of helix α21 from residues 668–680 is shifted and rotated by ~1.5 Å, and the side chains of Glu672, Phe676 and Tyr677 are moved a few angstroms to accommodate peptide interactions.

Conserved peptide interactions

The HIV-1 and EIAV peptides bind to the same ALIX surface and form similar interfaces. The late-domain structures have been modeled for a total of 11 (HIV-1) or 8 (EIAV) residues and were found to bury a total of approximately 570 $Å^2$ (HIV-1) and 450 $Å^2$ (EIAV) of solvent-accessible surface area. The structures are stabilized by numerous van der Waals contacts and several important hydrogen-bonding interactions. The two HIV-1 peptide structures are closely superimposable throughout.

In all three structures, the first well-ordered peptide residue is the leucine immediately preceding the late-domain tyrosine, and the three ordered N-terminal residues (LeuTyrPro, LYP) adopt superimposable conformations in the HIV-1 and EIAV peptides. This leucine side chain rests against a hydrophobic surface on the protein formed by ALIX Ala505, Gln508, Val509, Asn669 and Glu672, consistent with the loss of binding observed upon substitution with alanine[10] and the conservation of hydrophobic character at this position.

The late-domain tyrosine side chain has the most distinctive interaction. It plunges deep into a hydrophobic pocket that is lined by Ala502, Ala505, Asp506, Val509, Glu672, Gly673, Phe676 and Tyr677, with the phenolic hydroxyl projecting into the center of the arm 2 three-helix bundle, where it is specifically recognized by a hydrogen bond with the conserved side chain of Asp506 (**Fig. 1f**). This buried hydrogen bond shows good geometry and should be

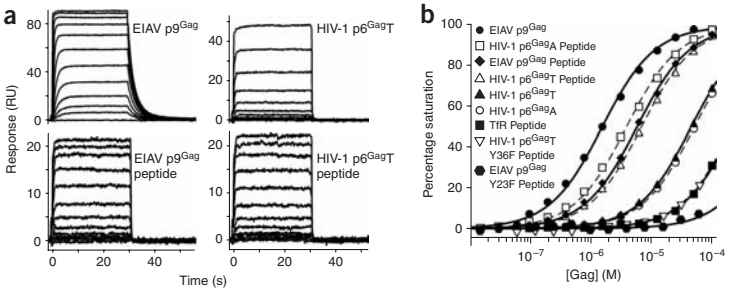

Figure 2 ALIX-YPX$_n$L binding affinities. (**a**) Representative biosensor sensograms for immobilized ALIX$_{Bro1\text{-}V}$ binding to HIV-1 p6^{Gag}T and EIAV p9^{Gag} proteins and to YPX$_n$L peptides used in crystallography. (**b**) Biosensor binding isotherms for ALIX$_{Bro1\text{-}V}$ binding to HIV-1 p6^{Gag}A/T and EIAV p9^{Gag} proteins, YPX$_n$L peptides and a peptide from transferrin receptor (TfR). Experiments with HIV-1 p6^{Gag}T and EIAV p9^{Gag} were reported in ref. 26 and are included here for reference.

strengthened by the relative acidity of the phenolic hydroxyl and by the orientation of Asp506 through a buttressing interaction with the conserved Tyr677 residue that occurs even in the absence of peptide. In addition to enhancing affinity, this hydrogen-bonding interaction should enhance specificity, including discriminating against substitution of the late-domain tyrosine for a phenylalanine.

The late-domain proline packs against Phe676, Ala502 and Val498, which explains why substitution of Phe676 or Val498 with aspartate severely impairs peptide binding[26,29]. The only hydrogen bond between the late-domain main chain and ALIX is formed by the NH group of the peptide tyrosine and the conserved ALIX side chain of Glu672. These interactions of the LYP tripeptide at the N termini of the different late-domain sequences provide a common anchor for ALIX binding.

HIV-1 and EIAV late domains adopt different conformations

The HIV-1 and EIAV late-domain peptides adopt quite different conformations immediately following the N-terminal LYP tripeptide that allow the leucine side chain of both YPX$_n$L sequences to bind to the same shallow pocket in ALIX. The side chains of the intervening X residues, three for HIV-1 and one for EIAV, all project away from the ALIX surface because the EIAV peptide is extended whereas HIV-1 forms a helical turn (**Fig. 1e**). These different conformations therefore allow sequences that contain different numbers of intervening residues to make equivalent contacts with ALIX.

The electron density maps become less clear toward the peptide C termini, and they are uninterpretable for the EIAV sequence more than one residue after the leucine residue of the YPX$_n$L core. The C-terminal density for the HIV-1 peptides is also weak, but appears to show the peptide continuing in the same direction along the groove (**Supplementary Fig. 1** online). The structure thereby places the HIV late-domain Leu44 side chain in a hydrophobic contact with the ALIX residues Phe495 and Ile683. This model is consistent with reports that binding to ALIX is greatly impaired upon mutation of p6^{Gag} Leu44 to proline[10] or alanine[36].

The structure rationalizes previous mutagenic analyses of the ALIX side of the late-domain binding interface. Point mutations of ALIX residues Val498, Phe676 and Ile683 (to Asp) all substantially reduced the binding affinity of EIAV p9^{Gag} and HIV-1 p6^{Gag} (>20-fold) and blocked the ability of ALIX to rescue TSG101-independent release of HIV-1 (ref. 26). The ALIX F676D and V509A mutations also blocked binding of an HIV-1 p6^{Gag} peptide and abrogated the ability of an ALIX V-domain construct to inhibit HIV-1 release[29]. All of these residues reside within the late-domain binding site and make important contacts with all these peptides.

ALIX binding to YPX$_n$L late domains

We carried out biosensor binding experiments to quantify the affinities of the ALIX-YPX$_n$L interactions (**Fig. 2**, **Table 1**). ALIX$_{Bro1\text{-}V}$ and ALIX$_V$ generally did not have any notable differences in their ligand-binding affinities, consistent with the idea that all determinants for late-domain binding reside within ALIX$_V$. Furthermore, ALIX bound HIV-1 p6^{Gag}A and p6^{Gag}T peptides with indistinguishable affinities (7 ± 7 μM and 8 ± 2 μM, respectively), consistent with their superimposable binding geometries. The EIAV p9^{Gag} peptide bound with a similar affinity (7 ± 1 μM). These data agree well with previously reported equilibrium dissociation constants for peptides spanning the HIV-1 (16-mer) and EIAV (15-mer) YPX$_n$L motifs (5–6 μM), obtained from solution-phase isothermal titration calorimetry[29,36]. Substitution of the late-domain tyrosine with phenylalanine reduced the binding affinity of both HIV-1 p6^{Gag} and EIAV p9^{Gag} more than 15-fold (**Table 1**). These results are consistent with the observed hydrogen-bond interaction with the tyrosine phenol and with the strict conservation of tyrosine in YPX$_n$L sequences in HIV-1, EIAV and SIV, but conflict with the conclusions of Munshi *et al.*, who reported that a phenylalanine substitution had no effect on ALIX binding[36]. The reasons for this discrepancy are not known at present.

HIV-1$_{NL4\text{-}3}$ p6^{Gag} YPX$_n$L Tyr is essential for late-domain function

Two different approaches were used to test the functional importance of the phenolic hydroxyl of the YPX$_n$L tyrosine residue for ALIX-mediated HIV-1$_{NL4\text{-}3}$ budding. In one case, we examined the release and infectivity of an HIV-1 mutant with a p6^{Gag} Tyr36Phe substitution (engineered to maintain the native sequence in the –1 reading frame for Pol expression). Previous studies showed that lack of ALIX

Table 1 ALIX binding to HIV-1 p6^{Gag}, EIAV p9^{Gag} and transferrin receptor

Equilibrium dissociation constants (μM, 20 °C)[a]	ALIX$_{Bro1\text{-}V}$	ALIX$_V$
HIV-1 p6^{Gag}A peptide	7 ± 7[b]	5 ± 3[b]
HIV-1 p6^{Gag}T peptide	8 ± 2[b]	6 ± 3[b]
HIV-1 p6^{Gag}T Y36F peptide	220 ± 20[b]	230 ± 50[b]
EIAV p9^{Gag} peptide	7 ± 1[b]	6 ± 1[b]
EIAV p9^{Gag} Y23F peptide	>1,000	>1,000
HIV-1 p6^{Gag}A	60 ± 20[b]	60 ± 15[b]
HIV-1 p6^{Gag}T	40 ± 10[b,c]	39 ± 1[b,c]
EIAV p9^{Gag}	1.5 ± 0.3[b,c]	1.2 ± 0.3[b,c]
TfR peptide	270 ± 140[b]	340 ± 90[b]

[a]Biosensor binding experiments were performed between immobilized GST-ALIX fusions and peptide sequences of HIV-1 p6^{Gag} ($_{32}$DKELYPL(A/T)SLRSLFG$_{46}$), EIAV p9^{Gag} ($_{19}$TQNLYPDLSEIKK$_{31}$), transferrin receptor 1 (TfR, $_{17}$PLSYTRFSLARQV$_{29}$) and purified HIV-1 p6^{Gag} and EIAV p9^{Gag}. [b]Average ± s.d. between 2–9 independent measurements. [c]Experiments with HIV-1 p6^{Gag}T and EIAV p9^{Gag} were reported in ref. 26 and are included here for reference.

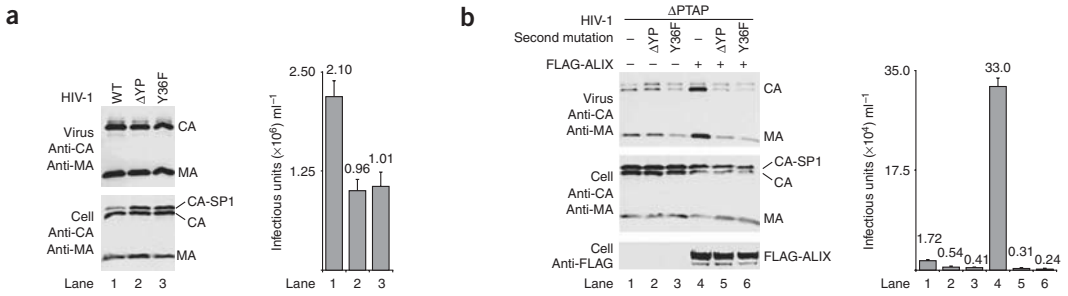

Figure 3 The HIV-1 p6^{Gag} YPX$_n$L tyrosine is essential for late-domain function. (**a**) The HIV-1 p6^{Gag} Tyr36Phe mutation reduces release and infectivity of otherwise wild-type HIV-1. Lanes 1, wild-type (WT) HIV-1 expressed in 293T cells (positive control); lanes 2, HIV-1 encoding a $_{36}$SR$_{37}$ mutation in the $_{36}$YPLTSL$_{41}$ late domain of p6^{Gag} (ΔYP); lanes 3, HIV-1 encoding a Y36F mutation in the $_{36}$YPLTSL$_{41}$ late domain of p6^{Gag}. Western blots showing virus production (top gel panel) and cellular Gag protein levels (bottom gel panel, antibodies to CA^{Gag} and to MA^{Gag}). Graph below shows viral titers measured in a single-cycle MAGIC assay ($n = 3 \pm$ s.d.). Cellular CA^{Gag} and MA^{Gag} levels were similar in all cases, but the CA-SP1 processing intermediate accumulated in the ΔYP and Tyr36Phe constructs, which is typically observed when virus budding is inhibited. (**b**) A secondary HIV-1 p6^{Gag} Tyr36Phe mutation blocks the rescue of HIV$_{ΔPTAP}$ virus release and infectivity that are normally induced by ALIX overexpression. Top gel panel, western blot showing HIV$_{ΔPTAP}$ virus release. Middle gel panel, cellular CA^{Gag} and MA^{Gag} protein levels. Bottom gel panel, exogenous ALIX expression. Graph below shows viral titers as analyzed in MAGIC infectivity assays ($n = 3 \pm$ s.d.). HIV$_{ΔPTAP}$ constructs were used in all experiments and were co-transfected with an empty pCI-neo vector control (lanes 1–3) or a vector expressing FLAG-ALIX (lanes 4–6). The HIV$_{ΔPTAP}$ constructs used in lanes 1 and 4 had no secondary mutations (negative control), whereas HIV$_{ΔPTAP}$ constructs with secondary mutations were used in lanes 2 and 5 (p6^{Gag} ΔYP, positive control) and in lanes 3 and 6 (p6^{Gag} Y36F). Note that overexpression raised ALIX levels ~50-fold over endogenous protein levels as estimated by western blotting with antibodies to ALIX (not shown).

recruitment results in a 50–75% reduction in HIV-1 infectivity and release from 293T cells[5,26], as seen for the control $_{36}$TyrPro$_{37}$ to $_{36}$SerArg$_{37}$ mutation (termed ΔYP) in HIV-1 p6^{Gag} (**Fig. 3a**). Notably, the HIV-1 p6^{Gag} Tyr36Phe mutation had the same effect, reducing the viral titer to 48% that of the control and inducing a modest increase in the accumulation of the CA-SP1 Gag processing intermediate, which is typically seen when viral budding is impaired. Thus, the Tyr36Phe mutation alone seems to abrogate the ability of p6^{Gag} to recruit ALIX.

We also examined budding and infectivity of an HIV-1 construct in which the p6^{Gag} PTAP late domain was mutated (HIV$_{ΔPTAP}$). This virus can no longer recruit ESCRT-I and only buds efficiently from 293T cells when ALIX is overexpressed. This system therefore provides a sensitive assay for testing whether p6^{Gag} mutants can support functional recruitment of exogenous ALIX protein[26,27]. The Tyr36Phe mutation blocked ALIX recruitment (**Fig. 3b**); notably, it also apparently blocked recruitment of endogenous ALIX protein, causing a further four-fold reduction in the (already low) release of HIV$_{ΔPTAP}$ from cells lacking exogenous ALIX. Taken together, these experiments demonstrate that removing the phenolic hydroxyl of the tyrosine residue within the YPX$_n$L motif blocks ALIX recruitment and HIV-1$_{NL4-3}$ late-domain function *in vivo*, consistent with our *in vitro* binding and structural studies.

Protein context modulates ALIX–late domain interactions

Our finding that p6^{Gag} and p9^{Gag} peptides bound ALIX with similar affinities (K_d ~7 μM) was in contrast to our previous observations that ALIX binds the full-length 52-residue HIV-1 p6^{Gag}A protein and the 51-residue EIAV p9^{Gag} protein with different affinities (57 ± 21 μM and 1.5 ± 0.3 μM, respectively)[26]. Munshi *et al.* also reported a similar difference between p6^{Gag} and p9^{Gag} binding affinities as quantified in biosensor binding measurements, but this difference was not observed in their isothermal titration calorimetry measurements[36]. Inspection of the dissociation phases in the upper panels of **Figure 2a** shows that p9^{Gag} dissociates more slowly (by >10-fold) than p6^{Gag}, which is consistent with the overall increase in thermodynamic stability that we observed for p9^{Gag}–ALIX complexes. These results indicate that late-domain YPX$_n$L sequences provide the primary recognition interface, but that binding affinity is modulated by the context in which the sequence is displayed. Similar context-dependent effects were observed when late domains were transferred between different viruses[37]. These observations further suggest that ALIX-binding affinities are not simply maximized but are selected for optimum performance *in vivo*. Viruses such as EIAV that contain a single known late domain present a high-affinity ALIX binding site to recruit ALIX for viral budding, whereas HIV-1, which also uses a PTAP late domain, presents its YPX$_n$L motif in a more weakly binding context.

To assess the efficiency with which the different YPX$_n$L late domains recruit ALIX *in vivo*, we measured the relative levels of ALIX incorporated by p6^{Gag} and p9^{Gag} polypeptides into different virus-like particles (VLPs). These experiments used HIV-1 Δp6 proviral constructs in which the Gag protein was fused to HIV-1 p6^{Gag} (control), to EIAV p9^{Gag} or to a minimal PTAP motif that lacked a YPX$_n$L sequence[15]. There was a marked increase in the extent of ALIX

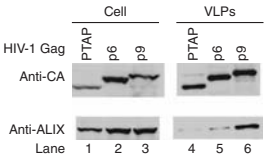

Figure 4 ALIX incorporation into HIV-1 virus-like particles. HIV-1 Δp6 proviral plasmids expressing a truncated HIV-1 Gag protein fused to either a minimal TSG101-binding motif (PEPTAPPEES, PTAP, lanes 1 and 4), HIV-1 p6^{Gag} (p6, lanes 2 and 5) or EIAV p9^{Gag} (p9, lanes 3 and 6) were used to generate HIV-1 virus-like particles (VLPs) in 293T cells. Expression of endogenous ALIX (lower left) and incorporation into VLPs (lower right) was measured by western blot with antibodies to ALIX, whereas HIV-1 Gag cellular expression levels (upper left) and VLP production (upper right) were measured by blotting with antibodies to CA. Note that VLP levels were normalized to show equivalent Gag protein levels (upper right) and that cellular Gag and ALIX expression levels were similar in all cases (left).

incorporation into VLPs from the artificial HIV-1 $p9^{Gag}$ construct relative to HIV-1 $p6^{Gag}$ (~12-fold) and to HIV-1 PTAP alone (~22-fold) (**Fig. 4**). These data are consistent with the higher affinity between ALIX and EIAV $p9^{Gag}$ measured *in vitro* and are in good agreement with earlier immunoprecipitation experiments[10], which showed greater association of ALIX with EIAV $p9^{Gag}$ than with HIV-1 $p6^{Gag}$. Therefore, although the isolated YPX_nL motifs bind ALIX with similar affinities, the affinities of the EIAV $p9^{Gag}$ and HIV $p6^{Gag}$ proteins differ owing to subtle protein context effects that could, for example, stabilize the extended conformation of the EIAV late domain and destabilize the helical conformation required for HIV-1 late-domain binding.

ALIX binding to endogenous cellular partners

Because the viral YPX_nL peptides bind to conserved residues on the ALIX surface, it seems likely that the viral late domains have evolved to mimic interactions of cellular ALIX binding partners. In support of this assumption, the pH-sensing protein PacC has been shown to use a YPXL/I motif to bind PalA, the ALIX homolog in *Aspergillus nidulans*[12]. Homologs of PacC are not apparent for species other than related filamentous fungi and yeast, however, so it is likely that there are other endogenous YPX_nL-containing ligands. ALIX was recently reported to bind the transferrin receptor (TfR) to facilitate its trafficking into exosomes[38]. This interaction was mapped to a YTRF motif in the TfR cytoplasmic tail, which resembles the consensus YPX_nL motif. To test whether ALIX can bind this site, we measured the affinity of $ALIX_{Bro1\text{-}V}$ for a 13-residue peptide fragment of TfR encompassing the YTRF sequence[38], and found that ALIX bound this fragment with a K_d of 267 ± 140 μM, which is ~40-fold weaker than the HIV-1 and EIAV YPX_nL late-domain peptides. Weak affinities of this magnitude can mediate biologically important interactions, but additional experiments will be necessary to determine whether TfR is an authentic ALIX binding partner. Regardless, it seems likely that other endogenous, higher-affinity ligands remain to be discovered.

Notably, the conserved surface of ALIX extends ~10 Å beyond the N-terminal ordered residues of the late-domain peptides, toward the base of the V domain (**Supplementary Fig. 2** online). In particular, Glu665 and Asn669 are invariant in an alignment of nine ALIX sequences[26]; they do not seem to perform structural roles but are potentially available for additional binding interactions. We therefore speculate that these residues are conserved because they function to bind cellular partners, whereas the viral late domains use only a portion of the binding site.

DISCUSSION

Our structural data show that ALIX recognizes viral YPX_nL motifs through a conserved hydrophobic groove on arm 2 of the V domain that is likely also to bind endogenous cellular partners. The most notable features of the interactions are the burial of the late-domain tyrosine side chain deep into a hydrophobic pocket and the formation of a hydrogen bond between the phenolic hydroxyl and a conserved aspartate. The importance of this interaction was confirmed by mutational analyses, both *in vitro* and *in vivo*, and the tyrosine residue is therefore an essential element of the YPX_nL late domains of HIV-$1_{NL4\text{-}3}$ and EIAV. The leucine and proline residues that flank this tyrosine residue are also conserved in the late domains of both HIV-$1_{NL4\text{-}3}$ and EIAV, and these residues make equivalent hydrophobic contacts with ALIX. The terminal leucine residues within the YPX_nL late domains of HIV-1 and EIAV also make equivalent ALIX interactions, despite spacing differences (HIV-1, $n = 3$; EIAV, $n = 1$); this is made possible by alternative helical (HIV) or extended (EIAV) main chain conformations. Thus, the structures presented here explain how ALIX recognizes (L)YPX_nL motifs (and its variants[39]) and can accommodate either one or three residues between the proline and leucine positions. We note that some HIV-2 and SIV strains can still bind and package ALIX even though their Gag proteins typically lack YPX_nL motifs[10], although the basis for these interactions is currently unknown.

Finally, we found that although the isolated HIV-1 and EIAV late-domain peptides have equivalent affinities, context-dependent effects modulate the binding to make it stronger (EIAV) or weaker (HIV-1) for the full-length $p6^{Gag}$ and $p9^{Gag}$ proteins. These observations are consistent with the model that binding of late domains is not simply maximized but is tuned for optimum selective advantage. In this regard, it is notable that EIAV $p9^{Gag}$, which lacks the ability to recruit TSG101, binds ALIX some 60-fold more tightly than does HIV-1 $p6^{Gag}$. Such fine tuning of binding affinities is likely to be especially important for complexes that must form and disassemble along a reaction pathway, as is expected to be the case during abscission, multivesicular body vesicle formation and virus budding.

METHODS

Protein purification and crystallization. $ALIX_{Bro1\text{-}V}$ (residues 1–698) harboring the $KK_{268,269}YY$ double mutation was purified as described[26]. HIV-1 $p6^{Gag}A$, HIV-1 $p6^{Gag}T$ and EIAV $p9^{Gag}$ peptides were synthesized with the sequences $_{32}$DKELYPLASLRSLFG$_{46}$, $_{32}$DKELYPLTSLRSLFG$_{46}$ and $_{19}$TQNLYPDLSEIKK$_{31}$, respectively. Peptide termini were blocked with acetyl (N) and amide (C) groups. Lyophilized peptides were resuspended in water and mixed with $ALIX_{Bro1\text{-}V}$ to a molar ratio of ~1:1.2 protein/peptide at a final ALIX concentration of 10 mg ml^{-1}. Crystals were grown by sitting-drop vapor diffusion at 13 °C, with the drops comprising 1–2 μl of reservoir solution (0.20–0.25 M $MgCl_2$, 7–10% (w/v) PEG-4000 and 0.1 M NaMES, pH 5.9–6.1) and 2 μl protein solution (1 mM DTT, 100 mM NaCl and 10 mM HEPES, pH 8.0).

Table 2 X-ray data collection and refinement statistics

	$p6^{Gag}A$	$p6^{Gag}T$	$p9^{Gag}$
Data collection			
Space group	*C*2	*C*2	*C*2
Cell dimensions			
a, *b*, *c* (Å)	146.1, 99.4, 73.5	145.9, 99.1, 73.2	146.4, 98.6, 72.8
α, β, γ (°)	90.0, 107.3, 90.0	90.0, 107.3, 90.0	90.0, 107.1, 90.0
Resolution (Å)	40–2.55 (2.64–2.55)	50–2.60 (2.69–2.60)	50–2.60 (2.69–2.60)
R_{sym}	12.6 (36.6)	6.0 (25.2)	15 (30.6)
$I / \sigma(I)$	14 (2.1)	13 (2.1)	7 (2.3)
Completeness (%)	98.6 (88.3)	98.4 (94.2)	98.2 (96.5)
Redundancy	5.6	3.7	3.0
Refinement			
Resolution (Å)	28–2.55	50–2.6	50–2.6
No. reflections	30,785	28,331	28,155
R_{work}/R_{free}	22.5/28.0	22.4/28.5	22.3/28.6
No. atoms			
Protein	5,574	5,574	5,552
Water	17	17	23
Average *B*-factor ($Å^2$)	95.8	88.4	84.7
R.m.s. deviations			
Bond lengths (Å)	0.013	0.017	0.014
Bond angles (°)	1.309	1.511	1.384

Diffraction data from one crystal were used to determine each structure. Values in parentheses are for the highest-resolution shell. R_{free} is calculated from 5% of reflections chosen randomly.

Data collection and refinement. Crystals were cryoprotected by transfer, in 5% (v/v) glycerol increments, to a solution of reservoir components made up with 30% (v/v) glycerol. Crystals were suspended in a nylon loop, plunged into liquid nitrogen, and maintained at 100 K for data collection at beamline 11-1 of the Stanford Synchrotron Radiation Laboratory ($\lambda = 1.00000$ Å ($p6^{Gag}A$) and 0.97946 Å ($p6^{Gag}T$, $p9^{Gag}$)). Data were processed using HKL2000 (ref. 40). The structures were isomorphous with the unliganded $ALIX_{Bro1\text{-}V}$ structure (PDB code 2OEV[26]) and were refined in REFMAC5[41] with TLS refinement using TLSMD[42–44] and TLSANL[45] in the CCP4 suite[46]. Model building was performed with O[47] and COOT[48]. Geometry was analyzed in PROCHECK[49], with no residues in disallowed regions of the Ramachandran plot. Statistics are given in **Table 2**.

Biosensor binding experiments. Surface plasmon resonance biosensor binding experiments were performed at 20 °C using a Biacore T100 optical biosensor equipped with a CM5 sensor chip. Antibody to glutathione *S*-transferase (GST) was immobilized by amine-coupling chemistry[50] onto the chip surface followed by application of soluble *Escherichia coli* lysates of GST and GST-ALIX fusion proteins diluted in running buffer (20 mM sodium phosphate, 150 mM NaCl, 0.2 mg ml^{-1} BSA, 0.005% (v/v) P20, pH 7.2) to densities of 3,000–3,500 response units. After GST-ALIX capture, chip surfaces were overcoated with recombinant GST to minimize nonspecific interactions with the GST antibody surface. Data for HIV-1 $p6^{Gag}A$, $p6^{Gag}T$ and EIAV $p9^{Gag}$ were previously reported[26] and are shown here for comparison. Lyophilized peptides of HIV-1 $p6^{Gag}A$, $p6^{Gag}T$, EIAV $p9^{Gag}$ and transferrin receptor 1 (TfR, $_{19}PLSYTRFSLARQV_{31}$)[38] were resuspended in 10 mM sodium phosphate, pH 7.2, 150 mM NaCl, diluted in running buffer and injected in duplicate from concentrations of 0 to 100 μM. Affinity parameters were obtained by plotting the equilibrium responses against the analyte concentration and fitting the data to simple 1:1 binding models[51]. Note that higher analyte concentrations gave rise to nonspecific surface binding.

HIV-1 infectivity and ALIX rescue experiments. The $p6^{Gag}$ Tyr36Phe mutation was introduced into wild-type $HIV\text{-}1_{NL4\text{-}3}$ and $HIV_{\Delta PTAP}$ R9 proviral constructs using the Megaprimer mutagenesis method (WISP07-85 and WISP07-86, respectively). Each mutation changed the $p6^{Gag}$ Tyr36 codon (TAT) to a Phe36 codon (TTT) without changing the p6*/Pol sequence in the −1 frame. Full cloning details are available upon request, and all other aspects of this experiment were performed as described previously[26].

HIV-1 VLP production. 293T cells were transfected (using Lipofectamine 2000) with HIV-1 Δp6 proviral plasmids expressing truncated HIV-1 Gag proteins fused to either HIV-1 $p6^{Gag}$ (p6, WISP07-87), EIAV $p9^{Gag}$ (p9, WISP07-88) or a minimal TSG101-binding motif (PEPTAPPEES, PTAP, WISP07-89)[15]. Cells were lysed in RIPA buffer and VLPs were harvested ~48 h after transfection through a 20% (w/v) sucrose cushion. Cell lysates and VLPs were analyzed by western blot with polyclonal antibodies to CA (1:10,000 dilution), MA (1:15,000) or ALIX (1:5,000)[11].

Accession codes. Protein Data Bank: Coordinates and structure-factor amplitudes have been deposited with accession codes 2R02 ($p6^{Gag}T$), 2R03 ($p9^{Gag}$) and 2R05 ($p6^{Gag}A$).

Note: Supplementary information is available on the Nature Structural & Molecular Biology website.

ACKNOWLEDGMENTS

We thank P. Bieniasz (Aaron Diamond AIDS Research Center) for kindly providing various HIV-1 proviral plasmids and H. Göttlinger (University of Massachusettes) for helpful discussions. This work was funded by US National Institutes of Health (NIH) grants GM082534 (C.P.H., W.I.S.) and AI051174 (W.I.S.). Portions of this research were performed at the Stanford Synchrotron Radiation Laboratory (SSRL), a national user facility operated by Stanford University on behalf of the US Department of Energy, Office of Basic Energy Sciences. The SSRL Structural Molecular Biology Program is supported by the Department of Energy, Office of Biological and Environmental Research, and by the NIH, National Center for Research Resources, Biomedical Technology Program and National Institute of General Medical Sciences. The Center for Biomolecular Interactions Analysis at the University of Utah is funded in part by NIH grant 1S10RR016787-01 (D.G.M.).

Published online at http://www.nature.com/nsmb/
Reprints and permissions information is available online at http://npg.nature.com/reprintsandpermissions

1. Demirov, D.G. & Freed, E.O. Retrovirus budding. *Virus Res.* **106**, 87–102 (2004).
2. Bieniasz, P.D. Late budding domains and host proteins in enveloped virus release. *Virology* **344**, 55–63 (2006).
3. Morita, E. & Sundquist, W.I. Retrovirus budding. *Annu. Rev. Cell Dev. Biol.* **20**, 395–425 (2004).
4. Garrus, J.E. *et al.* Tsg101 and the vacuolar protein sorting pathway are essential for HIV-1 budding. *Cell* **107**, 55–65 (2001).
5. Gottlinger, H.G., Dorfman, T., Sodroski, J.G. & Haseltine, W.A. Effect of mutations affecting the p6 gag protein on human immunodeficiency virus particle release. *Proc. Natl. Acad. Sci. USA* **88**, 3195–3199 (1991).
6. Huang, M., Orenstein, J.M., Martin, M.A. & Freed, E.O. p6Gag is required for particle production from full-length human immunodeficiency virus type 1 molecular clones expressing protease. *J. Virol.* **69**, 6810–6818 (1995).
7. Demirov, D.G., Ono, A., Orenstein, J.M. & Freed, E.O. Overexpression of the N-terminal domain of TSG101 inhibits HIV-1 budding by blocking late domain function. *Proc. Natl. Acad. Sci. USA* **99**, 955–960 (2002).
8. Martin-Serrano, J., Zang, T. & Bieniasz, P.D. HIV-1 and Ebola virus encode small peptide motifs that recruit Tsg101 to sites of particle assembly to facilitate egress. *Nat. Med.* **7**, 1313–1319 (2001).
9. VerPlank, L. *et al.* Tsg101, a homologue of ubiquitin-conjugating (E2) enzymes, binds the L domain in HIV type 1 Pr55(Gag). *Proc. Natl. Acad. Sci. USA* **98**, 7724–7729 (2001).
10. Strack, B., Calistri, A., Craig, S., Popova, E. & Gottlinger, H.G. AIP1/ALIX is a binding partner for HIV-1 p6 and EIAV p9 functioning in virus budding. *Cell* **114**, 689–699 (2003).
11. von Schwedler, U.K. *et al.* The protein network of HIV budding. *Cell* **114**, 701–713 (2003).
12. Vincent, O., Rainbow, L., Tilburn, J., Arst, H.N., Jr. & Penalva, M.A. YPXL/I is a protein interaction motif recognized by *Aspergillus* PalA and its human homologue, AIP1/Alix. *Mol. Cell. Biol.* **23**, 1647–1655 (2003).
13. Puffer, B.A., Parent, L.J., Wills, J.W. & Montelaro, R.C. Equine infectious anemia virus utilizes a YXXL motif within the late assembly domain of the Gag p9 protein. *J. Virol.* **71**, 6541–6546 (1997).
14. Chen, C., Vincent, O., Jin, J., Weisz, O.A. & Montelaro, R.C. Functions of early (AP-2) and late (AIP1/ALIX) endocytic proteins in equine infectious anemia virus budding. *J. Biol. Chem.* **280**, 40474–40480 (2005).
15. Martin-Serrano, J., Yarovoy, A., Perez-Caballero, D. & Bieniasz, P.D. Divergent retroviral late-budding domains recruit vacuolar protein sorting factors by using alternative adaptor proteins. *Proc. Natl. Acad. Sci. USA* **100**, 12414–12419 (2003).
16. Hurley, J.H. & Emr, S.D. The ESCRT complexes: structure and mechanism of a membrane-trafficking network. *Annu. Rev. Biophys. Biomol. Struct.* **35**, 277–298 (2006).
17. Odorizzi, G. The multiple personalities of Alix. *J. Cell Sci.* **119**, 3025–3032 (2006).
18. Williams, R.L. & Urbe, S. The emerging shape of the ESCRT machinery. *Nat. Rev. Mol. Cell Biol.* **8**, 355–368 (2007).
19. Carlton, J.G. & Martin-Serrano, J. Parallels between cytokinesis and retroviral budding-a role for the ESCRT machinery. *Science* **316**, 1908–1912 (2007).
20. Muziol, T. *et al.* Structural basis for budding by the ESCRT-III factor CHMP3. *Dev. Cell* **10**, 821–830 (2006).
21. Langelier, C. *et al.* Human ESCRT-II complex and its role in human immunodeficiency virus type 1 release. *J. Virol.* **80**, 9465–9480 (2006).
22. Kim, J. *et al.* Structural basis for endosomal targeting by the Bro1 domain. *Dev. Cell* **8**, 937–947 (2005).
23. Bowers, K. *et al.* Protein-protein interactions of ESCRT complexes in the yeast *Saccharomyces cerevisiae*. *Traffic* **5**, 194–210 (2004).
24. Pornillos, O., Alam, S.L., Davis, D.R. & Sundquist, W.I. Structure of the Tsg101 UEV domain in complex with the PTAP motif of the HIV-1 p6 protein. *Nat. Struct. Biol.* **9**, 812–817 (2002).
25. Pornillos, O. *et al.* Structure and functional interactions of the Tsg101 UEV domain. *EMBO J.* **21**, 2397–2406 (2002).
26. Fisher, R.D. *et al.* Structural and biochemical studies of ALIX/AIP1 and its role in retrovirus budding. *Cell* **128**, 841–852 (2007).
27. Usami, Y., Popov, S. & Gottlinger, H.G. Potent rescue of human immunodeficiency virus type 1 late domain mutants by ALIX/AIP1 that depends on its CHMP4 binding site. *J. Virol.* **81**, 6614–6622 (2007).
28. Bibollet-Ruche, F. *et al.* New simian immunodeficiency virus infecting De Brazza's monkeys (*Cercopithecus neglectus*): evidence for a cercopithecus monkey virus clade. *J. Virol.* **78**, 7748–7762 (2004).
29. Lee, S., Joshi, A., Nagashima, K., Freed, E.O. & Hurley, J.H. Structural basis for viral late-domain binding to Alix. *Nat. Struct. Mol. Biol.* **14**, 194–199 (2007).
30. Odorizzi, G., Katzmann, D.J., Babst, M., Audhya, A. & Emr, S.D. Bro1 is an endosome-associated protein that functions in the MVB pathway in *Saccharomyces cerevisiae*. *J. Cell Sci.* **116**, 1893–1903 (2003).
31. Vito, P., Pellegrini, L., Guiet, C. & D'Adamio, L. Cloning of AIP1, a novel protein that associates with the apoptosis-linked gene ALG-2 in a Ca^{2+}-dependent reaction. *J. Biol. Chem.* **274**, 1533–1540 (1999).

32. Missotten, M., Nichols, A., Rieger, K. & Sadoul, R. Alix, a novel mouse protein undergoing calcium-dependent interaction with the apoptosis-linked-gene 2 (ALG-2) protein. *Cell Death Differ.* **6**, 124–129 (1999).
33. Chen, B., Borinstein, S.C., Gillis, J., Sykes, V.W. & Bogler, O. The glioma-associated protein SETA interacts with AIP1/Alix and ALG-2 and modulates apoptosis in astrocytes. *J. Biol. Chem.* **275**, 19275–19281 (2000).
34. Chatellard-Causse, C. *et al.* Alix (ALG-2-interacting protein X), a protein involved in apoptosis, binds to endophilins and induces cytoplasmic vacuolization. *J. Biol. Chem.* **277**, 29108–29115 (2002).
35. Tsuda, M., Seong, K.H. & Aigaki, T. POSH, a scaffold protein for JNK signaling, binds to ALG-2 and ALIX in *Drosophila*. *FEBS Lett.* **580**, 3296–3300 (2006).
36. Munshi, U.M., Kim, J., Nagashima, K., Hurley, J.H. & Freed, E.O. An Alix fragment potently inhibits HIV-1 budding: characterization of binding to retroviral YPXL late domains. *J. Biol. Chem.* **282**, 3847–3855 (2007).
37. Martin-Serrano, J., Perez-Caballero, D. & Bieniasz, P.D. Context-dependent effects of L domains and ubiquitination on viral budding. *J. Virol.* **78**, 5554–5563 (2004).
38. Geminard, C., De Gassart, A., Blanc, L. & Vidal, M. Degradation of AP2 during reticulocyte maturation enhances binding of hsc70 and Alix to a common site on TFR for sorting into exosomes. *Traffic* **5**, 181–193 (2004).
39. Costa, L.J. *et al.* Interactions between Nef and AIP1 proliferate multivesicular bodies and facilitate egress of HIV-1. *Retrovirology* **3**, 33 (2006).
40. Otwinowski, Z. & Minor, W. Processing of X-ray diffraction data collected in oscillation mode. In *Methods in Enzymology* Vol. 276 (eds. Carter, C.W., Jr. & Sweet, R.M.) 307–326 (Academic Press, New York, 1997).
41. Murshudov, G.N., Vagin, A.A. & Dodson, E. Refinement of macromolecular structures by the maximum-likelihood method. *Acta Crystallogr. D* **53**, 240–255 (1997).
42. Merritt, E.A. & Painter, J. TLSMD web server for the generation of multi-group TLS models. *J. Appl. Cryst.* **39**, 109–111 (2006).
43. Painter, J. & Merritt, E.A. Optimal description of a protein structure in terms of multiple groups undergoing TLS motion. *Acta Crystallogr. D Biol. Crystallogr.* **62**, 439–450 (2006).
44. Murshudov, G.N., Vagin, A.A., Lebedev, A., Wilson, K.S. & Dodson, E.J. Efficient anisotropic refinement of macromolecular structures using FFT. *Acta Crystallogr. D* **55**, 247–255 (1999).
45. Howlin, B., Butler, S.A., Moss, D.S., Harris, G.W. & Driessen, H.P.C. TLSANL: TLS parameter analysis program for segmented anisotropic refinement of macromolecular structures. *J. Appl. Cryst.* **26**, 622–624 (1993).
46. CCP4. The CCP4 suite: programs for protein crystallography. *Acta Crystallogr. D* **50**, 760–763 (1994).
47. Jones, T.A., Zou, J.Y., Cowan, S.W. & Kjeldgaard, M. Improved methods for building protein models in electron density maps and the location of errors in these models. *Acta Crystallogr. A* **47**, 110–119 (1991).
48. Emsley, P. & Cowtan, K. Coot: model-building tools for molecular graphics. *Acta Crystallogr. D Biol. Crystallogr.* **60**, 2126–2132 (2004).
49. Laskowski, R.A., Moss, D.S. & Thornton, J.M. Main-chain bond lengths and bond angles in protein structures. *J. Mol. Biol.* **231**, 1049–1067 (1993).
50. Johnsson, B., Lofas, S. & Lindquist, G. Immobilization of proteins to a carboxymethyldextran-modified gold surface for biospecific interaction analysis in surface plasmon resonance sensors. *Anal. Biochem.* **198**, 268–277 (1991).
51. Myszka, D.G. Improving biosensor analysis. *J. Mol. Recognit.* **12**, 279–284 (1999).
52. DeLano, W.L. *The PyMOL Molecular Graphics System* (DeLano Scientific, San Carlos, California, USA, 2002).

Structural and Functional Studies of ALIX/AIP1 in Complex with the YPX$_n$L Late Domains from HIV-1 p6^{Gag} and EIAV p9^{Gag}

Qianting Zhai[1,3], Robert D. Fisher[1,3], Hyo-Young Chung[1], David G. Myszka[2], Wesley I. Sundquist[1]*, and Christopher P. Hill[1]*

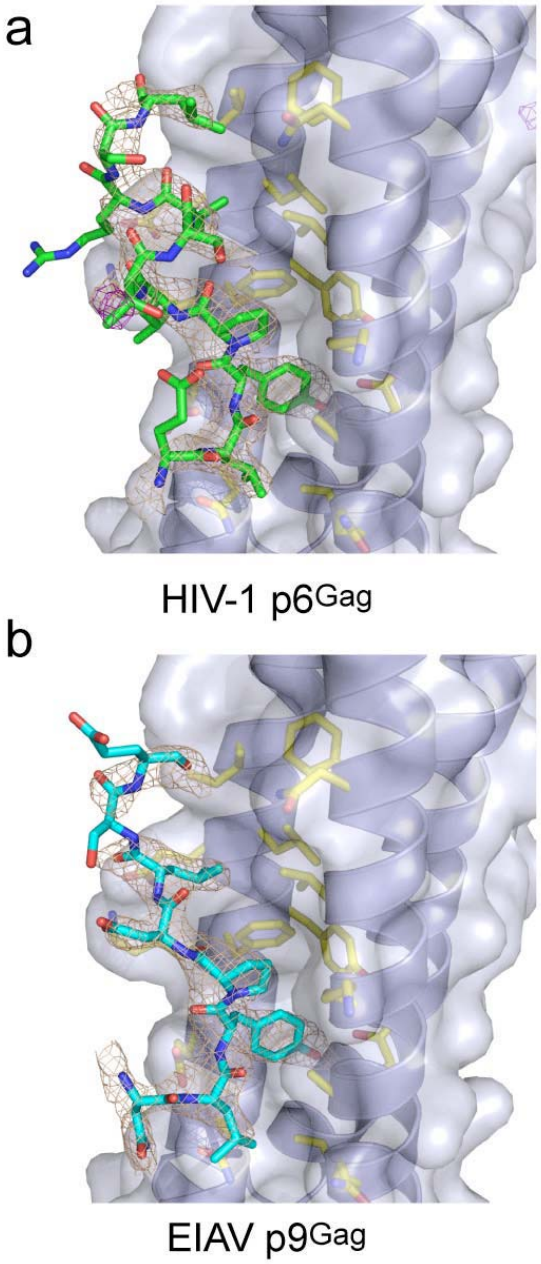

Supplementary Figure 1. HIV-1 $p6^{Gag}$ and EIAV $p9^{Gag}$ Peptide Omit Maps

Fo-Fc peptide omit maps (colored wheat, displayed at 2.2 x RMSD) were calculated from refined ALIX models that did not include peptide models for HIV-1 $p6^{Gag}$ (a) or EIAV $p9^{Gag}$ (b). An Fo($p6^{Gag}$T)-Fo($p6^{Gag}$A) difference map was calculated using phases from the ALIX:$p6^{Gag}$T model (magenta, displayed at 4.0 x RMSD). Since $p6^{Gag}$A/T peptides are identical except for threonine or alanine at position 39, the observed difference map peak corresponds to the location of Thr39 side chain atoms. This map further validated the helical structure of $p6^{Gag}$. The view is the same as that in Figures 1 c,d.

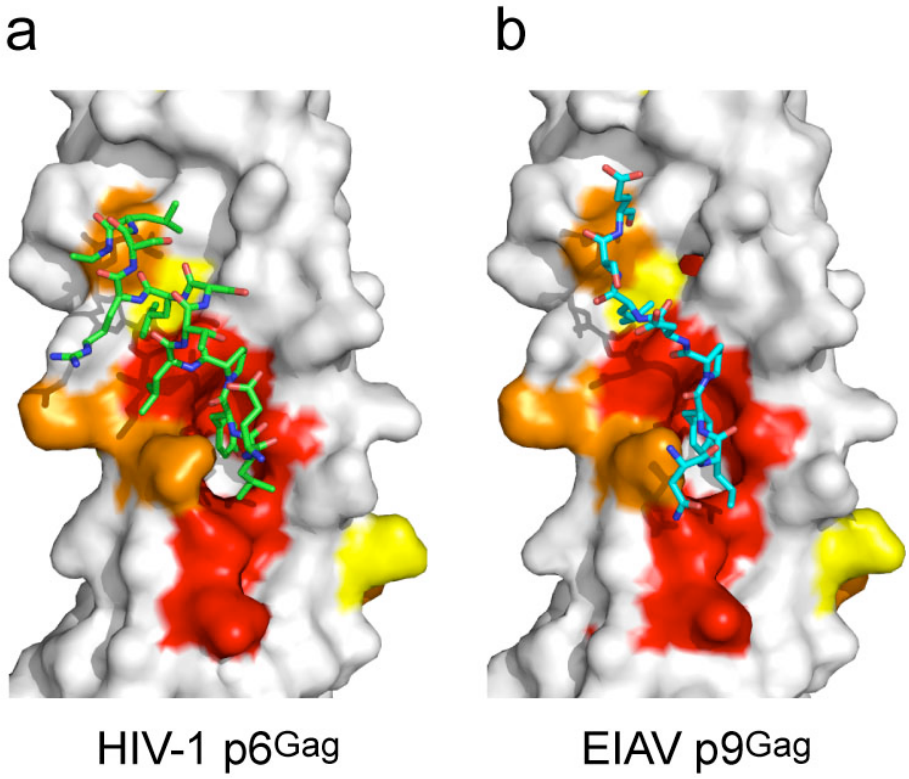

Supplementary Figure 2. ALIX Conservation at the Peptide Binding Site

HIV-1 $p6^{Gag}$ (a) and EIAV $p9^{Gag}$ (b) peptides (sticks) are shown binding to ALIX, which is shown as a surface that is colored according to sequence conservation from alignment of nine divergent species in ESPript[1]; residues with scaled similarity scores are color coded as follows: 85-100 are red, 68-84 are orange, and 50-67 are yellow (see also ref. 2). Extension of the conserved surface ~10 Å N-terminal to the late domain peptides suggests that endogenous ligands might bind to a larger region of the ALIX surface. The nine species used in the alignment to define conservation are: *Homo sapiens* (Human), *Mus musculus* (Mouse), *Gallus gallus* (Chicken), *Xenopus laevis* (African clawed frog),

Drosophila melanogaster (Fruit fly), *Caenorhabditis elegans*, *Dictyostelium discoideum* (Slime mold), *Arabidopsis thaliana* (Mouse-ear cress), and *Aspergillus oryzae*.

1. Gouet, P., Courcelle, E., Stuart, D.I. & Metoz, F. ESPript: analysis of multiple sequence alignments in PostScript. *Bioinformatics* **15**, 305-8 (1999).

2. Fisher, R.D. et al. Structural and Biochemical Studies of ALIX/AIP1 and Its Role in Retrovirus Budding. *Cell* **128**, 841-52 (2007).

CHAPTER 4

IDENTIFICATION AND STRUCTRUAL CHARACTERIZATION OF THE ALIX-BINDING LATE DOMAINS OF SIMIAN IMMUNODEFICIENCY VIRUS SIV_{MAC239} AND $SIV_{AGMTAN-1}$

Qianting Zhai, Michael B. Landesman, Howard Robinson,Wesley I. Sundquist, and Christopher P. Hill

This research was originally published in the Journal of Virology.
Reprinted with permission from American Society for Microbiology.

Identification and Structural Characterization of the ALIX-Binding Late Domains of Simian Immunodeficiency Virus SIV_{mac239} and $SIV_{agmTan-1}$ ▽

Qianting Zhai,[1]† Michael B. Landesman,[1]† Howard Robinson,[2]
Wesley I. Sundquist,[1]* and Christopher P. Hill[1]*

Department of Biochemistry, University of Utah School of Medicine, Salt Lake City, Utah 84112-5650,[1] and Department of Biology, Brookhaven National Laboratory, Upton, New York 11973[2]

Received 10 August 2010/Accepted 4 October 2010

Retroviral Gag proteins contain short late-domain motifs that recruit cellular ESCRT pathway proteins to facilitate virus budding. ALIX-binding late domains often contain the core consensus sequence YPX_nL (where X_n can vary in sequence and length). However, some simian immunodeficiency virus (SIV) Gag proteins lack this consensus sequence, yet still bind ALIX. We mapped divergent, ALIX-binding late domains within the $p6^{Gag}$ proteins of SIV_{mac239} ($_{40}$SREKPYKEVTEDLLHLNSLF$_{59}$) and $SIV_{agmTan-1}$ ($_{24}$AAGAYDPARKLLEQY AKK$_{41}$). Crystal structures revealed that anchoring tyrosines (in lightface) and nearby hydrophobic residues (underlined) contact the ALIX V domain, revealing how lentiviruses employ a diverse family of late-domain sequences to bind ALIX and promote virus budding.

Many enveloped viruses, including retroviruses, recruit proteins of the cellular ESCRT pathway to facilitate budding (reviewed in references 3, 11, and 35). Short sequence motifs, termed late domains, within retroviral Gag polyproteins bind directly to early-acting ESCRT factors, which then recruit and activate the downstream machinery necessary for membrane fission. The three well-characterized late domains are typically denoted by their canonical core amino acid sequences: PTAP late domains bind the ubiquitin E2 variant (UEV) domain of the TSG101 subunit of the ESCRT-I complex, PPXY late domains bind WW domains of NEDD4 family ubiquitin E3 ligases, and YPX_nL (where X_n can vary in sequence and length) late domains bind the V domain of ALIX (10, 20, 32, 37). In a number of cases, retroviral Gag proteins have been shown to utilize multiple late domains (e.g., see references 3, 4, 7, 11, 16, 31, 33, 34, and 35). We speculate that this phenomenon may be even more prevalent than is currently appreciated because mutations in auxiliary late domains often produce weak or cell-specific phenotypes and because late domains can be difficult to recognize owing to primary sequence divergence. It is therefore of interest to define the range of different sequences that can function as late domains and to learn how sequence variation is tolerated while late-domain function is retained.

Strack and colleagues initially reported that ALIX binds core sequences of $_{35}$LYPLTSL$_{41}$ and $_{22}$LYPDL$_{26}$ within the late domains of human immunodeficiency virus type 1 (HIV-1) $p6^{Gag}$ and equine infectious anemia virus (EIAV) $p9^{Gag}$, respectively (32) (anchoring tyrosines are shown in boldface, and nearby hydrophobic residues that contact ALIX are underlined). They also reported that $p6^{Gag}$ proteins from simian immunodeficiency virus SIV_{mac239} and $SIV_{agmTan-1}$ can bind and package ALIX into virions, but in those cases the ALIX-binding sites were not fully mapped and were not obvious, because the SIV $p6^{Gag}$ proteins lacked canonical YPX_nL ALIX-binding elements. We therefore performed biosensor binding experiments and deletion analyses to quantify and map the ALIX-binding sites. These experiments employed a recombinant ALIX protein that spanned the Bro1 and V domains (residues 1 to 698), here denoted $ALIX_{Bro1-V}$, but lacked the C-terminal proline-rich region (residues 699 to 868). As shown in Fig. 1, $ALIX_{Bro1-V}$ bound directly to the full-length $p6^{Gag}$ proteins from SIV_{mac239} (equilibrium dissociation constant [K_D], 66 ± 4 μM) and $SIV_{agmTan-1}$ (K_D, 24 ± 1 μM), with binding affinities that were comparable to those of HIV-1 $p6^{Gag}$ and EIAV $p9^{Gag}$ (K_D, 40 and 1.5 μM, respectively) (37).

Deletion experiments were performed to map the ALIX-binding sites to the following sequences: SIV_{mac239} $p6^{Gag}$, $_{40}$S REKPYKEVTEDLLHLNSLF$_{59}$; and $SIV_{agmTan-1}$ $p6^{Gag}$, $_{24}$A AGAYDPARKLLEQYAKK$_{41}$ (Fig. 1 and data not shown). In both cases, ALIX bound the full-length SIV $p6^{Gag}$ proteins and the minimal binding sites with comparable affinities, indicating that ALIX binding was not significantly influenced by $p6^{Gag}$ residues beyond the immediate binding site. The late domains of HIV-1 $p6^{Gag}$ and EIAV $p9^{Gag}$ both contain key tyrosine residues that bind in a deep pocket on the second arm of the ALIX V domain (37). The ALIX-binding sites within SIV_{mac239} and $SIV_{agmTan-1}$ $p6^{Gag}$ also contained single tyrosine residues (highlighted in boldface), and alanine point mutations in each of these tyrosines eliminated any detectable ALIX binding to the full-length SIV $p6^{Gag}$ proteins (Fig. 1). Thus, these tyrosines are also key determinants of ALIX binding to the SIV $p6^{Gag}$ proteins.

To learn how these SIV $p6^{Gag}$ proteins recognize and recruit ALIX, we crystallized and determined the structures of $ALIX_{Bro1-V}$ ($KK_{268,269}YY$ mutant) in complex with binding-site peptides from the $SIV_{agmTan-1}$ and SIV_{mac239} $p6^{Gag}$ proteins. Crystallization and data collection were performed as

* Corresponding author. Mailing address: Department of Biochemistry, University of Utah School of Medicine, 15 N. Medical Drive East, Room 4100, Salt Lake City, UT 84112-5650. Phone for W. I. Sundquist: (801) 585-5402. Fax: (801) 581-7959. E-mail: wes@biochem.utah.edu. Phone for C. P. Hill: (801) 585-5536. Fax: (801) 581-7959. E-mail: chris@biochem.utah.edu.

† Q.Z. and M.B.L. contributed equally.

▽ Published ahead of print on 20 October 2010.

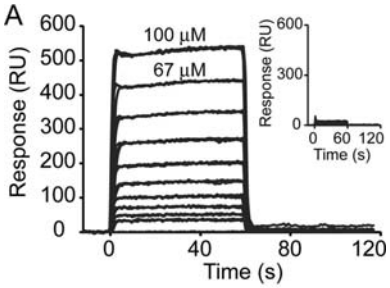

C

ALIX Binding Site	Equilibrium Dissociation Constant (K_D, μM)
SIV_{mac239} p6	66±4
SIV_{mac239} $p6_{40-59}$	82±8
SIV_{mac239} $p6_{Y45A}$	>2000
$SIV_{agmTan-1}$ p6	24.5±0.5
$SIV_{agmTan-1}$ $p6_{24-41}$	23±0
$SIV_{agmTan-1}$ $p6_{Y28A}$	>2000
HIV-1 p6	40±10
HIV-1 $p6_{32-46}$	8±2
EIAV p9	1.5±0.3
EIAV $p9_{19-31}$	7±1

FIG. 1. $ALIX_{Bro1-V}$ binding to different $p6^{Gag}$ proteins. (A) Representative biosensor sensograms for $ALIX_{Bro1-V}$ binding to immobilized wild-type (main graph) or Y45A mutant (inset) SIV_{mac239} glutathione *S*-transferase (GST)-$p6^{Gag}$ proteins. Samples were analyzed in triplicate. $p6^{Gag}$ proteins, minimal binding peptides (blocked N and C termini), were created, and the binding studies were performed and analyzed as described previously (37). RU, response units. (B) Representative biosensor binding isotherms for $ALIX_{Bro1-V}$ binding to SIV_{mac239} GST-$p6^{Gag}$ or $SIV_{agmTan-1}$ $p6^{Gag}$ proteins. (C) Summary of $ALIX_{Bro1-V}$ dissociation constants for different retroviral p6/p9 proteins/peptides. Values for SIV peptides are the means from two independent experiments (each measured in triplicate) ± ranges. Dissociation constants for the HIV-1 and EIAV peptides were reported previously (37) but are reprinted here for reference.

previously described (37). Crystallographic statistics are provided in Table 1. A comparison of the two SIV peptide complex structures with the previously reported HIV and EIAV late-domain complexes reveals that the ALIX protein structure is essentially invariant. In all cases, the dominant interaction is insertion of a tyrosine side chain of the p6 peptide into a deep hydrophobic pocket on ALIX (Fig. 2). The tyrosines of all four late-domain peptides superimpose closely and make the same contacts with ALIX, including a hydrogen bond between the tyrosine phenoxyl and the conserved ALIX Asp506 side chain. As described previously, the EIAV and HIV late-domain interfaces also bury a proline immediately following the tyrosine (the Y + 1 position) and a leucine at Y + 3 (EIAV) or Y + 5 (HIV), with the different leucine positions being accommodated by different conformations of the peptide backbone, either extended (EIAV, designated a type 1 ALIX-binding motif) or helical (HIV, designated type 2) from the Y + 2 position.

The two SIV peptides form equivalent ALIX interfaces but do so by adopting yet another conformation (termed a type 3 ALIX-binding motif). In both cases, they are helical from the Y + 1 residue, which results in the Y + 3 Val/Ala and Y + 7 Leu occupying the same locations as the Pro and Leu of EIAV and HIV (Fig. 2). The most notable difference between the two SIV peptides is that their helices project at an angle of 15° with respect to each other. This presumably results from differences in residues that contact ALIX, especially Val versus Ala at position Y + 3, and results in a 2.5-Å displacement of the $SIV_{agmTan-1}$ Y + 7 Leu compared to the structurally equivalent Leu of SIV_{mac239}, HIV, and EIAV. Thus, late-domain sequences adopt a range of conformations in order to preserve the interaction motif: $\Phi YX_{0/2}\Phi X_{1/3}L$, with the alternative 0/2 and 1/3 spacings of the intervening X residues accommodated by extended versus helical backbone conformations.

TABLE 1. Crystallographic statistics for ALIX complexes[a]

Parameter[b]	Value for indicated strain[c]	
	SIV_{mac239}	$SIV_{agmTan-1}$
Space group	C2	C2
Cell dimensions		
a (Å)	145.3	145.5
b (Å)	99.3	99.1
c (Å)	72.5	72.6
β (°)	106.9	106.6
Resolution (Å)	45–2.3 (2.38–2.3)	45–2.5 (2.59–2.5)
Completeness (%)	97.7 (82.6)	95.6 (70.8)
$I/\sigma(I)$	18.2 (3.9)	31.5 (3.5)
R_{sym} (%)[c]	9.6 (28.2)	5.5 (32.0)
No. of unique reflections	44,063	34,197
R_{factor}/R_{free} (%)[d]	20.5/25.2	20.4/26.1
No. of protein atoms	5,614	5,559
No. of water molecules	58	22
Avg B factor (Å^2)		
Protein atoms	77.6	86.5
Water molecules	58	63.6
RMSD from ideal geometry		
Bonds (Å)	0.007	0.008
Angles (°)	0.994	1.057

[a] Data were collected at beam line X29 of the National Synchrotron Light Source and processed using HKL2000 (23). The structures were determined using rigid-body refinement with the unliganded $ALIX_{Bro1-V}$ model and were refined in PHENIX (1) with TLS refinement (24, 25). Model building was performed with O (17) and COOT (9).

[b] $R_{sym} = (|(\Sigma I - \langle I \rangle)|)/(\Sigma I)$, where $\langle I \rangle$ is the average intensity of multiple measurements. $R_{factor} = \Sigma_{hkl}||F_{obs}(hkl)| - F_{calc}(hkl)||/\Sigma_{hkl}|F_{obs}(hkl)|$. R_{free} = the cross-validation R factor for the 5% of reflections against which the model was not refined.

[c] Values in parentheses are for the highest-resolution shell.

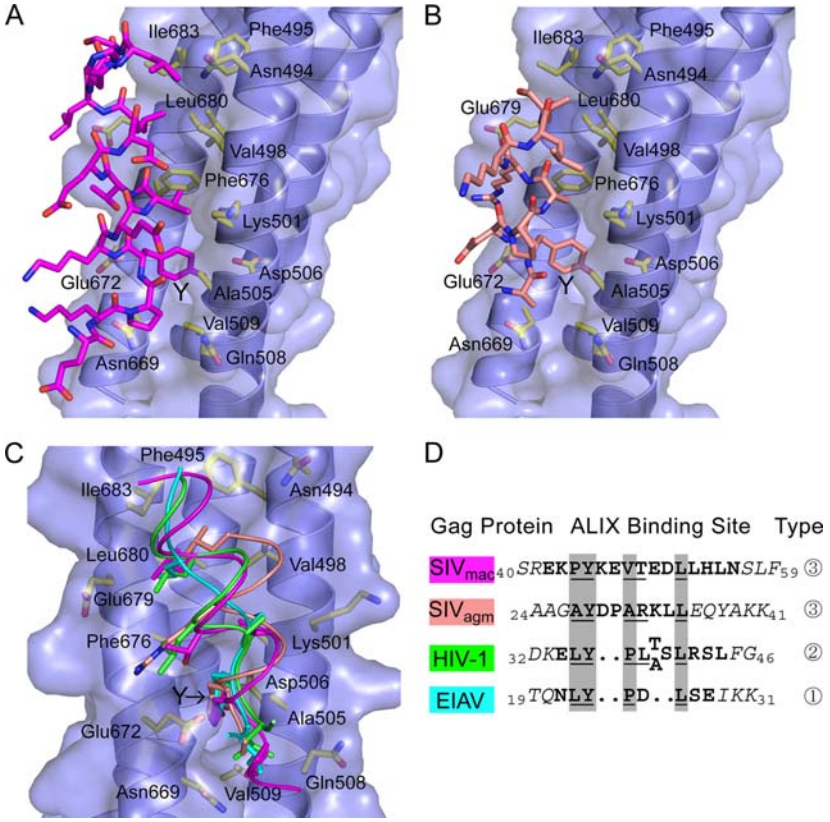

FIG. 2. Structures of SIV late domains bound to the second V-domain arm of human $ALIX_{Bro1\text{-}V}$. (A) SIV_{mac239} $p6^{Gag}$ late-domain peptide (magenta sticks) and human $ALIX_{Bro1\text{-}V}$ protein, represented as a blue ribbon and surface, with the side chains of binding-site residues shown explicitly and labeled. The p6 tyrosine is indicated with a Y. The p6 peptide is oriented with the N terminus at the bottom of the figure. (B) $SIV_{agmTam\text{-}1}$ $p6^{Gag}$ late-domain peptide and $ALIX_{Bro1\text{-}V}$ complex. (C) Overlay of the ALIX in complex with late-domain peptides of HIV-1 $p6^{Gag}$ (Protein Data Bank code 2R02; green), EIAV $p9^{Gag}$ (Protein Data Bank code 2R03; turquoise), SIV_{mac239} $p6^{Gag}$ (magenta), and $SIV_{agmTan\text{-}1}$ $p6^{Gag}$ (salmon). Panels A to C were generated using PyMOL (6). (D) Late-domain peptide sequences used for crystallography and binding studies, aligned on the basis of the crystal structures. Residues modeled in the crystal structures are in boldface, and those lacking electron density are in italics. Residues that are structurally equivalent in all four complexes are highlighted by a gray background. Residues that bury more than 50% of their solvent-accessible surface at the protein interface are underlined. Note that ALIX binds three different types of viral sequence motifs, which we have designated types 1 to 3.

Sequence analyses revealed that nearly all primate lentiviruses carry one of the three different types of ALIX-binding motifs, supporting the idea that type 3 ALIX-binding motifs can function as late domains that enhance virus budding (Fig. 3A). SIV_{mac239} $p6^{Gag}$ has been analyzed by deletion analysis (26), but unfortunately the functional importance of the key tyrosine residue in the ALIX-binding site was not tested. We therefore used a SIV_{mac251}-based system (21), for which a vector was available, to test whether noncanonical ALIX-binding sites within SIV $p6^{Gag}$ proteins can function as late domains. SIV_{mac251} and SIV_{mac239} are closely related and have identical $p6^{Gag}$ ALIX-binding sites. Both isolates also contain PTAP elements within $p6^{Gag}$ that presumably bind TSG101 and function as late domains.

Constructs were designed to mutate key residues in both candidate late domains within the SIV_{mac251} $p6^{Gag}$ proteins encoded by the pSIV3+ helper vector without altering the underlying Pol reading frame ($_{11}$PTAP$_{14}$ to $_{11}$LIAL$_{14}$, termed ΔPTAP; and $_{38}$EKPYKEVTEDLLHL$_{51}$ to $_{38}$EKP*S*KEVTED *S*LHL$_{51}$, termed ΔYL; mutated residues are italicized). Virions were produced in 293T cells and analyzed as described previously (30), with Western blotting used to detect virion-associated and cellular CA levels (anti-SIVmac CA mouse monoclonal antibody, 1:3,000 [14]) and cellular ALIX levels (anti-ALIX rabbit polyclonal antibody, 1:5,000 [10]). Viral titers were measured using flow cytometry to detect green fluorescent protein (GFP) expression from the packaged pSIVgaMES4sin vector in transduced 293T cells.

As expected, the ΔPTAP mutation inhibited SIV_{mac251} release, as measured by reductions in virion-associated CA (p27) protein levels (Fig. 3B, VIRION Western blot, compare lanes 1 and 2), without altering cellular CA expression levels (CELL

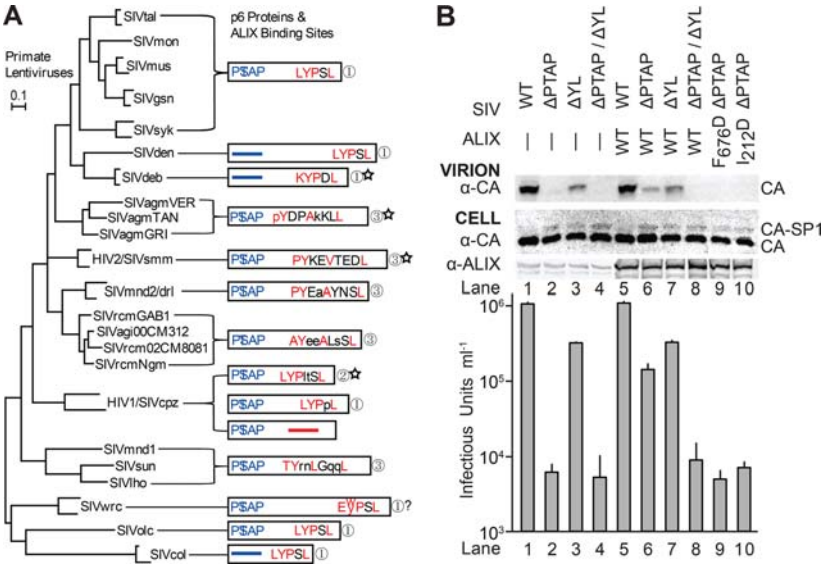

FIG. 3. Primary sequences and functional analyses of the late domains within primate lentiviral p6^{Gag} proteins. (A) Maximum likelihood phylogenetic tree showing the different primate lentiviral lineages and their p6^{Gag} proteins (drawn to scale as white boxes). TSG101-binding P(S/T)AP late domains are shown in blue, and putative ALIX-binding late domains are shown in red (predicted ALIX contact residues) or black (solvent exposed residues). ALIX-binding-site types are designated at right (see text for explanation). Sequences that most closely match the crystallographically characterized ALIX complexes are denoted with stars. Consensus sequences for the designated lineage(s) were derived from reference 19, and residues conserved at >85% identity are shown in capital letters. p6^{Gag} proteins from the HIV-1/SIV$_{cpz}$ lineage fall into three different classes that either have type 1 or 2 ALIX-binding sites or lack apparent ALIX-binding sites (and also lack tyrosines). Putative ALIX-binding sites within SIV$_{wrc}$ proteins can have either a Trp or Tyr residue in the second position, and the effect of the Trp substitution on ALIX binding has not been tested. The scale bar represents 0.1 substitution per site, and the tree was adapted from reference 1a. (B) Mutations in the SIV$_{mac251}$ p6^{Gag} $_{11}$PTAP$_{14}$ (ΔPTAP) and $_{38}$EKPYKEVTEDLLHL$_{51}$ (ΔYL) sequences inhibited virion release (Western blot, panel 1) and reduced viral titers (bottom graph, single-cycle infectivity assays), and ALIX overexpression stimulated release of the SIV$_{mac251}$ ΔPTAP construct. Cells were transfected with the designated SIV$_{mac251}$ vectors (WISP10-480-484), and cotransfected with either an empty pCI-neo vector control (lanes 1 to 4) or vectors expressing either wild-type (WT) FLAG-ALIX (lanes 5 to 8) or the designated mutant (lanes 9 and 10) FLAG-ALIX proteins. Vector transduction titers shown in the graph were measured in single-cycle infectivity assays (n = 5 assays; values are shown plus standard deviations). Western blots showing the levels of cell-associated CA and ALIX are also shown (CELL), with endogenous ALIX expression levels (lanes 1 to 4) enhanced 20-fold relative to exogenous ALIX expression levels (lanes 5 to 10) for ease of visualization.

blot). Vector titers were also dramatically reduced, essentially to background levels [from 1.06 (±0.06) × 10^6/ml to 6 (±2) × 10^3/ml; 180-fold reduction] (Fig. 3B, bottom panel, compare lanes 1 and 2). SIV$_{mac251}$ release and infectivity were also reduced by the ΔYL mutation in the ALIX-binding site, although the reduction was much less dramatic than for the ΔPTAP mutation (Fig. 3B, compare lanes 1 and 3; 3-fold infectivity reduction). The ΔPTAP/ΔYL double mutation inhibited virus release to an even greater extent than either single mutation alone (Fig. 3B, compare lanes 2 and 4), with viral titers again near background levels. Mutations in either (or both) late domains led to accumulation of the CA-SP1 processing intermediate within cells (Fig. 3B, CELL blot, compare lane 1 to lanes 2 to 4). This phenotype is also seen for HIV-1 late-domain mutants and is indicative of budding defects (13). Thus, both the $_{11}$PTAP$_{14}$ and $_{38}$EKPYKEVTEDLLHL$_{51}$ sequences within SIV$_{mac251}$ p6^{Gag} promote Gag processing, virion release, and viral infectivity, and the PTAP sequence serves as the dominant late domain under these experimental conditions. The situation is similar for HIV-1; both the ALIX- and TSG101-binding late domains are functional, but mutations in the PTAP element are more detrimental in most cell types (12).

To confirm that the SIV$_{mac251}$ p6^{Gag} $_{38}$EKPYKEVTEDLLHL$_{51}$late domain was ALIX responsive, we tested whether ALIX overexpression stimulated virus release via this sequence (10, 33). ALIX overexpression did not alter the release and infectivity of wild-type SIV$_{mac251}$, presumably because the $_{11}$PTAP$_{14}$ late domain was already highly active (Fig. 3B, compare lanes 1 and 5). In contrast, ALIX overexpression substantially stimulated the release and infectivity of an SIV$_{mac251}$ ΔPTAP construct [to 1.4 (±0.2) × 10^5; 23-fold infectivity increase] (Fig. 3B, compare lanes 2 and 6). This stimulation was dependent upon the ALIX-binding site within SIV$_{mac251}$ p6^{Gag}, because ALIX overexpression failed to stimulate either the ΔYL or the ΔPTAP/ΔYL mutant constructs significantly (compare lanes 3 to 7 and 4 to 8). Stimulation also required the YPX$_n$L-binding site of ALIX, because an inactivating point mutation within this site (F676D) blocked the ability of ALIX to stimulate release of the ΔPTAP construct (compare lanes 6 and 9). Thus, the $_{38}$EKPYKEVTEDLLHL$_{51}$ site within SIV$_{mac251}$ p6^{Gag} functions as an ALIX-dependent late domain.

As shown in Fig. 3A, $p6^{Gag}$ proteins from nearly every known primate lentiviral lineage contain a type 1, type 2, or type 3 ALIX-binding site, implying that (i) the ability to bind ALIX must provide primate lentiviruses with a strong selective advantage and (ii) these three types probably account for all (or nearly all) of the different ALIX-binding modes. The only exceptions are a subset of viruses within the HIV-1/SIV_{cpz} lineage, which lack identifiable ALIX-binding sites, and possibly also a subset of SIV_{wrc} viruses whose type 1 ALIX-binding sites have Trp in place of Tyr. Type 3 ALIX-binding sites are widespread throughout primate lentiviruses, and type 1 and 3 sites are more common than type 2 sites (which predominate only in HIV-1 strains). Interestingly, $p6^{Gag}$ proteins that lack the ability to bind TSG101 typically have type 1 ALIX-binding sites (2). Type 1 sites bind ALIX with relatively high affinities, at least in the cases examined to date (Fig. 1C), and this correlation may therefore reflect a need to recruit ALIX more efficiently when TSG101 cannot be recruited directly.

Although ALIX binds rather weakly to most isolated late domains, several factors likely enhance ALIX recruitment *in vivo*. First, p6-ALIX V domain interactions of the type studied here can be augmented by upstream interactions between the ALIX Bro1 domain and the HIV-1 Gag NC domain (8, 28, 29). Analogous SIV NC-ALIX Bro1 interactions are also possible, although such interactions alone are apparently not sufficient to stimulate virus release because ALIX overexpression does not substantially rescue SIV_{mac251} release or infectivity in the absence of the $p6^{Gag}$ ALIX-binding site. Second, activated ALIX is dimeric (27), which should enhance binding avidity to oligomeric Gag assemblies. Third, ALIX can associate with ubiquitin, and ubiquitylation of Gag (or associated proteins) could therefore enhance ALIX recruitment (18). Finally, both Gag and ALIX can associate with membranes, which may increase the effective local ALIX concentrations at budding sites. Thus, relatively weak ALIX-$p6^{Gag}$ interactions of the type described here are apparently sufficient to ensure that ALIX is recruited to function in virus budding.

Once recruited, ALIX can stimulate virus budding by recruiting the downstream ESCRT-III membrane fission machinery via direct interactions with CHMP4 subunits (10, 33) and also via additional stimulatory activities of the N-terminal Bro1 domain that may involve membrane deformation (28). CHMP4 recruitment appears to be important in the case of SIV_{mac251}, because the $ALIX_{I212D}$ mutant, which cannot bind CHMP4 (22), also failed to stimulate release of the ΔPTAP construct (Fig. 3B, compare lanes 6 and 10). Thus, the ALIX-binding site in SIV_{mac251} $p6^{Gag}$ functions, at least in part, to provide access to the membrane fission activity of the downstream ESCRT-III proteins.

Our results also have important implications for the identification of cellular ALIX-binding partners. The YPX_nL-binding site within the ALIX V domain presumably evolved to bind cellular partners, rather than viral late domains. To date, however, only one cellular interaction of this type has been identified: that between the *Aspergillus* ALIX homolog PalA and its binding partner PacC (36). PalA binds tandem YPXL/I motifs within PacC that match canonical EIAV late domains, and this interaction facilitates the pH-regulated cleavage of the PacC transcription factor. Such pH-sensing pathways are not conserved outside of fungi, however, suggesting that additional ALIX-binding partners have yet to be identified. Our studies show that ALIX can bind a broader range of sequences than previously appreciated, requiring only an anchoring tyrosine interaction and downstream hydrophobic residues that can vary in both identity and spacing. Cellular ALIX-binding partners (and possibly also other viruses) can presumably also employ this very loose consensus motif, which may help explain why the mammalian ALIX-binding partner(s) has thus far escaped detection.

Protein structure accession numbers. Coordinates and diffraction data for $ALIX_{Bro1\text{-}V}$ ($KK_{268,269}YY$ mutant) in complex with the SIV_{mac239} and $SIV_{agmTan\text{-}1}$ peptides have been deposited in the Protein Data Bank (PDB codes 2XS1 and 2XS8, respectively).

We thank Niels Pedersem for supplying the SIV_{mac} p27 monoclonal antibody (55-2F12) through the AIDS Research and Reference Reagent Program, Division of AIDS, NIAID, NIH, Jean-Luc Darlix for the gift of the SIV_{mac251} vector system, David Myszka and Rebecca Rich at the University of Utah HSC Protein Interactions Core Research Facility for assistance with the biosensor binding experiments, and Martine Peeters, Vanessa Hirsch, and Beatrice Hahn for helpful direction on primate lentivirus lineages.

Operations of the National Synchrotron Light Source (NSLS) are supported by the Office of Basic Energy Sciences at the U.S. Department of Energy and by the NIH. Data collection at the NSLS was funded by the National Center for Research Resources. This work was supported by NIH grants AI051174 (to W.I.S.) and P50 082545 (W.I.S. and C.P.H.).

REFERENCES

1. **Adams, P. D., P. V. Afonine, G. Bunkóezi, V. B. Chen, I. W. Davis, N. Echols, J. J. Headd, L.-W. Hung, G. J. Kapral, R. W. Grosse-Kunstleve, A. J. McCoy, N. W. Moriarty, R. Oeffner, R. J. Read, D. C. Richardson, J. S. Richardson, T. C. Terwilliger, and P. H. Zwart.** 2010. PHENIX: a comprehensive Python-based system for macromolecular structure solution. Acta Crystallogr. D Biol. Crystallogr. **66:**213–221.
1a. **Ahuka-Mundeke, S., F. Liegeois, A. Ayouba, Y. Foupouopouognini, E. Nerrienet, E. Delaporte, and M. Peeters.** 25 August 2010. Full-length genome sequence of a simian immunodeficiency virus infecting a captive agile mangabey (Cercocebus agilis) is closely related to SIVrcm infecting wild red-capped mangabeys (Cercocebus torquatus) in Cameroon. J. Gen. Virol. [Epub ahead of print.]
2. **Bibollet-Ruche, F., E. Bailes, F. Gao, X. Pourrut, K. L. Barlow, J. P. Clewley, J. M. Mwenda, D. K. Langat, G. K. Chege, H. M. McClure, E. Mpoudi-Ngole, E. Delaporte, M. Peeters, G. M. Shaw, P. M. Sharp, and B. H. Hahn.** 2004. New simian immunodeficiency virus infecting De Brazza's monkeys (Cercopithecus neglectus): evidence for a cercopithecus monkey virus clade. J. Virol. **78:**7748–7762.
3. **Bieniasz, P. D.** 2009. The cell biology of HIV-1 virion genesis. Cell Host Microbe **5:**550–558.
4. **Chung, H. Y., E. Morita, U. von Schwedler, B. Muller, H. G. Krausslich, and W. I. Sundquist.** 2008. NEDD4L overexpression rescues the release and infectivity of human immunodeficiency virus type 1 constructs lacking PTAP and YPXL late domains. J. Virol. **82:**4884–4897.
5. Reference deleted.
6. **DeLano, W. L.** 2008. The PyMOL molecular graphics system. DeLano Scientific LLC, Palo Alto, CA.
7. **Dilley, K. A., D. Gregory, M. C. Johnson, and V. M. Vogt.** 2010. An LYPSL late domain in the gag protein contributes to the efficient release and replication of Rous sarcoma virus. J. Virol. **84:**6276–6287.
8. **Dussupt, V., M. P. Javid, G. Abou-Jaoude, J. A. Jadwin, J. de La Cruz, K. Nagashima, and F. Bouamr.** 2009. The nucleocapsid region of HIV-1 Gag cooperates with the PTAP and LYPXnL late domains to recruit the cellular machinery necessary for viral budding. PLoS Pathog. **5:**e1000339.
9. **Emsley, P., and K. Cowtan.** 2004. Coot: model-building tools for molecular graphics. Acta Crystallogr. D Biol. Crystallogr. **60:**2126–2132.
10. **Fisher, R. D., H. Y. Chung, Q. Zhai, H. Robinson, W. I. Sundquist, and C. P. Hill.** 2007. Structural and biochemical studies of ALIX/AIP1 and its role in retrovirus budding. Cell **128:**841–852.
11. **Fujii, K., J. H. Hurley, and E. O. Freed.** 2007. Beyond Tsg101: the role of Alix in 'ESCRTing' HIV-1. Nat. Rev. Microbiol. **5:**912–916.
12. **Fujii, K., U. M. Munshi, S. D. Ablan, D. G. Demirov, F. Soheilian, K. Nagashima, A. G. Stephen, R. J. Fisher, and E. O. Freed.** 2009. Functional role of Alix in HIV-1 replication. Virology **391:**284–292.

13. **Göttlinger, H. G., T. Dorfman, J. G. Sodroski, and W. A. Haseltine.** 1991. Effect of mutations affecting the p6 gag protein on human immunodeficiency virus particle release. Proc. Natl. Acad. Sci. U. S. A. **88:**3195–3199.
14. **Higgins, J. R., S. Sutjipto, P. A. Marx, and N. C. Pedersen.** 1992. Shared antigenic epitopes of the major core proteins of human and simian immunodeficiency virus isolates. J. Med. Primatol. **21:**265–269.
15. Reference deleted.
16. **Jadwin, J. A., V. Rudd, P. Sette, S. Challa, and F. Bouamr.** 2010. Late domain-independent rescue of a release-deficient Moloney murine leukemia virus by the ubiquitin ligase itch. J. Virol. **84:**704–715.
17. **Jones, T. A., J. Y. Zou, S. W. Cowan, and Kjeldgaard.** 1991. Improved methods for binding protein models in electron density maps and the location of errors in these models. Acta Crystallogr. A **47:**110–119.
18. **Joshi, A., U. Munshi, S. D. Ablan, K. Nagashima, and E. O. Freed.** 2008. Functional replacement of a retroviral late domain by ubiquitin fusion. Traffic **9:**1972–1983.
19. **Kuiken, C., B. Foley, T. Leitner, C. Apetrei, B. Hahn, I. Mizrachi, J. Mullins, A. Rambaut, S. Wolinsky, and B. Korber (ed.).** 2010. HIV sequence compendium 2010. Los Alamos National Laboratory, Theoretical Biology and Biophysics Division, Los Alamos, NM.
20. **Lee, S., A. Joshi, K. Nagashima, E. O. Freed, and J. H. Hurley.** 2007. Structural basis for viral late-domain binding to Alix. Nat. Struct. Mol. Biol. **14:**194–199.
21. **Mangeot, P. E., D. Negre, B. Dubois, A. J. Winter, P. Leissner, M. Mehtali, D. Kaiserlian, F. L. Cosset, and J. L. Darlix.** 2000. Development of minimal lentivirus vectors derived from simian immunodeficiency virus (SIVmac251) and their use for gene transfer into human dendritic cells. J. Virol. **74:**8307–8315.
22. **McCullough, J., R. D. Fisher, F. G. Whitby, W. I. Sundquist, and C. P. Hill.** 2008. ALIX-CHMP4 interactions in the human ESCRT pathway. Proc. Natl. Acad. Sci. U. S. A. **105:**7687–7691.
23. **Otwinowski, Z., and W. Minor.** 1997. Processing of X-ray diffraction data collected in oscillation mode. Methods Enzymol. **276:**307–326.
24. **Painter, J., and E. A. Merritt.** 2005. A molecular viewer for the analysis of TLS rigid-body motion in macromolecules. Acta Crystallogr. D Biol. Crystallogr. **61:**465–471.
25. **Painter, J., and E. A. Merritt.** 2006. Optimal description of a protein structure in terms of multiple groups undergoing TLS motion. Acta Crystallogr. D Biol. Crystallogr. **62:**439–450.
26. **Pikora, C. A., C. Wittish, and R. C. Desrosiers.** 2006. p6gag of human and simian immunodeficiency viruses is tolerant to small in-frame deletions downstream of the late domain. Virology **346:**479–489.
27. **Pires, R., B. Hartlieb, L. Signor, G. Schoehn, S. Lata, M. Roessle, C. Moriscot, S. Popov, A. Hinz, M. Jamin, V. Boyer, R. Sadoul, E. Forest, D. I. Svergun, H. G. Göttlinger, and W. Weissenhorn.** 2009. A crescent-shaped ALIX dimer targets ESCRT-III CHMP4 filaments. Structure **17:**843–856.
28. **Popov, S., E. Popova, M. Inoue, and H. G. Göttlinger.** 2009. Divergent Bro1 domains share the capacity to bind human immunodeficiency virus type 1 nucleocapsid and to enhance virus-like particle production. J. Virol. **83:**7185–7193.
29. **Popov, S., E. Popova, M. Inoue, and H. G. Göttlinger.** 2008. Human immunodeficiency virus type 1 Gag engages the Bro1 domain of ALIX/AIP1 through the nucleocapsid. J. Virol. **82:**1389–1398.
30. **Sandrin, V., D. Muriaux, J. L. Darlix, and F. L. Cosset.** 2004. Intracellular trafficking of Gag and Env proteins and their interactions modulate pseudotyping of retroviruses. J. Virol. **78:**7153–7164.
31. **Segura-Morales, C., C. Pescia, C. Chatellard-Causse, R. Sadoul, E. Bertrand, and E. Basyuk.** 2005. Tsg101 and Alix interact with murine leukemia virus Gag and cooperate with Nedd4 ubiquitin ligases during budding. J. Biol. Chem. **280:**27004–27012.
32. **Strack, B., A. Calistri, S. Craig, E. Popova, and H. G. Göttlinger.** 2003. AIP1/ALIX is a binding partner for HIV-1 p6 and EIAV p9 functioning in virus budding. Cell **114:**689–699.
33. **Usami, Y., S. Popov, and H. G. Göttlinger.** 2007. Potent rescue of human immunodeficiency virus type 1 late domain mutants by ALIX/AIP1 depends on its CHMP4 binding site. J. Virol. **81:**6614–6622.
34. **Usami, Y., S. Popov, E. Popova, and H. G. Göttlinger.** 2008. Efficient and specific rescue of human immunodeficiency virus type 1 budding defects by a Nedd4-like ubiquitin ligase. J. Virol. **82:**4898–4907.
35. **Usami, Y., S. Popov, E. Popova, M. Inoue, W. Weissenhorn, and, G. G. H.** 2009. The ESCRT pathway and HIV-1 budding. Biochem. Soc. Trans. **37:**181–184.
36. **Vincent, O., L. Rainbow, J. Tilburn, H. N. Arst, Jr., and M. A. Penalva.** 2003. YPXL/I is a protein interaction motif recognized by *Aspergillus* PalA and its human homologue, AIP1/Alix. Mol. Cell. Biol. **23:**1647–1655.
37. **Zhai, Q., R. D. Fisher, H. Y. Chung, D. G. Myszka, W. I. Sundquist, and C. P. Hill.** 2008. Structural and functional studies of ALIX interactions with YPX(n)L late domains of HIV-1 and EIAV. Nat. Struct. Mol. Biol. **15:**43–49.

CHAPTER 5

ACTIVATION OF THE RETROVIRAL BUDDING FACTOR ALIX

Abstract

The cellular ALIX protein functions within the ESCRT pathway to facilitate intralumenal endosomal vesicle formation, the abscission stage of cytokinesis, and enveloped virus budding. Here, we report that the C-terminal proline-rich region (PRR) of ALIX folds back against the upstream domains and auto-inhibits V domain binding to viral late domains. Mutations designed to destabilize the closed conformation of the V domain opened the V domain, increased ALIX membrane association, and enhanced virus budding. These observations support a model in which ALIX activation requires dissociation of the autoinhibitory PRR and opening of the V domain arms.

Methods and Results

Retroviral Gag polyproteins contain short sequence motifs, termed "late domains", which facilitate virus budding by recruiting components of the cellular ESCRT pathway (Bieniasz, 2009; Usami et al., 2009). For example, the HIV-1 p6Gag protein contains "PTAP" and "YPXL" late domains (designated by their consensus sequences), that bind directly to the TSG101 and ALIX proteins, respectively (Demirov et al., 2002; Garrus et al., 2001; Martin-Serrano et al., 2001; Strack et al., 2003; VerPlank et al., 2001). ALIX, in turn, binds the CHMP4 subunits of the ESCRT-III complex, resulting in recruitment of the VPS4 ATPase, membrane fission, and virus release (Hurley and Hanson, 2010; Peel et al., 2010).

ALIX contains three distinct structural elements: an N-terminal Bro1

domain, a central V domain, and a C-terminal proline rich region (PRR). The boomerang-shaped Bro1 domain binds CHMP4 proteins (Fisher et al., 2007; Kim et al., 2005; McCullough et al., 2008), the V domain comprises two extended three-helix bundles and binds YPXL late domains (Fisher et al., 2007; Lee et al., 2007; Zhai et al., 2008; Zhai et al., 2011), and the PRR binds a series of other proteins, but is predicted to lack a persistent secondary or tertiary structure (Fisher et al., 2007; Fujii et al., 2007; Odorizzi, 2006). Like other ESCRT factors, ALIX must cycle between soluble (inactive) and membrane-associated (active) states. Several lines of evidence suggest that conformational changes accompany (or induce) these transitions. Firstly, recombinant ALIX proteins can form stable monomers and dimers (Fisher et al., 2007; Munshi et al., 2007), and biochemical evidence suggests that the dimer is the active conformation (Carlton et al., 2008; Fisher et al., 2007; Munshi et al., 2007; Pires et al., 2009). Secondly, small angle X-ray scattering (SAXS) profiles indicate that the two arms of the V domain may open and associate in an anti-parallel fashion when the protein dimerizes (Pires et al., 2009). Thirdly, recent reports show that the PRR can inhibit ALIX binding to conformationally-sensitive monoclonal antibodies, CHMP4 proteins, and viral Gag proteins (Zhou et al., 2009; Zhou et al., 2008; Zhou et al., 2010). However, previous studies have not characterized the structure or conformational transitions of pure, full-length ALIX because this protein has not been available.

Although we were unable to express full-length human ALIX protein in E. coli, we could produce multi-milligram quantities of pure recombinant ALIX in insect cells using a baculoviral expression system. Briefly, 2 L of SF21 cells were infected with a BaculoDirect (Invitrogen) expression vector, which encoded His6-ALIX (ALIX residues 1-868, WISP10-643). The cells were lysed by sonication 48 hours post infection (300 mM NaCl, 10 mM imidazole, 5% v/v glycerol, and 1% v/v Triton X-100, 50 mM Tris, pH 8.0). ALIX was purified from the clarified lysate by Ni2+ chromatography (Qiagen, elution with 250 mM imadazole), anion exchange chromatography (Q sepharose, GE Healthcare, 0.025-1.0 M NaCl gradient, 25 mM Tris, pH 8.8) and size exclusion chromatography (Superdex 200, GE Healthcare, monomeric species collected) (Figure 5.1A). This procedure typically yielded 5 mg of pure monomeric ALIX, and the protein identity was confirmed by electrospray ionization mass spectrometry. ALIX constructs that lacked the PRR (ALIX residues 1-698, denoted ALIXBro1-V (WISP10-648) ALIXBro1-V-R649E (WISP11-296) were expressed and purified in E. coli as described previously (Fisher et al., 2007).

SAXS experiments were performed to examine the conformation of the C-terminal PRR. These measurements were performed using an Anton Paar SAXSess line-collimation instrument as described (Jeffries et al., 2008). Analysis of the forward scattering intensity, I(0) (Orthaber et al., 2000), gave a solution molecular mass for ALIX (102.5 kDa, see Table S1) that agrees

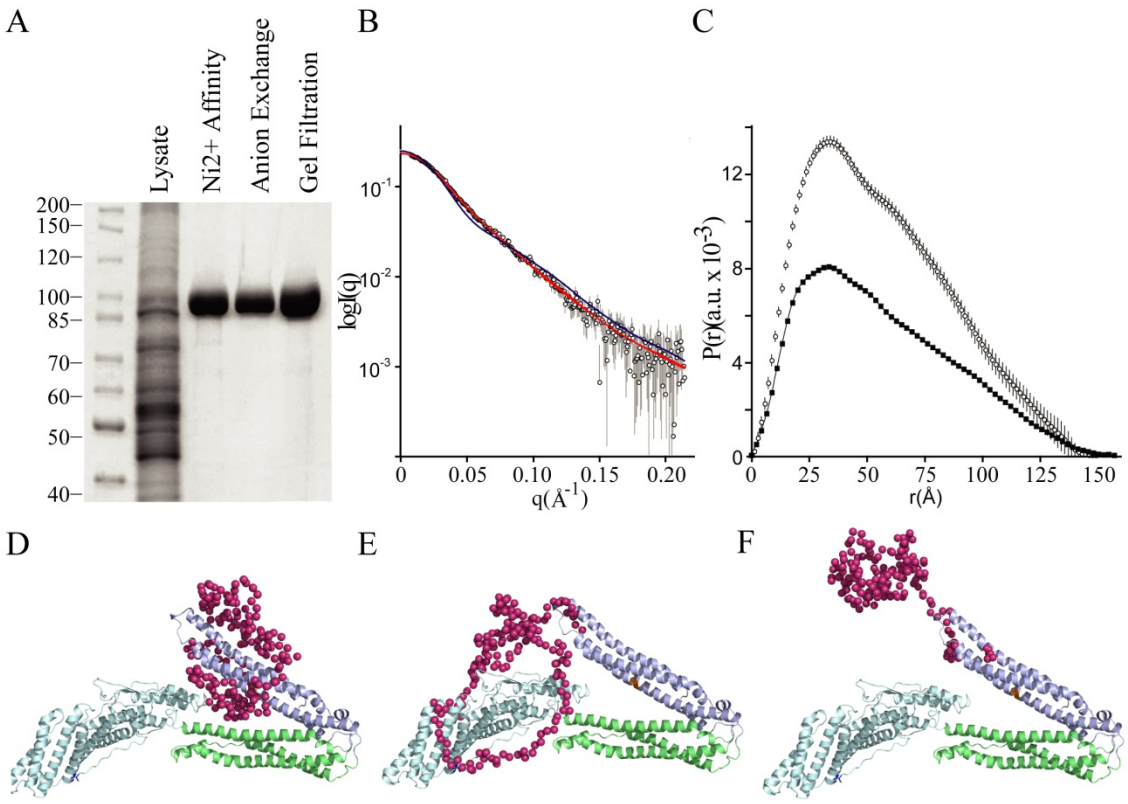

Figure 5.1 Small Angle X-ray Scattering Analyses of Recombinant ALIX.
(A) SDS-PAGE analysis (Coomassie blue staining) showing the stepwise expression and purification of full length human His_6-ALIX protein following: baculoviral expression in SF21 insect cells (lane 1), nickel affinity chromatography (lane 2), anion-exchange chromatography (lane 3), and gel filtration chromatography (lane 4). (B) Log I(q) vs. q solution small angle X-ray scattering profile for ALIX (circles) and $ALIX_{Bro1\text{-}VR649E}$ (grey diamonds). Fits to the ALIX scattering data are shown in red (models depicted in panels D and E) or blue (model depicted in F). For clarity, the data have been offset on the $I(q)$ axis. (C) Probable atom-pair distance distributions ($P(r)$ vs r) for ALIX (open circles), the crystal structure of $ALIX_{Bro1\text{-}V}$ (black squares) and $ALIX_{Bro1\text{-}V,R649E}$ (grey diamonds). The crystal structure $P(r)$ was calculated as for the experimental data except that the intensity profile was generated using CRYSOL26 (Svergun et al., 1995) and the coordinates of $ALIX_{Bro1\text{-}V}$ (7). The areas under the $P(r)$ curves are proportional to $I(0)$ and correctly scaled according to the ratios of the square of the molecular masses of the proteins. (D and E) ALIX models that fit the scattering data (red lines in B). The Bro1 domain is shown in light blue, the two arms of the V domain are shown in green and blue, respectively, and PRR dummy atoms are shown in magenta. (F) A model in which the PRR projects into solution does not fit the SAXS data (blue line in B.)

well with the calculated monomeric mass (100.8 kDa), indicating that the protein was monodisperse and monomeric. The Log I(q) vs. q SAXS profile for ALIX (open circles) is shown in Figure 5.1B. Indirect Fourier transformation of the SAXS profile using the program GIFT (Bergmann et al., 2000) yielded the probable atom-pair distance distribution within ALIX (P(r) vs. r plot, Figure 5.1C), the radius of gyration (Rg), 44.8 ± 1.5Å, and the maximum linear dimension (Dmax), 155 ± 5 Å. These structural parameters are very similar to the Rg (45.3 Å) and Dmax (158 Å) values calculated from the P(r) profile derived from the ALIXBro1-V crystal structure (Figure 5.1C, black squares). The overall shapes of the experimentally-derived and crystal structure based P(r) curves are also similar, indicating that the mass of the PRR must pack near the center of mass of the Bro1-V core structure. In contrast, a recent SAXS analysis of an ALIX construct that lacked the Bro1 domain and the final 108 PRR residues indicated that in this context the truncated PRR projected away from the V domain (Shi et al., 2010). These observations support a role for the Bro1 domain and/or the C-terminal two-thirds of the PRR in mediating the fold-back structure.

Atomic models for ALIX were generated using the ALIXBro1-V crystal structure (Fisher et al., 2007), and dummy atom representations of PRR residues. The ALIXBro1-V structure was fixed as a single rigid-body and the PRR positioned by refinement against the SAXS data using the program BUNCH (Petoukhov and Svergun, 2005). In the absence of any distance

constraints, the PRR consistently refined toward the second arm of the V domain (Figure 5.1D and red line fit in Figure 5.1B, $\chi 2$=0.54, calculated using CRYSOL26 (Svergun et al., 1995)). Models in which the PRR center was constrained to be within 5 Å of the center of the Bro1 domain fit the scattering data equally well (Figure 5.1E and red line fit in Figure 5.1B, $\chi 2$ = 0.54). In contrast, models in which the PRR was rotated away from the V domain and into solution did not fit the experimental data (Figure 5.1F and blue line fit in Figure 5.1B; $\chi 2$ = 4.70). Thus, the SAXS data indicate that the ALIX PRR lies close to the Bro1-V core in solution, probably interacting with arm2 of the V domain and possibly also with the Bro1 domain.

Isothermal titration calorimetry was performed to test whether the PRR influenced ALIX binding to a high-affinity late domain peptide from EIAV p9Gag (19TQNLYPDLSEIKK31; bold residues contact arm2 of the ALIX V domain (Zhai et al., 2008)). As expected, the control ALIXBro1-V protein bound the EIAV p9Gag peptide with a KD of 3.6 μM (Figure 5.2, black squares), which matches our previous biosensor-based analyses (KD = 6 μM, see (Zhai et al., 2008)). In contrast, full length ALIX did not bind detectably to the EIAV p9Gag peptide under these conditions (open circles). Similarly, the EIAV p9Gag peptide bound approximately 100-fold less tightly to ALIX than to ALIXBro1-V in biosensor binding experiments (data not shown). In contrast, both ALIX constructs bound with similar affinities to a peptide that corresponded to the binding epitope on CHMP4B

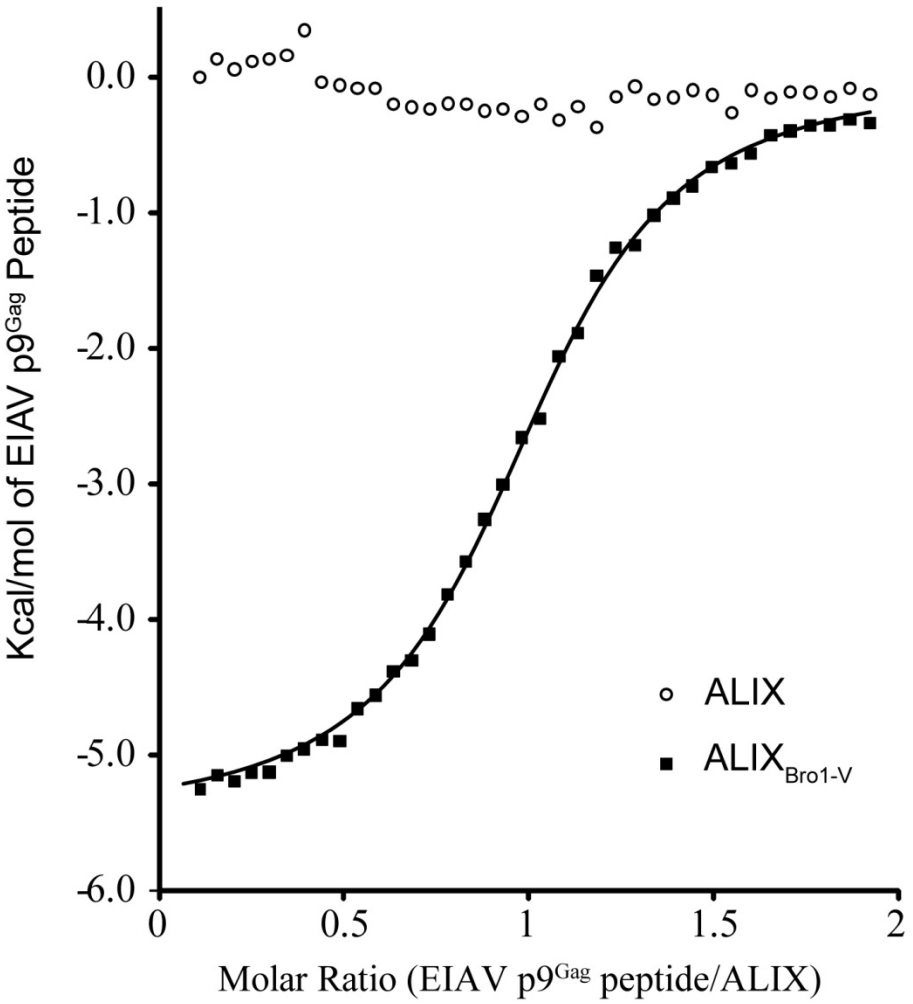

Figure 5.2. ALIX protein binding to an EIAV $p9^{Gag}$ late domain peptide. Isothermal calorimetry titrations of an EIAV $p9^{Gag}$ peptide (750 μM) into 70 μM $ALIX_{Bro1-V}$ (filled squares) or ALIX (open circles) in a solution of 20mM sodium phosphate pH 7.2, 150 mM NaCl, 1 mM DTT (25°C). The solid line shows the theoretical curve for a 1:1 peptide: $ALIX_{Bro1-V}$ complex with a dissociation constant of 3.6 μM (N=1.01±0.004, $\Delta G_{25°C}$= -7.42±0.02 Kcal/mol, $\Delta H_{25°C}$= -5.55±0.03 Kcal/mol, $\Delta S_{25°C}$= 6.30±0.17 eu, MicroCal Origin software). The peptide was added in 39 0.5 μl injections (180 s intervals) using a MicroCal iTC_{200}.

(205KKKEEEDDDMKELENWAGSM224, bold residues contact the ALIX Bro1 domain, see (McCullough et al., 2008), ALIX KD = 112±57 μM, ALIXBro1-V KD = 75±24 μM, n=6). In this respect, our results differ from those of Zhou et al., who observed that the PRR also inhibited CHMP4 binding (Zhou et al., 2010). However, our experiments were performed using pure monomeric ALIX and CHMP4B peptides, whereas theirs were performed with full-length proteins in crude extracts and could have been influenced by additional factors such as avidity effects resulting from protein oligomerization. Our data indicate that the PRR does not significantly alter the intrinsic affinity of the CHMP4 binding site on the Bro1 domain, but strongly inhibits YPXL late domain binding to arm2 of the V domain.

The two arms of the ALIX V domain are juxtaposed at an acute angle of ~30º in crystal structures of the monomeric protein (termed the "closed" conformation) (Fisher et al., 2007; Lee et al., 2007; Zhai et al., 2008; Zhai et al., 2011). The suggestion that the linker connecting the two arms functions as a hinge that opens further under some conditions (Fisher et al., 2007) is consistent with SAXS data, which indicate that that the two arms are indeed more open in the ALIX dimer (Pires et al., 2009). We therefore hypothesized that mutations that destabilize the closed conformation might promote ALIX dimerization, membrane association, binding to the oligomeric Gag protein, and virus budding. This idea was tested by examining whether mutation of ALIX Arg649 localized the protein to cellular membranes or stimulated virus

release. Arg649 forms an array of hydrogen bonding interactions that connect the three linker strands in the closed conformation, and the Arg649Glu mutation is therefore expected to destabilize the closed conformation of the V domain. Structural parameters derived from SAXS data collected from ALIXBro1-V-R649E show that there is a mass redistribution in the mutant compared to the ALIXBro1-V crystal structure as indicated by a change in the probable atom-pair distribution (Figure 5.1 C, grey diamonds), which extends out to ~190 Å. The Rg of ALIXBro1-V,R649E is ~8 Å greater than the ALIXBro1-V crystal structure (53.5 Å vs 45.3 Å), while the average radius of gyration of cross section of the mutant (calculated in PRIMUS (Konarev et al., 2003)) is smaller (Rgc ~12 Å vs ALIXBro1-V ~14.5 Å). These data show that the Arg649Glu mutation causes ALIXBro1-V to extend and become 'thinner', indicating that the mutation causes the V-domain to occupy a more 'open' configuration.

Membrane flotation experiments were performed as previously described (Ono and Freed, 1999) to test whether the Arg649Glu mutation enhanced ALIX membrane association. Briefly, transfected 293T cells were collected 6 hours post-transfection, washed three times with cold NTE (150 mM NaCl, 10 mM Tris-HCl, 1 mM EDTA), and suspended in 800 µl NTE containing 6% (wt/vol) sucrose, and a protease inhibitor cocktail (Sigma). Cells were disrupted by sonication (Figure 5.3A, lane 1, "Lysate"), nuclei and protein aggregates were removed by low-speed centrifugation (800×g, 15min,

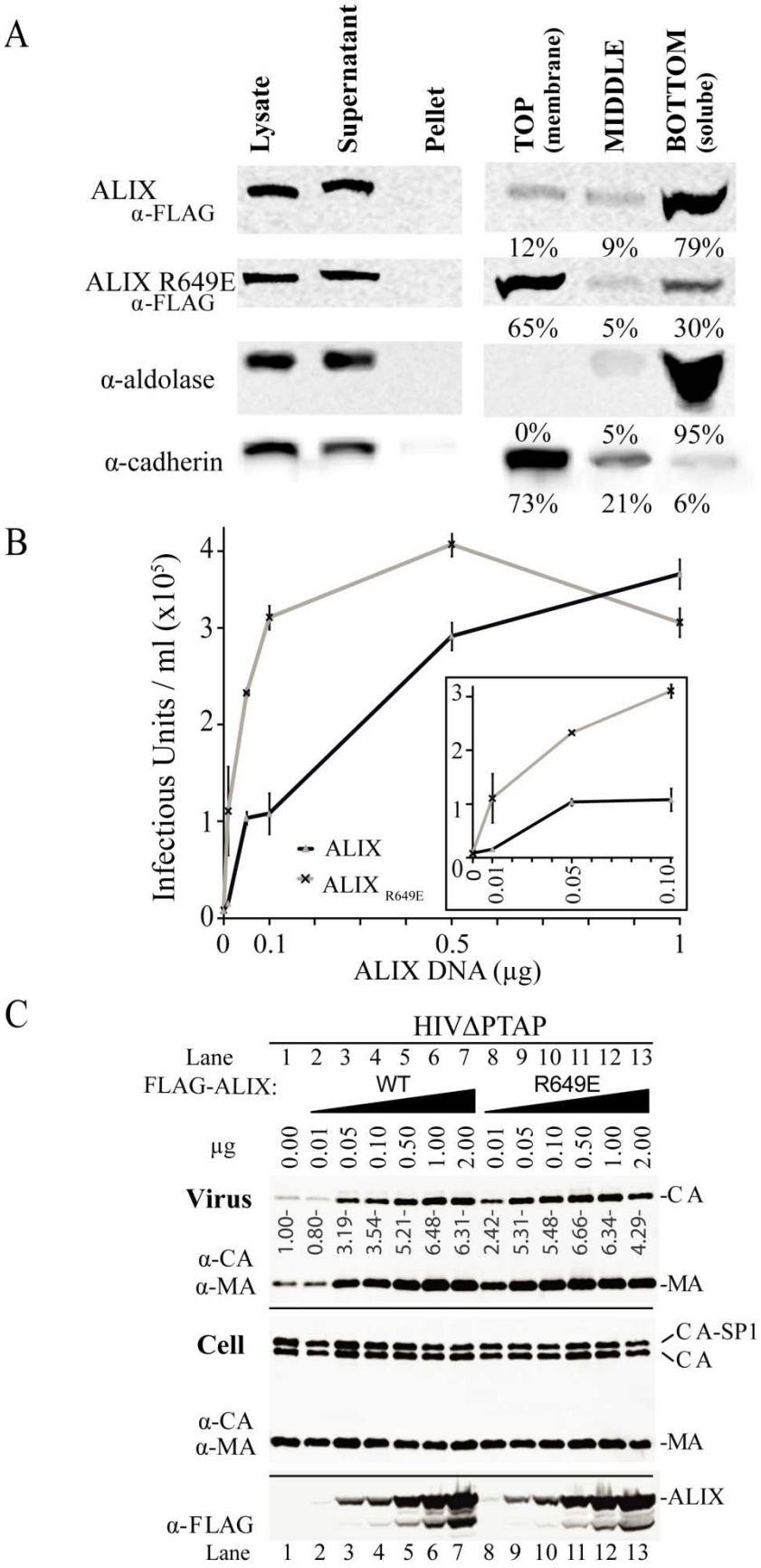
A
Lysate
Supernatant
Pellet
TOP (membrane)
MIDDLE
BOTTOM (solube)
ALIX α-FLAG
12% 9% 79%
ALIX R649E α-FLAG
65% 5% 30%
α-aldolase
0% 5% 95%
α-cadherin
73% 21% 6%
B
Infectious Units / ml (x10^5)
ALIX
ALIX R649E
ALIX DNA (µg)
C
HIVΔPTAP
Lane 1 2 3 4 5 6 7 8 9 10 11 12 13
FLAG-ALIX: WT R649E
µg 0.00 0.01 0.05 0.10 0.50 1.00 2.00 0.01 0.05 0.10 0.50 1.00 2.00
Virus
1.00- 0.80- 3.19- 3.54- 5.21- 6.48- 6.31- 2.42- 5.31- 5.48- 6.66- 6.34- 4.29-
α-CA
α-MA
-CA
-MA
Cell
CA-SP1
CA
α-CA
α-MA
-MA
α-FLAG
-ALIX
Lane 1 2 3 4 5 6 7 8 9 10 11 12 13

Figure5.3. The Arg649Glu mutation activates ALIX for membrane association and virus budding.

(A) Floatation analysis showing the degree of membrane association of ALIX and $ALIX_{R649E}$. Lanes 1-3 show the crude fractionation of 293T cell lysates (lane 1) expressing either: ALIX (row 1, WISP03-308), $ALIX_{R649E}$ (row 2, WISP06-180), or no protein (control, rows 3 and 4). The data demonstrate that neither ALIX nor $ALIX_{R649E}$ forms insoluble aggregates (compare lanes 2 and 3 and see text for details). Lanes 4-6 show the percentages of ALIX (row 1) $ALIX_{R649E}$ (row 2), aldolase (soluble protein control, row 3) and cadherin (integral membrane protein control, row 4) that partitioned into the membrane-containing (lane 4), soluble (lane 6) or intermediate (row 5) fractions. (B) HIV-1 ΔPTAP viral titers released by 293T cells (6 well plates, 1 µg plasmid DNA) co-transfected with an empty vector control or with the indicated quantities of pCl-neo-FLAG vectors expressing wild type ALIX (grey triangles, black line) or $ALIX_{R649E}$ (black crosses, grey line). Titers were measured in triplicate using single-cycle MAGIC infectivity assays. (C) Western blots of supernatants and cells corresponding to the experiment described in panel B, showing levels of virion-associated CA and MA released into the media (panel 1), and cellular levels of viral Gag, (α-CA and α-MA, panel 2), and ALIX protein levels (α-FLAG, panel 3)

resolubilized in 10% triton/NTE, lane 3, “Insoluble”). ALIX and ALIXR649E remained in the non-pelleted fractions (lane 2, “Soluble”). This fraction was adjusted to 80% (wt/vol) sucrose in NTE, placed on the bottom of a 14×89 mm centrifuge tube (Beckman, 331372), and the membrane fractions were “floated” by sedimentation (35,000 RPM for 24 h, 4°C, Beckman SW41 rotor) through layers of 65% sucrose (6 ml) and 10% sucrose (2.5 ml). Fractions containing membrane-bound proteins (4 ml, lane 4), soluble proteins (5 ml, lane 6), and an intermediate fraction (3 ml, lane 5) were collected and their protein contents were analyzed by Western blotting. Control soluble (aldolase) and integral membrane proteins (cadherin) concentrated in the soluble and membrane fractions, respectively, as expected (Figure 5.3A, rows 3 and 4, respectively). The wild type FLAG-ALIX protein remained predominantly (79%) in the soluble fraction (Figure 5.3A, row 1, compare lanes 4 and 6), whereas most (65%) of the ALIXR649E mutant associated with membranes (Figure 5.3A, row 2, compare lanes 4 and 6). Thus, these data indicate that V domain opening activates ALIX for membrane binding.

To test whether the ALIXR649E mutant was also hyperactive in stimulating virus release, we measured the release and infectivity of an HIV-1NL4-3 virus that could not bind TSG101 (HIV-1 ΔPTAP) and was therefore highly dependent upon expression of exogenous ALIX for budding (Fisher et al., 2007; Usami et al., 2007). As shown in Figure 5.3B and 3C,

ALIXR649E was more potent than the wild type protein in stimulating virus release and infectivity, particularly when ALIX levels were limiting. For example, viral infectivity was 7-fold higher when cells were transfected with 0.01 μg of the ALIXR649E expression construct (see Figure 5.3B, inset) even though both proteins were expressed at equivalent levels (Figure 5.3C, panel 3, compare lanes 2 and 8). Similarly, 0.1 μg of the ALIXR649E expression construct stimulated virus release and infectivity to levels that were comparable to those induced by 1.0 μg of the wild-type ALIX expression construct (Figure 5.3B, inset and Figure 5.3C, panel 3, compare lanes 7 and 11). Thus, the Arg649Glu mutation activates ALIX to facilitate HIV-1 release, further supporting the idea that destabilizing the closed conformation of the ALIX V domain produces a constitutively active protein.

Together with previous reports (Carlton et al., 2008; Pires et al., 2009; Zhou et al., 2010), our studies support a model in which ALIX is activated to facilitate virus budding through a series of conformational changes that: 1) release the PRR from the Bro1-V domains and expose the YPXL late domain binding site, 2) open the V domain, 3) stimulate membrane recruitment of ALIX, and 4) induce protein dimerization (Figure 5.4). These conformational changes are likely to be concerted and mutually reinforcing because: 1) ALIX dimerization appears to require V domain opening (Pires et al., 2009) and to be regulated by PRR residues (Carlton et al., 2008), 2) membrane recruitment will tend to increase local ALIX concentrations and thereby drive

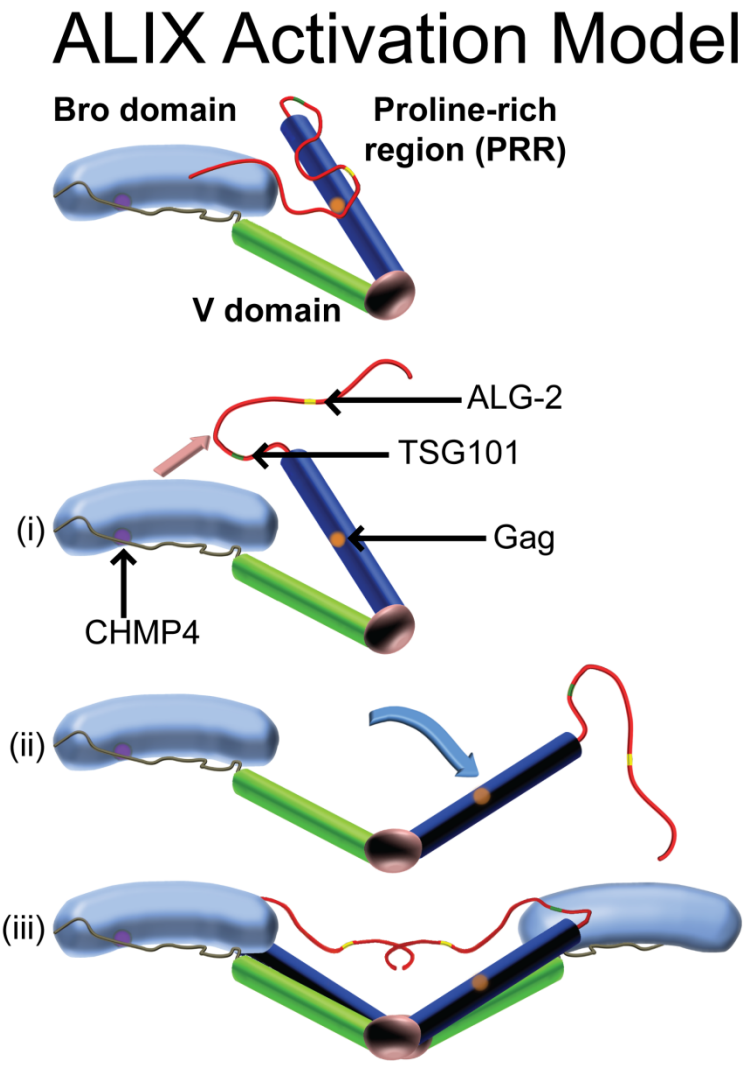

Figure 5.4. Model depicting different stages of ALIX activation. (i) Monomeric ALIX adopts an autoinhibited state in the cytosol in which the two V domain arms (blue and green) adopt a "closed" conformation, the PRR (red) folds back onto the V domain to occlude the YPXL late domain binding site (orange), and onto the Bro1 domain (light blue with the CHMP4 binding site shown in purple). ALIX activation requires: (ii) dissociation of the PRR from the Bro1-V core (pink arrow), (iii) opening of the V domain (blue arrow), and (iv) protein dimerization, denoted in brackets because dimeric species were characterized in references (Carlton et al., 2008; Pires et al., 2009), not in the present study.

dimerization, and 3) ALIX dimerization will tend to promote binding to oligomeric Gag complexes owing to avidity. Thus, all of these effects likely combine to stimulate ALIX recruitment during viral Gag protein assembly at the plasma membrane. Other factors that may also contribute to ALIX activation include ubiquitin association (Joshi et al., 2008), phosphorylation (Schmidt et al., 2005), the ubiquitin E3-ligase POSH (Alroy et al., 2005; Tsuda et al., 2006; Votteler et al., 2009), and factors that bind the PRR such as CEP55, endophilins, TSG101, ALG-2, PYK2, Src kinases, and the Cbl-SET/CIN85-endophilin complex (Carlton et al., 2008; Fisher et al., 2007; Martin-Serrano et al., 2003; Missotten et al., 1999; Morita et al., 2007; Schmidt et al., 2003; Shi et al., 2010; Strack et al., 2003; Tsuda et al., 2006; Vito et al., 1999; von Schwedler et al., 2003).

In addition to providing a regulatable step in ESCRT complex assembly, ALIX dimerization may nucleate the assembly of two strands of CHMP4, which is thought to form filaments within the necks of budding vesicles (Hurley and Hanson, 2010; Peel et al., 2010). During yeast intralumenal endosomal vesicle formation, the ESCRT-II complex performs an analogous function in nucleating the polymerization of two CHMP4 strands (Teis et al., 2010). In that case, two CHMP4 filaments are formed because the ESCRT-II complex contains two copies of the ESCRT-III binding protein Vps25p (Hurley and Hanson, 2010; Peel et al., 2010). Similarly, the mechanism of PRR autoinhibition described here for ALIX is analogous to

autoinhibition of the ESCRT-III proteins, whose C-terminal tails also fold back on the body of the protein to prevent protein oligomerization and membrane binding until they are released by binding to upstream factors (Bajorek et al., 2009; Lata et al., 2008; Lin et al., 2005; Xiao et al., 2009). Once the proteins are opened, the oligomerization domains can polymerize, and the C-terminal tails are free to recruit additional downstream factors. Thus, different ESCRT factors employ common principles to cycle on and off membranes and maintain the sequential protein assembly pathways required for regulated membrane fission.

References

Alroy, I., Tuvia, S., Greener, T., Gordon, D., Barr, H.M., Taglicht, D., Mandil-Levin, R., Ben-Avraham, D., Konforty, D., Nir, A.*, et al.* (2005). The trans-Golgi network-associated human ubiquitin-protein ligase POSH is essential for HIV type 1 production. Proc Natl Acad Sci USA *102*, 1478-1483.

Bajorek, M., Schubert, H.L., McCullough, J., Langelier, C., Eckert, D.M., Stubblefield, W.M., Uter, N.T., Myszka, D.G., Hill, C.P., and Sundquist, W.I. (2009). Structural basis for ESCRT-III protein autoinhibition. Nat Struct Mol Biol *16*, 754-762.

Bergmann, A., Fritz, G., and Glatter, O. (2000). Solving the generalized indirect Fourier transformation (GIFT) by Boltzmann simplex simulated annealing (BSSA). JAppl Crystallogr *33*, 1212-1216.

Bieniasz, P.D. (2009). The cell biology of HIV-1 virion genesis. Cell Host Microbe *5*, 550-558.

Carlton, J.G., Agromayor, M., and Martin-Serrano, J. (2008). Differential requirements for Alix and ESCRT-III in cytokinesis and HIV-1 release. Proc Natl Acad Sci USA *105*, 10541-10546.

Demirov, D.G., Ono, A., Orenstein, J.M., and Freed, E.O. (2002). Overexpression of the N-terminal domain of TSG101 inhibits HIV-1 budding by blocking late domain function. Proc Natl Acad Sci USA *99*, 955-960.

Fisher, R.D., Chung, H.Y., Zhai, Q., Robinson, H., Sundquist, W.I., and Hill, C.P. (2007). Structural and biochemical studies of ALIX/AIP1 and its role in retrovirus budding. Cell *128*, 841-852.

Fujii, K., Hurley, J.H., and Freed, E.O. (2007). Beyond Tsg101: the role of Alix in 'ESCRTing' HIV-1. Nat Rev Microbiol *5*, 912-916.

Garrus, J.E., von Schwedler, U.K., Pornillos, O.W., Morham, S.G., Zavitz, K.H., Wang, H.E., Wettstein, D.A., Stray, K.M., Cote, M., Rich, R.L.*, et al.* (2001). Tsg101 and the vacuolar protein sorting pathway are essential for HIV-1 budding. Cell *107*, 55-65.

Hurley, J.H., and Hanson, P.I. (2010). Membrane budding and scission by the ESCRT machinery: it's all in the neck. Nat Rev Mol Cell Biol *11*, 556-566.

Jeffries, C.M., Whitten, A.E., Harris, S.P., and Trewhella, J. (2008). Small-angle X-ray scattering reveals the N-terminal domain organization of cardiac myosin binding protein C. J Mol Biol *377*, 1186-1199.

Joshi, A., Munshi, U., Ablan, S.D., Nagashima, K., and Freed, E.O. (2008). Functional replacement of a retroviral late domain by ubiquitin fusion. Traffic *9*, 1972-1983.

Kim, J., Sitaraman, S., Hierro, A., Beach, B.M., Odorizzi, G., and Hurley, J.H. (2005). Structural basis for endosomal targeting by the Bro1 domain. Dev Cell *8*, 937-947.

Konarev, P.K., Volkov, V.V., Sokolova, A.V., Koch, M.H.J., and Svergun, D.I. (2003). PRIMUS: a Windows PC-based system for small-angle scattering data analysis. J Appl Cryst *36*, 1277-1282.

Lata, S., Roessle, M., Solomons, J., Jamin, M., Gottlinger, H.G., Svergun, D.I., and Weissenhorn, W. (2008). Structural basis for autoinhibition of ESCRT-III CHMP3. J Mol Biol *378*, 816-825.

Lee, S., Joshi, A., Nagashima, K., Freed, E.O., and Hurley, J.H. (2007). Structural basis for viral late-domain binding to Alix. Nat Struct Mol Biol *14*, 194-199.

Lin, Y., Kimpler, L.A., Naismith, T.V., Lauer, J.M., and Hanson, P.I. (2005). Interaction of the mammalian endosomal sorting complex required for transport (ESCRT) III protein hSnf7-1 with itself, membranes, and the AAA+ ATPase SKD1. J Biol Chem *280*, 12799-12809.

Martin-Serrano, J., Yaravoy, A., Perez-Caballero, D., and Bieniasz, P.D. (2003). Divergent retroviral late-budding domains recruit vacuolar protein

sorting factors by using alternative adaptor proteins. Proc Natl Acad Sci USA *100*, 12414-12419.

Martin-Serrano, J., Zang, T., and Bieniasz, P.D. (2001). HIV-1 and Ebola virus encode small peptide motifs that recruit Tsg101 to sites of particle assembly to facilitate egress. Nat Med *7*, 1313-1319.

McCullough, J., Fisher, R.D., Whitby, F.G., Sundquist, W.I., and Hill, C.P. (2008). ALIX-CHMP4 interactions in the human ESCRT pathway. Proc Natl Acad Sci USA *105*, 7687-7691.

Missotten, M., Nichols, A., Rieger, K., and Sadoul, R. (1999). Alix, a novel mouse protein undergoing calcium-dependent interaction with the apoptosis-linked-gene 2 (ALG-2) protein. Cell Death Differ *6*, 124-129.

Morita, E., Sandrin, V., Chung, H.Y., Morham, S.G., Gygi, S.P., Rodesch, C.K., and Sundquist, W.I. (2007). Human ESCRT and ALIX proteins interact with proteins of the midbody and function in cytokinesis. Embo J *26*, 4215-4227.

Munshi, U.M., Kim, J., Nagashima, K., Hurley, J.H., and Freed, E.O. (2007). An Alix fragment potently inhibits HIV-1 budding: characterization of binding to retroviral YPXL late domains. J Biol Chem *282*, 3847-3855.

Odorizzi, G. (2006). The multiple personalities of Alix. J Cell Sci *119*, 3025-3032.

Ono, A., and Freed, E.O. (1999). Binding of human immunodeficiency virus type 1 Gag to membrane: role of the matrix amino terminus. J Virol *73*, 4136-4144.

Orthaber, D., Bergmann, A., and Glatter, O. (2000). SAXS experiments on absolute scale with Kratky systems using water as a secondary standard. J Applied Cryst *33*, 218-225.

Peel, S., Macheboeuf, P., Martinelli, N., and Weissenhorn, W. (2010). Divergent pathways lead to ESCRT-III-catalyzed membrane fission. Trends Biochem Sci.

Petoukhov, M.V., and Svergun, D.I. (2005). Global rigid body modeling of macromolecular complexes against small-angle scattering data. Biophys J *89*, 1237-1250.

Pires, R., Hartlieb, B., Signor, L., Schoehn, G., Lata, S., Roessle, M., Moriscot, C., Popov, S., Hinz, A., Jamin, M., *et al.* (2009). A Crescent-Shaped ALIX Dimer Targets ESCRT-III CHMP4 Filaments. Structure *17*, 843-856.

Schmidt, M.H., Chen, B., Randazzo, L.M., and Bogler, O. (2003). SETA/CIN85/Ruk and its binding partner AIP1 associate with diverse cytoskeletal elements, including FAKs, and modulate cell adhesion. J Cell Sci *116*, 2845-2855.

Schmidt, M.H., Dikic, I., and Bogler, O. (2005). Src phosphorylation of Alix/AIP1 modulates its interaction with binding partners and antagonizes its activities. J Biol Chem *280*, 3414-3425.

Shi, X., Opi, S., Lugari, A., Restouin, A., Coursindel, T., Parrot, I., Perez, J., Madore, E., Zimmermann, P., Corbeil, J.*, et al.* (2010). Identification and biophysical assessment of the molecular recognition mechanisms between the human haemopoietic cell kinase Src homology domain 3 and ALG-2-interacting protein X. Biochem J *431*, 93-102.

Strack, B., Calistri, A., Craig, S., Popova, E., and Gottlinger, H.G. (2003). AIP1/ALIX Is a Binding Partner for HIV-1 p6 and EIAV p9 Functioning in Virus Budding. Cell *114*, 689-699.

Svergun, D., Barberato, C., and Koch, M.H.J. (1995). CRYSOL - a program to evaluate X-ray solution scattering of biological macromolecules from atomic coordinates. J Appl Crystallogr *28*, 768-773.

Teis, D., Saksena, S., Judson, B.L., and Emr, S.D. (2010). ESCRT-II coordinates the assembly of ESCRT-III filaments for cargo sorting and multivesicular body vesicle formation. EMBO J *29*, 871-883.

Tsuda, M., Seong, K.H., and Aigaki, T. (2006). POSH, a scaffold protein for JNK signaling, binds to ALG-2 and ALIX in Drosophila. FEBS Lett *580*, 3296-3300.

Usami, Y., Popov, S., and Gottlinger, H.G. (2007). Potent rescue of human immunodeficiency virus type 1 late domain mutants by ALIX/AIP1 depends on its CHMP4 binding site. J Virol *81*, 6614-6622.

Usami, Y., Popov, S., Popova, E., Inoue, M., Weissenhorn, W., and H, G.G. (2009). The ESCRT pathway and HIV-1 budding. Biochem Soc Trans *37*, 181-184.

VerPlank, L., Bouamr, F., LaGrassa, T.J., Agresta, B., Kikonyogo, A., Leis, J., and Carter, C.A. (2001). Tsg101, a homologue of ubiquitin-conjugating (E2) enzymes, binds the L domain in HIV type 1 Pr55Gag. Proc Natl Acad Sci USA *98*, 7724-7729.

Vito, P., Pellegrini, L., Guiet, C., and D'Adamio, L. (1999). Cloning of AIP1, a novel protein that associates with the apoptosis- linked gene ALG-2 in a Ca2+-dependent reaction. J Biol Chem *274*, 1533-1540.

von Schwedler, U.K., Stuchell, M., Muller, B., Ward, D.M., Chung, H.Y., Morita, E., Wang, H.E., Davis, T., He, G.P., Cimbora, D.M.*, et al.* (2003). The protein network of HIV budding. Cell *114*, 701-713.

Votteler, J., Iavnilovitch, E., Fingrut, O., Shemesh, V., Taglicht, D., Erez, O., Sorgel, S., Walther, T., Bannert, N., Schubert, U.*, et al.* (2009). Exploring the functional interaction between POSH and ALIX and the relevance to HIV-1 release. BMC Biochem *10*, 12.

Xiao, J., Chen, X.W., Davies, B.A., Saltiel, A.R., Katzmann, D.J., and Xu, Z. (2009). Structural basis of Ist1 function and Ist1-Did2 interaction in the multivesicular body pathway and cytokinesis. Mol Biol Cell *20*, 3514-3524.

Zhai, Q., Fisher, R.D., Chung, H.Y., Myszka, D.G., Sundquist, W.I., and Hill, C.P. (2008). Structural and functional studies of ALIX interactions with YPX(n)L late domains of HIV-1 and EIAV. Nat Struct Mol Biol *15*, 43-49.

Zhai, Q., Landesman, M.B., Robinson, H., Sundquist, W.I., and Hill, C.P. (2011). Identification and structural characterization of the ALIX-binding late domains of simian immunodeficiency virus SIVmac239 and SIVagmTan-1. J Virol *85*, 632-637.

Zhou, X., Pan, S., Sun, L., Corvera, J., Lee, Y.C., Lin, S.H., and Kuang, J. (2009). The CHMP4b- and Src-docking sites in the Bro1 domain are autoinhibited in the native state of Alix. Biochem J *418*, 277-284.

Zhou, X., Pan, S., Sun, L., Corvera, J., Lin, S.H., and Kuang, J. (2008). The HIV-1 p6/EIAV p9 docking site in Alix is autoinhibited as revealed by a conformation-sensitive anti-Alix monoclonal antibody. Biochem J *414*, 215-220.

Zhou, X., Si, J., Corvera, J., Gallick, G.E., and Kuang, J. (2010). Decoding the intrinsic mechanism that prohibits ALIX interaction with ESCRT and viral proteins. Biochem J *432*, 525-534.

CHAPTER 6

STRUCTURAL AND FUNCTIONAL STUDIES OF BROX IN VIRUS BUDDING

Introduction

ALIX functions in the MVB pathway, retroviral budding, and abscission of mother and daughter cells. ALIX and its yeast orthologue Bro1 each contain an N-terminal Bro1 domain that binds directly to CHMP4 and Snf7, respectively. During biogenesis of MVBs in yeast, Bro1 (the yeast homolog of mammalian ALIX) functions in the sorting of carboxypeptidase S and Ga1 permease to the lysosome (Odorizzi et al., 2003). The Bro1-Snf7 interaction coordinates recruitment of the deubiquitylating enzyme Doa4 to recycle ubiquitin prior to MVB sorting and subsequent lysosomal degradation (Kim et al., 2005; Richter et al., 2007). In addition, binding of Bro1 to Snf7 enhances the stability of ESCRT-III and inhibits Vps4-mediated disassembly of the ESCRT-III complex (Wemmer et al., 2011). Moreover, the interaction between the Bro1 domain and CHMP4 is essential for ALIX to promote retrovirus budding and membrane scission of cytokinesis, when ALIX is recruited by viral Gag and CEP55 proteins respectively (Carlton and Martin-Serrano, 2007; Fisher et al., 2007; Morita et al., 2007; Teis et al., 2008; Usami et al., 2007; Wollert et al., 2009).

In addition to ALIX, two other proteins encoded by the human genome contain Bro1-like domains. One is HD-PTP (also called PTPN23), which contains a similar domain organization of ALIX and an additional putative protein tyrosine phosphatase domain. HD-PTP has been shown to function in endosomal cargo sorting and MVB pathways (Doyotte et al., 2008). The other

ALIX homolog is named Brox, which contains an N-terminal Bro1 domain and a C-terminal farnesylation site (CaaX motif, C standing for cysteine, a for any aliphatic amino acid, and X for any amino acid) (Figure 6.1) (Ichioka et al., 2008). Brox shares 21.8% sequence identity with the human ALIX Bro1 domain or the yeast Bro1 domain.

Although the function of Brox remains unclear, it is likely functions in membrane scission events involving ESCRT proteins. First, Brox was identified from a proteomic analysis of urinary exosomes, in which many ESCRT proteins were identified, including ALIX, TSG101, CHMP4, VPS4A and VPS4B (Pisitkun et al., 2004). Notably, ALIX was also revealed to be abundant in exosomes by an independent proteomic analysis of dendritic cell-derived exosomes (Thery et al., 2001). Exosomes are luminal MVB vesicles released from the cell when MVBs fuse with the plasma membrane rather than lysosomes, so the association of Brox suggests that it, like ALIX, can function in the MVB pathway-driven formation of exosomes. Second, Brox can bind CHMP4 and, upon overexpression of a dominant negative mutant of VPS4B, is partly localized to the Golgi and endosomes (Ichioka et al., 2008). Third, Gottlinger and colleagues reported that the NC domain of the HIV-1 Gag protein can associate with the Bro1 domain of ALIX and provide an additional site for ALIX recruitment, and further demonstrated that the Bro1 domains of ALIX, HD-PTP and Brox were capable of enhancing the release of virus like particles (VLPs) comprised of a minimal Gag molecule (Popov et al.,

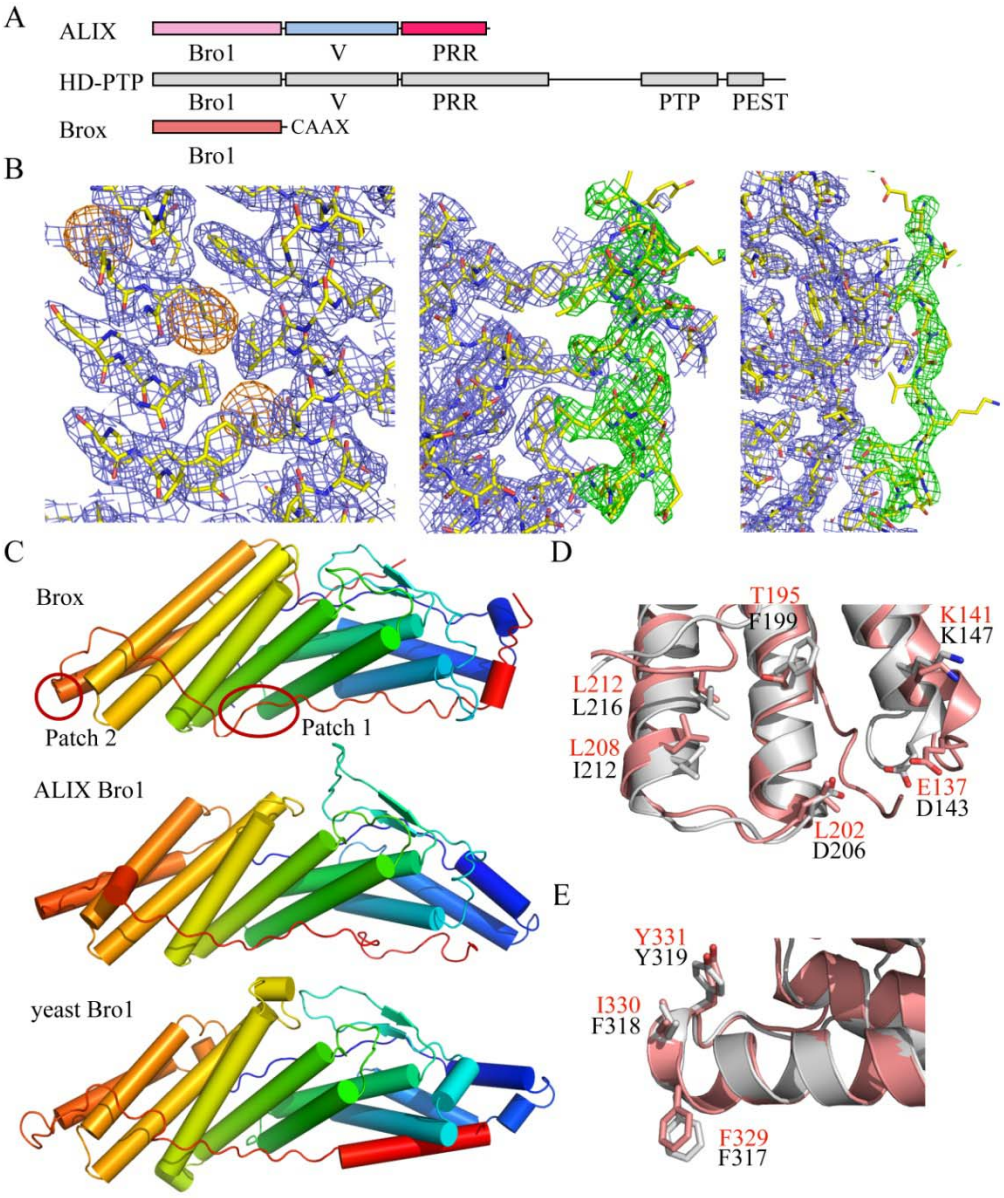

Figure 6.1 Domain organization and structure of Brox.
(A) Domain organization of ALIX, HD-PTP and Brox.
(B) The electron-density maps. Left: 2Fo-Fc electron density map (blue, 1X RMSD). The anomalous difference Fourier map (5X RMSD and orange). Middle: the omit map for regions (residues 366-378) is colored green. Right: the omit map for regions (residues 390-401) is colored green.
(C) Structural comparison of Brox to other known Bro1 domains. Proteins are colored in rainbow from blue at the N-terminus to red at the C-terminus.
(D) Top: Zoom-in view of the CHMP4 binding site (patch 1). ALIX is colored gray, Brox is colored pink. Bottom: Zoom-in view of patch 2.

2009). In apparent conflict with this finding, Bouamer's group observed that overexpression of the ALIX Bro1 domain, but not overexpression of other Bro1 domains, rescued the release of HIV-1 PTAP-/YP- (Dussupt et al., 2009). Therefore, the function of Brox remains elusive. In order to better characterize Brox, we determined the crystal structure of human Brox, measured its binding to CHMP4, and determined its importance in viral budding.

Methods and Results

Structure Determination of Brox

In order to determine the crystal structure of Brox, the construct (residues 1-401) was cloned into pET151/D topo vector (Invitrogen) and expressed as an N-terminal 6XHis-tagged selenomethionine-substituted protein in BL21(DE3) Codon+ (RIL) *E. Coli* in auto-induction media PASM5052 (Studier, 2005). Cells were lysed with lysozyme treatment and sonication, and the lysate clarified by cenrifugation. Following purification on Ni^{2+} resin, the eluted protein was dialyzed against 25 mM Tris pH 8.0, 100 mM NaCl, 1 mM DTT, 5% glycerol, and TEV protease overnight. The cleaved protein was collected as flow-through from a second Ni^{2+} resin column and applied to a HiTrap Q Sepharase Fast Flow Column (GE Healthcare). The protein was eluted by a NaCl gradient from 25 mM to 1 M (25 mM Tris pH 8.8, 1 mM DTT and 5% glycerol), applied to size exclusion chromatography (10 mM Tris pH 8.0, 100 mM NaCl, 1 mM DTT), and concentrated to 10

mg/ml. Crystals were grown in sitting drops (reservoir: 20% PEG 1500, 0.1 M MMT pH 6.6, 13 ℃) and cryoprotected in a solution of reservoir components made up with 30% glycerol.

Diffraction data were collected to 2.6 Å resolution at three wavelengths at beam line X-29 of the National Synchrotron Light Source and processed using HKL2000 (Otwinowski and Minor, 1997). The Brox structure was determined by the MAD method using the PHENIX AutoSol wizard (Grosse-Kunstleve and Adams, 2003; McCoy et al., 2004; Terwilliger, 1994; Terwilliger et al., 2009). Fourteen Se sites identified from MAD and the ALIX Bro1 domain structure were used to guide model building. The model was first refined in REFMAC5 with 3-fold NCS in the CCP4 suite (Group, November 4. 1994), and then refined in PHENIX with TLS refinement (Adams et al., 2010; Painter and Merritt, 2005, 2006) to R/Rfree values of 19.2/25.5 (Table 6.1). For the most part the electron-density map is clearly defined, including for most side chains, although residues 379-390 are not apparent and the C-terminal residues 391-401 are only marginally observed (Figure 6.1).

Most of the Brox structure overlaps closely with the known structures of other Bro1 domains. Brox is mainly composed of α-helices, and contains just two ß-strands, to form an extended and slightly curved structure that resembles a banana (Fisher et al., 2007; Kim et al., 2005). Similar to other unknown Bro1 domain, an extended loop, residues 332-365, traverses the

Table 6.1. Crystallographic Statistics for Brox(1-401)

	Brox (1-401)		
Data Collection			
Wavelength (Å)	0.97910	0.97940	0.9611
Space group	C2	C2	C2
Cell dimensions (Å,°)	a = 227.6 b = 67.2 c = 103.5 ß = 96.6	a = 227.7 b = 67.2 c = 103.6 ß = 96.6	a = 227.8 b = 67.3 c = 103.6 ß = 96.6
Resolution (Å)	40-2.7 (2.8-2.7)	40-2.7 (2.8-2.7)	40-2.7 (2.8-2.7)
Completeness (%)	98.8 (98.5)	99.6 (97.2)	98.8 (98.9)
I/σ(I)	18.1 (3.6)	21.3 (3.0)	21.4 (3.3)
Rsym (%)	9.3 (45.3)	9.1 (47.2)	9.0 (49.0)
Number of unique reflections	43,199	43,233	43,242
Refinement			
Rfactor/Rfree (%)	19.2/25.5		
Number of protein atoms	9294		
Number of water molecules	31		
Average B-factor (Å^2)			
protein atoms	60.9		
water molecules	44.5		
RMSD from ideal geometry	0.008		
Bonds (Å)	1.156		
Angles (°)			

length of the Bro1 domain on the concave surface (Figure 6.1). The RMSD of C-alpha atoms of Brox (residues 1-367) is 2.6 Å to ALIX-Bro1 domain (residues 2-360) and 3.0 Å to the yeast Bro1 domain (residues 1-367). The unique feature of Brox rises from its C-terminal residues (residue 366-401). Instead of entering the V domain at residue 366, as for ALIX, Brox forms a helix (residues 366-378), then extends over the convex face (Figure 6.1).

Interactions Between Brox and CHMP4

Two hydrophobic patches that have been described for the ALIX Bro1 domain are also conserved on the Brox surface. Patch 1 of ALIX Bro1 domain mediates the CHMP4 interaction. Several groups have shown that Brox can also bind to CHMP4 via patch 1 by immune-precipitation experiments (Ichioka et al., 2008; Popov et al., 2009). The Brox residues that correspond to the CHMP4 binding site of ALIX are highlighted in Figure 6.1. The interactions between the ALIX Bro1 domain and all three of the CHMP4 isoforms are similar, although CHMP4B is the primary interaction partner of ALIX, because CHMP4B is expressed highest in the tested tissues (Katoh et al., 2004; McCullough et al., 2008).

Surface Plasmon Resonance (SPR) was performed to test whether CHMP4 interacts with Brox directly through the putative binding site. Binding experiments used Biacore 2000 and T100 optical biosensor instruments. CM5 sensor chips were derivatized with anti-GST antibody using amine coupling, and were used to capture GST-CHMP4B$_{205\text{-}224}$ or GST

alone. Pure Brox proteins each at 400 μM as the highest concentrations in a 1.5-fold dilution series were injected in duplicate. All interactions reached equilibrium rapidly and dissociated with seconds during the dissociation phase. Binding responses were fit to 1:1 binding isotherms to obtain equilibrium constants. Brox binds to the N-terminal GST-tagged $CHMP4B_{205-224}$ with an affinity of 98.3 μM (SD = 22.0 μM), which is similar to the ALIX-CHMP4 interactions (McCullough et al., 2008). Single point mutations of K144E or L212D on Brox completely abolished the interaction with CHMP4B, indicating that Brox binds CHMP4B directly through patch 1 (Figure 6.2). To determine whether the CHMP4 binding site plays an important role in the function of Brox, Michael Landesman in the Sundquist lab performed a minimal Gag budding assay. As expected, Brox stimulated VLP formation of the minimal Gag construct and was incorporated into the viral particles, whereas the K144E or L212D mutations that disrupted CHMP4 interaction failed to promote VLP production of the minimal Gag.

Association Between Brox and NC

Accumulating observations show that HIV-1 Gag can engage the Bro1 domain of ALIX through NC. All the Bro1 domains tested, including the ALIX Bro1 domain and Brox, are sufficient to stimulate virus-like particle production in a minimal Gag rescue assay (Dussupt et al., 2009; Popov et al., 2008, 2009. However, direct interactions between NC and the Bro1 domains remain to be determined.

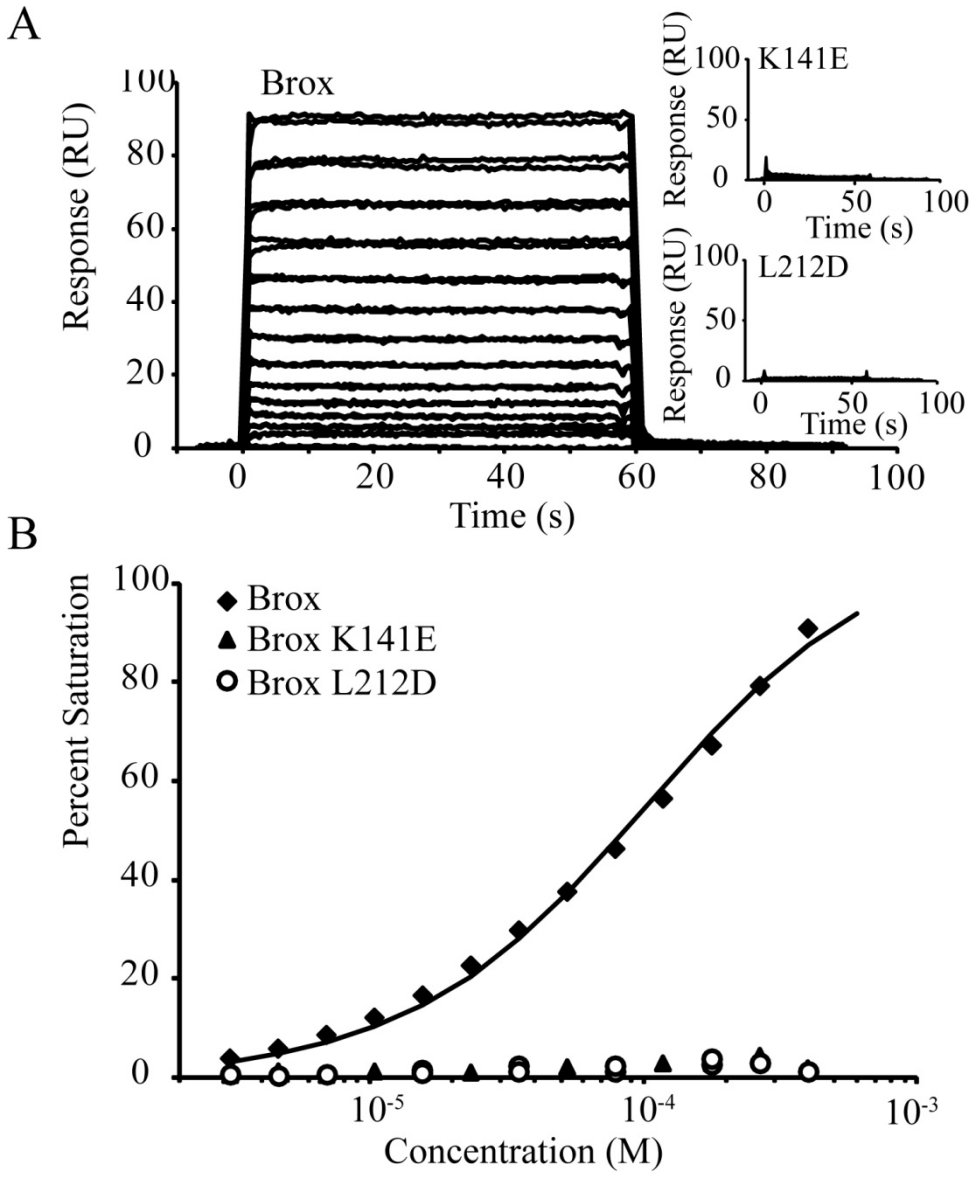

Figure 6.2 Brox binding to CHMP4.
(A) Representative biosensor sensograms for Brox and mutants binding to the immobilized GST-CHMP4B$_{204-224}$.
(B) Biosensor binding isotherms for Brox, Brox$_{K141E}$ and Brox$_{L212D}$ binding to the CHMP4B$_{204-224}$.

The HIV-1 NC was cloned into the PET-3a vector with *Nde1* and *BahmH1* restriction sites (Novagen). The plasmid was transformed into BL2l-Codonplus® (DE3)-RIPL competent cells. A starter culture of 200ml PA-0.5G media grown at 37 °C overnight was added to 2 L of P-5052 media supplemented with 0.1 mM $ZnCl_2$ and grown for 8 h at 37 °C and 48 h at 19 °C (Tyler et al., 2005). The purification scheme for the HIV-1 NC was adapted from Lee et al (Lee et al., 1998). Cells were lysed by sonication, and the nucleic acids were precipitated by adding 4% (w/v) polyethyleneimine (pH 7.9) dropwise to a final concentration of 0.4% and stirred for 15 minutes. The supernatant was applied onto a 5 ml HiTrap Q-Sepharase and a HiTrap SP-Sepharase column (GE Healthcare) connected in series. After washing with 25 ml buffer A (50 mM Tris-HCl pH 8.0, 0.1M NaCl, 0.1 mM $ZnCl_2$, 10 mM BME, 10% glycerol), the Q column was detached. The protein was eluted from 0.1M to 1 M NaCl and applied to size exclusion chromatography. Because Brox is more soluble and expressed to a higher level than the ALIX Bro1 domain, the experiment was done using Brox. NMR samples were made by titrating Brox into NC, resulting in 200 μM NC alone or with Brox at concentrations of 200 μM, 400 μM, 600 μM, 800 μM and 1000 μM in 25 mM Sodium Acetate pH 6.5, 25 mM NaCl, 100 μM $ZnCl_2$ 1mM DTT and 10% (v/v) H_2O. NMR HSQC spectra were recorded at 25 °C on a Varian INOVA 600 MHz spectrometer. NC residues were assigned by comparing with the published NC spectra (De Guzman et al., 1998). The resonance of NC E51

showed a small shift upon the addition of Brox, and several resonances, including F6, R7, Q9 and R10, were found to disappear in the presence of Brox (Figure 6.3). Curiously, the NMR structure of NC in complex with RNA indicates that F6 and Q9 contact one RNA recognition element, and R7 and R10 contact a different RNA recognition element (Amarasinghe et al., 2000; De Guzman et al., 1998).

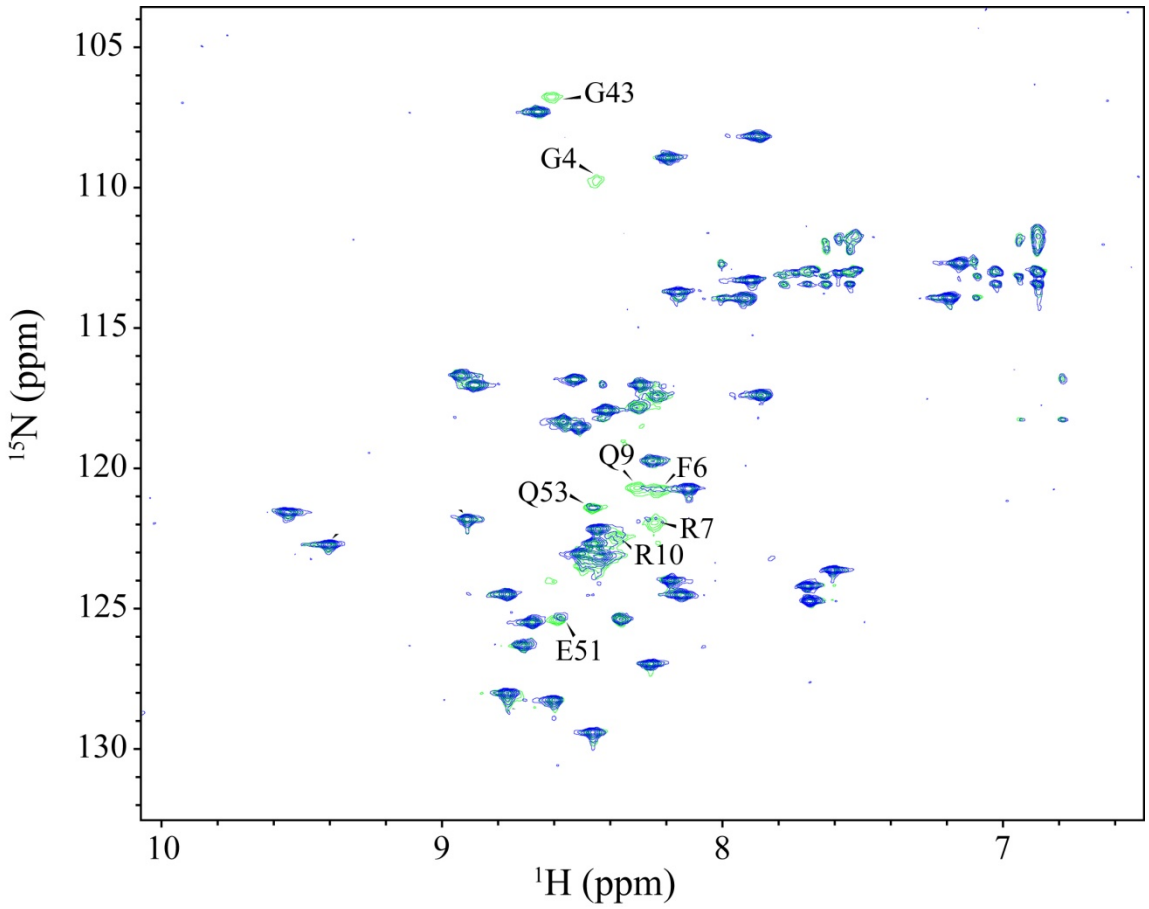

Figure 6.3. Overlaid ^{15}N -^{1}H HSQC spectra of pure ^{15}N-NC protein either free (green) or with Brox with a final molar ratio of 1:3 (Blue). The resonances that shifted and disappeared are labeled with the residue identities.

To determine whether the observed resonance shifts are caused by a direct NC-Bro1 interaction, SPR was performed to determine binding affinities of Bro1-V to NC. Cells that expressed GST-NC constructs were treated with lysozyme, DNase and sonication. The supernatants were treated with 4% (w/v) PEI (pH 7.9) dropwise to a final concentration of 0.4% in order to remove nucleic acids. GST-NC proteins were then precipitated by adding saturated ammonium sulfate to a final concentration of 1M, and resuspended with buffer (20 mM phosphate pH 7.4, 150mM NaCl, 10 μM $ZnCl_2$ and 1mM DTT). Pure $ALIX_{Bro1\text{-}V}$ proteins at 340 μM as the highest concentrations in a 2 fold dilution series were injected in duplicate. First, the binding signal of $ALIX_{Bro1\text{-}V}$ to GST-NC was every close to that of the GST-free construct (Figure 6.4), while the control GST-p6 and GST-CHMP4B bound to $ALIX_{Bro1\text{-}V}$ with dissociation affinities of 41 μM and 26 μM. Second, DNase and PEI treatment, which removes nucleic acid, did not alter the affinity. Third, affinities of $ALIX_{Bro1\text{-}V}$ to NCp1p6 and p6 constructs were indistinguishable, which was not surprising given the large uncertainty associated with the extremely weak NC-Bro1 interaction. Fourth, double mutants, such as F6A-Q9A, R7A-R10A and E51A-Q53A, did not completely abolish the interaction between the Bro1 domains and NC. Even C28S and C49S double mutations on NC, which disrupt its zinc finger structure, did not change the K_D. Therefore, these results show that there is not a direct interaction between

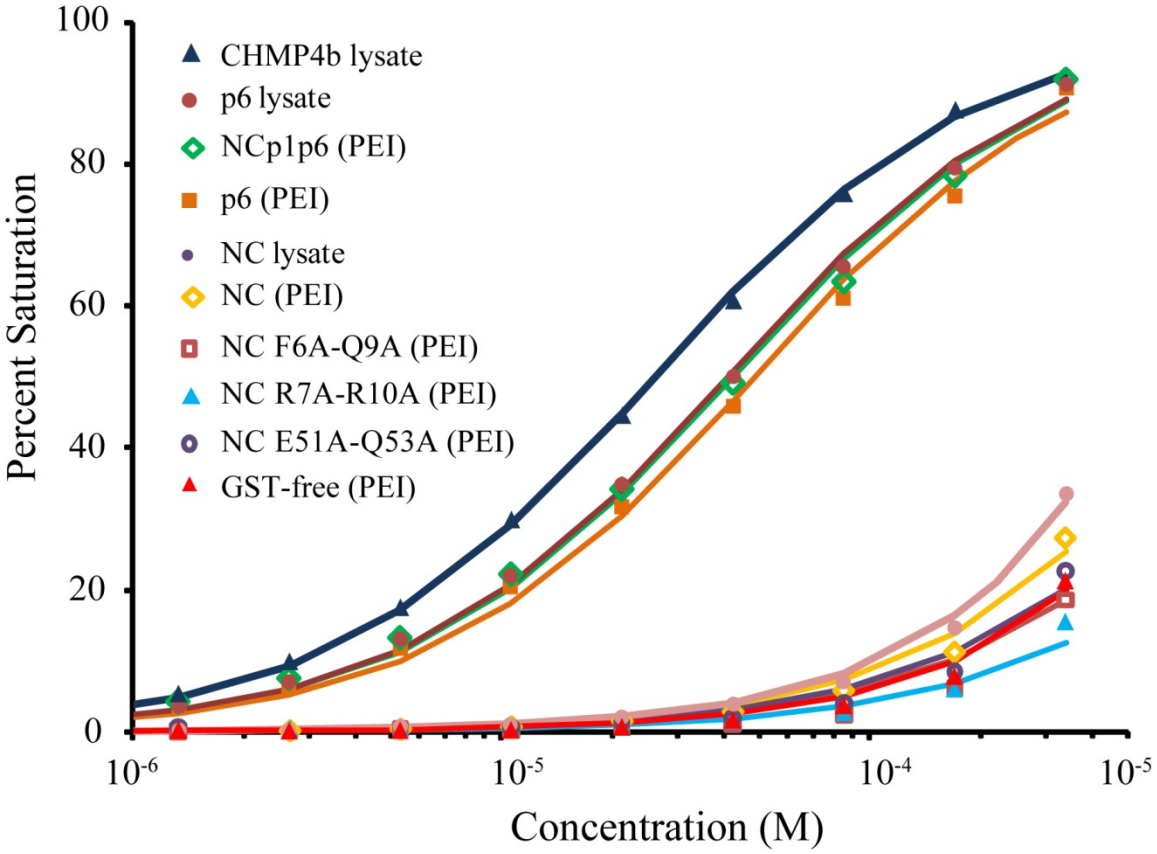

Figure 6.4. Representative biosensor binding Isotherms for $ALIX_{Bro1\text{-}V}$ binding to GST-NC construct.
$ALIX_{Bro1\text{-}V}$ binds to GST-$CHMP4b_{205\text{-}224}$ (K_D = 26 μM), GST-p6 (K_D = 41 μM), as expected. Treatment of PEI and SAS did not impair ALIX-p6 interaction (K_D = 48 μM). GST-NCp1p6 binds to $ALIX_{Bro1\text{-}V}$ with a K_D of 42 μM similar to GST-p6. The binding curves of GST-NC (PEI) and GST-NC (lysate) are close to that of GST-free. Both presence of nucleic acids and mutations did not make notable differences in NC binding to ALIX.

purified NC and Bro1 domains, at least within the affinity (tighter than ~1 mM) that is detectable by SPR.

References

Adams, P.D., Afonine, P.V., Bunkoczi, G., Chen, V.B., Davis, I.W., Echols, N., Headd, J.J., Hung, L.W., Kapral, G.J., Grosse-Kunstleve, R.W., *et al.* (2010). PHENIX: a comprehensive Python-based system for macromolecular structure solution. Acta Crystallogr D Biol Crystallogr *66*, 213-221.

Amarasinghe, G.K., De Guzman, R.N., Turner, R.B., Chancellor, K.J., Wu, Z.R., and Summers, M.F. (2000). NMR structure of the HIV-1 nucleocapsid protein bound to stem-loop SL2 of the psi-RNA packaging signal. Implications for genome recognition. J Mol Biol *301*, 491-511.

Carlton, J.G., and Martin-Serrano, J. (2007). Parallels between cytokinesis and retroviral budding: a role for the ESCRT machinery. Science *316*, 1908-1912.

De Guzman, R.N., Wu, Z.R., Stalling, C.C., Pappalardo, L., Borer, P.N., and Summers, M.F. (1998). Structure of the HIV-1 nucleocapsid protein bound to the SL3 psi-RNA recognition element. Science *279*, 384-388.

Doyotte, A., Mironov, A., McKenzie, E., and Woodman, P. (2008). The Bro1-related protein HD-PTP/PTPN23 is required for endosomal cargo sorting and multivesicular body morphogenesis. Proc Natl Acad Sci U S A *105*, 6308-6313.

Dussupt, V., Javid, M.P., Abou-Jaoude, G., Jadwin, J.A., de La Cruz, J., Nagashima, K., and Bouamr, F. (2009). The nucleocapsid region of HIV-1 Gag cooperates with the PTAP and LYPXnL late domains to recruit the cellular machinery necessary for viral budding. PLoS Pathog *5*, e1000339.

Fisher, R.D., Chung, H.Y., Zhai, Q., Robinson, H., Sundquist, W.I., and Hill, C.P. (2007). Structural and biochemical studies of ALIX/AIP1 and its role in retrovirus budding. Cell *128*, 841-852.

Grosse-Kunstleve, R.W., and Adams, P.D. (2003). Substructure search procedures for macromolecular structures. Acta Crystallogr D Biol Crystallogr *59*, 1966-1973.

Group, C.C.P. (November 4. 1994). The CCP4 Suite:Programs for Protein Crystallography. Acta Crystallogr D50 *50*, 760-763.

Ichioka, F., Kobayashi, R., Katoh, K., Shibata, H., and Maki, M. (2008). Brox, a novel farnesylated Bro1 domain-containing protein that associates with charged multivesicular body protein 4 (CHMP4). Febs J *275*, 682-692.

Katoh, K., Shibata, H., Hatta, K., and Maki, M. (2004). CHMP4b is a major binding partner of the ALG-2-interacting protein Alix among the three CHMP4 isoforms. Arch Biochem Biophys *421*, 159-165.

Kim, J., Sitaraman, S., Hierro, A., Beach, B.M., Odorizzi, G., and Hurley, J.H. (2005). Structural basis for endosomal targeting by the Bro1 domain. Dev Cell *8*, 937-947.

Lee, B.M., De Guzman, R.N., Turner, B.G., Tjandra, N., and Summers, M.F. (1998). Dynamical behavior of the HIV-1 nucleocapsid protein. J Mol Biol *279*, 633-649.

McCoy, A.J., Storoni, L.C., and Read, R.J. (2004). Simple algorithm for a maximum-likelihood SAD function. Acta Crystallogr D Biol Crystallogr *60*, 1220-1228.

McCullough, J., Fisher, R.D., Whitby, F.G., Sundquist, W.I., and Hill, C.P. (2008). ALIX-CHMP4 interactions in the human ESCRT pathway. Proc Natl Acad Sci U S A *105*, 7687-7691.

Morita, E., Sandrin, V., Chung, H.Y., Morham, S.G., Gygi, S.P., Rodesch, C.K., and Sundquist, W.I. (2007). Human ESCRT and ALIX proteins interact with proteins of the midbody and function in cytokinesis. Embo J *26*, 4215-4227.

Odorizzi, G., Katzmann, D.J., Babst, M., Audhya, A., and Emr, S.D. (2003). Bro1 is an endosome-associated protein that functions in the MVB pathway in Saccharomyces cerevisiae. J Cell Sci *116*, 1893-1903.

Otwinowski, Z., and Minor, W. (1997). Processing of X-ray Diffraction Data Collected in Oscillation Mode. Methods in Enzymology *276*.

Painter, J., and Merritt, E.A. (2005). A molecular viewer for the analysis of TLS rigid-body motion in macromolecules. Acta Crystallogr D Biol Crystallogr *61*, 465-471.

Painter, J., and Merritt, E.A. (2006). Optimal description of a protein structure in terms of multiple groups undergoing TLS motion. Acta Crystallogr D Biol Crystallogr *62*, 439-450.

Pisitkun, T., Shen, R.F., and Knepper, M.A. (2004). Identification and proteomic profiling of exosomes in human urine. Proc Natl Acad Sci U S A *101*, 13368-13373.

Popov, S., Popova, E., Inoue, M., and Gottlinger, H.G. (2009). Divergent Bro1 domains share the capacity to bind human immunodeficiency virus type 1 nucleocapsid and to enhance virus-like particle production. J Virol *83*, 7185-7193.

Richter, C., West, M., and Odorizzi, G. (2007). Dual mechanisms specify Doa4-mediated deubiquitination at multivesicular bodies. Embo J *26*, 2454-2464.

Studier, F.W. (2005). Protein production by auto-induction in high density shaking cultures. Protein Expr Purif *41*, 207-234.

Teis, D., Saksena, S., and Emr, S.D. (2008). Ordered assembly of the ESCRT-III complex on endosomes is required to sequester cargo during MVB formation. Dev Cell *15*, 578-589.

Terwilliger, T.C. (1994). MAD phasing: Bayesian estimates of F(A). Acta Crystallogr D Biol Crystallogr *50*, 11-16.

Terwilliger, T.C., Adams, P.D., Read, R.J., McCoy, A.J., Moriarty, N.W., Grosse-Kunstleve, R.W., Afonine, P.V., Zwart, P.H., and Hung, L.W. (2009). Decision-making in structure solution using Bayesian estimates of map quality: the PHENIX AutoSol wizard. Acta Crystallogr D Biol Crystallogr *65*, 582-601.

Thery, C., Boussac, M., Veron, P., Ricciardi-Castagnoli, P., Raposo, G., Garin, J., and Amigorena, S. (2001). Proteomic analysis of dendritic cell-derived exosomes: a secreted subcellular compartment distinct from apoptotic vesicles. J Immunol *166*, 7309-7318.

Tyler, R.C., Sreenath, H.K., Singh, S., Aceti, D.J., Bingman, C.A., Markley, J.L., and Fox, B.G. (2005). Auto-induction medium for the production of [U-15N]- and [U-13C, U-15N]-labeled proteins for NMR screening and structure determination. Protein Expr Purif *40*, 268-278.

Usami, Y., Popov, S., and Gottlinger, H.G. (2007). Potent rescue of human immunodeficiency virus type 1 late domain mutants by ALIX/AIP1 depends on its CHMP4 binding site. J Virol *81*, 6614-6622.

Wemmer, M., Azmi, I., West, M., Davies, B., Katzmann, D., and Odorizzi, G. (2011). Bro1 binding to Snf7 regulates ESCRT-III membrane scission activity in yeast. J Cell Biol *192*, 295-306.

Wollert, T., Wunder, C., Lippincott-Schwartz, J., and Hurley, J.H. (2009). Membrane scission by the ESCRT-III complex. Nature *458*, 172-177.

CHAPTER 7

SUMMARY AND PERSPECTIVE

ALIX Functions in Virus Budding

Many membrane scission events that separate the nascent viral envelope from host membranes co-opt the cellular ESCRT machinery (Bieniasz, 2009; Usami et al., 2009). ESCRT proteins play important roles in topologically equivalent cellular membrane scission events, including biogenesis of MVBs, and membrane abscission at the end of cell division (Carlton and Martin-Serrano, 2007; Hurley and Emr, 2006). Viral Gag mimics the upstream complexes of ESCRT machinery to enrich cargoes, induce and stabilize membrane curvature, because Gag proteins are able to assemble on the plasma membrane into an approximately spherical lollipop-like structure (Freed, 1998). Gag then recruits downstream of the ESCRT pathway to complete membrane abscission. HIV-1 and EIAV encode "YPXnL" late domains that recruit ALIX and other ESCRT components to facilitate virus budding. ALIX contains three distinct structural elements: an N-terminal Bro1 domain, a central V domain, and a C-terminal proline rich region (PRR).

We determined the crystal structures of $ALIX_{Bro1}$, $ALIX_{V}$, $ALIX_{Bro1-V}$, identified new ALIX-binding peptides from SIV strains, and determined structure of ALIX in complex with all characterized ALIX binding peptides, which likely cover all the ALIX-binding modes adopted by the viral Gag proteins. Furthermore, we determined the structure of a human ALIX homologue Brox, which interacts with CHMP4 via the same hydrophobic

patch of the ALIX Bro1 domain (McCullough et al., 2008). Therefore, we showed that ALIX serves as a scaffold that connects retroviral Gag proteins to ESCRT-III.

ALIX-TSG101

Many binding partners of ALIX have been reported, and can potentially participate in viral budding. The most notable of these is TSG101, which is itself the receptor for the primary late domain of HIV-1, a P(S/T)AP motif that binds the TSG101 UEV domain (Garrus et al., 2001). Curiously, a $_{717}$PSAP$_{720}$ motif is found in the ALIX PRR and can directly bind to the UEV domain of TSG101 (von Schwedler et al., 2003). However, overexpression of ALIX$_{P720L}$ rescued HIV-1 ΔPTAP release and infectivity (Fisher et al., 2007), indicating that this potential ALIX-TSG101 contact is not essential for viral budding.

Nevertheless, the C-terminal region of ALIX contains additional TSG101 binding sites. Residues $_{852}$PSYP$_{855}$, Y864 and Y865 can mediate ALIX self-association and ALIX-TSG101 interaction. Thus, those residues could contact TSG101 directly or contribute to ALIX dimerization, which may produce an additional binding site (Carlton et al., 2008). Furthermore, both TSG101 and ALIX are recruited directly by the same interface of CEP55 to the midbody at the conclusion of cytokinsis (Carlton et al., 2008; Lee et al., 2008; Morita et al., 2007). It remains a puzzle why depletion of TSG101 inhibits the abscission step of cell cytokinesis, even though theoretically

ALIX alone is sufficient to recruit ESCRT-III subunits. Likewise, both ALIX and TSG101 are required to rescue VPL release of ubiquitin-fused EIAV Gag that lacks a YPXL motif (Joshi et al., 2008). These results indicate that TSG101 likely regulates ALIX, and the role of TSG101-ALIX interaction in viral release remains to be dissected.

ALIX-ubiquitin

Ubiquitin serves an important sorting signal during MVB biogenesis. Many ESCRT complexes contain ubiquitin-binding domains and can be ubiquitylated (Raiborg and Stenmark, 2009). Although the role of ubiquitin in viral budding remains elusive, several observations support a positive role for ubiquitin in viral particle release: (1) High levels of free ubiquitin and ubiquitylated Gag are incorporated in retroviruses (Ott et al., 1998; Putterman et al., 1990). (2) Mutation of multiple lysine residues, which are candidate sites of ubiquitylation, in Gag inhibits virus budding (Gottwein et al., 2006; Ott et al., 2000; Spidel et al., 2004). (3) Several independent observations show that different HECT ubiquitin ligases can drive viral budding, likely through multiple ways that can involve ubiquitylation of Gag or ubiquitylation of Gag cofactors (Chung et al., 2008; Jouvenet et al., 2011; Usami et al., 2008). (4) An unrelated ubiquitin ligase, the ring-finger containing protein POSH, was shown to promote viral production (Alroy et al., 2005). POSH can form a complex with ALIX in a calcium-dependent manner, and can ubiquitylate multiple sites on ALIX (Votteler et al., 2009). Although

silencing of POSH by RNAi and disruption the POSH-ALIX interaction did not impair ALIX-dependent viral release (Votteler et al., 2009; unpublished data). (5) Virginie Sandrin, a postdoc in the Sundquist group, has discovered that the majority of ALIX incorporated into budded virions is mono-ubiquitylated (personal communication). (6) Fusion of ubiquitin to EIAV Gag lacking of a late domain rescued VLP release, which can be abolished by depletion of either cellular ALIX or TSG101 (Joshi et al., 2008).

Motivated by these observations, I tested whether ALIX can directly interact with ubiquitin by performing SPR experiments. Cells expressing ubiquitin or I44A mutant cloned in pET3a vector were lysed with lysozyme treatment and sonication. Other proteins in the supernatant were precipitated with 70% perchloric acid with 1% (v/v) final concentration. The clarified supernatant was dialyzed overnight against 50mM ammonium acetate pH 4.5, and applied to HiTrap SP column (GE Healthcare). The protein was eluted by a NaCl gradient from 0 to 500 mM and further purified by size exclusion chromatography. SPR experiments were performed by immobilizing GST-ALIX constructs and injecting purified ubiquitin protein. Ubiquitin binds to the ALIX V domain with a K_D of 1.07 mM (SD = 0.104 mM) (Figure 7.1). Like ubiquitin binding to ESCRT-0, -I and -II, and many other ubiquitin binding proteins, this interaction was severely impaired by the ubiquitin I44A mutation.

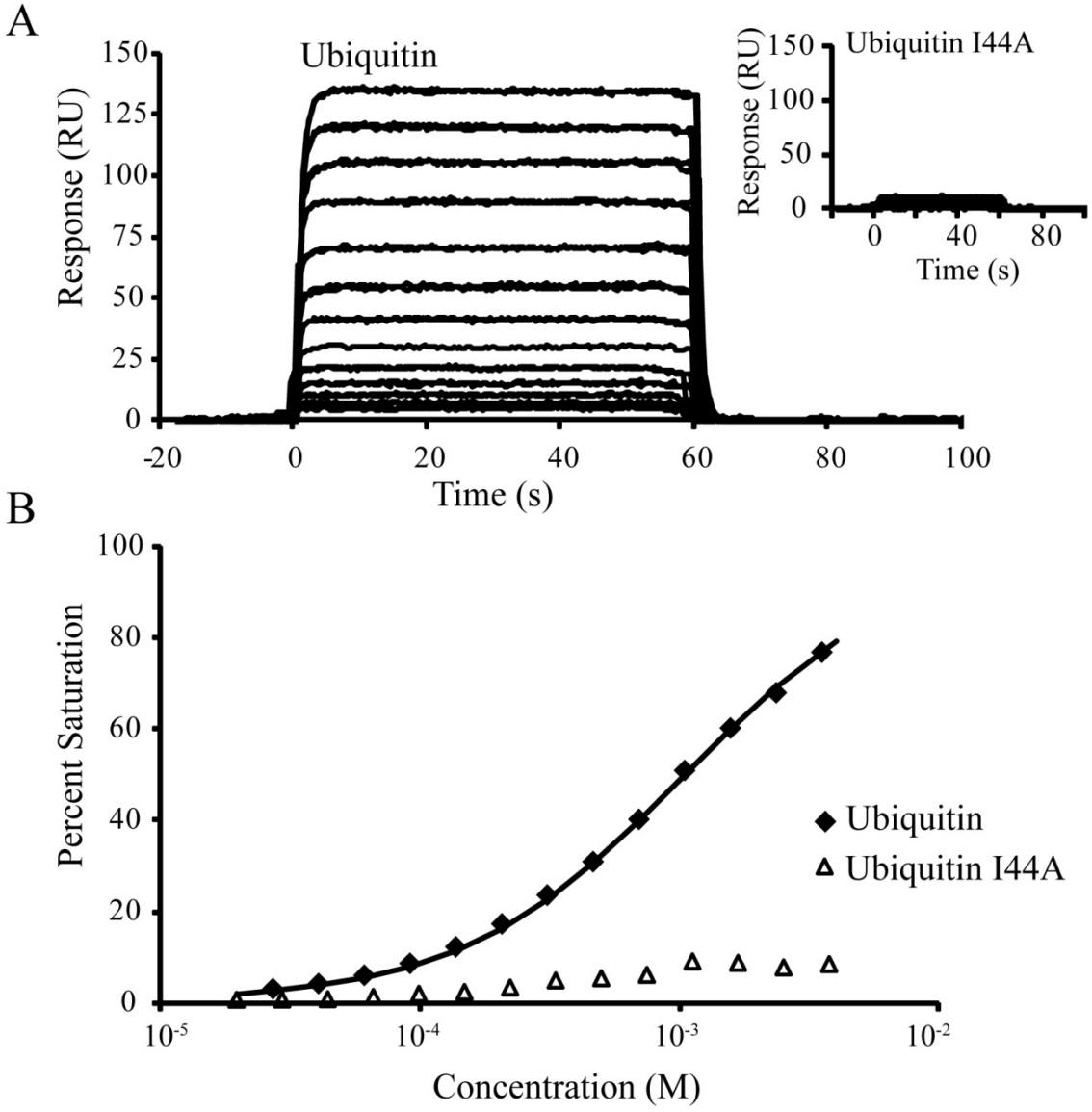

Figure 7.1. ALIX$_V$ binding ubiquitin.
(A) Representative biosensor sensograms for wild type (blue) and I44A mutant (black) ubiquitin proteins binding to immobilized GST-ALIX$_V$. Samples were analyzed twice at 25 ℃. Ubiquitin and Ubiquitin_I44A were tested at a high concentration of 3.5 mM in a 1.5-fold dilution series in duplicate over the GST captured surfaces in 10 mM Tris pH 8.0, 100 mM NaCl, 1 mM DTT with 0.01% Tween-20 and 0.1 mg/ml BSA. (B) Representative biosensor binding isotherms for the ALIXV binding to ubiquitin proteins.

I have worked on mapping the ubiquitin binding site on ALIX. Fifty GST-ALIX$_V$ mutants were made and analyzed for ubiquitin interaction. Effects were modest, but mutations that weakened the ALIX-ubiquitin interaction by at least two fold are I382A, A388E, L391A and L619A, and all belong to the arm 1 of the V domain (Table 7.1). In support of the ubiquitin binding site being located on arm 1, we found that a construct corresponding to just arm 1 also interacted with ubiquitin. We were unable, however, to identify a mutation that eliminated ALIX-ubiquitin association, including a double mutation of A388E and L619A. This effort is made challenging by the extremely weak binding affinity, which causes measurement errors that are so large that the effect of mutation is underestimated.

Based on these data, it is attractive to speculate that ubiquitin binding and ubiquitylation of ALIX contributes to virus production under physiological expression levels of ALIX. One method to overcome the problem of detecting low affinity interaction is to use purified dimeric ALIX proteins and di-ubiquitin chains to perform SPR and affinity purification experiments, because dimerization can greatly increase binding affinity. Another approach is NMR chemical shift perturbation, which might indicate specific residues at the ALIX-ubiquitin interface. Another approach would be to cocrystallize ALIX and ubiquitin to visualize the interaction directly. Furthermore, a possible approach to determine the functional importance of ALIX-ubiquitin interactions would be to assay mutants that do not bind ubiquitin non-

Table 7.1. Summary of K_D for Ubiquitin to GST-$ALIX_V$ proteins.

	Constructs	K_D (mM)
wt	GST-V	1.12
1	GST-V-L626A	Not expressed
2	GST-V-L443A	0.98
3	GST-V-T674A	1.58
4	GST-V-L585A	1.31
5	GST-V-F676D	1.40
6	GST-V-K374A	0.98
7	GST-V-V378A	2.19
8	GST-V-K574	0.93
9	GST-V-I382A	3.78
10	GST-V-N393A	1.05
11	GST-V-K563A	1.52
12	GST-V-E406A	0.78
13	GST-V-K565A	1.23
14	GST-V-E617A	0.94
15	GST-V-E623A	1.26
16	GST-V-Q616A	0.92
17	GST-V-L619A	3.92
18	GST-V-Q622A	1.36
19	GST-V-A388E	8.78
20	GST-V-Q384E	1.07
21	GST-V-L443A	0.70
22	GST-V-R446A	2.81
23	GST-V-N678A	1.61
24	GST-V-I450A	1.28
25	GST-V-T674A	1.20
26	GST-V-K671A	1.10
27	GST-V-L588A	0.98
28	GST-V-L585A	0.92
29	GST-V-Q445A	1.71
30	GST-V-E449A	1.05
31	GST-V-E453A	1.47
32	GST-V-R456A	1.29
33	GST-V-E460A	0.98
34	GST-V-S515D	0.86
35	GST-V-A533E	0.81
36	GST-V-V593D	0.61
37	GST-V-R380A	0.96
38	GST-V-E387A	1.49
39	GST-V-L391A	2.21

Table 7.1. Continued.

	Constructs	K_D (mM)
40	GST-V-A383E	0.73
41	GST-V-R386A	0.97
42	GST-V-N379A	1.13
43	GST-V-R373A	0.68
44	GST-V-E567A	1.23
45	GST-V-N571A	1.11
46	GST-V-L626K	Not expressed
47	GST-V-K614A	1.06
48	GST-V-K620A	1.01
49	GST-V-K621A	1.06
50	GST-V-L619A-A388E	4.80

covalently or are resistant to ubiquitylation. It would be important to use physiological levels of ALIX in these experiments, and it may be informative to assay for both viral budding and cytokinesis defects.

ALIX-membrane

The known structures of Bro1 domains all reveal an extended curved banana-shaped conformation, even when the different homologs share only low levels of sequence similarity (Fisher et al., 2007; Kim et al., 2005). The concave surface of Bro1 domains has been speculated to bind curved membrane or to induce membrane deformation (Kim et al., 2005). Moreover, ALIX has been reported to associate with LBPA, which is abundant in MVBs and can induce formation of vesicles (Kobayashi et al., 1998; Lebrand et al., 2002; Matsuo et al., 2004). However, ALIX was also reported to antagonize internal vesicle formation in LBPA liposomes, which is apparently contradictory to the positive function of ALIX in virus production. It is still unclear whether ALIX can directly associate with membrane and regulate membrane curvature. Possible approaches to investigating this problem would be to visualize purified ALIX proteins incubated with lipids by electron microscopy and by FRET.

ALIX Activation

In Chapter 6, we reported that the C-terminal PRR of ALIX folds back against the V domain and inhibits access by viral late domains. A mutation (R649E) that opens the closed conformation of the V domain was more potent

than the wild type protein in stimulating virus release and infectivity. Weissenhorn and colleagues also argued that the active ALIX conformation is one in which the two arms of the V domain are in an open orientation (Pires et al., 2009). They further argue that ALIX dimerizes upon activation, with the arms of the open V domain packing against each other in an anti-parallel fashion (Pires et al., 2009). We have also noted that ALIX preparations include a significant fraction of dimerized protein that does not rapidly interconvert with the monomeric species, although our activated R649E mutant is primarily monomeric. Based on all these observations, we propose that ALIX is activated to facilitate virus budding through a series of conformational changes, including PRR release from Bro1-V domains, opening of the V domain, membrane recruitment of ALIX, and dimerization.

A more precise description of the active conformation is an important objective for future studies. For example, what mechanism might trigger ALIX activation? Are certain ALIX-binding partners, protein modifications or ALIX localization involved in ALIX activation? From a structural perspective, a crystal structure of $ALIX_{R649E}$ might provide insight to conformational changes that underlie ALIX activation. Another attractive target for future structural studies is the dimeric form for ALIX, which likely represents an activated state.

References

Alroy, I., Tuvia, S., Greener, T., Gordon, D., Barr, H.M., Taglicht, D., Mandil-Levin, R., Ben-Avraham, D., Konforty, D., Nir, A.*, et al.* (2005). The trans-

Golgi network-associated human ubiquitin-protein ligase POSH is essential for HIV type 1 production. Proc Natl Acad Sci U S A *102*, 1478-1483.

Bieniasz, P.D. (2009). The cell biology of HIV-1 virion genesis. Cell Host Microbe *5*, 550-558.

Carlton, J.G., Agromayor, M., and Martin-Serrano, J. (2008). Differential requirements for Alix and ESCRT-III in cytokinesis and HIV-1 release. Proc Natl Acad Sci U S A *105*, 10541-10546.

Carlton, J.G., and Martin-Serrano, J. (2007). Parallels between cytokinesis and retroviral budding: a role for the ESCRT machinery. Science *316*, 1908-1912.

Chung, H.Y., Morita, E., von Schwedler, U., Muller, B., Krausslich, H.G., and Sundquist, W.I. (2008). NEDD4L overexpression rescues the release and infectivity of human immunodeficiency virus type 1 constructs lacking PTAP and YPXL late domains. J Virol *82*, 4884-4897.

Fisher, R.D., Chung, H.Y., Zhai, Q., Robinson, H., Sundquist, W.I., and Hill, C.P. (2007). Structural and biochemical studies of ALIX/AIP1 and its role in retrovirus budding. Cell *128*, 841-852.

Freed, E.O. (1998). HIV-1 gag proteins: diverse functions in the virus life cycle. Virology *251*, 1-15.

Garrus, J.E., von Schwedler, U.K., Pornillos, O.W., Morham, S.G., Zavitz, K.H., Wang, H.E., Wettstein, D.A., Stray, K.M., Cote, M., Rich, R.L.*, et al.* (2001). Tsg101 and the vacuolar protein sorting pathway are essential for HIV-1 budding. Cell *107*, 55-65.

Gottwein, E., Jager, S., Habermann, A., and Krausslich, H.G. (2006). Cumulative mutations of ubiquitin acceptor sites in human immunodeficiency virus type 1 gag cause a late budding defect. J Virol *80*, 6267-6275.

Hurley, J.H., and Emr, S.D. (2006). The ESCRT complexes: structure and mechanism of a membrane-trafficking network. Annu Rev Biophys Biomol Struct *35*, 277-298.

Joshi, A., Munshi, U., Ablan, S.D., Nagashima, K., and Freed, E.O. (2008). Functional replacement of a retroviral late domain by ubiquitin fusion. Traffic *9*, 1972-1983.

Jouvenet, N., Zhadina, M., Bieniasz, P.D., and Simon, S.M. (2011). Dynamics of ESCRT protein recruitment during retroviral assembly. Nat Cell Biol.

Kim, J., Sitaraman, S., Hierro, A., Beach, B.M., Odorizzi, G., and Hurley, J.H. (2005). Structural basis for endosomal targeting by the Bro1 domain. Dev Cell *8*, 937-947.

Kobayashi, T., Stang, E., Fang, K.S., de Moerloose, P., Parton, R.G., and Gruenberg, J. (1998). A lipid associated with the antiphospholipid syndrome regulates endosome structure and function. Nature *392*, 193-197.

Lebrand, C., Corti, M., Goodson, H., Cosson, P., Cavalli, V., Mayran, N., Faure, J., and Gruenberg, J. (2002). Late endosome motility depends on lipids via the small GTPase Rab7. Embo J *21*, 1289-1300.

Lee, H.H., Elia, N., Ghirlando, R., Lippincott-Schwartz, J., and Hurley, J.H. (2008). Midbody targeting of the ESCRT machinery by a noncanonical coiled coil in CEP55. Science *322*, 576-580.

Matsuo, H., Chevallier, J., Mayran, N., Le Blanc, I., Ferguson, C., Faure, J., Blanc, N.S., Matile, S., Dubochet, J., Sadoul, R.*, et al.* (2004). Role of LBPA and Alix in multivesicular liposome formation and endosome organization. Science *303*, 531-534.

McCullough, J., Fisher, R.D., Whitby, F.G., Sundquist, W.I., and Hill, C.P. (2008). ALIX-CHMP4 interactions in the human ESCRT pathway. Proc Natl Acad Sci U S A *105*, 7687-7691.

Morita, E., Sandrin, V., Chung, H.Y., Morham, S.G., Gygi, S.P., Rodesch, C.K., and Sundquist, W.I. (2007). Human ESCRT and ALIX proteins interact with proteins of the midbody and function in cytokinesis. Embo J *26*, 4215-4227.

Ott, D.E., Coren, L.V., Chertova, E.N., Gagliardi, T.D., and Schubert, U. (2000). Ubiquitination of HIV-1 and MuLV Gag. Virology *278*, 111-121.

Ott, D.E., Coren, L.V., Copeland, T.D., Kane, B.P., Johnson, D.G., Sowder, R.C., 2nd, Yoshinaka, Y., Oroszlan, S., Arthur, L.O., and Henderson, L.E. (1998). Ubiquitin is covalently attached to the p6Gag proteins of human immunodeficiency virus type 1 and simian immunodeficiency virus and to the p12Gag protein of Moloney murine leukemia virus. J Virol *72*, 2962-2968.

Pires, R., Hartlieb, B., Signor, L., Schoehn, G., Lata, S., Roessle, M., Moriscot, C., Popov, S., Hinz, A., Jamin, M.*, et al.* (2009). A Crescent-Shaped ALIX Dimer Targets ESCRT-III CHMP4 Filaments. Structure *17*, 843-856.

Putterman, D., Pepinsky, R.B., and Vogt, V.M. (1990). Ubiquitin in avian leukosis virus particles. Virology *176*, 633-637.

Raiborg, C., and Stenmark, H. (2009). The ESCRT machinery in endosomal sorting of ubiquitylated membrane proteins. Nature *458*, 445-452.

Spidel, J.L., Craven, R.C., Wilson, C.B., Patnaik, A., Wang, H., Mansky, L.M., and Wills, J.W. (2004). Lysines close to the Rous sarcoma virus late domain critical for budding. J Virol *78*, 10606-10616.

Usami, Y., Popov, S., Popova, E., and Gottlinger, H.G. (2008). Efficient and specific rescue of human immunodeficiency virus type 1 budding defects by a Nedd4-like ubiquitin ligase. J Virol *82*, 4898-4907.

Usami, Y., Popov, S., Popova, E., Inoue, M., Weissenhorn, W., and H, G.G. (2009). The ESCRT pathway and HIV-1 budding. Biochem Soc Trans *37*, 181-184.

von Schwedler, U.K., Stuchell, M., Muller, B., Ward, D.M., Chung, H.Y., Morita, E., Wang, H.E., Davis, T., He, G.P., Cimbora, D.M.*, et al.* (2003). The protein network of HIV budding. Cell *114*, 701-713.

Votteler, J., Iavnilovitch, E., Fingrut, O., Shemesh, V., Taglicht, D., Erez, O., Sorgel, S., Walther, T., Bannert, N., Schubert, U.*, et al.* (2009). Exploring the functional interaction between POSH and ALIX and the relevance to HIV-1 release. BMC Biochem *10*, 12.

APPENDIX

STRUCTURAL AND FUNCTIONAL STUDIES ON THE EXTRACELLULAR DOMAIN OF BST2/TETHERIN IN REDUCED AND OXIDIZED CONFORMATIONS

Heidi L. Schubert, Qianting Zhai, Virginie Sandrin, Debra M. Eckert, Mitla Garcia-Maya, Louise Saul, Wesley I. Sundquist, Roberto A. Steiner, and Christopher P. Hill

This research was originally published in the Proceeding of the National Academy of Sciences of the United States of America. 107(42):17951-6.2010.

Structural and functional studies on the extracellular domain of BST2/tetherin in reduced and oxidized conformations

Heidi L. Schubert[a,1], Qianting Zhai[a,1], Virginie Sandrin[a], Debra M. Eckert[a], Mitla Garcia-Maya[b], Louise Saul[b], Wesley I. Sundquist[a,2], Roberto A. Steiner[b,2], and Christopher P. Hill[a,2]

[a]Department of Biochemistry, University of Utah School of Medicine, Salt Lake City, UT 84112-5650; and [b]Randall Division of Cell and Molecular Biophysics, King's College London, New Hunt's House, Guy's Campus, London, SE1 1UL, United Kingdom

Edited* by Stephen C. Harrison, Harvard Medical School, Boston, MA, and approved August 17, 2010 (received for review June 11, 2010)

HIV-1 and other enveloped viruses can be restricted by a host cellular protein called BST2/tetherin that prevents release of budded viruses from the cell surface. Mature BST2 contains a small cytosolic region, a predicted transmembrane helix, and an extracellular domain with a C-terminal GPI anchor. To advance understanding of BST2 function, we have determined a 2.6 Å crystal structure of the extracellular domain of the bacterially expressed recombinant human protein, residues 47–152, under reducing conditions. The structure forms a single long helix that associates as a parallel dimeric coiled coil over its C-terminal two-thirds, while the N-terminal third forms an antiparallel four-helix bundle with another dimer, creating a global tetramer. We also report the 3.45 Å resolution structure of BST2(51-151) prepared by expression as a secreted protein in HEK293T cells. This oxidized construct forms a dimer in the crystal that is superimposable with the reduced protein over the C-terminal two-thirds of the molecule, and its N terminus suggests pronounced flexibility. Hydrodynamic data demonstrated that BST2 formed a stable tetramer under reducing conditions and a dimer when oxidized to form disulfide bonds. A mutation that selectively disrupted the tetramer (L70D) increased protein expression modestly but only reduced antiviral activity by approximately threefold. Our data raise the possibility that BST2 may function as a tetramer at some stage, such as during trafficking, and strongly support a model in which the primary functional state of BST2 is a parallel disulfide-bound coiled coil that displays flexibility toward its N terminus.

coiled coil | crystal structures | HIV | innate immunity | restriction factor

Viral infection can induce a type I interferon response, which in turn stimulates the expression of many genes that encode innate immunity factors (1). One of the upregulated proteins, bone marrow stromal cell antigen 2 (BST2/tetherin/CD317/HM1.24), inhibits the release of HIV-1 and other enveloped viruses from the surface of cells in which it is expressed (2–10). HIV-1 virions retained at the cell surface in the presence of BST2 are fully formed and mature but remain attached to the cell surface by a protease-sensitive linkage (11, 12) that contains BST2 (13, 14). The retained virions can subsequently be internalized and have been visualized in early and late endosomes, and they may ultimately be degraded following fusion with lysosomes (12).

HIV-1 escapes BST2-mediated restriction through the activity of its accessory protein viral protein U (Vpu) (15–17). Most, but not all (18), studies have found that Vpu reduces cell surface levels of BST2, and the two proteins appear to interact through their transmembrane (TM) domains (19–25). Various mechanisms for BST2 surface downregulation have been proposed, including lysosomal degradation, proteasomal degradation, and/or sequestration/retargeting of BST2 to the trans-Golgi network (reviewed in ref. 8). The general importance of BST2 is indicated by the findings that other viruses use different proteins to overcome BST2 restriction, including the Env/glycoproteins of Ebola virus and some strains of SIV and HIV-2, (4, 26, 27), the negative factor (Nef) protein of other SIV strains (24, 28, 29), and the K5 protein of Kaposi's Herpes Sarcoma virus (30, 31).

The mature BST2 protein has an unusual architecture, comprising a small cytosolic domain and a TM helix at the N terminus (residues 22–44), a glycophosphatidylinositol (GPI) anchor at the C-terminal Ser160 residue, and an approximately 105-residues-long disulfide-rich coiled coil structure predicted for the extracellular domain (32–34). This configuration appears central to function, with the leading model being that virions are held at the cell surface by a bridge in which the extracellular domain of one or, more likely, multiple molecules of BST2 spans the gap between plasma membrane and the membrane of the otherwise detached viral particle (13, 14, 34). It has been argued that the GPI modification targets BST2 to cholesterol-rich regions of the plasma membrane (33), which may concentrate the protein at sites of viral budding. However, removal of the GPI anchor reportedly does not release virions from their tethered state (14). Finally, functions for BST2, independent of viral restriction, have also been proposed in trafficking and signaling (33), and in organization of the subapical actin cytoskeleton (35).

It has been proposed that BST2 forms a parallel dimeric coiled coil that is stabilized by C53–C53, C63–C63, and C91–C91 disulfide bonds. This model is supported by nonreducing SDS/PAGE analyses of mutant proteins isolated from the surface of HEK293T cells (32, 34) and by a recent crystal structure of residues 89–147 of the BST2 extracellular domain (36). Both the N-terminal TM helix and the C-terminal GPI can be incorporated into HIV-1 virions, and it has therefore been suggested that BST2 either forms an antiparallel dimer (14) or that it forms a parallel dimer whose tethering orientation is not critical for viral restriction (34). We also note that the importance of BST2 dimerization has been disputed (37). Remarkably, HIV-1 restriction is preserved (at approximately 10% levels) in cells that express an engineered protein that was designed to maintain the overall BST2 architecture but does not conserve the specific amino acid residue identities (34). Finally, the efficiency of BST2-mediated HIV-1 inhibition appears to be concentration-dependent, because virions that contain BST2 can be released under

Author contributions: H.L.S., Q.Z., V.S., D.M.E., M.G.-M., L.S., W.I.S., R.A.S., and C.P.H. designed research; H.L.S., Q.Z., V.S., D.M.E., M.G.-M., L.S., and R.A.S. performed research; H.L.S., Q.Z., V.S., D.M.E., M.G.-M., L.S., W.I.S., R.A.S., and C.P.H. analyzed data; and H.L.S., V.S., D.M.E., W.I.S., R.A.S., and C.P.H. wrote the paper.

The authors declare no conflict of interest.

*This Direct Submission article had a prearranged editor.

Data deposition: The atomic coordinates and structure factors have been deposited in the Protein Data Bank, www.pdb.org [ID codes 3nwh (reduced BST2) and 2xg7 (oxidized BST2)].

[1]H.L.S. and Q.Z. contributed equally to this work.

[2]To whom correspondence may be addressed. E-mail: wes@biochem.utah.edu, roberto.steiner@kcl.ac.uk, or chris@biochem.utah.edu.

This article contains supporting information online at www.pnas.org/lookup/suppl/doi:10.1073/pnas.1008206107/-/DCSupplemental.

conditions of low BST2 expression (34). These considerations emphasize the importance of determining the oligomeric state(s) of BST2. In an effort to understand the mechanistic basis for BST2 activity better, we have determined crystal structures and solution oligomerization states of oxidized and reduced BST2 proteins and tested the restriction activity of a structure-based mutant that cannot switch oligomerization states when reduced.

Results

Reduced BST2 Crystal Structure. We determined a structure of the human BST2 extracellular domain (residues 47-152) produced in *Escherichia coli* and crystallized in the presence of reductant to 2.6 Å resolution and R/R_{free} values of 26.0%/27.8% (Fig. 1 and Table S1). All but a few of the BST2 residues at the termini of the four molecules in the asymmetric unit were visible, although the central regions (residues 92–117) have relatively weak density and high B values.

Subunits are arranged as parallel dimers that splay apart slightly to form an antiparallel 4-helix bundle over the N-terminal 40 residues and generate a 245 Å-long tetramer in the asymmetric unit (Fig. 1*A*). The remaining two-thirds forms a dimeric coiled coil, with residues 118–150 displaying the standard "knobs-into-holes" packing of *a* and *d* heptad repeat residues seen in classical coiled coils (38–40), and residues 92–117 packing more loosely to display some but not all of the *a* and *d* residue knobs-into-holes interactions (Fig. S1). Equivalent packing for the C-terminal two-thirds was reported by Hinz et al. (36).

Although each of the subunits forms one continuous helix that is devoid of sharp turns, the helices do not all superpose closely over their entire length. The two parallel dimers in the asymmetric unit are very similar to each other and superpose with a root mean square deviation of 0.79 Å over all Cα atoms (Fig. 1*B*), but the two subunits within one parallel dimer show an approximately 30° deflection in the vicinity of residue 90, near the tetramer-dimer transition (Fig. 1*C*). This asymmetry results from small differences spread over several residues and may indicate that the BST2 sequence encodes an asymmetric dimeric structure, although we prefer the explanation that the molecule has inherent flexibility.

C53 and C63 are contained within the N-terminal four-helix bundle while C91 is immediately C-terminal to the bundle. All three cysteines are reduced in this structure, whereas biochemical data indicate that BST2 forms disulfide bonds in the oxidizing environment of the cell exterior (34). Residues C53 and C63 are too far from their partners to form disulfide bonds without disrupting packing of the four-helix bundle region. In contrast, neighboring C91 residues could form a disulfide bond without substantial movement of their main chains from the crystal structure. We have built C91 residues with their sulfur atoms separated by 4.7 Å in this structure because the density, which is relatively poor in this region, does not indicate formation of a disulfide.

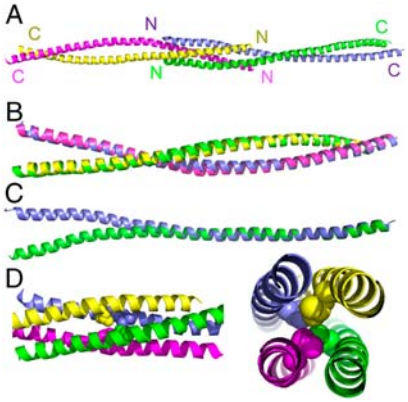

Fig. 1. Structure of reduced BST2(47–152). (*A*) The four molecules in the asymmetric unit. Yellow/magenta and blue/green subunits form parallel dimers. (*B*) Overlap of the two parallel dimers. (*C*) Overlap of the blue and green subunits on residues 90–152. (*D*) Orthogonal views showing the L70 side chain buried at the center of the tetramer.

Oligomeric States in Solution. Equilibrium analytical ultracentrifugation (AUC) was used to determine the association state of recombinant BST2 proteins in solution. This method provides shape-independent estimates of mass and is therefore ideally suited for studies of highly extended assemblies such as BST2. These studies employed slightly longer BST2(47–154) constructs in order to include two tyrosine residues and thereby increase optical absorbance. The AUC data showed that the recombinant protein is a tetramer in solution under the reducing conditions used in crystallization, over an initial concentration range of 0.5–2.0 mg/ml (41.7–166.7 μM). Equilibrium protein distributions could be globally fit to a single species tetramer model (Fig. S2) and also indicated a tetrameric association when the molecular weight was allowed to float (Fig. 2*A*).

To determine if oligomerization was altered by oxidation, purified reduced BST2 was dialyzed for one week against identical buffer that lacked reductant. Mass spectrometry showed that this protein was a fully disulfide-linked dimer (Fig. S3). The protein eluted from a sizing column primarily as a well-defined peak but also included a broad peak at shorter retention times that presumably corresponded to oxidized aggregates. AUC showed that protein from the main peak is dimeric over the concentration range tested (0.5–2.0 mg/ml), either by fitting to a dimer (Fig. S2) or by allowing the molecular weight to float (Fig. 2*B*). These data indicate that BST2 forms a stable tetramer under reducing conditions and converts into a stable dimer upon oxidation.

Oxidized Crystal Structure. To determine the BST2 extracellular domain structure under oxidizing conditions, we expressed secreted BST2(51–151) in HEK293T cells and completed purification and crystallization in the absence of reductant. Crystals of Endo-H treated BST2(51–151) diffracted anisotropically to a maximum resolution of 3.45 Å resolution. This structure, with one dimer in the asymmetric unit, was determined by molecular replacement using residues 89–151 of the reduced structure as a search model. The refined model (R/R_{free} = 26.9%/29.8%) comprises residues 72–151 for one of the two molecules in the asymmetric unit and residues 77–151 for the other molecule. The oxidized and reduced structures overlap closely from residue 90 to the C terminus but diverge toward the N terminus where the reduced protein tetramerizes (Fig. 3). For example, the Cβ–Cβ distance of juxtaposed A88 residues, which occupy an *a* coiled coil position, is 4.2 Å in the oxidized structure and 7.4 Å in the reduced structure. Clear electron density, confirmed by kicked omit maps, is observed for a disulfide bridge linking C91 residues validating the oxidized state of the molecule (Fig. 3). Two sugar moieties extending from N92 and positioned perpendicular to the C91–C91 disulfide could be located in the electron density (Fig. S4). Finally, additional N-terminal residues could be modeled in a helical conformation (Fig. S5), although due to the modest resolution, gaps in the density, and appearance of disorder, we have not included those residues in the deposited model. Thus, the dimeric coiled coil extends into the region that is tetrameric in the reduced structure, and residual density suggests that the coiled coil continues most of the way to the N terminus of this construct, albeit with pronounced flexibility.

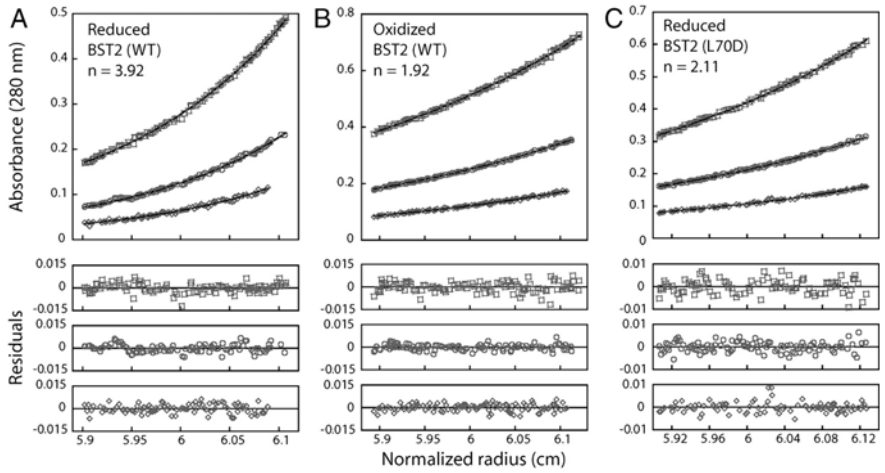

Fig. 2. Analytical equilibrium sedimentation analyses of BST2(47–154) with (*A*) and without (*B*) reductant and of BST2(47–154)L70D with reductant (*C*). Bottom, residual differences between the data and fit. Rotor speeds shown here were 12,000 rpm. Data from two rotor speeds were globally fit to single species models in which the molecular weights were allowed to float. Estimated molecular weights were 50,070 Da for reduced BST2(47–154) ($MW_{obs}/MW_{calc} = 3.92$), 24,497 Da for oxidized BST2(47–154) ($MW_{obs}/MW_{calc} = 1.92$), and 26,908 Da for reduced BST2(47–154)L70D ($MW_{obs}/MW_{calc} = 2.11$).

The Role of the BST2 Tetramer in HIV-1 Restriction. Although the functional importance of many BST2 residues has been tested by mutagenesis (34), the tetramer has not been reported previously. To create a mutant protein that was defective in tetramerization, we mutated Leu70, which lies at the heart of the four-helix bundle (Fig. 1*D*). Mutation to Asp destabilized the tetramer, so that the BST2(147-154)L70D protein remained dimeric, even under reducing conditions (Fig. 2*C* and Fig. S6). Thus, this mutation allowed us to test the restriction activity of a protein that dimerized but did not detectably tetramerize in vitro.

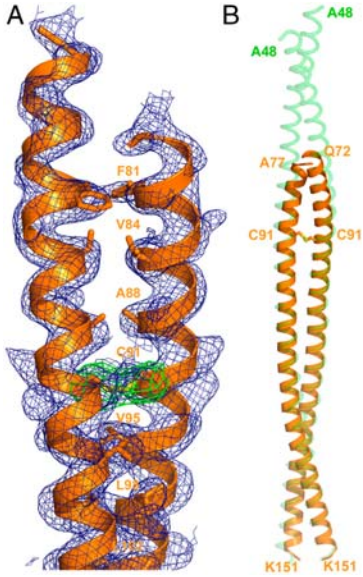

Fig. 3. Structure of oxidized BST2(51–151). (*A*) Electron density for the N-terminal region of oxidized BST2. B-factor sharpening was set at the median B value of refined atoms. $2mF_o$-DF_c map is shown in blue at 1 σ. Maximum-likelihood weighted averaged kick omit map (average size = 100, kick = 0.8 Å) for the C91 disulfide is colored green at 4 σ. Residues at the coiled coil interface are shown. (*B*) Overlap of the reduced (green) and oxidized (orange) structures.

To assay restriction, HEK293T cells (which do not express BST2) were cotransfected with expression constructs for wild-type or mutant BST2 and an HIV-1_{NL4-3} proviral expression construct that lacked Vpu (HIV-$1_{\Delta Vpu}$). BST2(L70D) expression was modestly increased (~1.5-fold) across a series of different concentrations of expression construct (Fig. 4*A*, "Cell" bottom panel). Virus released from cells that expressed wild-type and mutant BST2 was analyzed by (*i*) Western blotting of virion-associated MA and CA proteins in the culture media (Fig. 4*A*, "Virus") and (*ii*) measuring the infectious titers of released virions (Fig. 4*B*). These data showed that both the wild-type and mutant BST2 proteins were effective restriction factors because they reduced the release of infectious viral particles more than 5,000-fold when expressed at high levels. However, the restriction potency of BST2(L70D) was consistently about half that of the wild-type protein, despite higher expression levels (Fig. 4). The strong but attenuated activity of BST2(L70D) indicates that BST2 tetramerization is not essential, although it remains possible that it may contribute to the potency of viral restriction.

Discussion

We have determined crystal structures of the extracellular domain of BST2 under reducing and oxidizing conditions. The C-terminal two-thirds of the structure forms a parallel dimeric coiled coil. The C-terminal third adopts a classical knobs-into-holes packing, while the central third is less well-defined. At the N-terminal third of the protein, the two parallel helices splay apart to form an antiparallel four-helix bundle in the reduced state, but when the protein is oxidized these helices continue, at least initially, as a dimeric coiled coil that is stabilized by a C91–C91 disulfide and probably also by C53–C53 and C63–C63 disulfides. AUC data indicated that the crystal structures recapitulate the predominant solution oligomerization states because the reduced protein forms a stable tetramer but becomes dimeric upon oxidation (Fig. 2). The latter observation is consistent with an earlier study, which concluded that BST2 forms a disulfide-crosslinked dimer on the cell surface (34). Our data therefore indicate that BST2 can tether budded virions to the plasma membrane as a disulfide-linked coiled coil dimer.

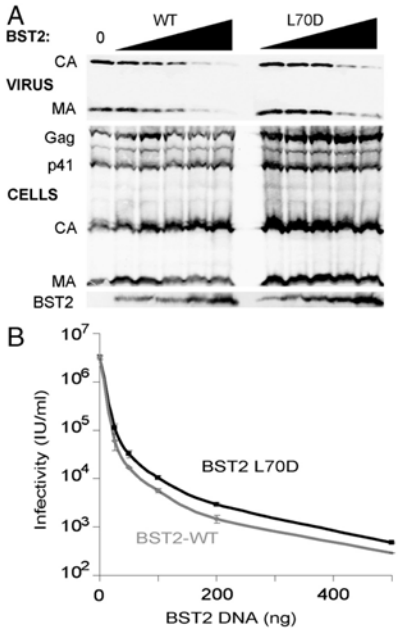

Fig. 4. Inhibition of HIV-1 release and infectivity by BST2 proteins. (*A*) Western blot of samples from 293 T cells that expressed HIV-$1_{\Delta Vpu}$ and either lacked BST2 (lane 1, unrestricted control) or expressed increasing levels of wild-type BST2 (lanes 2–6) or BST2(L70D) (lanes 7–11). Panel 1, levels of virion-associated viral Gag proteins released into the supernatant (VIRUS, anti-CA and anti-MA). Panel 2, intracellular Gag protein levels (CELLS, anti-CA and anti-MA). Panel 3, intracellular BST2 levels (CELLS, anti-BST2). The first lane of Panel 1 contains 25-fold less sample than the other lanes. Quantification showed that, on average, cells transfected with BST2(L70D) expressed 1.4 ± 0.3-fold more protein than those transfected with the wild-type BST2 ($n = 5$, $\pm$s.d.). Nevertheless, cells expressing BST2(L70D) released 2.5 ± 1.3-fold more virion-associated CA and MA protein ($n = 10$, $\pm$s.d.). (*B*) Graph showing HIV-1 titers in the presence of increasing quantities of expression vectors. Wild-type BST2 (light curve), BST2(L70D) (dark curve). Each data point corresponds to a sample analyzed in the Western blots shown in panel *A*. On average, viral titers were 1.9 ± 0.1-fold higher in cells expressing BST2(L70D) mutant (vs. wild-type BST2, $n = 10$, $\pm$s.d.).

While our manuscript was in preparation, a structure of the bacterially expressed C-terminal two-thirds of BST2 (residues 80–147) was reported by Hinz and colleagues (36). This structure showed formation of the C91–C91 disulfide bond, was ordered over residues 89–147, and superimposes closely with our BST2 structures (RMSD = 0.5–0.8 Å over essentially all Cα atoms). This reinforces the impression that the C-terminal two-thirds of the BST2 extracellular domain forms a dimeric coiled coil over both the well packed C-terminal third and over the less regularly associated central third.

Hinz et al. (36) also reported small angle X-ray scattering (SAXS) analysis of dimeric BST2(80–147) and BST2(47–159) proteins. Their data indicate an elongated structure that has a bend at about one third from the N terminus. An attractive possibility is that the N-terminal third of the molecule is flexible, with one specific possibility being that the coiled coil conformation continues toward the N terminus but can hinge about residues approximately 80–90. This apparent flexibility is consistent with (*i*) our finding that residues in this region adopt different conformations in our reduced and oxidized structures (Fig. 3) and in different subunits in the reduced structure (Fig. 1*C*), (*ii*) the appearance of electron density maps for our oxidized BST2(51–151) structure (Fig. 3 and Fig. S5), (*iii*) the protein's protease sensitivity at residue 80 (36), and (*iv*) the retention of tethering activity when an HA tag is introduced following residue 82 (36).

In addition to a hinging motion, it is possible that the N-terminal third of the BST2 extracellular domain has internal flexibility. This would be consistent with the absence of favored buried coiled coil residues in this region of the sequence and our finding that L70D, which corresponds to a buried *d* position in a simple coiled coil model derived from our crystal structures, expresses and purifies like the wild-type sequence and retains activity in a viral restriction assay (Fig. 4). The distribution of cystine residues is compatible with formation of a standard coiled coil throughout the length of the molecule because these residues would occupy *a* (C53), *d* (C63), and *d* (C91) positions in the model extended from the crystal structure. Disulfides can typically be accommodated in these positions, although they are expected to cause some structural perturbation when introduced into an *a* site (41). Just one disulfide is required for stability because constructs lacking any two cystines retain viral restriction activity, albeit with reduced potency (34). The conservation of all three cystines in a region of presumably loose-packed coiled coil is probably not simply due to a requirement for stability because coiled coils can be very stable in the absence of any disulfides. Rather, the cyteine conservation likely reflects a balance between requirements of stability and flexibility for optimal BST2 function.

The model in which BST2 forms a coiled coil from residue 47 to 152 predicts an overall length of 140 Å. This compares with the finding from SAXS measurements that the BST2(47–159) construct has an overall length of 170 Å (36). This 30 Å length difference might be explained by extended conformation(s) for residues 153–159, which are not present in any of the crystal structures plus a few additional residues at the ends of the molecule, which tend to be poorly defined in electron density. Partial unwinding of helices of the N-terminal disulfide-bound portion of the coiled coils is also a possibility.

A number of observations indicate that the N-terminal region of the BST2 extracellular domain is functionally important, including the findings that activity is lost when all disulfide bonds are disrupted (34) or when seven residues within 62–73 are mutated (36). Although we find that the L70D protein retains activity, thereby indicating that formation of a stable reduced tetramer is not essential for viral restriction, the restriction activity is reduced by approximately twofold compared to wild-type, even though expression of the mutant increases slightly. This reduction in potency indicates that L70 contributes to restriction, likely by stabilizing a functional conformation. Indeed, the activity reduction in the L70D mutant approaches the 10-fold loss of activity seen in an "artificial" BST2 molecule that replaces essentially all of the amino acid residues (34). L70D may diminish restriction activity by impacting the conformation or stability of the parallel coiled coil conformation. Alternatively, L70D may diminish activity by inhibiting formation of the reduced BST2 tetramer that, though not absolutely essential for HIV-1 restriction, might contribute to the efficiency of restriction or to some other BST2 function. It is striking that BST2 forms a stable tetramer in solution, indicating that the four-helix bundle is an energetically stable conformation, although we note that isolated coiled coil peptides can adopt nonphysiological association states (42). In principle, tetramerization could occur at several different stages of the BST2 "life cycle." One possibility is that BST2 could become reduced upon localization to a cellular compartment that induces disulfide bond reduction (43, 44), in which case tetramerization could serve as a signal that alters protein trafficking (e.g., promoting BST2 recycling or retention).

Finally, the structure raises the general question, why is BST2 dimeric? Because the leading model is that virions are tethered by the TM helix and GPI anchors binging plasma and viral membranes, one can question why a single isolated subunit is not

sufficient for activity. There are a number of possible explanations, which are not mutually exclusive. Consistent with a report that the GPI anchor is dispensable for restriction (14), one possibility is that virions can be tethered by the two TM helices of a dimer embedding separately in plasma and virion membranes. A second possibility is that dimerization provides a more structured extracellular domain that is better able to fold and resist proteolysis. Third, formation of an extended coiled coil, rather than a more flexible isolated single subunit, may optimally separate the TM helices and GPI anchors, thereby increasing the chance that virions will bud between them and become tethered to the cell. Finally, dimerization may strengthen the tether through avidity effects that result from having two attachments to each membrane. Avidity effects may also explain why higher concentrations of BST2 molecules produce more efficient virion retention (34) because higher order BST2 dimer–dimer interactions could be stabilized in the constrained environment of the cell surface. Although important questions remain regarding the structure of the tether that connects virus and cell, our data indicate that a BST2 parallel coiled coil is likely to be a fundamental component.

Methods

Structure Determination of Reduced BST2. Human BST2(47–152) was expressed in *E.coli*, purified under reducing conditions, and concentrated to 9–16 mg/ml for crystallization (see *SI Text* for details). Crystals grew in sitting drops comprising 2 μl of protein solution and 2 μl of reservoir solution (18% PEG-MME 2K, 0.1 M BisTris pH 7.2, 4 μM TCEP). Crystals were transferred to reservoir solution made up with 30% MPD and plunged into liquid nitrogen. Data were collected from a selenomethione-substituted crystal at SSRL beamline 7.2 and processed with *HKL2000* (45). Eight of the expected twelve Se sites were located using the auto solve option in *Phenix* (46) and phased to 3.0 Å resolution. The model was built using COOT (47) and refined to 2.6 Å with REFMAC5 (48, 49) using translation/libration/screw (TLS) parameters (50) and programs in the CCP4 suite (51). The crystallized construct includes six additional residues (GIDPFT) at the N terminus that are not visible in electron density maps. The following residues lack defined density; molecule A (K47); B (K152); C (K47, K152); D (K47, A48, N49, K151, K152).

Structure Determination of Oxidized BST2. Human BST2(51–151) was expressed in HEK293T cells, purified, and concentrated to approximately 80 mg/ml (Bradford) for crystallization (see *SI Text* for details). MRC crystallization plate sitting drops were set up using a Mosquito crystallization robot by mixing 100 nl of protein solution with an equivalent amount of reservoir. Stacks of platelike crystals grew using a reservoir of 8% PEG8000, 100 mM Tris-HCl pH 8.5 at 18 °C. Crystals were vitrified in crystallization reservoir supplemented with 25% glycerol for data collection at the Diamond Light Source I04 beamline. Data were integrated and scaled using the programs MOSFLM (52) and SCALA (53) of the CCP4 suite. The structure of BST2(51–151) was determined by molecular replacement using PHASER (54) and residues 89–151 of reduced BST2(47–152) as the search model. 20 cycles of rigid-body refinement were followed by 10 cycles of positional refinement using REFMAC5 (48, 49) with the occupancy of C91 residues set to 0.01. $2mF_o$-DF_c and mF_o-DF_c maps indicated the existence of the C91–C91 disulfide and helical density was visible N-terminal to the template. Model building used COOT (47). Final refinement cycles used secondary structure restraints between hydrogen bonded helical N-O atoms. Phenix.refine (55) was used to generate secondary structure restraints and to calculate maximum likelihood averaged kick omit maps (56). The refined model lacks a substantial portion of the N terminus, which could not be reliably built, although residual density is present, particularly in proximity to neighboring molecules in the lattice (Fig. S5).

Analytical Equilibrium Ultracentrifugation. Data were collected at 4 °C in an Optima XL-A centrifuge (Beckman). Reduced BST2(47–154) samples were in a buffer containing 20 mM Tris pH 7.4, 300 mM NaCl, and 4 mM TCEP. Alternatively, BST2(47–154) was oxidized by extensive (1 week) dialysis against the same buffer lacking reductant. Formation of a disulfide-linked dimer upon oxidation was verified by mass spectrometry (Fig. S3). Oxidized and reduced protein samples were centrifuged at 12,000 rpm and 16,000 rpm with initial protein concentrations of 2.1, 1.06, and 0.53 mg/ml (166.7 μM, 83.3 μM, 41.7 μM). Data were globally fit to ideal single species models with fixed or floating molecular masses using the non linear least squares algorithms in the HETEROANALYSIS software (57). Protein partial specific volumes and solvent densities were calculated with the program SEDNTERP (version 1.09) (58).

BST2 Restriction of Virus Release and Infectivity. 293T and HeLa-TZM reporter cells (obtained from Drs. J. C. Kappes and X. Wu through the AIDS Research and Reference Reagent Program, Division of AIDS, NIAID, NIH) were maintained using standard procedures. Wild-type and mutant BST2 proteins were expressed from a pCAG vector under the control of a constitutively active CMV promoter. The HIV-1(ΔVpu) version of the HIV-1 molecular clone NL4-3 has been described previously (12). Virus was produced by calcium phosphate transfection of semiconfluent six well-plates of 293T cells with 1 μg of viral DNA and with increasing quantities of vectors expressing wild-type BST2 WISP10-435 or BST2(L70D) WISP10-436 (0, 25, 50, 100, 200, and 500 ng) or an empty pCAG control vector.

For Western blotting experiments, virus-containing media was harvested 40 h posttransfection. Virions (1 ml) were pelleted through a 20% sucrose cushion at 15,000 × *g*, and the pellet was resuspended in 30 μl 1X SDS/PAGE loading buffer (12 μl loaded/lane). Cells from the same samples were harvested, pelleted, lysed in 60 μl SDS-loading buffer, and boiled for 10 min (6 μl loaded/lane). Levels of virion-associated CA and MA proteins in the culture media (Virus) and cellular Gag-derived and BST2 proteins (Cells) were analyzed by Western blotting using a mouse anti-BST2 (kindly provided by Chugai Pharmaceutical, 1:500 dilutions) or our own rabbit anti-HIV CA and MA antisera (both mixed at 1:1,000). The secondary antibodies were antimouse IgG (goat) polyclonal conjugated to Alexa680 (1:10,000, Invitrogen) and antirabbit IgG (donkey) polyclonal conjugated to IRdye800 (1:10,000, Rockland). Western blots were visualized and quantified using an Odyssey scanner (Li-Cor Biosciences).

Infectious titers were determined from viral supernatants by the numbers of β-galactosidase-positive foci formed on HeLa-TZM indicator cells. Titers provided in Fig. 4*B* show the mean± the range from two independent repetitions of the experiment.

ACKNOWLEDGMENTS. We thank Dr. Stuart J. Neil (King's College London) for contribution in the early stages of the project and Dr. R. Aricescu (University of Oxford) for advice on the mammalian expression system. Portions of this research were carried out at the Stanford Synchrotron Radiation Light Source, (SSRL), a national user facility operated by Stanford University on behalf of the U.S. Department of Energy, Office of Basic Energy Sciences, and at the Diamond Light Source (UK). The SSRL Structural Molecular Biology Program is supported by the Department of Energy, Office of Biological and Environmental Research, and by the National Institutes of Health (NIH), National Center for Research Resources, Biomedical Technology Program, and the National Institute of General Medical Sciences. This work was supported by NIH Grant P50 082545 (W.I.S. and C.P.H.) and a Royal Society Research grant (R.A.S.).

1. Sadler AJ, Williams BR (2008) Interferon-inducible antiviral effectors. *Nat Rev Immunol* 8(7):559–568.
2. Neil SJD, Zang T, Bieniasz PD (2008) Tetherin inhibits retrovirus release and is antagonized by HIV-1 Vpu. *Nature* 451(7177):425–430.
3. Van Damme N, et al. (2008) The interferon-induced protein BST-2 restricts HIV-1 release and is downregulated from the cell surface by the viral Vpu protein. *Cell Host Microbe* 3(4):245–252.
4. Kaletsky RL, Francica JR, Agrawal-Gamse C, Bates P (2009) Tetherin-mediated restriction of filovirus budding is antagonized by the Ebola glycoprotein. *Proc Natl Acad Sci USA* 106(8):2886–2891.
5. Sakuma T, Noda T, Urata S, Kawaoka Y, Yasuda J (2009) Inhibition of Lassa and Marburg virus production by tetherin. *J Virol* 83(5):2382–2385.
6. Jouvenet N, et al. (2009) Broad-spectrum inhibition of retroviral and filoviral particle release by tetherin. *J Virol* 83(4):1837–1844.
7. Groom HC, Yap MW, Galao RP, Neil SJ, Bishop KN (2010) Susceptibility of xenotropic murine leukemia virus-related virus (XMRV) to retroviral restriction factors. *Proc Natl Acad Sci USA* 107(11):5166–5171.
8. Douglas JL, et al. (2010) The great escape: Viral strategies to counter BST-2/tetherin. *PLoS Pathog* 6(5):e1000913.
9. Sauter D, Specht A, Kirchhoff F (2010) Tetherin: Holding on and letting go. *Cell* 141(3):392–398.
10. Arnaud F, et al. (2010) Interplay between ovine bone marrow stromal cell antigen 2/tetherin and endogenous retroviruses. *J Virol* 84(9):4415–4425.
11. Neil SJD, Sandrin V, Sundquist WI, Bieniasz PD (2007) An interferon-[alpha]-induced tethering mechanism inhibits HIV-1 and Ebola virus particle release but is counteracted by the HIV-1 Vpu protein. *Cell Host Microbe* 2(3):193–203.
12. Neil SJD, Eastman SW, Jouvenet N, Bieniasz PD (2006) HIV-1 Vpu promotes release and prevents endocytosis of nascent retrovirus particles from the plasma membrane. *PLoS Pathog* 2(5):e39.

13. Hammonds J, Wang JJ, Yi H, Spearman P (2010) Immunoelectron microscopic evidence for Tetherin/BST2 as the physical bridge between HIV-1 virions and the plasma membrane. *PLoS Pathog* 6(2):e1000749.
14. Fitzpatrick K, et al. (2010) Direct restriction of virus release and incorporation of the interferon-induced protein BST-2 into HIV-1 particles. *PLoS Pathog* 6(3):e1000701.
15. Klimkait T, Strebel K, Hoggan MD, Martin MA, Orenstein JM (1990) The human immunodeficiency virus type 1-specific protein vpu is required for efficient virus maturation and release. *J Virol* 64(2):621–629.
16. Göttlinger HG, Dorfman T, Cohen EA, Haseltine WA (1993) Vpu protein of human immunodeficiency virus type 1 enhances the release of capsids produced by gag gene constructs of widely divergent retroviruses. *Proc Natl Acad Sci USA* 90(14):7381–7385.
17. Varthakavi V, Smith RM, Bour SP, Strebel K, Spearman P (2003) Viral protein U counteracts a human host cell restriction that inhibits HIV-1 particle production. *Proc Natl Acad Sci USA* 100:15154–15159.
18. Miyagi E, Andrew AJ, Kao S, Strebel K (2009) Vpu enhances HIV-1 virus release in the absence of Bst-2 cell surface down-modulation and intracellular depletion. *Proc Natl Acad Sci USA* 106(8):2868–2873.
19. Iwabu Y, et al. (2009) HIV-1 accessory protein Vpu internalizes cell-surface BST-2/tetherin through transmembrane interactions leading to lysosomes. *J Biol Chem* 284(50):35060–35072.
20. Schubert U, et al. (1996) Identification of an ion channel activity of the Vpu transmembrane domain and its involvement in the regulation of virus release from HIV-1-infected cells. *FEBS Lett* 398(1):12–18.
21. McNatt MW, et al. (2009) Species-specific activity of HIV-1 Vpu and positive selection of tetherin transmembrane domain variants. *PLoS Pathog* 5(2):e1000300.
22. Banning C, et al. (2010) A flow cytometry-based FRET assay to identify and analyse protein-protein interactions in living cells. *PLoS One* 5(2):e9344.
23. Rong L, et al. (2009) The transmembrane domain of BST-2 determines its sensitivity to down-modulation by human immunodeficiency virus type 1 Vpu. *J Virol* 83(15): 7536–7546.
24. Jia B, et al. (2009) Species-specific activity of SIV Nef and HIV-1 Vpu in overcoming restriction by tetherin/BST2. *PLoS Pathog* 5(5):e1000429.
25. Lim ES, Malik HS, Emerman M (2010) Ancient adaptive evolution of Tetherin shaped Vpu and Nef functions in human immunodeficiency virus and primate lentiviruses. *J Virol* 84(14):7124–7134.
26. Le Tortorec A, Neil SJ (2009) Antagonism to and intracellular sequestration of human tetherin by the human immunodeficiency virus type 2 envelope glycoprotein. *J Virol* 83(22):11966–11978.
27. Gupta RK, et al. (2009) Simian immunodeficiency virus envelope glycoprotein counteracts tetherin/BST-2/CD317 by intracellular sequestration. *Proc Natl Acad Sci USA* 106 (49):20889–20894.
28. Zhang F, et al. (2009) Nef proteins from simian immunodeficiency viruses are tetherin antagonists. *Cell Host Microbe* 6(1):54–67.
29. Yang SJ, et al. (2010) Anti-tetherin activities in Vpu-expressing primate lentiviruses. *Retrovirology* 7:13.
30. Bartee E, McCormack A, Fruh K (2006) Quantitative membrane proteomics reveals new cellular targets of viral immune modulators. *PLoS Pathog* 2(10):e107.
31. Pardieu C, et al. (2010) The RING-CH ligase K5 antagonizes restriction of KSHV and HIV-1 particle release by mediating ubiquitin-dependent endosomal degradation of tetherin. *PLoS Pathog* 6(4):e1000843.
32. Ohtomo T, et al. (1999) Molecular cloning and characterization of a surface antigen preferentially overexpressed on multiple myeloma cells. *Biochem Bioph Res Co* 258(3):583–591.
33. Kupzig S, et al. (2003) Bst-2/HM1.24 is a raft-associated apical membrane protein with an unusual topology. *Traffic* 4(10):694–709.
34. Perez-Caballero D, et al. (2009) Tetherin inhibits HIV-1 release by directly tethering virions to cells. *Cell* 139(3):499–511.
35. Rollason R, Korolchuk V, Hamilton C, Jepson M, Banting G (2009) A CD317/tetherin-RICH2 complex plays a critical role in the organization of the subapical actin cytoskeleton in polarized epithelial cells. *J Cell Biol* 184(5):721–736.
36. Hinz A, et al. (2010) Structural basis of HIV-1 tethering to membranes by the BST-2/tetherin ectodomain. *Cell Host Microbe* 7(4):314–323.
37. Sakuma T, Sakurai A, Yasuda J (2009) Dimerization of tetherin is not essential for its antiviral activity against Lassa and Marburg viruses. *PLoS One* 4(9):e6934.
38. Crick FH (1953) The packing of α-helices: Simple coiled-coils. *Acta Crystallogr* 6:689–697.
39. O'Shea EK, Klemm JD, Kim PS, Alber T (1991) X-ray structure of the GCN4 leucine zipper, a two-stranded, parallel coiled coil. *Science* 254(5031):539–544.
40. Walshaw J, Woolfson DN (2001) Socket: a program for identifying and analysing coiled-coil motifs within protein structures. *J Mol Biol* 307(5):1427–1450.
41. Zhou NE, Kay CM, Hodges RS (1993) Disulfide bond contribution to protein stability: positional effects of substitution in the hydrophobic core of the two-stranded alpha-helical coiled-coil. *Biochemistry* 32(12):3178–3187.
42. Garcia P, et al. (2006) Molecular insights into the self-assembly mechanism of dystrophia myotonica kinase. *FASEB J* 20(8):1142–1151.
43. Dube M, et al. (2010) Antagonism of tetherin restriction of HIV-1 release by Vpu involves binding and sequestration of the restriction factor in a perinuclear compartment. *PLoS Pathog* 6(4):e1000856 (in eng).
44. Feener EP, Shen WC, Ryser HJ (1990) Cleavage of disulfide bonds in endocytosed macromolecules. A processing not associated with lysosomes or endosomes. *J Biol Chem* 265(31):18780–18785.
45. Otwinowski Z, Minor W (1997) Processing of X-ray diffraction data collected in oscillation mode. *Methods Enzymol* 276:307–326.
46. Adams PD, et al. (2010) PHENIX: A comprehensive Python-based system for macromolecular structure solution. *Acta Crystallogr D* 66(Pt 2):213–221.
47. Emsley P, Cowtan K (2004) Coot: Model-building tools for molecular graphics. *Acta Crystallogr D* 60(Pt 12 Pt 1):2126–2132.
48. Murshudov GN, Vagin AA, Dodson EJ (1997) Refinement of macromolecular structures by the maximum-likelihood method. *Acta Crystallogr D* 53(Pt 3):240–255.
49. Steiner RA, Lebedev AA, Murshudov GN (2003) Fisher's information in maximum-likelihood macromolecular crystallographic refinement. *Acta Crystallogr D* 59(Pt 12): 2114–2124.
50. Painter J, Merritt EA (2006) Optimal description of a protein structure in terms of multiple groups undergoing TLS motion. *Acta Crystallogr D* 62(Pt 4):439–450.
51. CCP4 (1994) The CCP4 suite: Programs for protein crystallography. *Acta Crystallogr D* 50(Pt 5):760–763.
52. Leslie AGW (1992) Recent changes to the MOSFLM package for processing film and image plate data. *Joint CCP4 + ESF-EAMCB Newsletter on Protein Crystallography* No. 26:27–33.
53. Evans P (2006) Scaling and assessment of data quality. *Acta Crystallogr D* 62(Pt 1): 72–82.
54. McCoy AJ, et al. (2007) Phaser crystallographic software. *J Appl Crystallogr* 40(Pt 4): 658–674.
55. Adams PD, et al. (2002) PHENIX: Building new software for automated crystallographic structure determination. *Acta Crystallogr D* 58(Pt 11):1948–1954.
56. Praaenikar J, Afonine PV, Guncar G, Adams PD, Turk D (2009) Averaged kick maps: Less noise, more signal… and probably less bias. *Acta Crystallogr D* 65(Pt 9):921–931.
57. Cole JL (2004) Analysis of heterogeneous interactions. *Methods Enzymol* 384:212–232.
58. Laue T, Shah B, Ridgeway T, Pelletier S (1992) *Computer-aided interpretation of analytical sedimentation data for proteins* (Royal Society of Chemistry, Cambridge, UK), pp 90–125.

Supporting Information

Schubert et al. 10.1073/pnas.1008206107

Supporting Methods

Expression and Purification of Reduced BST2. Human BST2(47–152) was cloned into pET151/D-TOPO (Invitrogen) and expressed in BL21(DE3)RIL cells using the autoinduction technique (1). Ni-NTA affinity chromatography, dialysis against 20 mM Tris, pH 8.0, 100 mM NaCl, 2 mM DTT, and cleavage of the His-tag with TEV protease overnight at room temperature, was followed by Q (Buffer A: 20 mM Tris 8.8, 10 mM NaCl, 1 mM DTT; Buffer B: 20 mM Tris 8.8, 1 M NaCl, 1 mM DTT) and size-exclusion chromatography in 20 mM HEPES pH 7.0, 100 mM NaCl, 2 mM DTT. Protein was concentrated to 9–16 mg/ml for crystallization. Identical procedures were used for BST2(47–154) and selenomethionine-substituted BST2(47–152).

Expression and Purification of Oxidized BST2. Human BST2(51–151) was cloned into a pHLsec vector (a kind gift of Dr. Aricescu, Oxford) between the *AgeI* and *KpnI* cloning sites with a C-terminal $GTKH_6$ tag. After secretion signal cleavage, an EGT tripeptide is left at the N terminus resulting in the final EGT-(BST2 E51–K151)-$GTKH_6$ protein product [BST2(51–151)]. Transient protein expression was performed in HEK293T cells essentially as described (2). To facilitate protein deglycosylation, the *N*-glycosylation inhibitor swainsonine was added at a final concentration of 20 μM during DNA-PEI complex formation (3). Four days after transfection, the supernatant was collected for protein purification under nonreducing conditions. Following overnight binding to a His-Trap column (GE Healthcare), BST2(51–151) was eluted in 50 mM phosphate buffer pH 7.5, 300 mM NaCl with a linear (10–300 mM) imidazole gradient. The protein was then dialyzed against 50 mM Tris-HCl buffer, 50 mM NaCl with pH adjusted to 5.5 with a 1 M sodium citrate solution prior to overnight deglycosylation at 37 °C with Endoglycosidase-H (New England Biosciences) according to the manufacturer's instructions. Deglycosylated BST2(51–151) was further purified by size-exclusion chromatography on a S200 16/60 column (GE Healthcare) in 50 mM Tris-HCl pH 7.5, 100 mM NaCl buffer.

1. Studier FW (2005) Protein production by auto-induction in high density shaking cultures. *Protein Expres Purif* 41(1):207–234.
2. Aricescu AR, Lu W, & Jones EY (2006) A time- and cost-efficient system for high-level protein production in mammalian cells. *Acta Crystallogr D* 62(Pt 10):1243–1250.
3. Chang VT et al. (2007) Glycoprotein structural genomics: Solving the glycosylation problem. *Structure* 15(3):267–273.

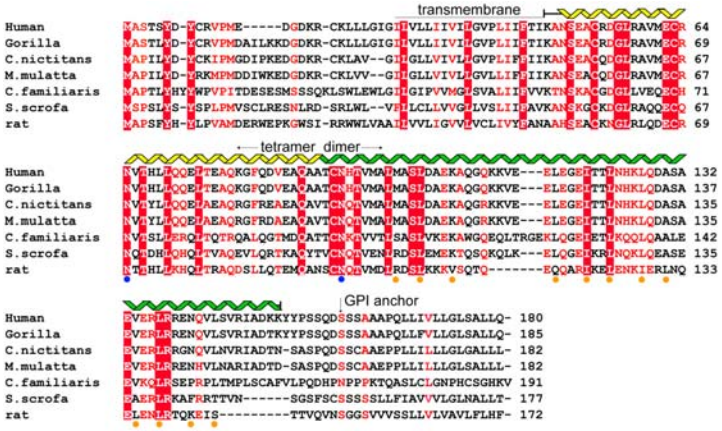

Fig. S1. Sequence alignment with knobs and holes analysis. An alignment of representative sequences with secondary structure observed in the reduced structure shown above. The mature human protein is truncated at Ser160, the site of GPI anchor attachment. The glycosylation sites, Asn65 and Asn92, are indicated with blue dots and are solvent exposed in the crystal structures. Residues that display *a* or *d* knobs into holes packing, as defined by the program SOCKET (1), are indicated with orange dots. Residues that are invariant in this alignment are highlighted in red boxes, and residues that are highly conserved are shown in red.

1. Walshaw J & Woolfson DN (2001) Socket: A program for identifying and analysing coiled-coil motifs within protein structures. *J Mol Biol* 307(5):1427–1450.

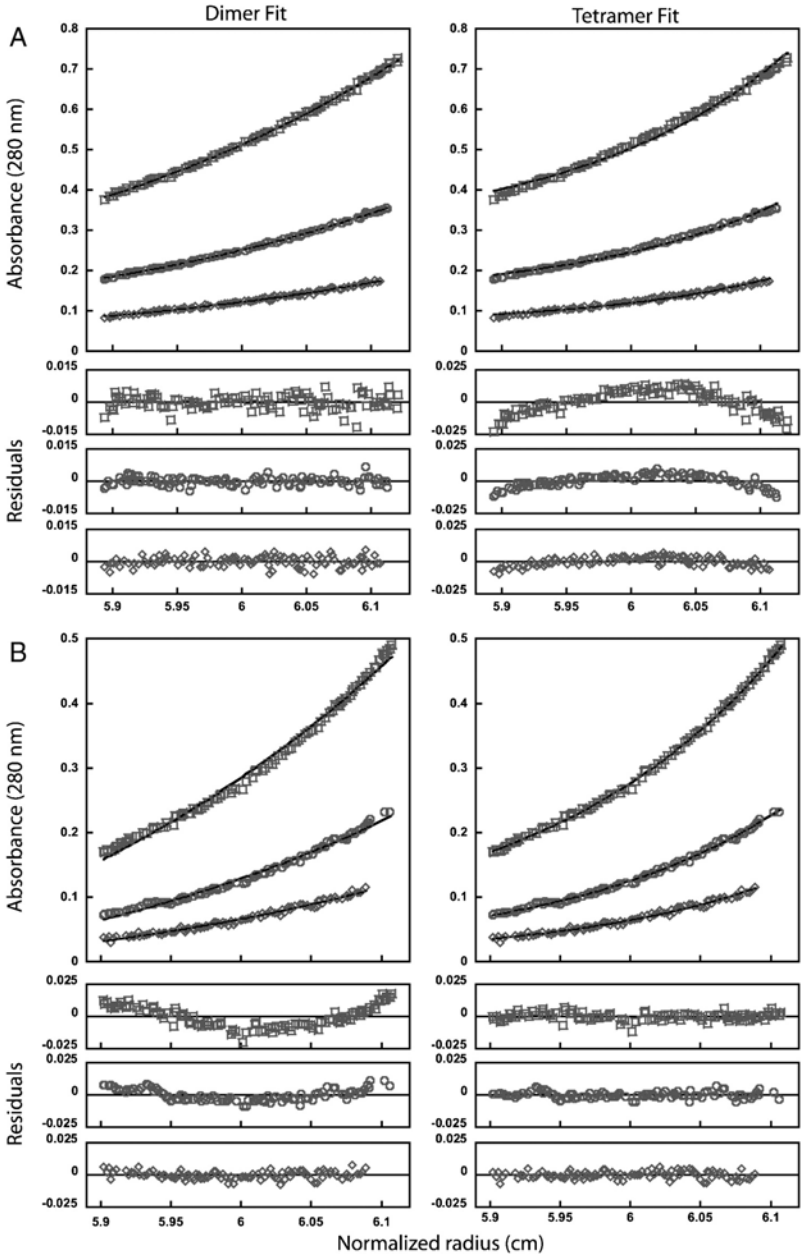

Fig. S2. Analytical equilibrium ultracentrifugation analyses of BST2(47–154). Equilibrium distributions without (*A*) and with (*B*) reductant (4 mM TCEP). Residual differences between the data and the fits are shown below. Rotor speeds were 12,000 rpm in these experiments. Data sets were also collected at 16,000 rpm. Data were collected at three concentrations and were globally fit to single species models in which the molecular weights were fixed to either a tetramer (left panel; 51,100 Da) or dimer (right panel, 25,550 Da). Note that the reduced BST2 protein is well fit by the tetramer model and the oxidized protein is well fit by the dimer model.

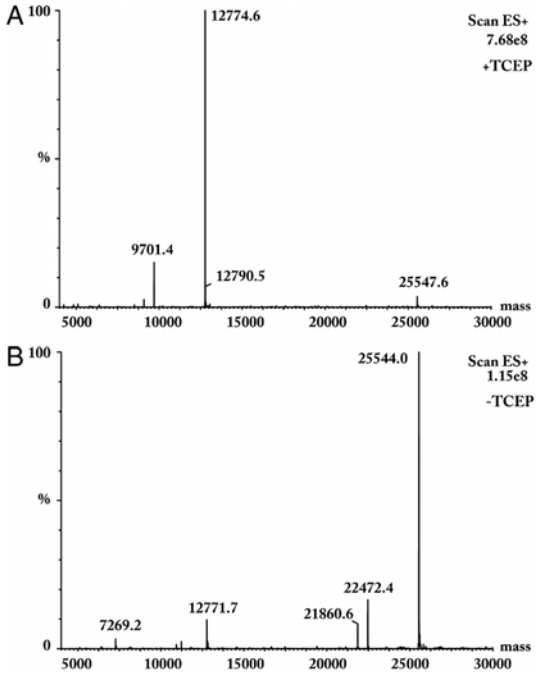

Fig. S3. Mass spectrometry of reduced and oxidized BST2(47–154). (*A*) Reduced and (*B*) oxidized BST2(47–154) were desalted for electrospray ionization mass spectrometry using a C18 Ziptip (Millipore) and analyzed on a Quattro-II mass spectrometer (Micromass, Inc.). Data were acquired with a cone voltage of 50 eV, a spray voltage of 2.8 kV, and scanning from 800 to 1,400 m/z in 4 s. Spectra were combined, and the multiply charged molecular ions were deconvoluted into a molecular-mass spectrum by using MaxEnt software (Micromass, Inc.). The mass of the reduced species corresponded to a BST2(47–154) monomer (MW_{obs} = 12,774.6 g/mol, MW_{calc} = 12,775.4 g/mol), indicating no disulfide formation in the presence of reductant. In contrast, the majority of BST2(47–154) formed a disulfide crosslinked dimer in the absence of TCEP (MW_{obs} = 25,544.0 g/mol, MW_{calc} = 25544.8 g/mol, assuming formation of three disulfide bonds).

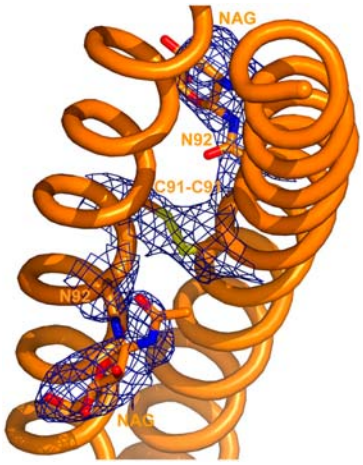

Fig. S4. Density showing glycosylation of N92 in BST2(51–151) expressed in HEK293T cells. $2mF_o$-DF_c electron density (1.0σ, blue) indicates the position of discernible sugar moieties extending from N92 residues after Endo-H treatment. N-acetylglucosamine (NAG) residues are approximately perpendicular to the C91–C91 disulfide bond.

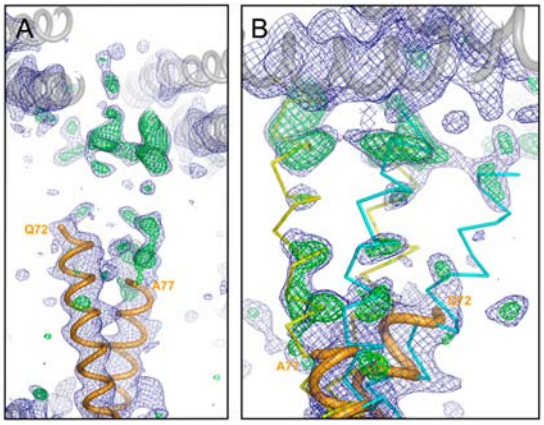

Fig. S5. Residual electron density at the N terminus of oxidized BST2(51–151). (*A*) Density in the $2mF_o$-DF_c (blue, 1.0 σ) and mF_o-DF_c (green, 3.0 σ) maps is visible at the N terminus of BST2(51–151) (orange). It is mostly evident in proximity to symmetry related molecules (gray). (*B*) Residual density suggests the possibility of alternative helical conformation for the N-terminus, which we have tentatively modeled in this figure. Flexibility at the N terminus could generate alternative coiled-coil dimers shown here in cyan and yellow, respectively.

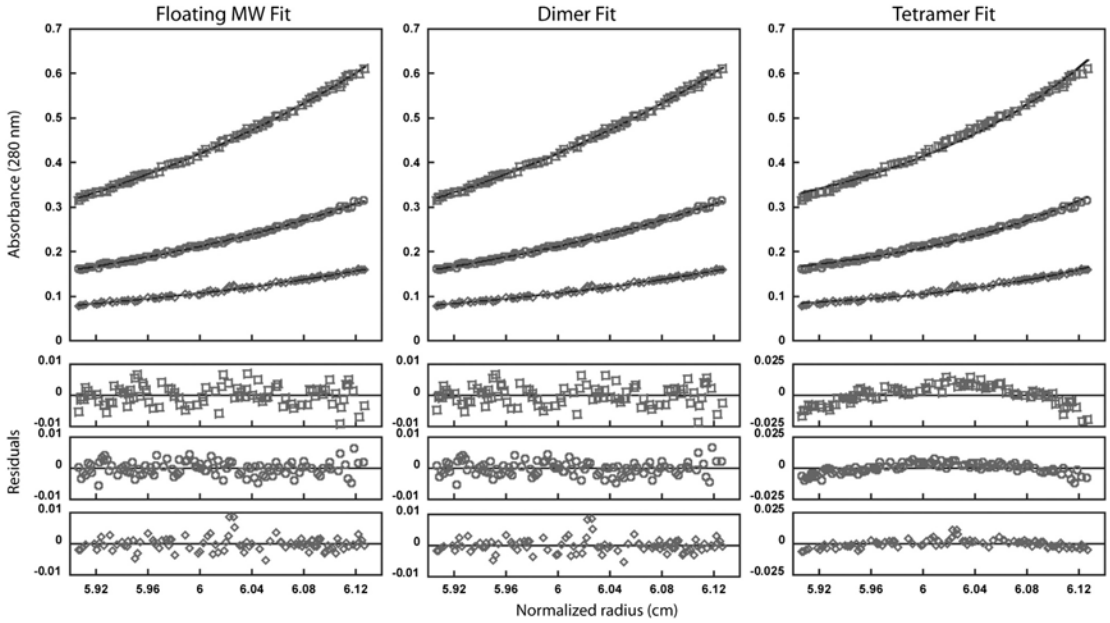

Fig. S6. Analytical equilibrium ultracentrifugation analyses of wt BST2(47–154)L70D. Equilibrium sedimentation distributions of BST2(47–154)L70D with reductant (4 mM TCEP). Corresponding residual differences are shown below. Rotor speeds for the data shown here were 12,000 rpm. Data sets were also collected at 16,000 rpm. Data were collected at three concentrations, and all of the data were globally fit to single species models in which the molecular weight was allowed to float (left panel; $MW_{obs} = 26{,}908$ Da), fixed as a dimer (middle panel; 25,554 Da) and fixed as a tetramer (right panel; 51,108 Da). Note that the reduced BST2(47–154) L70D protein is well fit by the dimer model.

Table S1. Data collection and crystallographic refinement statistics

Data set	Reduced BST2(47-152)	Oxidized BST2(51-151)
PDB code	3nwh	2xg7
Space group	$P2_1$	$P2_12_12_1$
Cell dimensions (Å,°)	$a = 26.6$	$a = 28.86$
	$b = 59.6$	$b = 91.86$
	$c = 159.5$	$c = 146.96$
	$\beta = 91.6$	
Solvent content (%)	57	70
Resolution (Å)	50.00-2.60 (2.69-2.60)	38.95-3.45 (3.64-3.45)
Completeness (%)	97.5 (93.2)	99.4 (97.6)
$I/\sigma(I)$	17.2 (4.0)	8.9 (2.5)
Multiplicity	3.6 (3.3)	6.8 (6.5)
R_{sym} (%) *	5.8 (26.9)	11.3 (70.9)
# Unique reflections	15,096	5,576
Wilson B ($Å^2$)	46.9	133.4
R factor (%)	26.0	26.9
R_{free} (%) †	28.7	29.8
# of protein atoms	3,266	1,209
# water molecules	18	0
# sugar molecules	-	2
$\langle B \rangle$($Å^2$)		
protein atoms	16.4	126.6
water molecules	37.4	-
sugar molecules		181.5
RMSD from ideality		
Bonds (Å)	0.018	0.012
Angles (°)	1.64	1.38
Phi/Psi angles:		
Favored (%)	98	98.04
Allowed (%)	2.0	1.96
Disallowed (%)	0.0	0.0

Values in parentheses are for the highest-resolution shell.

*$R_{sym} = \sum |I - \langle I \rangle| / \sum I$, where $\langle I \rangle$ is the average intensity from multiple observations of equivalent reflections.

†$R_{factor} = 100 \times \sum ||F_o| - |F_c|| / \sum |F_o|$. R_{free} is the R_{factor} computed from the 7.6% of reflections in the case of 3nwh and 4.5% in the case of 2xg7 that were chosen randomly and excluded from the refinement calculations.